DEPARTMENT OF
LIFE SCIENCES

IDENTIFICATION AND CHARACTERIZATION OF INCL: A *CHLAMYDIA TRACHOMATIS* PROTEIN ASSOCIATING WITH HOST CELL LIPID DROPLETS AND 14-3-3 PROTEINS

JOANA MARGARIDA NUNES BUGALHÃO

Master in Applied Microbiology

DOCTORATE IN MOLECULAR BIOSCIENCES

NOVA University Lisbon

November, 2021

DEPARTMENT OF
LIFE SCIENCES

IDENTIFICATION AND CHARACTERIZATION OF INCL: A *CHLAMYDIA TRACHOMATIS* PROTEIN ASSOCIATING WITH HOST CELL LIPID DROPLETS AND 14-3-3 PROTEINS

JOANA MARGARIDA NUNES BUGALHÃO

Master in Applied Microbiology

DOCTORATE IN MOLECULAR BIOSCIENCES

NOVA University Lisbon

November, 2021

NOVA SCHOOL OF SCIENCE & TECHNOLOGY

DEPARTMENT OF
LIFE SCIENCES

IDENTIFICATION AND CHARACTERIZATION OF INCL: A *CHLAMYDIA TRACHOMATIS* PROTEIN ASSOCIATING WITH HOST CELL LIPID DROPLETS AND 14-3-3 PROTEINS

JOANA MARGARIDA NUNES BUGALHÃO

Master in Applied Microbiology

Adviser: Luís Jaime Gomes Ferreira da Silva Mota
Assistant Professor, NOVA School of Science and Technology, NOVA University Lisbon

Examination Committee:

Chair: Isabel Maria Godinho de Sá Nogueira,
Full Professor, NOVA School of Science and Technology,
NOVA University Lisbon

Rapporteurs: Agathe Subtil,
Directrice de Recherche, Unité de Biologie Cellulaire de Infection Microbienne do Centre National de la Recherche Scientifique (CNRS), Institut Pasteur

Víctor Jimenez Cid,
Full Professor, Facultad de Farmacia da Universidad Complutense de Madrid

Adviser: Luís Jaime Gomes Ferreira da Silva Mota,
Assistant Professor, NOVA School of Science and Technology,
NOVA University Lisbon

Members: Maria José Borrego,
Assistant Researcher / Coordinator of the National Reference Laboratory of Sexually Transmitted Infections at National Institute of Health Dr. Ricardo Jorge

Isabel Maria dos Santos Leitão Couto,
Associate Professor, Instituto de Higiene e Medicina Tropical,
NOVA University Lisbon

DOCTORATE IN MOLECULAR BIOSCIENCES

NOVA University Lisbon
November, 2021

Identification and characterization of IncL: a *Chlamydia trachomatis* protein associating with host cell lipid droplets and 14-3-3 proteins

ACKNOWLEDGMENTS

My sincere acknowledgment to all who have supported me during my PhD thesis. My gratitude can only be properly expressed in Portuguese.

O meu sincero agradecimento a todos os que me apoiaram durante a minha tese de doutoramento.

Ao meu orientador, Prof. Luís Jaime Mota, por me ter aceitado no seu grupo de investigação, por contribuir para o meu desenvolvimento científico e pela revisão da minha tese. Por ser um orientador que se preocupa e valoriza todos os seus alunos, independentemente do seu nível académico. Por ter uma capacidade de trabalho inesgotável que nos motiva todos os dias. Pela oportunidade de aprender com o seu conhecimento e também pela recetividade em ouvir as minhas ideias, as melhores e as menos realistas, e permitir que as explorasse. Por todas as discussões, principalmente nas que discordámos, porque com a maioria eu concordaria mais tarde. Pela confiança e pela experiência que me proporcionou em desenvolver o meu doutoramento de forma mais independente, permitindo-me errar, explorar alternativas, voltar a errar, sabendo sempre que ao esgotar as minhas soluções estaria disponível para me apoiar. Serei sempre grata e consciente de que este caminho foi menos difícil por ter um orientador que respeito, admiro, e em quem sempre confiei.

Aos membros da minha comissão de tese, Prof. Isabel Couto, Prof. Rita Sobral e Prof. Sérgio Filipe, pela disponibilidade e pelas suas sugestões e críticas construtivas.

A todos os meus colegas do laboratório de Biologia da Infeção, Filipe Almeida, Nuno Charro, Sara Pais, Lia Domingues, Beatriz Costa, Irina Franco, Maria da Cunha, Maria Luís, Inês Pereira, Carolina Brizida, Joana Saraiva, Catarina Simões e Inês Leal, por me acompanharem durante os meus primeiros anos no laboratório e/ou durante o desenvolvimento da minha tese de doutoramento. Agradeço particularmente a entreajuda no contexto da pandemia de COVID-19, com trabalho limitado por turnos, que nos permitiu manter um ritmo de trabalho tão normal quanto possível. Agradeço à Maria da Cunha pela sua amizade, pelos seus conselhos e pela forma como inspira os mais novos com uma

mistura de sensibilidade e determinação. Agradeço à Inês Pereira pela sua força e por nunca desistir. Agradeço à Maria Luís por todos os nossos risos descontrolados e por me ter deixado conhecer a miúda inteligente e divertida que se esconde por trás de um sorriso tímido. Agradeço à Irina Franco pelo apoio e pela amizade. Por me ter integrado no seu projeto quando ingressei no laboratório e por ter sido uma orientadora entusiasta que me fez ter vontade de continuar em investigação. Acho que fomos uma "*Legionella* team" incrível e desejo que o seu talento para ensinar possa ser aproveitado por muitos mais. Agradeço também aos alunos de licenciatura e mestrado, Adriana Vieira, Joana Milão e Carolina Brizida, pela oportunidade de evoluir como orientadora e por tentarmos explorar alternativas que contribuíram para a progressão do trabalho. Agradeço à Sara Pais por ser uma presença constante, por partilharmos entusiasticamente a nossa vida pessoal e profissional e pelas conversas intermináveis sobre as possíveis funções das "nossas proteínas". Agradeço ao Nuno Charro pela amizade e por continuar sempre presente.

A todos os colegas, técnicos, investigadores e professores da FCT NOVA e ITQB pelos convívios e pela partilha de conhecimentos. À Prof. Isabel Sá Nogueira, Lia e Inês. À Prof. Rita Sobral, Bárbara, Inês e Gonçalo. Ao Prof. Sérgio Filipe e Joana. À Nicole, Ruth e Tânia por darem sempre o seu melhor. À Raquel Portela por todas as nossas conversas e pela sua boa disposição contagiante. Ao Prof. Pedro Viana Baptista e Prof. Mariana Pinho pela coordenação do programa doutoral em Biociências Moleculares. Aos meus colegas do programa doutoral pela boa energia e por tornarem mais simples os desafios que enfrentámos juntos.

Aos meus amigos Ourienses, de sempre e para sempre, em especial ao Dany de Sousa, Inês de Sousa, César Bucete, João Pereira, Cláudio Fernandes e Ricardo Simões, por todas as nossas aventuras e pelo privilégio de pertencer a este núcleo duro que vai sobrevivendo ao tempo e às mudanças.

À Joana Marques e à Margarida Pinheiro, pelo conforto de ter na minha vida pessoas tão especiais com quem tenho sempre vontade de partilhar tudo. Pela amizade incondicional, por me dizerem com sinceridade o que preciso de ouvir e por tolerarem todas as minhas facetas. Agradeço à Joana por nunca deixar que a distância seja uma barreira. Agradeço à Margarida por continuar a precoupar-se comigo, mesmo tendo uma bebé maravilhosa.

À minha família, por ser o meu refúgio. Aos meus avós António, Francisco e Joaquina (com saudade) e avó Tina, pelos incentivos ao longo da minha vida, pelo carinho e por me adorarem por nenhum motivo em especial, apenas por existir.

Aos meus tios e primos pelo seu apoio e pelos momentos de convívio. Ao meu afilhado Gabriel, que tem a mesma idade que a minha tese, pela simplicidade com que decide se somos amigos consoante a minha disponibilidade para brincar e com os seus mimos torna os meus dias mais felizes.

À família Sousa, em especial ao Tó-Zé, à Linda e ao Pedro, por estarem sempre presentes e me tratarem como família desde o primeiro dia.

Aos meus pais, pelo seu amor, pelos valores que me transmitiram e por tudo o que tenho alcançado na vida. Por serem pessoas incríveis que me apoiam sempre. Por continuarem a ser o meu primeiro telefonema na partilha dos bons e maus momentos. Por todas as suas lutas e conquistas, que me permitiram escolher todos os meus caminhos. A determinação com que enfrentam as adversidades continua a ser uma inspiração para mim. Ao meu pai pelo perfecionismo e dedicação em tudo o que faz, que me incentiva a ser melhor. À minha mãe por ser tão sensível como destemida e me inspirar quando a coragem me falha.

Ao meu Vítor, por não entender, mas aceitar o meu fascínio por bactérias que provocam doenças. Pela paciência e compreensão por todas as horas dedicadas a este trabalho. Por acreditar nas minhas capacidades sem nunca me deixar desistir. Por me dizer TRS (tu resolves sempre) quando estou ansiosa para algum desafio. Pelo seu sorriso intrigado nos dias em que cheguei a casa aos pulos sem ter descoberto "uma vacina para *Chlamydia*", mas a agir como tal. Pelo seu amor e carinho quando meses de trabalho não deram frutos. Por ser o meu companheiro de vida. Por demonstrar que a sua felicidade depende da minha. Por manter há 15 anos o desafio pessoal de me fazer rir todos os dias.

Funding

This work was supported by Fundação para a Ciência e Tecnologia (FCT) through grants PTDC/BIA-MIC/28503/2017 and PTDC/IMI-MIC/1300/2014, and in the scope of the projects UIDP/04378/2020 and UIDB/04378/2020 of the Research Unit on Applied Molecular Biosciences – UCIBIO, and LA/P/0140/2020 of the Associate Laboratory Institute for Health and Bioeconomy - i4HB. JNB was supported by PhD fellowship PD/BD/128214/2016, within the scope of the PhD program Molecular Biosciences (PD/00133/2012) funded by FCT.

ABSTRACT

Chlamydia trachomatis causes genital and ocular infections in humans. This obligate intracellular bacterial pathogen multiplies within a characteristic vacuole, known as inclusion, and utilizes a type III secretion system to deliver chlamydial proteins, such as inclusion membrane proteins (Incs), into host cells. This work aimed to increase the knowledge on *C. trachomatis* Incs. A screen using *Saccharomyces cerevisiae* led to the identification of two Incs causing vacuolar protein sorting defects and seven Incs showing tropism for eukaryotic organelles. In particular, the transient production in yeast and mammalian cells of different fragments of CT006 (renamed IncL) revealed its tropism for the endoplasmic reticulum and lipid droplets (LDs), an organelle that regulates storage and hydrolysis of neutral lipids. We identified a LD-targeting region within the first 88 amino acid residues of IncL and positively charged residues important for this targeting. Comparing with the parental *C. trachomatis* strain, cells infected by a strain overproducing IncL showed a slight increase in the area occupied by LDs within the inclusion region. However, we could not correlate this effect with the LD-targeting regions within IncL. In addition, a previous proteomics screen suggested that IncL could bind mammalian 14-3-3 proteins, which regulate several signaling pathways in host cells. Here, co-immunoprecipitation assays validated the predicted interactions between IncL and 14-3-3β, η and γ isoforms and revealed an interaction with the 14-3-3σ isoform. The carboxy-terminal region of IncL was essential and sufficient for the IncL-14-3-3β interaction. We further showed that both the amino and carboxy-terminal regions of IncL, flanking the Inc-characteristic bilobed hydrophobic domain, are exposed to the host cell cytosol during *C. trachomatis* infection, and therefore available to interact with host cell targets. In conclusion, we characterized a chlamydial protein interacting with host cell LDs and 14-3-3 proteins via different protein regions, thus expanding the understanding of *C. trachomatis*-host cell interactions.

Keywords: Host-pathogen interactions, *Chlamydia trachomatis*, Inc proteins, vesicular trafficking, lipid droplets, 14-3-3 proteins

RESUMO

Chlamydia trachomatis é uma bactéria intracelular obrigatória que provoca infeções oculares e genitais em humanos. *C. trachomatis* tem a capacidade de proliferar no interior de um vacúolo, denominado de inclusão, e transporta várias proteínas bacterianas para o citosol das células hospedeiras, incluindo proteínas que se localizam na membrana da inclusão (Incs). Este trabalho teve como objetivo aprofundar o conhecimento sobre proteínas Inc de *C. trachomatis*. Um rastreio usando *Saccharomyces cerevisiae* permitiu a identificação de duas Incs que interferem com o tráfego de proteínas para o vacúolo e sete Incs com tropismo para organelos eucarióticos. A produção transiente de diferentes fragmentos de CT006 (designada de IncL) revelou o seu tropismo para o retículo endoplasmático e para gotículas de lípidos (GLs), um organelo que regula o armazenamento e hidrólise de lípidos neutros. Identificámos os primeiros 88 aminoácidos de IncL como a região que se associa às GLs e aminoácidos importantes para esta localização. Em células infetadas com uma estirpe de *C. trachomatis* a sobre-produzir IncL foi observado um ligeiro aumento na área ocupada pelas GLs na região das inclusões, por comparação com uma estirpe selvagem. Adicionalmente, um rastreio de proteómica tinha sugerido que IncL poderia interagir com proteínas de mamífero 14-3-3, que regulam várias vias de sinalização da célula hospedeira. Neste trabalho, validámos a interação entre IncL e as isoformas 14-3-3β, η e γ e revelámos uma interação com a isoforma 14-3-3σ. A região carboxi-terminal de IncL mostrou ser essencial e suficiente para interagir com 14-3-3β. Demonstrámos ainda que as regiões amino e carboxi-terminais de IncL, que flanqueiam o domínio hidrofóbico bilobal característico das Incs, estão expostas ao citosol da célula hospedeira. Em conclusão, neste trabalho foi caracterizada uma proteína de *Chlamydia* que interage com GLs e com as proteínas 14-3-3, expandindo assim o conhecimento acerca das interações entre *C. trachomatis* e células hospedeiras.

Palavras chave: Interação bactéria-hospedeiro, *Chlamydia trachomatis*, Proteínas Inc, Tráfego vesicular, Gotículas de lípidos, Proteínas 14-3-3

CONTENTS

1 INTRODUCTION 1

1.1 Discovery and Taxonomy of *Chlamydiae* 1

1.2 The human pathogen *C. trachomatis* 3

1.2.1 The different tissue tropism of *C. trachomatis* strains 4

1.2.2 *C. trachomatis* diagnosis, treatment and vaccine 5

1.2.3 Experimental models to study *C. trachomatis* infections 6

1.3 The chlamydial biology and developmental cycle 6

1.4 Genetic tools to study *C. trachomatis* infections 10

1.4.1 The *C. trachomatis* genome 10

1.4.2 The development of protocols for *C. trachomatis* transformation 12

1.4.3 Advances in *C. trachomatis* mutagenesis 13

1.5 Secretion systems in *Chlamydiae* 16

1.5.1 The *C. trachomatis* T3S system 16

1.5.2 *C. trachomatis* T3S system effectors 18

1.6 Thesis Goals 33

2 MATERIALS AND METHODS 35

2.1 Plasmids and oligonucleotides 35

2.2 *Escherichia coli* strains and growth conditions 35

2.3 Yeast strains and vacuolar protein sorting assays 36

2.4 Mammalian cell lines 36

2.5 Transient transfection of mammalian cells 36

2.6 Manipulation of *C. trachomatis* 37

2.6.1 Infection of HeLa 229 cells by *C. trachomatis* 37

2.6.2 Transformation of *C. trachomatis* 37
2.6.3 Clone isolation of *C. trachomatis* strains by plaque purification 38
2.7 Co-immunoprecipitation assays 39
2.8 Antibodies, fluorescent dyes and treatment with oleic acid 40
2.9 Fluorescence microscopy 40
2.10 Immunoblotting 41
2.11 Statistical analyses 42
3 RESULTS 43
3.1 Screening of *C. trachomatis* Incs interfering with eukaryotic trafficking and/or showing tropism for eukaryotic organelles 43
3.1.1 *C. trachomatis* Incs cause vacuolar protein sorting mistrafficking in yeast 43
3.1.2 *C. trachomatis* Incs co-localize with yeast organelles 46
3.1.3 The first 88 amino acid residues of IncL fused to mEGFP co-localize with LDs in mammalian cells 52
3.1.4 Positively charged amino acids within $IncL_{1-88}$ are essential to target mEGFP-$IncL_{1-88}$ to LDs in mammalian cells 56
3.2 IncL-2HA produced by *C. trachomatis* slightly increases the area of LDs at the region of inclusions 59
3.2.1 The putative cytosolic regions of IncL are exposed to the host cell cytosol 59
3.2.2 Characterization of IncL-2HA during *C. trachomatis* infection 62
3.2.3 The effect of IncL-2HA produced by *C. trachomatis* on host cell LDs 65
3.3 Identification and validation of IncL host cell interacting proteins 72
3.3.1 IncL interacts with 14-3-3β in mammalian cells 72
3.3.2 The seven mammalian 14-3-3s are recruited to the periphery of *C. trachomatis* inclusions and IncL interacts with four isoforms 74
3.3.3 IncL interacts via the carboxy-terminal region with 14-3-3β 79
4 DISCUSSION AND CONCLUSIONS 83
4.1 Using yeasts as a model to identify bacterial effector proteins subverting host cell pathways 84

4.2 The dual intracellular localization of $IncL_{1-88}$ when ectopically produced in mammalian cells 86
4.3 A possible role for IncL during *C. trachomatis* infection 87
4.4 Searching for IncL host cell interacting proteins 89
4.5 Model for the role of IncL during *C. trachomatis* infection 92
4.6 Concluding remarks and future directions 93
REFERENCES 97
ANNEXES 117

LIST OF FIGURES

Figure 1.1 Phylogenetic reconstruction of the *Chlamydia* genus 3
Figure 1.2 The chlamydial developmental cycle 8
Figure 1.3 The *Chlamydia*-host cell interactions 9
Figure 1.4 Schematic representation of the *C. trachomatis* T3S system 17
Figure 1.5 *C. trachomatis* Incs interfering with host cell trafficking, acquisition of lipids and cytoskeleton remodeling 32
Figure 3.1 Schematic representation of vacuolar protein sorting assays 45
Figure 3.2 *C. trachomatis* Incs cause vacuolar protein sorting mistrafficking in yeast 46
Figure 3.3 Intracellular localization of Inc-GFP and Inc-GFP-Pep12$_{L\text{-}TM}$ proteins in yeast 47
Figure 3.4 Co-localization analyses between Inc-GFP proteins and mitochondria or endosomal compartments 48
Figure 3.5 IncL$_{1\text{-}88}$-GFP localizes at LDs in yeast 49
Figure 3.6 Schematic representation of *C. trachomatis* IncL 52
Figure 3.7 Prediction of transmembrane helices in IncL 53
Figure 3.8 Analysis of the production and intracellular localization of IncL versions in mammalian cells 54
Figure 3.9 The first 88 amino acid residues of IncL fused to mEGFP co-localize with LDs in mammalian cells 55
Figure 3.10 Full-length IncL and IncL$_{1\text{-}88}$ fused to mEGFP partially co-localize with the ER in mammalian cells 56
Figure 3.11 Analysis of the production of mEGFP-IncL$_{1\text{-}88}$ versions with positively charged amino acids replaced by glycines in mammalian cells 57
Figure 3.12 Positively charged amino acids within IncL$_{1\text{-}88}$ are important to target mEGFP-IncL$_{1\text{-}88}$ to LDs in mammalian cells 58
Figure 3.13 Analysis of the topology of IncL at the inclusion membrane 61
Figure 3.14 Characterization of *C. trachomatis* L2/434 strain harboring pIncL-2HA 63

Figure 3.15 Plasmid-encoded IncL-2HA is produced at early times post-infection and accumulates at the periphery of the inclusion 64
Figure 3.16 mEGFP-CT449 does not localize at lipid droplets in mammalian cells 66
Figure 3.17 Analysis of the production of plasmid-encoded CT449-2HA, $IncL_{5G}$-2HA and $IncL_{\Delta 47-67}$-2HA by *C. trachomatis* 67
Figure 3.18 Analysis of the intracellular localization of plasmid-encoded IncL-2HA, CT449-2HA, $IncL_{5G}$-2HA and $IncL_{\Delta 47-67}$-2HA 68
Figure 3.19 Analysis of the localization of LDs in cells infected by *C. trachomatis* 70
Figure 3.20 The effect of IncL-2HA produced by *C. trachomatis* on host cell lipid droplets 71
Figure 3.21 FLAG-HA-14-3-3β accumulates at the periphery of the inclusion membrane during *C. trachomatis* infection 73
Figure 3.22 FLAG-HA-14-3-3β and mEGFP-IncL interact after their transient production in mammalian cells 74
Figure 3.23 The seven mammalian isoforms of 14-3-3 proteins are recruited to the periphery of the inclusion membrane during *C. trachomatis* infection 75
Figure 3.24 mEGFP-IncL interacts with FLAG-HA-14-3-3β, HA-14-3-3η, FLAG-HA-14-3-3γ and HA-14-3-3σ after transient production in HEK 293T cells 77
Figure 3.25 Alignment of the amino acid sequences of 14-3-3 isoforms 78
Figure 3.26 IncL interacts via the carboxy-terminal region with 14-3-3β 79
Figure 3.27 Analysis of the interaction between IncL mutant proteins and 14-3-3β 80
Figure 3.28 The substitution by alanines of all the serine residues within putative IncL 14-3-3 binding motifs does not affect IncL-14-3-3β interaction 81
Figure 4.1 Model for the role of IncL during *C. trachomatis* infection 92

LIST OF TABLES

Table 1.1 *C. trachomatis* Incs confirmed to localize at the inclusion membrane and their validated host cell interacting proteins and proposed functions 25
Table 3.1 Inc-GFP fusion proteins - summary of production and localization in *S. cerevisiae*, and induction of a vacuolar protein sorting (Vps) defect..... 50
Table 3.2 Inc-GFP-Pep12$_{L\text{-}TM}$ fusion proteins - summary of production and localization in *S. cerevisiae*, and induction of a vacuolar protein sorting (Vps) defect 51
Table 3.3 Percentage (%) of identity between 14-3-3 isoforms..... 78

ABBREVIATIONS

14-3-3s	14-3-3 proteins
ATP	Adenosine triphosphate
ATPase	ATP hydrolase
Cas	CRISPR associated protein
CI-M6PR	Cation-independent mannose 6-phosphate receptor
co-IP	Co-immunoprecipitation
CLO	Chlamydia-like organisms
CPY-Inv	Carboxipeptidase Y-Invertase
CRISPRi	Clustered regularly interspaced short palindromic repeats interference
dCas	Catalytically inactive Cas
DMEM	Dulbecco's modified eagle medium
DNA	Deoxyribonucleic acid
EB	Elementary body
ESCRT	Endosomal sorting complexes required for transport
ER	Endoplasmic reticulum
EMS	Ethyl methanesulfonate
FBS	Fetal bovine serum
FRAEM	Fluorescence-reported allelic exchange mutagenesis
GSK	Glycogen synthase kinase
GEF	Guanine nucleotide exchange factor
GFP	Green fluorescent protein

gRNA	Guide RNA
GTP	Guanosine triphosphate
GTPase	Guanosine triphosphate hydrolases
HBSS	Hank's balanced salt solution
Hsp60	Heat-shock protein 60
HSPG	Heparin sulfate proteoglycans
IDO	Indoleamine 2,3- dioxygenase
IFN-γ	Interferon-gamma
Inc	Inclusion membrane protein
LD	Lipid droplet
LGV	Lymphogranuloma venereum
M6PRs	Mannose 6-phosphate receptor
MCS	Membrane contact sites
mEGFP	Monomeric enhanced green fluorescent protein
mRNA	Messenger RNA
MOMP	Major outer membrane protein
MTOC	Microtubule organizing center
MVB	Multivesicular bodies
NAAT	Nucleic Acid Amplification Test
NF-κB	Nuclear factor-κB
OD_{600}	Optical density at 600 nm
PAM	Protospacer-adjacent motif
pGP	Plasmid glycoprotein
PIP3	Phosphatidylinositol 3,4,5-triphosphate
Pmp	Polymorphic membrane protein
PMSF	Phenylmethylsulfonyl fluoride
PAM	Protospacer-adjacent motif

PBS	Phosphate-buffered saline
RB	Reticulate body
RNA	Ribonucleic acid
rRNA	Ribosomal RNA
SDS	Sodium dodecyl sulphate
SDS-PAGE	SDS-polyacrylamide gel electrophoresis
siRNA	Small interfering RNA
SNARE	Soluble N-ethylmaleimide-sensitive factor receptor
SNX	Sorting nexins
STI	Sexually Transmitted Infection
T3S	Type III secretion (equivalent nomenclature for Type II, IV, V and VI)
TGN	*trans*-Golgi network
VPS	Vacuolar protein sorting
VAMP	Vesicle-associated membrane protein
WGS	Whole genome sequencing
WHO	World health organization
YNB	Yeast nitrogen base
YNB-Ura	Yeast nitrogen base uracil dropout
α	Alpha
β	Beta
γ	Gamma
ε	Epsilon
ζ	Zeta
η	Eta
σ	Sigma
τ	Tau

1

INTRODUCTION

1.1 Discovery and Taxonomy of *Chlamydiae*

Chlamydiae are obligate intracellular bacteria, discovered in 1907 by Ludwig Halberstädter and Stanislaus von Prowazek. The researchers observed inclusion bodies near the nuclei of ocular conjunctival epithelial cells obtained from scrapings of an experimentally infected orangutan (Halberstädter and Prowazek, 1907). Inclusion bodies were named Chlamydozoa, a derivative from the Greek word "khlamús", meaning mantle. During the same decade, similar intracellular inclusions were reported in cervical and urethral cells from parents of newborns with inclusion conjunctivitis, in men with urethritis (Lindner, 1910; Lindner, 1911) and also from patients with lymphogranuloma venereum (LGV) (Durand *et al.*, 1913). As exemplified in the title of the article "Studies on the virus of lymphogranuloma inguinale" from Miyagwa (Miyagwa *et al.*, 1935), chlamydial organisms were thought to be viruses for many years, due to their small size and inability to replicate outside host cells. Only in 1966, along with advances in electronic microscopy, Moulder demonstrated the bacterial nature of *Chlamydiae*, including the presence of DNA and RNA, reproduction by binary fission and a cell wall similar to those of Gram-negative bacteria (Moulder, 1966).

The Phylum *Chlamydiae*, which comprises one Class (*Chlamydiia*) and one Order (*Chlamydiales*), was thought to include only the *Chlamydiaceae* family. The increasing knowledge about the diversity of these organisms led to the recognition of 8 additional families (*Parachlamydiaceae*, *Waddliaceae*, *Simkaniaceae, Rhabdochlamydiaceae*, *Criblamydiaceae*, *Piscichlamydiaceae, Chlavichlamydiaceae* and *Parilichamydiaceae*), which are frequently called "Chlamydia-like organisms" (CLO) or environmental *Chlamydiae*. Although CLOs were mainly isolated from environmental sources, it is currently known their ability to infect a wide host range [reviewed in (Taylor-Brown *et al.*, 2015)].

The *Chlamydia* genus belongs to the *Chlamydiaceae* family and comprises 16 species, all pathogenic to humans or animals (Figure 1.1). *Chlamydia trachomatis*, which exclusively infects humans, causes ocular and genital infections, which can have severe consequences (see section 1.2). Another relevant human pathogen is *C. pneumoniae*, which causes respiratory tract infection through the inhalation of contaminated droplets. It is one of the main causative agents of community-acquired pneumonia and it has also been associated with other pathologies, such as pharyngitis and chronic obstructive pulmonary disease (Brown, 2012; Falck *et al.*, 1995; Karnak *et al.*, 2001). The diversity of hosts targeted by this pathogen includes other mammalian animals, amphibians and reptiles [Reviewed in (Bodetti *et al.*, 2002)].

The remaining 14 species of the *Chlamydia* genus have non-human animals as their primary host, although some might be threatening to humans due to their zoonotic potential, especially *C. abortus*, *C. felis, C. psittacci*, *C. caviae* and *C. suis*.

C. abortus has the capacity to infect pregnant women exposed to contaminated ruminants, who become at risk of pregnancy loss. This bacterial species has been a major concern for livestock industry, as it targets the placenta of small ruminants, such as goat and sheep, which results in abortion in later stages of gestation or weaker offspring (Essig & Longbottom, 2015; Pospischil *et al.*, 2002).

C. felis typically causes conjunctivitis in cats and is transmitted via ocular secretions. Although only a few cases of human transmission have been confirmed, close interactions with these animals increase the probability of zoonosis (Cai *et al.*, 2002; Wons *et al.*, 2017).

C. psittacci infects preferentially birds, including psittacine birds, ducks, pigeons and turkeys, but it is also the causative agent of zoonotic psittacosis, also known as parrot fever (Harkinezhad *et al.*, 2009). Other species infecting the respiratory tract of birds are *C. avium*, *C. ibidis* and *C. gallinacea*.

C. caviae causes conjunctivitis and genital tract infections in guinea pigs, with only a few reported cases of transmission to humans. Guinea pigs infected with *C. caviae* are used as a model to study chlamydial genital infections (De Clercq *et al.*, 2013; Lutz-Wohlgroth *et al.*, 2006).

C. suis infects the conjunctiva, gastrointestinal tract and respiratory tract of pigs and have been detected in farm workers, although without any symptoms. It is the only *Chlamydia* species with reported cases of antibiotic resistance, specifically with tetracycline-resistance strains. This is a major concern in farming industry, due to the possibility of transference of the tetracycline-resistant gene to human pathogens (De Puysseleyr *et al.*, 2017; Unterweger *et al.*, 2020).

Other *Chlamydia* species with unknown capacity to infect humans are *C. pecorum* and *C. muridarum*. *C. pecorum* infects livestock and is endemic among koalas, contributing to their population decline (Fabijan *et al.*, 2019; Mohamad & Rodolakis, 2010). *C. muridarum*, which is predominantly a rodent pathogen, causes pneumonitis. This pathogen does not naturally infect the reproductive tract of mice, but it is manipulated to be widely used as a model to study genital *C. trachomatis* infections (De Clercq *et al.*, 2013).

More recently, *C. serpentis*, *C. poikilothermis* and *C. corallus* were discovered in snakes and *C. sanzini* was detected in snakes and turtles (Phillips *et al.*, 2019). Little is known regarding the zoonotic potential of these newly identified species.

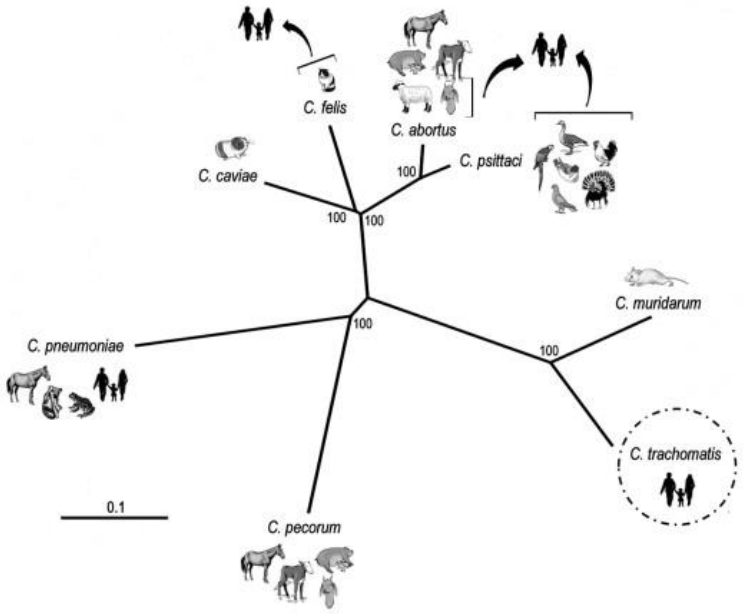

Figure 1.1 Phylogenetic reconstruction of the *Chlamydia* genus. Evolutionary relationships among *Chlamydiaceae* species and their natural hosts. The tree is based on 600 orthologous genes shared among the species for which genomes were fully sequenced and the arrows indicate cases of zoonotic transmission. Reprinted from (Nunes & Gomes, 2014) with permission from Elsevier.

1.2 The human pathogen *C. trachomatis*

Infections by *C. trachomatis* are a significant public health concern. Urogenital strains are the leading cause of sexually transmitted bacterial infections worldwide and ocular strains are the most common cause of preventable infectious blindness, with a higher incidence in developing countries.

1.2.1 The different tissue tropism of *C. trachomatis* strains

C. trachomatis strains comprise three biovars causing different pathologies, which are subtyped in different serovars based on the immunoreactivity of the surface major outer membrane protein (MOMP) or the genotyping and sequencing of the MOMP-encoding gene, *ompA*.

The trachoma biovar (serovars A to C and Ba) infects ocular epithelial cells and is transmitted via contact with eye or nose discharges. Inflammation and scaring of the conjunctiva can lead to irreversible blindness trachoma, which affects about 1.9 million people globally and is endemic mostly in the poorest areas of Africa and Middle East with limited access to healthcare (Taylor *et al.*, 2014; Trachoma Fact Sheets, World Health Organization (WHO), 2021).

The genital biovar (serovars D to K) is sexually transmitted and infects urogenital epithelial cells, causing cervicitis in women, and urethritis and epididymitis in men. Most cases are asymptomatic or with minimal signs, which facilitates the dissemination of the disease. Moreover, in women without treatment, 15-40% of infections ascend to the upper genital tract, which can lead to pelvic inflammatory disease, ectopic pregnancy, infertility and chronic pelvic pain (O'Connel & Ferone, 2016). In addition to serious reproductive sequelae, *C. trachomatis* infections have been considered a possible risk factor for cervical cancer (Paba *et al.*, 2008). In 2016, total estimated incident urogenital chlamydial cases were 127.2 million (Rowley *et al.*, 2019). A recent study reported a prevalence of genital *C. trachomatis* infections of 2.9% in general population, with higher incidence in females. The prevalence was higher in the region of Americas, especially in Latin America, followed by Europe, Africa, and the Western Pacific regions, and lowest in South-East Asia. This study highlighted the importance of prioritizing the design and delivery of chlamydial control programs by world health organization (WHO) to Latin America, especially females, and women in Africa (Huai *et al.*, 2020).

The LGV biovar (serovars L1 to L3), also sexually transmitted, causes invasive urogenital or anorectal infections, including genital papules or ulcers followed by painful inguinal and/or femoral lymphadenopathy (Ceovic & Gulin, 2015). Besides infecting epithelial cells, LGV strains are capable of infecting monocytes and macrophages, thus spreading to the lymphatic system. LGV is endemic in certain areas of Africa, Southeast Asia, India, the Caribbean, and South America, although outbreaks of proctitis, particularly among men who have sex with men, have been increasing in North America, Europe, and the United Kingdom (Ceovic & Gulin, 2015). The incidence of infections with LGV strains is lower comparing with ocular and genital strains, with 2389 cases reported in

2018. However, this is a 19% increment in comparison to 2017. As only 22 countries provided LGV surveillance data, these numbers are likely to be underestimated (European Centre for Disease Prevention and Control. Lymphogranuloma venereum, 2020) .

In Portugal, little is known about the prevalence of *C. trachomatis* infections. Recently, a study conducted with data from a 4-years period (2015-2018) aimed to set a baseline for the recently created national strategy for sexually transmitted infections (STI) control. This study demonstrated that, in general, several STIs are rising in Portugal. With respect to *C. trachomatis* infections, they found a total of 1267 cases: 70% occurred in males, 66.3% in people aged 18-35, 52.9% in heterosexuals and 42.9% in men who have sex with men (Pinho-Bandeira *et al.*, 2020).

1.2.2 *C. trachomatis* diagnosis, treatment and vaccine

The intracellular lifestyle and the asymptomatic nature of *C. trachomatis* infections is a drawback for accurate diagnosis and treatments before progression of the disease. For localized infections, assays to directly detect *C. trachomatis* are preferred, such as culturing, antigen tests and nucleic acid amplification tests (NAATs). As NAATs have the highest sensitivity and a specificity similar to cell culture assays, they are considered the method of choice for *C. trachomatis* detection in medical samples. For chronic or invasive infections, where the pathogen might not be detected in swabs, indirect methods using antibodies against *C. trachomatis* are more suitable (Meyer, 2016).

Ocular *C. trachomatis* infections are mostly endemic in areas with poor environmental and healthcare conditions, where programs to eliminate trachoma are being implemented using the WHO strategy "SAFE". SAFE stands for Surgery to treat the blinding state of the disease, Antibiotic treatment to clear infection, Facial cleanliness and Environmental improvement, including access to water and sanitation. As of 2020, ten countries successfully eliminated trachoma as a public health problem, however these efforts need to continue as it is still causing major economic costs in terms of lost in productivity from blindness and visual impairment (Trachoma Fact Sheets, World Health Organization (WHO), 2021).

Sexually transmitted *C. trachomatis* infections are generally curable with antibiotics (azythromycin or doxycycline). However, all patients are susceptible to re-infections and it is important to treat the disease at an early stage to avoid clinical symptoms and severe sequelae. *C. trachomatis* infections cause a high morbidity, however low efforts and investments have been made to develop preventive medicines. Recently, the vaccine antigen CTH522, which is a recombinant version of the *C. trachomatis* MOMP, became the first genital *Chlamydia* vaccine candidate trialed in humans, in phase I, and it demonstrated to be safe and immunogenic (Abraham *et al.*, 2019).

1.2.3 Experimental models to study *C. trachomatis* infections

Research on *C. trachomatis*-host cell interactions have been mostly relying on cultured non-polarized cells, such as HeLa, a cancer cell line derived from human cervical cells (Scherer *et al.*, 1953) and a few studies also used polarized cells, such as HEC-1, a human endometrial adenocarcinoma cell line (Kurarmoto *et al.*, 2002). Despite lacking several components of *in vivo* environments, cultured cells are more feasible to experimental manipulation, being widely used in the chlamydial research field. In fact, *in vitro* and *ex vivo* studies have been made major contributions for a better understating on the mechanisms employed by *C. trachomatis* to subvert host cell pathways and most of the current knowledge arose from these studies. Recently, organoids, which are three-dimensional structures that recapitulate the microanatomy of an organ's epithelial layer, have been developed to study *C. trachomatis* infections, trying to bridge the gap between *in vitro* and *in vivo* systems (Bishop *et al.*, 2020; Kessler *et al.*, 2019). Animal models to study chlamydial infections include mice, guinea pigs, nonhuman primates, pigs, rats, and rabbits [reviewed in (De Clercq *et al.*, 2013)]. In particular, as the female mouse genital tract is susceptible to both *C. muridarum* and *C. trachomatis* infections, these two mice models are primarily used to mimic human genital infections. In the case of *C. trachomatis*, the establishment of infection requires the pre-treatment of mice with hormones and the inoculation with high numbers of infectious particles. The choice between these models for a specific research topic should take into account the differences in pathogenicity and immunity between these two *Chlamydia* species (De Clercq *et al.*, 2013).

In comparison with *in vitro* or *ex vivo* approaches, animal models might reproduce more accurately the environment of human infections. However, they have ethical and practical disadvantages, which explain the preferential use of cell lines to study human pathogens.

1.3 The chlamydial biology and developmental cycle

Chlamydiae possess a cell wall similar to other Gram-negative bacteria, including an inner membrane and a lipopolysaccharides-containing outer membrane, separated by a periplasmic space with peptidoglycan. The chlamydial peptidoglycan was not detected for a long time, despite its existence being supported both by genetic studies and by the chlamydial susceptibility to β-lactams. Recently, peptidoglycan labeling techniques coupled with super resolution microscopy revealed that *Chlamydiae* possess a limited and transient peptidoglycan ring structure during its replicative phase (Liechti *et al.*, 2014; Liechti *et al.*, 2016).

C. trachomatis shares with all *Chlamydiae* a characteristic developmental cycle, where the bacteria alternate between two main morphological and functionally different forms. The extracellular small (~0.3 µm in diameter), infectious and non-replicative forms are designated as elementary bodies (EBs), while the intracellular larger (~1 µm in diameter), non-infectious and replicative forms are known as reticulate bodies (RBs) (AbdelRahman & Belland, 2005). In addition, intermediate forms in the transition from RBs to EBs were observed by electron microscopy and enlarged aberrant RBs are induced by stress factors such as cytokines, starvation and antibiotics (Hogan *et al.*, 2004; Phillips *et al.*, 1984). Aberrant RBs are formed when *Chlamydia* enters in a persistence state characterized by a low metabolic activity and impaired RBs to EBs transition, which can be reverted if the stress is removed (Hogan *et al.*, 2004).

Chlamydial EBs are surrounded by an outer membrane complex composed of proteins cross-linked by disulfide bonds, being able to resist in extracellular environments to osmotic and physical stresses. Although EBs have a compact nucleoid, they still have metabolic and biosynthetic activities. As RBs have a more relaxed chromatin and do not possess a cross-linked outer membrane, RBs are capable of intracellular replication, but are more susceptible to the extracellular environment (AbdelRahman & Belland, 2005; Omsland *et al.*, 2014).

The chlamydial developmental cycle (Figure 1.2) takes between 36-96 h. This varies between strains and is about 48 h for *C. trachomatis* LGV strains (Figure 1.2). Briefly, EBs attach to host cells and promote their entry into a membrane-bound vacuolar compartment, known as inclusion. The lipid and protein composition of the inclusion membrane is remodeled to selectively interact with host cell factors. The inclusion escapes from the phago-lysosomal pathway, migrates along microtubules to the perinuclear region near the centrosome and EBs differentiate into RBs, which actively divide by binary fission from ~6 to ~24 hours post-infection. Then, RBs start an asynchronous re-differentiation into EBs, and the chlamydiae subvert the host cytoskeleton and calcium-signaling to exit the cell by host cell lysis or extrusion of the inclusion. The released EBs can then infect neighboring cells (Figure 1.2).

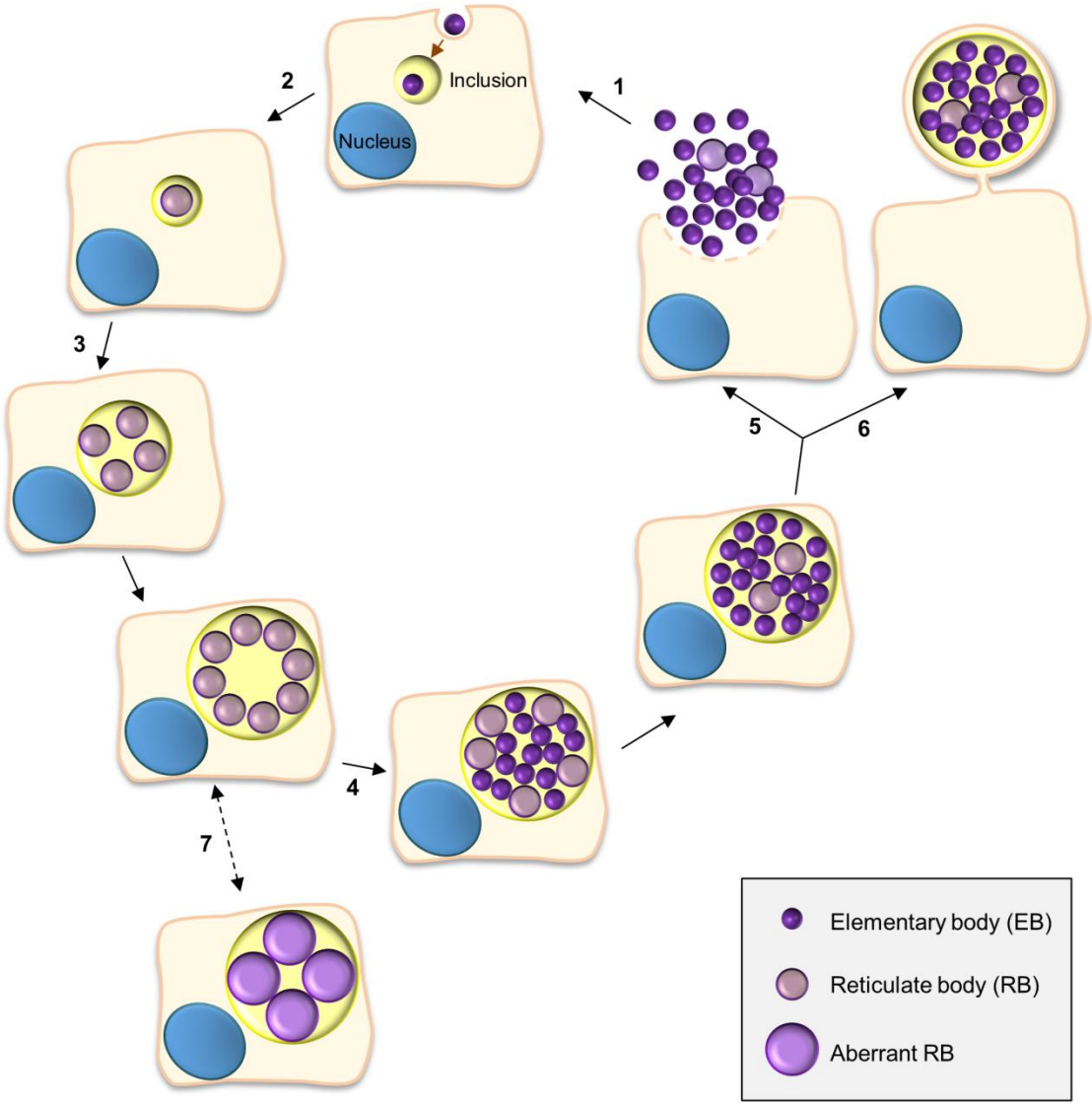

Figure 1.2 The chlamydial developmental cycle. (1) Adhesion to host cells by *C. trachomatis* EBs triggers the delivery of bacterial effectors that mediate actin rearrangements resulting in chlamydial invasion, subversion of the endocytic pathway and modulation of host cell survival and immune signaling (~ 0-2 h post-infection). (2) The nascent inclusion segregates from the phago-lysosomal pathway, the EBs differentiate into RBs, and the inclusion migrates along microtubules to a perinuclear centrosomal region (~ 2-6 h post-infection). (3) The RBs start replicating exponentially leading to a large inclusion occupying most of the host cell cytoplasm (~ 6-24 h post-infection). (4) The RBs re-differentiate asynchronously into EBs (~ 24-48 h post-infection). (5) e (6) The EBs (infectious progeny) and a few lasting RBs are released by host cell lysis (5) or extrusion (6) (~ 48-72 h post-infection). (7) Under certain stress conditions (antibiotics or cytokines) there is the reversible formation of aberrant RBs. Reprinted from (Bugalhão & Mota, 2019).

Throughout the cycle, besides avoiding the phago-lysosomal pathway, *C. trachomatis* mediates the recruitment to the inclusion of membrane and nutrients by interaction with Golgi-derived vesicles, multivesicular bodies (MVB), lipid droplets (LD), lysosome-degraded materials, endoplasmic reticulum (ER) (Figure 1.3), and also interferes with host cell survival and death and with innate immune signaling (Bastidas *et al.*, 2013; Elwell *et al.*, 2016). As *C. trachomatis* is confined within the inclusion, subversion of host processes is achieved through the delivery of bacterial proteins, called effectors, into the host cell cytosol and/or the inclusion membrane via specialized secretion systems (section 1.5).

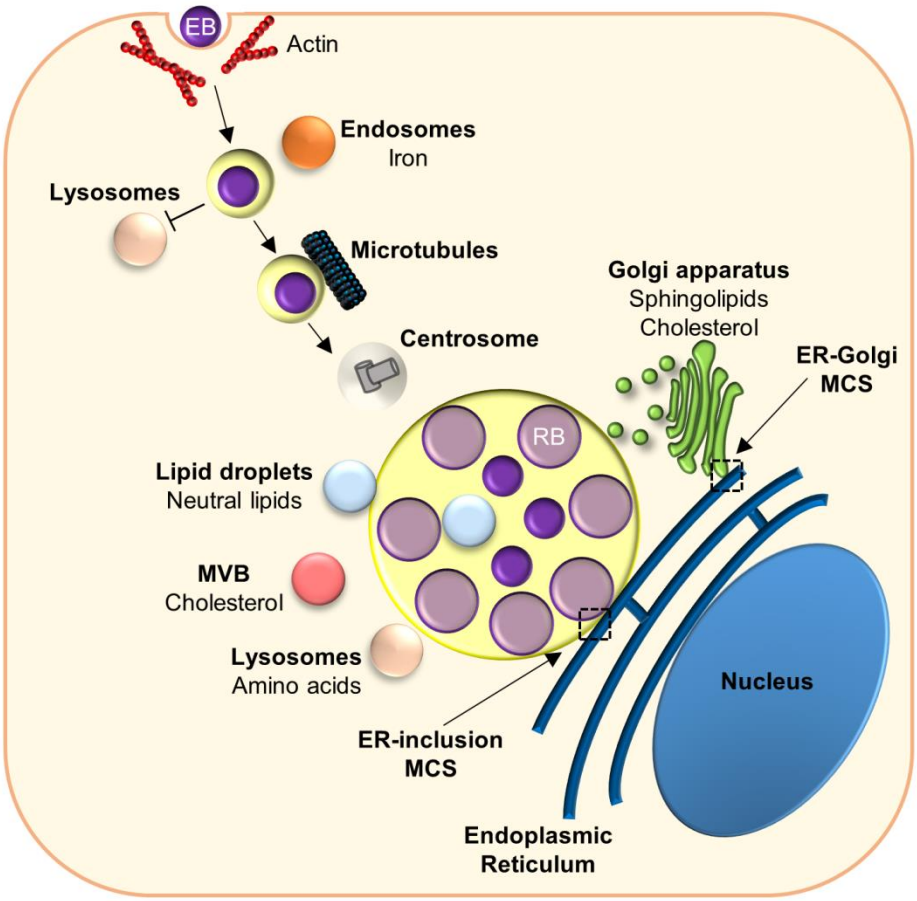

Figure 1.3 The *Chlamydia*-host cell interactions. *Chlamydia* enters host cells by an actin-dependent mechanism. The EBs are internalized into a membrane-bound vacuolar compartment, the inclusion, which escapes fusion with lysosomes and interacts with endosomes for iron acquisition. The nascent inclusion is transported along microtubules to the centrosome and EBs differentiate into RBs. The inclusion interacts with host-cell organelles, including the Golgi apparatus, the ER, LDs and MVBs. The acquisition of lipids involves vesicular trafficking from Golgi and MVBs and nonvesicular trafficking from LDs and membrane contact sites (MCS) formed between the ER and the inclusion. Essential amino acids might derive from host-protein degradation within lysosomes. The information to design this figure was adapted from (Bastidas *et al.*, 2013).

1.4 Genetic tools to study *C. trachomatis* infections

1.4.1 The *C. trachomatis* genome

The first *C. trachomatis* genome was published in 1998 for serovar D. It consists of a ~1 Mb chromosome and a ~7.5 kb plasmid, with 894 likely protein-coding genes (Stephens *et al.*, 1998; Lovett 1980). Subsequent studies revealed that genome sequences from all *C. trachomatis* serovars are very similar in size, with highly conserved gene order and content, showing more than 99% nucleotide sequence identity (Stephens *et al.*, 2009; Harris *et al.*, 2012; Seth-Smith *et al.*, 2013). The obligate intracellular nature of *Chlamydiae* is greatly explained by the presence of incomplete metabolic pathways, as the tricarboxilic acid cycle or the biosynthesis of amino acids, thus depending on the host for nutrient acquisition. However, all *C. trachomatis* genomes encode for proteins required for DNA replication, transcription, and translation, secretion systems from protein transport, recombination systems and essential functions in aerobic respiration.

Despite the similarities, differences should exist to explain the different cellular tropisms and pathologies caused by different *C. trachomatis* serovars. In fact, this is explained in part by the existence of a hypervariable region called "plasticity zone", which includes genes such as the *trpBA* operon and the *ct166*[F1] gene. Within the *trpBA* operon, specific mutations differ between genital strains, which possess an intact *trpBA* operon encoding a functional tryptophan synthase, and ocular strains, where the operon contains polymorphisms resulting in a non-functional enzyme (Fehlner-Gardiner *et al.*, 2002). Host cells produce interferon γ (IFN-γ) during *C. trachomatis* infection, inducing indoleamine 2,3-dioxygenase (IDO), an enzyme that degrades tryptophan, thus limiting bacterial growth. *In vivo*, genital chlamydial strains greatly rely on their own functional tryptophan synthase to synthesize tryptophan from the indole produced by the genital tract microbiome. This explains in part why ocular serovars are rarely associated with genital infections. The cytotoxin-encoding gene *ct166* presents different mutations and deletions among different serovars. For instance, the region encoding a glycosyltransferase domain, which is normally involved in the disassembling of the actin cytoskeleton, is intact in genital strains, partially deleted in ocular strains and completely absent in LGV strains (Carlson *et al.*, 2004).

Outside the "plasticity zone", variations are observed in other protein families, such as polymorphic membrane proteins (Pmps) (Gomes *et al.*, 2006) and inclusion membrane proteins (Inc) containing predicted bilobed hydrophobic motifs (Almeida *et al.*, 2012). Pmps

[F1] Throughout this work we used the nomenclature of the annotated *C. trachomatis* D/UW3 strain (Stephens *et al.*, 1998) or the general name.

have been shown to be involved in the adhesion process during infection (Becker & Hegemann, 2014) and Incs have diverse functions in *Chlamydia*-host cell interactions (section 1.5.2.2).

The chlamydial plasmid is highly conserved among *C. trachomatis* strains and between *Chlamydia* species, suggesting that there is a high selective pressure for plasmid maintenance (Zhong, 2017). Interestingly, a study suggested that the transcriptional dynamics of the plasmid might be related with different tissue tropisms. For instance, the plasmids from ocular strains showed, in general, lower gene expression levels than those from genital and LGV strains (Ferreira *et al.*, 2013). In opposition to plasmid-bearing strains, the inclusions of plasmidless strains have an abnormal morphology, reduced bacterial movement, lack the characteristic intrainclusion glycogen accumulation and the expression of several bacterial chromosome-encoded genes is reduced (Carlson *et al.*, 2008; Matsumoto *et al.*, 1998; O'Connell *et al.*, 2011; O'Connell & Nicks, 2006). Altogether, the chlamydial plasmid is considered a virulence factor. Clinical strains without the plasmid are rarely isolated and both plasmidless or plasmid-cured strains are more attenuated in virulence (O'Connell & Nicks, 2006; Sigar *et al.*, 2014; Zhong, 2017).

The plasmid has a low copy number (up to 8 copies per cell) and is non-conjugative, non-integrative, and lacks antibiotic resistance markers (except the plasmid from *C. suis*). It encodes 8 plasmid glycoproteins, pGP 1-8, and 2 small RNAs, sRNA-2 (antisense to *pgp8*) and sRNA-7 (antisense to *pgp5*) (Ferreira *et al.*, 2013; Pickett *et al.*, 2005). pGP1 encodes a predicted DNA helicase, and pGP2 and pGP6 are proteins with unknown function. However, it is known that *pgp1*, *-2*, *-6*, *-8*, and possibly sRNA-2, but not pGP8 (a putative integrase/recombinase), are essential for plasmid maintenance, in opposition to *pgp3*, *-4*, *-5* , -7 and sRNA-7 (Gong *et al.*, 2013; Liu, *et al.*, 2014a; Song *et al.*, 2013).

The abnormal morphology of inclusions and the lack of glycogen accumulation reported for plasmidless strains (Matsumoto *et al.*, 1998; O'Connell & Nicks, 2006) are also observed with *pgp4* deletion mutants (Song *et al.*, 2013). pGP4 is a transcriptional regulator of *pgp3*, and is also required for the normal expression of several chromosomal genes, including the glycogen synthase gene *glgA*, which is involved in the accumulation of glycogen within the inclusion lumen (Carlson *et al.*, 2008; Song *et al.*, 2013). Moreover, pGP4 was shown to be required for chlamydia lytic exit from host cells (Yang *et al.*, 2015). pGP5 negatively regulates the genes regulated by pGP4, suggesting that chromosomal gene expression might be modulated by the plasmid depending on the environment (Liu *et al.*, 2014a).

pGP3 is a protein that localizes at the bacterial outer membrane (Comanducci *et al.*, 1993), but it is also secreted into the inclusion lumen and host cell cytosol by unknown mechanisms (Li *et al.*, 2008b). Recently, a plasmid-dependent secretion system for the

cytosolic delivery of Pgp3 and GlgA was described (Lei *et al.*, 2021). This system is proposed to consist of a segregated population of globular structures containing Pgp3, GlgA and other chlamydial proteins (Lei *et al.*, 2021). pGP3 targets the antimicrobial peptide cathelicidin LL-37 neutralizing its activity (Hou *et al.*, 2015), modulates immune responses (Hou *et al.*, 2015) and is involved in inhibition of host cell apoptosis (Zou *et al.*, 2019). In addition, in *C. muridarum* strains lacking pGP3, virulence was attenuated (Liu *et al.*, 2014b).

1.4.2 The development of protocols for *C. trachomatis* transformation

The knowledge about *Chlamydiae* biology, and consequently the development of therapeutics and vaccines, was greatly delayed by the lack of genetic tools to overcome the constraints related with their obligate intracellular lifestyle.

In 1994, Tam and colleagues successfully transformed *C. trachomatis* for the first time. A chimeric plasmid, pPBW100, was generated comprising an *Escherichia coli* plasmid fused to 7000 bp of the *C. trachomatis* virulence plasmid. This plasmid was successfully introduced into *C. trachomatis* by electroporation, however transformants were rarely observed after four passages (Tam *et al.*, 1994). Based on the current knowledge, the generation of transient transformants was probably caused by a 500 bp deletion within *pgp1*, which is essential for plasmid maintenance (Song *et al.*, 2013). Therefore, and unfortunately, it took another 17 years for a stable transformation method to be developed, which could have been achieved much earlier if the *E. coli* vector had been inserted within a non-essential region of the *C. trachomatis* plasmid.

In the mid-time, Binet and Maurelli showed that *Chlamydiae* were potentially more feasible to genetic manipulation than previously anticipated. The authors reported the first gene replacement in *Chlamydia* by allelic exchange, which resulted in the insertion of point mutations within the region of the 16S rRNA in *C. psitacci* (Binet & Maurelli, 2009). Also, the authors showed that recovery of transformants could be improved using high amounts of circular (instead of linear) nonmethylated DNA during transformation by electroporation (Binet & Maurelli, 2009).

In 2011, a breakthrough in the research field was undoubtedly the description of a more efficient protocol to stably transform *Chlamydiae* using calcium chloride (Wang *et al.*, 2011). Wang and colleagues generated a shuttle vector comprising the native *C. trachomatis* virulence plasmid fused to an *E. coli* cloning vector encoding penicillin resistance. Briefly, EBs previously incubated with the recombinant plasmid DNA in a $CaCl_2$ buffer were added to epithelial cells, and penicillin was added throughout several rounds of infection. As the transformation plasmid and the native *C. trachomatis* plasmid share the same origin of

replication, selection for the shuttle vector cured transformed *C. trachomatis* strains from the native plasmid. Also, transformants were maintained after several passages, even in the absence of penicillin. In the presence of β-lactams, the *C. trachomatis* developmental cycle is arrested and the bacteria are maintained in the aberrant enlarged and non-dividing persistent form. Therefore, the presence of transformants with morphologically normal penicillin-resistant bacterial forms were easily distinguished from aberrant bacteria by light microscopy. In addition, by using a selection marker that induces a persistent state instead of death, the time for phenotypic transition increased, enhancing the probability of successful transformations. This study was the starting point for the development of transformation vectors with multiple cloning sites, selective markers and genes encoding reporter fluorescent proteins, and they have been widely used for native or inducible expression of chlamydial genes (Agaisse & Derré, 2013; Bauler & Hackstadt, 2014; Mueller & Fields, 2015; Wang *et al.*, 2018; Wickstrum *et al.*, 2013).

1.4.3 Advances in *C. trachomatis* mutagenesis

1.4.3.1 Random mutagenesis in *C. trachomatis*

The first successful strategies to mutagenize *C. trachomatis* relied on random mutagenesis approaches. In 2011, Kari and colleagues applied reverse genetics to generate isogenic *C. trachomatis* mutants containing one mutation per genome (Kari *et al.*, 2011). The authors applied low levels of the chemical mutagenic agent ethyl methanesulfonate (EMS) and screened for mutagenized strains in the *trpBA* operon. PCR products of the target gene were hybridized against the wild type gene and digested with CEL1 endonuclease, an enzyme that targets mismatches in double-strand DNA. Subpopulations with mutations were sequenced and plaque-cloned. This led to the identification of a nonsense mutation in *trpB* (Kari *et al.*, 2011).

Nguyen and Valdivia developed a forward genetic approach using random chemical mutagenesis coupled with whole genome sequencing (WGS) and DNA exchange (Nguyen & Valdivia, 2013). The authors treated rifampin-resistant *C. trachomatis* strains with higher levels of EMS, comparing with Kary *et al.*, to generate 3 to 20 mutations per genome. Mutants with aberrant plaque morphologies were screened, analyzed and mutant strains were identified by co-infecting cells with each rifampin-resistant strain and a spectinomycin-resistant wild type strain. Recombinant strains generated by lateral gene transfer were selected in the presence of both rifampin and spectinomycin and genotyped (Nguyen & Valdivia, 2013).

Kokes optimized these methods and generated a collection of 934 chemically mutagenized strains with mutations identified by WGS. Among these, 99 mutations led to nonsense codons that set the basis for reverse genetic analyses (Kokes *et al.*, 2015). Despite being very time-consuming and expensive, these types of approaches were crucial to expand the knowledge on recalcitrant microorganisms, such as *C. trachomatis*, that are less amenable to genetic manipulation. As an alternative to chemical mutagenesis, a single-insertion system was recently developed using transposon mutagenesis including a selection marker, thus facilitating the identification of insertion sites and consequently the discovery of genes associated with selected phenotypes (Labrie *et al.*, 2019).

1.4.3.2 Site-directed mutagenesis in *C. trachomatis*

The ability to stably transform *C. trachomatis* enabled the subsequent development of strategies for directed gene inactivation. In 2013, Johnson and Fisher adapted a technology marketed as TargeTron™ by Sigma to be used for *C. trachomatis* (Johnson & Fisher, 2013). The system is based on group II introns that naturally target prokaryotic genes and can be retargeted to mutagenize the genes of interest by altering the DNA sequences within these introns. To optimize the TargeTron vector for *C. trachomatis*, a chlamydial promoter was added upstream of the intron to allow the production of the machinery required for intron insertion within the target gene, and the *bla* gene was also inserted into the intron for β-lactamase production and selection of mutant strains. As a proof of principle, the system was successfully used to insertionally inactivate the gene encoding CT119/IncA, which is a *C. trachomatis* protein that localizes at the inclusion membrane during infection (Johnson & Fisher, 2013). Also, it was further confirmed the stability of the intron and that the TargeTron method could be used with spectinomycin by inserting the *aadA* gene as the selection marker, thus facilitating complementation studies and the generation of site-specific double mutants (Lowden *et al.*, 2015). To date, more than 15 *C. trachomatis* mutants were generated based on the TargeTron technology, including mutations in chaperonins (Illingworth *et al.*, 2017), inclusion membrane proteins (Almeida *et al.*, 2018; Carpenter *et al.*, 2017; Johnson & Fisher, 2013; Nguyen *et al.*, 2018; Shaw *et al.*, 2018; Sixt *et al.*, 2017; Stanhope *et al.*, 2017; Weber *et al.*, 2017; Wesolowski *et al.*, 2017) and proteins delivered into the host cell cytosol during infection (Cossé *et al.*, 2018; Pais *et al.*, 2013).

In the TargeTron method, the DNA sequence of the target gene is analyzed by a proprietary algorithm, which highlights potential insertion sites (Johnson & Fisher, 2013). This means that the regions where the intron can be inserted are limited, and the probability to succeed might be lower for genes lacking sites considered to be efficient. In 2016, an alternative method to generate *C. trachomatis* mutants called gene deletion by fluorescence-

reported allelic exchange mutagenesis (FRAEM) was developed by Mueller and Fields (Mueller *et al.*, 2016). The main features of the generated vector, pSUmC, are the gene encoding the red fluorescent protein mCherry; a *bla-gfp* cassette flanked by the sequences upstream and downstream from the gene of interest to promote homologous recombination and the replacement of the gene by *bla-gfp*; and the expression of *pgp6*, essential for plasmid maintenance, under the control of the inducible *tet* promoter. Initially, penicillin-resistant transformants are detected by green and red fluorescence and maintained in the presence of anhydrotetracycline to induce *pgp6* expression and plasmid maintenance. In the first recombination event, the plasmid inserts into the target gene. Then, the removal of anhydrotetracycline leads to a second recombination event and loss of the plasmid. Therefore, successful mutagenized strains are detected exclusively by green fluorescence due to the replacement of the target gene by *bla-gfp* and loss of the plasmid-encoded mCherry. The applicability of FRAEM for different sites in the *C. trachomatis* genome was validated with the generation of *C. trachomatis* mutants lacking *ct694*/*tmeA*, *ct695*/*tmeB* or *ct696* (Mueller *et al.*, 2016). FRAEM was further optimized to allow the deletion of the selection marker to reduce the risk of polar effects and to expand the use of this technique for genes within polycistronic operons (Keb *et al.*, 2018).

Despite the important outcomes from these landmark studies, the reduced genome of *C. trachomatis* suggests that a great number of genes might be essential for chlamydial development. Therefore, the generation of conditional mutants using CRISPR interference (CRISPRi) will be crucial to understand the function of essential proteins. Ouellette created the first protocol to mutagenize *C. trachomatis* genes using CRISPRi (Ouellette, 2018). A single plasmid was created to allow both the inducible production of the catalytically inactive Cas9 variant (dCas9) of *Staphylococcus aureus*, which reversibly repress gene expression, and the constitutive expression of a guide RNA (gRNA) recognizing a complementary chromosomal sequence next to a protospacer-adjacent motif (PAM) sequence. The feasibility of this technique was demonstrated with the conditional and reversible knockout of *incA* (Ouellette, 2018). However, some drawbacks for quantification analyses were related with leaky production of dCas9 in the absence of induction, off-target effects and plasmid instability, which originated a mixed population containing mutagenized and non-mutagenized bacteria (Ouellette, 2018). To overcome these limitations, the technology was recently optimized with the use of a different plasmid backbone. Also, dCas9 efficiency and stability was reduced by modifying the ribosome binding site that drives dCas9 translation initiation and by adding a carboxy-terminal degradation tag to dCas9 (Ouellette *et al.*, 2021). In addition, a CRISPRi system based on a dCas12 ortholog that

utilizes a different PAM sequence was also created, thus expanding the tools available to mutagenize chlamydial genes (Ouellette *et al.*, 2021).

1.5 Secretion systems in *Chlamydiae*

Diverse secretion systems mediate interactions between Gram-negative bacteria with other bacteria, host cells or the extracellular environment. These secretion systems are macromolecular nanomachines involved in the transport of different substrates to the outside of the bacterial cytoplasm. Depending on the secretion system, the substrates can be small molecules, DNA and/or proteins, which can be transported into the periplasm, the bacterial outer membrane, the extracellular space or directly injected into a prokaryotic or eukaryotic host cell (Costa *et al.*, 2015). In the case of Gram-negative bacteria, there are systems capable of spanning only the inner [e.g. SecYEG translocon and twin-arginine translocation (Tat) system] or the outer membrane (e.g. Type 5 secretion system; T5S system) and systems capable of spanning both the inner and outer membrane (e.g. T2S, T3S, T4S and T6S systems) (Costa *et al.*, 2015). The T2S and T5S systems require two steps for transport, where proteins are delivered into the periplasmic space by inner membrane transporters and then inserted into the outer membrane or delivered into the extracellular space by outer membrane transporters. Other double-membrane secretion systems, including the T3S, T4S and T6S systems are injecting devices involving only a one-step mechanism and the substrates are delivered directly from the bacterial cytoplasm into the extracellular space or into a target cell (Costa *et al.*, 2015).

In the case of *C. trachomatis*, its genome encodes for a Sec system, Sec-exported Pmps containing T5S system/autotransporter signals, other outer membrane proteins and a T2S and T3S systems (Stephens *et al.*, 1998).

1.5.1 The *C. trachomatis* T3S system

The T3S system is present in many bacterial pathogens of animals and plants, but it is also involved in symbiotic interactions. The T3S system is a major virulence factor essential for bacterial survival and manipulation of host cells (Costa *et al.*, 2015). In general, the genes encoding T3S system proteins are normally clustered in pathogenicity islands in chromosomes or in plasmids and can be identified by a lower G+C content. In the case of *C. trachomatis*, T3S system genes have a G+C content similar to the remaining genome and they are organized in several operons distributed in four main clusters. This is an indication that, in *Chlamydiae*, this system was not a result of recent gene integration and might constitute a

primordial system (Betts-Hampikian & Fields, 2010; Stephens *et al.*, 1998).

The T3S system apparatus is composed of an injectisome containing a multi-protein complex forming a basal structure and a needle protruding from the bacterial surface, which allows the transport of proteins across the two bacterial membranes, and a translocon, which is a pore formed in a host cell membrane by two T3S system proteins named translocators (Figure 1.4). In some systems, these translocator proteins have been shown to be connected to the needle by the tip complex formed by other translocator protein, creating a continuous channel between bacteria and host cells. The other components of this system are the T3S system effectors, which are transported into host cells to exert a variety of functions, and specific chaperones that assist in protein secretion. Chaperones can bind either to proteins of the T3S system apparatus or to the proteins to be translocated and they are essential to regulate the timings of secretion and to maintain substrates in a partially unfolded secretion-competent state, thus avoiding protein aggregation (Betts-Hampikian & Fields, 2010; Cornelis, 2006; Galán *et al.*, 2014).

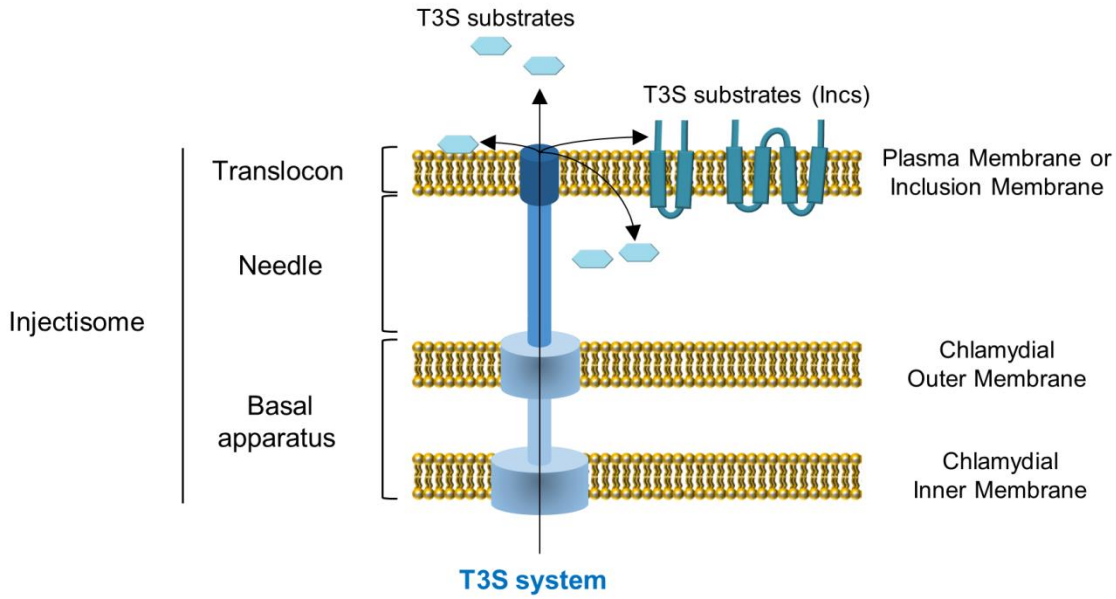

Figure 1.4 Schematic representation of the *C. trachomatis* T3S system. The T3S system is composed of an injectisome containing a multi-protein complex forming a basal structure and a needle protruding from the bacterial surface, and a translocon, which is a pore formed in the inclusion membrane or host cell plasma membrane. This system allows the delivery of T3S substrates directly from the bacteria into the host cell cytosol, inclusion membrane or inclusion lumen. Incs are T3S system effectors predicted to localize at the inclusion membrane via putative hydrophobic domains. Reprinted from (Bugalhão & Mota, 2019).

1.5.2 *C. trachomatis* T3S system effectors

In general, bacterial T3S system effectors can exert their functions by associating directly with host cell targets, by enzymatic modifications or by mimicking the roles of host factors. These proteins usually contain a disordered and not cleavable domain within their first 100 amino acids, which is rich in serine, threonine, isoleucine and proline and can be recognized by the T3S systems of other bacteria (Costa *et al.*, 2015). In spite of the development of bioinformatic tools to identify T3S substrates (Hui *et al.*, 2020; Samudrala *et al.*, 2009), as T3S system effectors lack a clear predictable secretion signal, the early identification of *C. trachomatis* effectors relied in the combination of several approaches, including study of chlamydial proteins in heterologous T3S systems (*Shigella*, *Salmonella*, *Yersinia*) (Da Cunha *et al.*, 2014; Ho & Starnbach, 2005; Subtil *et al.*, 2005). Also, the overproduction of candidate effectors in *S. cerevisiae* have also been used to identify potential chlamydial effector proteins (Kumar *et al.*, 2006; Sisko *et al.*, 2006). The validation of *C. trachomatis* effectors has been made essentially via their detection in the cytosol of infected cells or at the inclusion membrane by immunofluorescence microscopy [e.g. of studies (Fields & Hackstadt, 2000; Pais *et al.*, 2019; Subtil *et al.*, 2005; Weber *et al.*, 2015)] and using reporter assays to monitor protein translocation into host cells [e.g. of studies (Bauler & Hackstadt, 2014; Mueller & Fields, 2015; Wang *et al.*, 2018; Yanatori *et al.*, 2021)]. An example was the study of chlamydial proteins tagged with a 13-residue peptide derived from glycogen synthase kinase (GSK)3β, which is phosphorylated by cytosolic eukaryotic protein kinases (Garcia *et al.*, 2006). Detection of phosphorylated proteins using phospho-specific GSK antibodies demonstrated their localization outside the inclusion (Bauler & Hackstadt, 2014; Garcia *et al.*, 2006; Yanatori *et al.*, 2021).

Indirect evidence of an effector function has been obtained also through protein-protein interaction assays [e.g. of studies (Almeida *et al.*, 2018; Scidmore & Hackstadt, 2001; Vromman *et al.*, 2016)] and transient production in eukaryotic cells [e.g. of studies (Cocchiaro *et al.*, 2008; Pais *et al.*, 2019; Saka *et al.*, 2015)]. The recently developed techniques to genetically manipulate *Chlamydia* have been aiding in the functional characterization of these effectors. Some localize at the host cell cytosol, while others accumulate at the inclusion membrane. The later include a family of proteins called inclusion membrane proteins (Incs) characterized by the presence of a bilobed hydrophobic motif composed of two or more transmembrane segments separated by short loops of amino acids, which likely mediates their insertion into the inclusion membrane. Incs have predicted amino and/or carboxy-terminal regions exposed to the host cell cytosol, supporting their relevance in *Chlamydia*-host cell interactions (Bannantine *et al.*, 2000; Dehoux *et al.*, 2011; Lutter *et al.*, 2012; Rockey *et al.*, 2002).

Altogether, chlamydial effectors mediate the subversion of host cell pathways throughout the chlamydial developmental cycle, including invasion and exit mechanisms, avoidance of bacterial clearance and nutrients acquisition [Reviewed in (Bugalhão & Mota, 2019)].

In the following sections, the current knowledge on *C. trachomatis* effectors, including their main targets and roles are divided between Inc and non-Inc (proteins lacking a predicted bilobed hydrophobic domain) effectors.

1.5.2.1 Non-Inc *C. trachomatis* effectors

1.5.2.1.1 Non-Inc T3S system effectors packed in EBs and involved in the early steps of the infectious cycle

The mechanisms involved in binding and internalization of EBs into host cells varies between different chlamydial species and is likely related to the different tissue/host tropisms. In the case of *C. trachomatis*, the adhesion process is firstly mediated by a reversible and low-affinity electrostatic interaction of EBs with heparin sulfate proteoglycans (HSPGs), followed by a high-affinity binding of EBs ligands (e.g. OmcB, PmpD and MOMP) to host cell receptors [e.g. manose-6-phosphate receptor (M6PR), PDGFRβ, β1-integrin, and Ephrin A92] (Gitsels *et al.*, 2019). During invasion, EBs manipulate the actin cytoskeleton to force their entry and a few T3S system effectors were found to be pre packed in EBs and delivered into host cells.

The extensively studied effector CT456/Chlamydial translocated actin-recruiting phosphoprotein (TarP) contains a carboxy-terminal region involved in self-oligomerization and in actin binding and polymerization, and an amino-terminal tyrosine-rich repeat domain that upon phosphorylation by host kinases leads to the activation of the Arp2/3 complex and triggers intracellular signaling promoting host cell survival. The presence of a carboxy-terminal WH2-like domain that binds to globular actin (G-actin) combined with TarP oligomerization capacity promotes actin nucleation. In addition, filamentous actin (F-actin) binding domains allow the bundle of actin microfilaments (Jewett *et al.*, 2006; Jiwani *et al.*, 2013). TarP was found to be a substrate for multiple host tyrosine kinases, which results in the activation of complex signaling pathways (Elwell *et al.*, 2008; Jewett *et al.*, 2008; Mehlitz *et al.*, 2008). Phosphorylated TarP, in the presence of phosphatidylinositol 3,4,5-triphosphate (PIP3), regulates two Rac guanine nucleotide exchange factors (GEFs): Vav2 and the complex Sos1/Eps8/Abi1, which activates the Rac GTPases-dependent signaling cascade (Lane *et al.*, 2008). In addition, TarP binds to human adaptor protein SHC1, a protein involved in the regulation of apoptosis, possibly promoting host cell survival at early stages

of infection (Mehlitz *et al.*, 2010). Recently, a study using a *tarP* mutant strain generated using the FRAEM method showed the relevance of the carboxy-terminal F-actin binding domains for invasion efficiency and the requirement of TarP for *in vivo* infections (Ghosh *et al.*, 2020). In summary, after delivery into host cells, TarP activates several signaling pathways and manipulates the actin cytoskeleton to promote *C. trachomatis* invasion. Interestingly, TarP seems to be related with the different tissue tropisms of *C. trachomatis* strains. While LGV strains contain the highest levels of tyrosine-rich repeat regions and the fewest predicted actin binding domains, the opposite was found for ocular strains (Lutter *et al.*, 2010).

The effectors CT694/Translocated membrane-associated effector (Tme) A and CT695/TmeB are encoded in the *tmeAB* operon. Early after invasion, TmeA and TmeB are detected near the nascent inclusion. After 24 h, while TmeB remains exclusively associated with the inclusion membrane, TmeA also localizes at the host cell plasma membrane (Hower *et al.*, 2009; Mueller & Fields, 2015; Wang *et al.*, 2018). It is known that TmeA binds AHNAK nucleoprotein, being able to inhibit AHNAK-mediated F-actin bundling *in vitro*. However, the recruitment of AHNAK to the nascent inclusion was found to be independent of TmeA. While mutant strains in *tmeB* are not affected in their ability to invade host cells, *tmeA* mutants showed defects in invasion of tissue cultured cells and in a mouse model. However, invasion defects seem to be independent of TmeA-AHNAK interaction, as this defect is observed both in AHNAK-positive or AHNAK knock-out cells (Hower *et al.*, 2009; Keb *et al.*, 2018; McKuen *et al.*, 2017). Two recent studies further elucidated the mode of action of TmeA. TmeA interacts with the GTPase binding domain of the nucleation promoting factor N-WASP, which leads to the recruitment of the Arp2/3 complex to the sites of bacterial entry to promote actin polymerization (Faris *et al.*, 2020; Keb *et al.*, 2021). Moreover, TmeA and TarP seem to activate the Arp2/3 complex via different signaling pathways, acting sinergistically to promote chlamydial invasion (Faris *et al.*, 2020; Keb *et al.*, 2021).

CT622 was firstly detected within the inclusion lumen as early as 6 h post-infection and at the host cell cytosol only from 36 h post-infection (Gong *et al.*, 2011). In a subsequent study, CT622 was found to be abundant in EBs and to be delivered into host cells throughout the chlamydial cycle. In addition, *C. trachomatis ct622* mutant strains displayed defects in the production of infectious progeny and a reduced *C. trachomatis*-dependent protein tyrosine phosphorylation, strongly indicating its role at early stages of infection (Cossé *et al.*, 2018). Recently, CT622 was found to target the autophagy related protein 16-1 (ATG16L1) and it was renamed translocated ATG16L1 interacting protein (TaiP) (Hamaoui *et al.*, 2020). According to this study, the carboxy-terminal region of TaiP mediates the interaction with ATG16L1, which supports *C. trachomatis* growth by disrupting the interaction between

ATG16L1 and the integral membrane protein TMEM59. The results show that this effect is Rab6-dependent and it is proposed that Rab6-positive compartments, such as exocytic pathways emerging from the Golgi apparatus, are re-routed to the inclusion as a supply of membrane for inclusion growth (Hamaoui *et al.*, 2020).

CT875/Translocated early phosphoprotein (TepP) is another protein that is tyrosine-phosphorylated by host kinases upon delivery into host cells and it is also phosphorylated in serine residues. TepP is able to bind and to recruit to the nascent inclusion the CRK proto-oncogene, adaptor protein (CRK), CRK like proto-oncogene, adaptor protein (CRKL), GSK3β, and different subunits of class I phosphoinositide-3-kinase (PI3K). A *C. trachomatis tepP* insertional mutant strain presented growth defects in cultured cells. Moreover, in cells infected by this mutant the expression of genes associated with innate immune responses was reduced. TepP seems to modulate host responses at early stages of infection to support chlamydial growth (Carpenter *et al.*, 2017; Chen *et al.*, 2014).

1.5.2.1.2 Non-Inc T3S system effectors targeting the host cytosol, nucleus, or the inclusion membrane

CT847 is delivery into host cell and interacts with a transcription regulator controlling cell proliferation, the Grap2 cyclin D-interacting protein (GCIP). As the levels of GCIP were found to decrease during infection and siRNA-mediated depletion of GCIP leads to increased production of *C. trachomatis* progeny, the interaction of CT847 with GCIP seems to be important for chlamydial infection (Chellas-Géry *et al.*, 2007).

CT737/nuclear effector (NUE) was the first chlamydial effector found to localize at the host cell nucleus. NUE is a histone methyl-transferase targeting host histones, being probably involved in chromatin remodeling (Pennini *et al.*, 2010).

The effectors CT619, CT620, CT621, CT711 and CT712 share a *Chlamydiacea*-specific domain of unknown function (DUF582) within their carboxy-terminal region. Among these proteins, it is known that CT620 and CT621 localize in the cytosol and nucleus and CT711 localizes only in the nucleus of infected cells (Hobolt-Pedersen *et al.*, 2009; Muschiol *et al.*, 2011). These proteins interact with components of endosomal sorting complexes required for transport (ESCRT), which are involved in the formation of MVBs. With the exception of CT712, all these proteins were found to interact with the ESCRT component Hrs through their carboxy-terminal region and CT619 is also able to bind another component, the tumor susceptibility 101 (TSG101), via its amino-terminal region. The meaning of these interactions is still unclear, as the depletion of Hrs or TSG101 does not interfere with the *C. trachomatis* capacity to invade or multiply within host cells (Vromman *et al.*, 2016). Nevertheless, the ESCRT machinery is also required for abscission during cytokinesis, which was recently

proposed to be involved in *C. trachomatis* exit by extrusion (Zuck & Hybiske, 2019). This suggests that DUF582-containing effectors might be involved in the regulation of chlamydial exit.

CT089/CopN and CT529/Cap1, which do not possess the characteristic hydrophobic domain of Incs, were observed associated with the inclusion membrane during infection (Fling *et al.*, 2001; Rockey *et al.*, 2002). Although the functions of these proteins remain unclear, Cap1 was found to associate with LDs when transiently produced in mammalian cells (Saka *et al.*, 2015) and CopN is thought to be a T3S system gatekeeper required for secretion of translocators and control of the delivery of effectors into host cells (Archuleta & Spiller, 2014). The interference of CopN from *C. pneumoniae*, but not from *C. trachomatis*, with host cell microtubules suggests an effector role for this protein (Huang *et al.*, 2008).

CT105/*C. trachomatis* effector associated with the Golgi (CteG) has a dual intracellular localization during *C. trachomatis* infection. CteG first associates with the Golgi complex and later in infection it localizes predominantly at the host cell plasma membrane. CteG caused mistrafficking when transiently produced in yeast, which means that CteG possibly interferes with host cell vesicular trafficking (Pais *et al.*, 2019).

1.5.2.1.3 Non-Inc T3S system-candidate/independent effectors

Several T3S candidate effectors of *C. trachomatis* are delivered into the host cells by unknown mechanisms. The CT166 cytotoxin, already mentioned in section 1.4.1, causes a cytopathic effect in host cells, which is characterized by cell rounding and disassembly of actin filaments during bacterial internalization. This effect is also observed when the protein is transiently produced in mammalian cells and might involve the glycosylation of the Rho-family protein Rac1. CT166 possibly inactivates the TarP-dependent activation of Rac1 to promote actin rearrangements required for *C. trachomatis* invasion (Belland *et al.*, 2001; Thalmann *et al.*, 2010).

CT868/*Chlamydia* deubiquitinases (Cdu) 1/ChlaDUB1 and CT867/Cdu2/ChlaDUB2 possess deubiquitinase and deneddylase activities when transiently produced in mammalian cells, and Cdu1 also displays an acetyltransferase activity (Misaghi *et al.*, 2006; Pruneda *et al.*, 2018). At 24 h post-infection, these proteins localize at the inclusion membrane, a localization that is maintained after 48 h for Cdu1, while Cdu2 also accumulates at the host cell plasma membrane (Fischer *et al.*, 2017; Wang *et al.*, 2018). While *C. trachomatis cdu2*-null mutants showed a normal capacity to generate infectious progeny, growth defects were observed for *C. trachomatis* strains lacking Cdu1 in two types of mammalian cells and in a mouse model of infection (Fischer *et al.*, 2017; Pruneda *et al.*, 2018). Also, Golgi fragmentation and redistribution around the inclusion, characteristic of *C. trachomatis* infection, was not

observed in cells infected by *C. trachomatis cdu1* or *cdu2*-null mutants (Pruneda *et al.*, 2018). The role of these proteins in this process is further supported by the observation of Golgi fragmentation in cells transiently producing Cdu1 or Cdu2. In addition, host targets were identified for Cdu1, although the relevance of these interactions is still unclear. Cdu1 binds the nuclear factor-κB (NF-κB) inhibitor (IκNα) to impair its ubiquitination and degradation, thus suppressing the activation of NF-κB, which controls several genes related with immunity (Le Negrate *et al.*, 2008). In addition, Cdu1 deubiquitinates the apoptosis regulator MCL1, probably stabilizing this anti-apoptotic protein and contributing to avoid host cell apoptosis during *C. trachomatis* infection (Fischer *et al.*, 2017; Sharma *et al.*, 2011).

The effectors CT311 and CT795 are poorly characterized, however they were found to localize both at the inclusion lumen and host cell cytosol, and CT311 was also observed at the host cell nucleus (Lei *et al.*, 2011; Lei *et al.* 2013; Qi *et al.*, 2011).

CT156/Lipid droplets (LD)-associated protein (Lda) 1 (Lda1), CT163/Lda2, CT473/Lda3 and CT257/Lda4 were found to associate with eukaryotic LDs when transiently produced in yeast. This localization was further confirmed both in transfected mammalian cells and during *C. trachomatis* infection for Lda1, 2 and 3. As LDs were found to localize within the inclusion lumen, possibly to be used as a source of lipids and proteins for the bacteria, Ldas are likely involved in the acquisition of these organelles (Cocchiaro *et al.*, 2008; Kumar *et al.*, 2006; Sisko *et al.*, 2006).

A few *C. trachomatis* proteins were found to be delivered into the host cells independently of the T3S system, including Pgp3, mentioned in section 1.4.1, CT441/Tail-specific protease (Tsp) and CT858/Chlamydia protease-like activity factor (CPAF).

CT441/Tsp has chaperone activity and it is involved in protein quality control. Tsp has not been detected within the host cell cytosol, however it was found to bind to the human steroid RNA activator 1 (SRA1) and to cleave the p65 subunit of NF-κB. As p65 is not cleaved during *C. trachomatis* infection, the precise role of Tsp remains unclear (Borth *et al.*, 2010; Kohlmann *et al.*, 2015; Lad *et al.*, 2007).

CT858/CPAF is a serine protease produced by *Chlamydiae* and the amount of host cell targets and functions attributed to a single protein have been made very complex to clearly understand its role during *C. trachomatis* infection. Initial studies proposed a high number of *Chlamydia* and host cell proteins as CPAF targets, but it was later demonstrated that the cleavage of many of these proteins were an artifact and occurred only after cell lysis (Chen *et al.*, 2012; Zhong, 2011). CPAF is produced as an inactive zymogen, which autocatalyzes into an active protease after being transported into the inclusion lumen (Dong *et al.*, 2004; Huang *et al.*, 2008; Paschen *et al.*, 2008). CPAF was also found to localize within the host cell cytosol and to target vimentin and the nuclear envelope protein lamin-associated protein-1 (LAP-1)

prior to host cell lysis, which suggests a role for CPAF in the exit phase of the developmental cycle (Snavely *et al.*, 2014). CPAF also plays important roles in the evasion of the host immune system by targeting antimicrobial peptides to degradation, inhibiting the translocation of NF-κB p65 to the nucleus and interfering with the activation of neutrophils (Patton *et al.*, 2018; Rajeeve *et al.*, 2018; Tang *et al.*, 2015). CPAF-deficient mutants were found to be defective in intracellular growth, which could be expected taking into account the diverse functions exerted by a single effector (Snavely *et al.*, 2014).

1.5.2.1.4 Non-Inc effectors delivered into the inclusion lumen

There are a few *C. trachomatis* proteins of unknown function, which so far were observed within the inclusion lumen, outside of *Chlamydia*, but not in the host cell cytosol. Some of these proteins were found to be substrates of the T3S system, namely CT142, CT143 and CT144 (Da Cunha *et al.*, 2014), which were observed as globular structures co-localizing with each other within the lumen of the inclusion, possibly forming a protein complex (Da Cunha *et al.*, 2017). In particular, CT143 was found to be highly immunogenic and stimulates the secretion of inflammatory cytokines in macrophages (Jia *et al.*, 2019; Wang *et al.*, 2010). There are also glycogen metabolizing enzymes that were shown (GlgA and GlgX) or deduced (GlgB, GlgP, MalQ and MrsA) to localize within the inclusion lumen and recently it was demonstrated that GlgA, CT143, CT144 and Pgp3 co-localize in the same globular structure (Lei *et al.*, 2021) and therefore their functions might be related.

CT049/Pmp-like secreted (Pls) protein 1 (Pls1) and CT050/Pls2 were also observed as globular structures in the inclusion lumen, however they lack a sec-dependent secretion signal and the mechanism of transport is still unknown. These proteins seem to be important for *C. trachomatis* growth, as the co-injection of anti-Pls1 and Pls2 antibodies into infected cells partially inhibited the expansion of the inclusion (Jorgensen & Valdivia, 2008).

The putative protease Ptr has a putative sec-dependent secretion signal, being possibly delivered into the inclusion lumen by the T2S system. A *C. trachomatis ptr* mutant strain showed a defect in recovering from stress induced by IFNγ, but not by penicillin (Panzetta *et al.*, 2019).

1.5.2.2 *C. trachomatis* Incs

C. trachomatis Incs constitute a family of proteins unique of *Chlamydiae*, with little similarity with each other or with other known proteins. A large proteomics study identified several potential interactions of 38 putative Incs with host cell proteins, however most remain to be validated (Mirrashidi *et al.*, 2015). Incs were first identified in 1995 and subsequent studies relied on bioinformatic approaches using the hydrophobic bilobed

domain to search the genome for additional Incs. To date, ~60 *C. trachomatis* Incs were identified and their predicted localization has been experimentally confirmed for 36 of them (Table 1.1). About 25 Incs are conserved among *Chlamydiae* species and therefore species specific Incs might be related with the different host tropisms (Bannantine *et al.*, 2000; Dehoux *et al.*, 2011; Lutter *et al.*, 2012; Rockey *et al.*, 2002).

To date, a few Incs were shown to be able to form homotypic or heterotypic complexes supposedly contributing to inclusion stability and several Incs have been implicated in the subversion of a wide range of host processes, including inclusion tethering to the centrosome, subversion of vesicular and non-vesicular trafficking, actin cytoskeleton rearrangements and resistance to apoptosis (Table 1.1) [Reviewed in (Bugalhão & Mota, 2019)].

Table 1.1 *C. trachomatis* Incs confirmed to localize at the inclusion membrane and their validated host cell interacting proteins and proposed functions. Adapted from (Bugalhão & Mota, 2019)

Inc (annotation/name)			Host cell protein targets	Proposed functions	References
Strain D/UW3	Strain L2/434	General			
CT005	CTL0260	IncV	VAPA/B	Formation of ER-inclusion MCS; non-vesicle lipid uptake by *C. trachomatis*.	(Shaw *et al.*, 2000; Stanhope *et al.*, 2017; Wang *et al.*, 2018; Weber *et al.*, 2015)
CT006	CTL0261	-	Unknown	Unknown.	(Weber *et al.*, 2015)
CT101	CTL0356	MrcA	ITPR3	Promotion of chlamydial extrusion; localize at inclusion microdomains.	(Mital *et al.*, 2010; Nguyen *et al.*, 2018; Shaw *et al.*, 2000)
CT115	CTL0370	IncD	CERT	Formation of ER-inclusion MCS; non-vesicle lipid uptake by *C. trachomatis*.	(Agaisse & Derré, 2014; Derré *et al.*, 2011; Li *et al.*, 2008a; Scidmore-Carlson *et al.*, 1999)
CT116	CTL0371	IncE	SNX5/6	Modulation of retromer-dependent trafficking.	(Elwell *et al.*, 2017; Li *et al.*, 2008a; Paul *et al.*, 2017; Scidmore-Carlson *et al.*, 1999; Sun *et al.*, 2017; Weber *et al.*, 2015)
CT117	CTL0372	IncF	VAMP3	Heterophilic Inc-Inc interactions.	(Bui *et al.*, 2021; Gauliard *et al.*, 2015; Li *et al.*, 2008a; Scidmore-Carlson *et al.*, 1999; Weber *et al.*, 2015)

CT118	CTL0373	IncG	14-3-3β, VAMP3	Unknown; associates with LDs.	(Bui *et al.*, 2021; Li *et al.*, 2008a; Saka *et al.*, 2015; Scidmore-Carlson *et al.*, 1999; Scidmore & Hackstadt, 2001)
CT119	CTL0374	IncA	VAMP3/7/8	Homotypic inclusion fusion; regulation of host cell vesicular trafficking; associates with LDs.	(Bannantine *et al.*, 2000; Cingolani *et al.*, 2019; Cocchiaro *et al.*, 2008; Delevoye *et al.*, 2008; Johnson & Fisher, 2013; Li, *et al.*, 2008; Ouellette, 2018; Ouellette *et al.*, 2021; Ronzone & Paumet, 2013; Scidmore-Carlson *et al.*, 1999; Suchland *et al.*, 2000;Wang *et al.*, 2018)
CT134	CTL0389	-	Unknown	Unknown.	(Weber *et al.*, 2015)
CT135	CTL0390	-	Unknown	Important for chlamydial virulence in a mouse infection model.	(Sturdevant *et al.*, 2010; Sturdevant *et al.*, 2014; Weber *et al.*, 2015)
CT147	CTL0402	-	Unknown	Unknown.	(Belland *et al.*, 2003; Li *et al.*, 2008a; Suchland *et al.*, 2000)
CT179	CTL0431	-	Unknown	Unknown.	(Weber *et al.*, 2015)
CT192	CTL0444	-	Unknown	Unknown.	(Weber *et al.*, 2015)
CT222	CTL0475	-	Unknown	Heterophilic Inc-Inc interactions; localizes at inclusion microdomains.	(Gauliard *et al.*, 2015; Mital *et al.*, 2010; Shaw *et al.*, 2000; Weber *et al.*, 2015)
CT223	CTL0476	IPAM	CEP170	Modulation of the microtubule network; inhibition of host cell cytokinesis; localizes at inclusion microdomains.	(Alzhanov *et al.*, 2009; Bannantine *et al.*, 2000; Dumoux *et al.*, 2015; Li *et al.*, 2008a; Shaw *et al.*, 2000; Weber *et al.*, 2015)
CT224	CTL0477	-	Unknown	Inhibition of host cell cytokinesis; localizes at inclusion microdomains.	(Alzhanov *et al.*, 2009; Shaw *et al.*, 2000; Weber *et al.*, 2015)
CT225	CTL0477A	-	Unknown	Inhibition of host cell cytokinesis.	(Alzhanov *et al.*, 2009; Li *et al.*, 2008a; Shaw *et al.*, 2000)
CT226	CTL0478	-	Unknown	Unknown.	(Li *et al.*, 2008a; Sharma *et al.*, 2006; Shaw *et al.*, 2000; Weber *et al.*, 2015)
CT227	CTL0479	-	Unknown	Unknown.	(Li *et al.*, 2008a; Shaw *et al.*, 21000)
CT228	CTL0480	-	MYPT1	Inhibition of chlamydial extrusion; localizes at inclusion microdomains.	(Li *et al.*, 2008a; Lutter *et al.*, 2013; Sharma *et al.*, 2018; Shaw *et al.*, 2000)

CT229	CTL0481 CpoS	Rabs	Control of inclusion membrane stability and/or host cell death, and of host cell vesicular trafficking.	(Bannantine *et al.*, 2000; Faris *et al.*, 2019; Li *et al.*, 2008a; Rzomp *et al.*, 2006; Shaw *et al.*, 2000; Sixt *et al.*, 2017; Weber *et al.*, 2015; Weber *et al.*, 2017)
CT232	CTL0484 IncB	Unknown	Localizes at inclusion microdomains.	(Li *et al.*, 2008a; Mital *et al.*, 2010; Weber *et al.*, 2015)
CT233	CTL0485 IncC	Unknown	Control of inclusion membrane stability; localizes at inclusion microdomains.	(Bannantine *et al.*, 2000; Li *et al.*, 2008a; Weber *et al.*, 2015; Weber *et al.*, 2017)
CT249	CTL500A-	Unknown	Unknown.	(Jia *et al.*, 2007; Li *et al.*, 2008a; Shaw *et al.*, 2000)
CT288	CTL0540 -	CCDC146	Localizes at inclusion microdomains.	(Almeida *et al.*, 2018; Bannantine *et al.*, 2000; Li *et al.*, 2008a; Weber *et al.*, 2015)
CT345	CTL0599 -	Unknown	Unknown.	(Weber *et al.*, 2015)
CT358	CTL0612 -	Unknown	Unknown.	(Li , *et al.*, 2008)
CT383	CTL0639 -	Unknown	Modulation of inclusion membrane stability.	(Weber *et al.*, 2015; Weber *et al.*, 2017)
CT440	CTL0699 -	Unknown	Unknown.	(Li, *et al.*, 2008a)
CT442	CTL0701 CrpA	VAMP3	Unknown.	(Bui *et al.*, 2021; Bannantine *et al.*, 2000; Li *et al.*, 2008a; Starnbach *et al.*, 2003; Weber *et al.*, 2015)
CT449	CTL0709 -	VAMP3	Unknown.	(Bui *et al.*, 2021; Weber *et al.*, 2015)
CT483	CTL0744 -	Unknown	Unknown.	(Shaw *et al.*, 2000)
CT565	CTL0828 -	Unknown	Unknown.	(Shaw *et al.*, 2000)
CT618	CTL0882 -	Unknown	Associates with LDs.	(Li *et al.*, 2008a; Saka *et al.*, 2015; Sisko *et al.*, 2006)
CT813	CTL0184 InaC	14-3-3 proteins, ARF1/4, VAMP3/7/8	Modulation of post-translational modification of microtubules, and of F-actin and Golgi redistribution around the inclusion.	(Bui *et al.*, 2021; Chen *et al.*, 2006; Delevoye *et al.*, 2008; Kokes *et al.*, 2015; Li *et al.*, 2008a; Shaw *et al.*, 2000; Wesolowski *et al.*, 2017)
CT850	CTL0223 -	DYNLT1	Inclusion positioning at centrosome; localizes at inclusion microdomains.	(Mital *et al.*, 2010: Mital *et al.*, 2015; Shaw *et al.*, 2000)

1.5.2.2.1 Incs localizing at inclusion microdomains

Several Incs (CT222, CT223/Inclusion protein acting on microtubules (IPAM), CT224, CT228, CT232/IncB, CT233/IncC, CT288 and CT850) were found to accumulate in patches at the inclusion membrane near the centrosome called inclusion microdomains, which contain cholesterol and phosphorylated active forms of Src family kinases. These microdomains have been proposed to facilitate the interaction of the inclusion with the centrosome, microtubules and the actin-myosin cytoskeleton (Mital *et al.*, 2010; Mital *et al.,* 2015).

CT223/IPAM interacts with the host centrosomal protein CEP170 (Figure 1.5a), which was found to be required for microtubules accumulation in a nest-like structure around the inclusion and for normal inclusion morphology and *C. trachomatis* growth. When transiently produced in mammalian cells, IPAM associates with the centrosome and is able to alter the organization of microtubules in a CEP170-dependent manner. This indicates that IPAM potentially interferes with microtubules via its interaction with CEP170 (Dumoux *et al.*, 2015; Mital *et al.*, 2010; Mital *et al.*, 2015; Weber *et al.*, 2015). Also, IPAM and the Incs CT224 and CT225 (not shown to localize at microdomains) inhibit cytokinesis when overproduced in mammalian cells (Alzhanov *et al.*, 2009).

CT288 binds the centrosomal protein coiled-coil domain containing 146 (CCDC146). CCDC146 is recruited to the periphery of the inclusion in a CT288-independent manner, suggesting that other Incs might interact with CCDC146 (Almeida *et al.*, 2018).

CT850 binds a dynein subunit, dynein light chain Tctex-type 1 (DYNLT1). DYNLT1 accumulates at inclusion microdomains and its depletion disrupts the association of the inclusion with centrosomes. As *C. trachomatis* subverts the minus-end directed microtubule motor, dynein, to traffic along microtubules to the microtubule organizing center (MTOC), it is proposed that CT850 interacts with DYNLT1 to facilitate the trafficking of the inclusion to the MTOC (Mital *et al.*, 2015).

CT228 binds human myosin phosphatase target subunit 1 (MYPT1), and CT101/MrcA binds inositol 1,4,5-trisphosphate receptor type 3 (ITPR3), a channel mediating the release of Ca^{2+} from intracellular stores. It was demonstrated that CT228 and MrcA are required for the localization of MYPT1 and ITPR3, respectively, at the inclusion membrane. These results combined with further experiments indicated that these Incs target the enzymes that control the phosphorylated state of myosin light chain 2 (MLC2) to regulate the inclusion extrusion process, by modulating the activity of myosin II. MrcA is proposed to promote chlamydial exit by extrusion and CT228 to inhibit it (Lutter *et al.*, 2013; Nguyen *et al.*, 2018; Shaw *et al.*, 2018).

1.5.2.2.2 Incs modulating the actin cytoskeleton and Golgi redistribution around the inclusion

During *C. trachomatis* infection, the Golgi complex fragments into mini stacks around the inclusion, which is thought to facilitate the acquisition of sphingolipids (Heuer *et al.*, 2009; Kumar & Valdivia, 2008).

CT813/Inclusion membrane protein for actin assembly (InaC) was first reported to accumulate at the inclusion membrane during infection and to localize at cytoskeleton-like structures when transiently produced in mammalian cells (Chen *et al.*, 2006). Later, InaC was identified in a screen for genes involved in the accumulation of F-actin around the inclusion using chemically mutagenized *C. trachomatis* strains. InaC was found to interfere with actin remodeling and Golgi redistribution around the inclusion by unrelated processes (Kokes *et al.*, 2015; Kumar & Valdivia, 2008; Wesolowski *et al.*, 2017). InaC binds and recruits to the periphery of the inclusion host cell Arf GTPases (Arf1 and 4), which regulate eukaryotic vesicular trafficking and the structure of the Golgi complex (Kokes *et al.*, 2015; Wesolowski *et al.*, 2017). In *C. trachomatis*-infected cells, InaC mediates the activation of Arf1 and Arf4, which induces post-translational modifications of microtubules resulting in Golgi redistribution around the inclusion (Figure 1.5a). So far, a relationship between InaC-Arfs interactions and F-actin remodeling has not been established (Wesolowski *et al.*, 2017). It is also unclear whether InaC is essential or not for *C. trachomatis* growth, as only one out of the three generated *inaC* mutants affected the generation of infectious progeny in mammalian cells. Moreover, absence of InaC did not affect the trafficking of sphingolipids to the inclusion (Kokes *et al.*, 2015; Wesolowski *et al.*, 2017). InaC was also found to interact with the vesicle-associated membrane proteins (VAMPs) VAMP3/7/8 and also with 14-3-3 proteins (14-3-3s), which are phosphoserine/threonine binding proteins involved in several signaling pathways (Bui *et al.*, 2021; Delevoye *et al.*, 2008; Kokes *et al.*, 2015; Mirrashidi *et al.*, 2015). In addition to InaC, another two Incs of unknown function were shown (CT118/IncG) or predicted (CT006) to interact with some isoforms of 14-3-3s (Mirrashidi *et al.*, 2015; Scidmore & Hackstadt, 2001). It was suggested that the recruitment of 14-3-3β by Incs might sequester BCL2-associated agonist of cell death (BAD) protein at the inclusion membrane away from mitochondria, thus protecting host cell from apoptosis (Verbeke *et al.*, 2006). IncG, together with Incs CT618 and IncA, was also found associated with LDs isolated from *C. trachomatis* infected cells (Cocchiaro *et al.*, 2008; Saka *et al.*, 2015).

1.5.2.2.3 Incs targeting the ER

The Incs CT115/IncD and CT005/IncV localize at ER-inclusion MCS, possibly involved in the acquisition of lipids to chlamydial inclusions (Figure 1.5b). IncD is able to interact with the host ceramide transporter (CERT) and the overproduction of IncD increases the recruitment of CERT and its interacting partners, VAMP-associated protein (VAP) A (VAPA) and VAPB, to the inclusion membrane (Agaisse & Derré, 2014; Derré *et al.*, 2011). Therefore, the transport of ceramide from the ER into the inclusion lumen is thought to occur at ER-inclusion MCS involving the VAPA/B-CERT-IncD complex (Figure 1.5b). It is still unclear how ceramide is converted into sphingomyelin within the inclusion (Agaisse & Derré, 2014; Derré *et al.*, 2011). IncV interacts with VAPA and VAPB (Figure 1.5b) and in *C. trachomatis* strains overproducing or lacking IncV the recruitment of VAPA/B to the periphery of the inclusion increases or decreases, respectively (Mirrashidi *et al.*, 2015; Stanhope *et al.*, 2017). However, *incV* mutant strains do not display defects in intracellular growth, suggesting that IncV is more likely involved in the tethering of the ER to the inclusion than in the import of ceramide (Stanhope *et al.*, 2017; Weber *et al.*, 2017).

1.5.2.2.4 Incs interfering with eukaryotic vesicular trafficking

CT119/IncA is able to interact with itself and to mediate homotypic fusion between inclusions (Figure 1.5c) (Cingolani *et al.*, 2019; Delevoye *et al.*, 2004; Gauliard *et al.*, 2015; Hackstadt *et al.*, 1999; Ronzone *et al.*, 2014; Ronzone & Paumet, 2013). Infection of mammalian cells with *C. trachomatis incA* mutants results in non-fusogenic inclusions without affecting chlamydial growth (Weber *et al.*, 2016). IncA has two soluble N-ethylmaleimide-sensitive factor receptor (SNARE)-like domains (SLD1 and SLD2). The carboxy-terminal SLD2 is required for homotypic interactions and SLD1 and part of SLD2 are needed for fusion between inclusions. In addition, SLDs mediate the interactions of IncA with VAMP3, 7 and 8 (Figure 1.5c), and the recruitment of these SNAREs to the inclusion membrane decreases in cells infected by *incA* mutant strains (Delevoye *et al.*, 2004, Delevoye *et al.*, 2008; Gauliard *et al.*, 2015; Ronzone & Paumet, 2013). As IncA has the capacity to inhibit endocytic SNARE-mediated fusion, it seems that IncA might interact with VAMPs to inhibit their functions and selectively prevent fusion of host vesicles with the inclusion (Figure 1.5c) (Paumet *et al.*, 2009; Ronzone & Paumet, 2013).

CT116/IncE modulates the retromer-dependent trafficking, which is associated with the recycling of cargo from endosomes to the plasma membrane or trans-Golgi network (TGN). Several sorting nexins (SNX), which can be part of the retromer protein complex, accumulate at the periphery of the inclusion and at least SNX5 and SNX6 were found to interact with IncE (Figure 1.5c). IncE competes with cation-independent (CI) mannose 6-

phosphate receptor (M6PR) (CI-M6PR) for binding to SNX5 (Figure 1.5c), and M6PRs are involved in the transport of lysosomal enzymes from the TGN to endosomes and then their recycling to Golgi depends on the retromer. Taking into account that *C. trachomatis* growth is enhanced by the depletion of retromer components, including SNX5, this indicates that the retromer restricts chlamydial development and that IncE might subvert the retromer and lysosomal functions via its interaction with SNXs (Aeberhard *et al.*, 2015; Elwell *et al.*, 2017; Mirrashidi *et al.*, 2015; Sun *et al.*, 2017).

CT229/*Chlamydia* promoter of survival (CpoS) interacts with multiple Rab GTPases (Rabs 1, 2, 6, 8, 10, 14, 18, 33, 34, and 35) (Figure 1.5c), which are master regulators of vesicular trafficking, and several other Rabs were observed at or near the inclusion. CpoS interacting Rabs were absence from inclusions in cells infected with a *cpoS* null mutant and at least the depletion of Rab 4, 6, 14 and 35 negatively affected *C. trachomatis* growth (Capmany & Damiani, 2010; Faris *et al.*, 2019; Lipinski *et al.*, 2009; Mirrashidi *et al.*, 2015; Sixt *et al.*, 2017).

Faris *et al.* found that the production of CpoS in yeast cells is toxic and that CpoS-mediated toxicity could be suppressed by the overproduction of proteins related with clathrin-coated vesicles (Faris *et al.*, 2019). In addition, they showed that the accumulation of CI-M6PR (clathrin-dependent transport from the TGN) and transferrin (clathrin-dependent transport from the plasma membrane) at the inclusion membrane requires CpoS, and in the case of transferrin the recruitment also depends on Rab4 and 35 (Figure 1.5c) (Faris *et al.*, 2019). Also, *cpoS* mutants were found to be attenuated in their ability to generate infectious progeny both in cultured cells and in a mice infection model (Sixt *et al.*, 2017; Weber *et al.*, 2017). Besides interfering with vesicular trafficking, CpoS, together with CT383 and IncC, were suggested to be involved in maintaining the integrity and stability of the inclusion, which is essential to support bacterial growth and to prevent host cell death. A cytotoxic effect caused by *cpoS* null mutants was observed by two independent studies, which differ in the explanation for this phenomenon (Sixt *et al.*, 2017; Weber *et al.*, 2017). Increased host cell death was observed by Weber *et al.* in cells infected by *C. trachomatis* strains with *cpoS*, *incC* or *ct383* insertionally inactivated and each one of these mutations decreased bacterial growth. In addition, multiple inclusions and premature lysis of the inclusion membrane were observed. This, together with other results, indicated that the cytotoxic effect was caused by the release of *Chlamydiae* into the host cell cytosol leading to autophagy-dependent host cell death (Weber *et al.*, 2017). Sixt *et al.* reported that *cpoS* mutants activate the stimulator of interferon genes (STING), resulting in the re-localization of STING from the ER to perinuclear vesicles and enhanced interferon response. However, as host cell death was reduced in STING-deficient cells infected by *cpoS* mutant, but not if the transport of STING

was pharmacologically inhibited, it seemed that the interferon response and host cell death driven by *cpoS* mutant were not related. Also, further experiments indicated that the cytotoxic effect could be related with control of calcium pools at the ER (Sixt *et al.*, 2017).

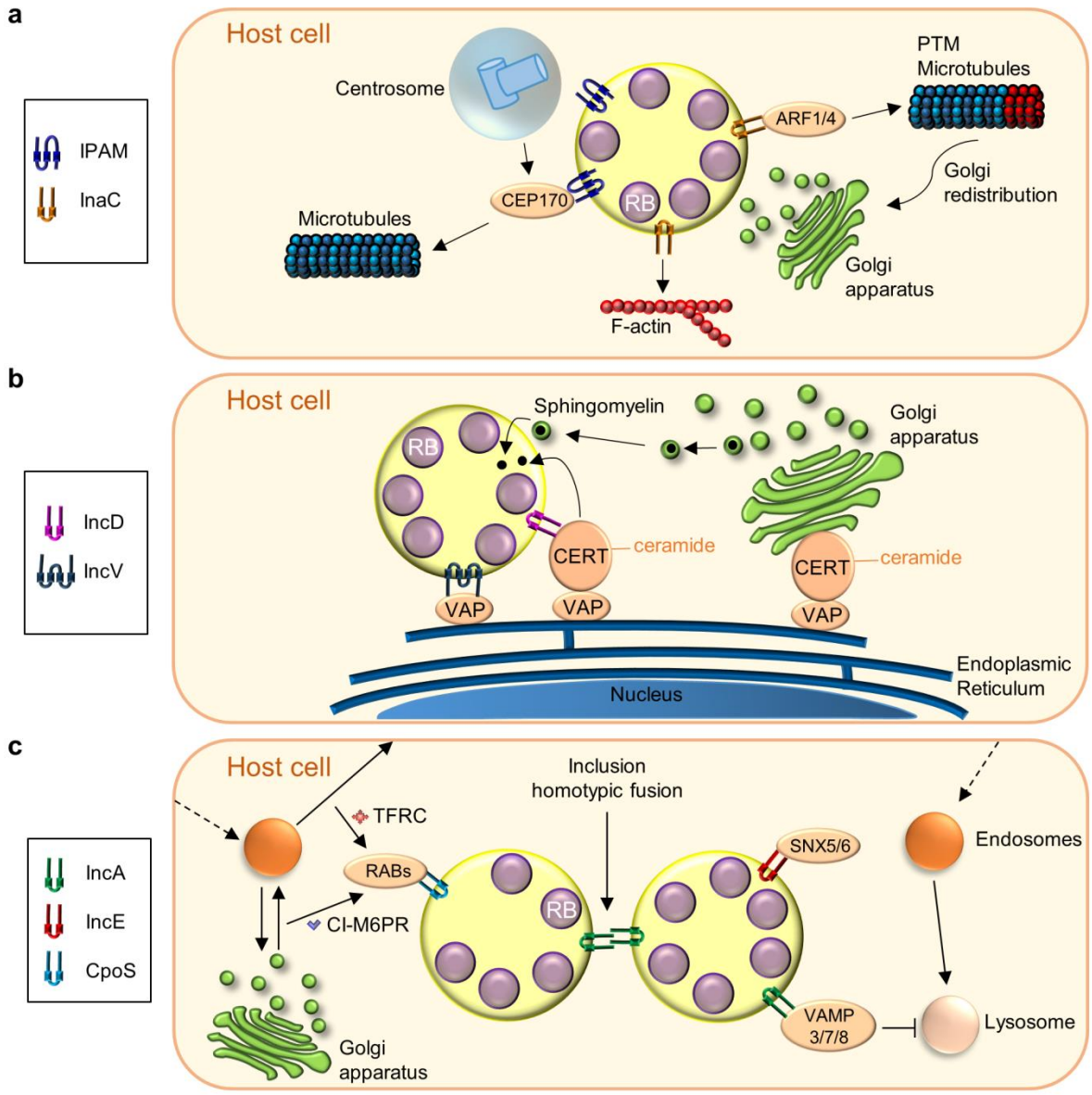

Figure 1.5 ***C. trachomatis*** **Incs interfering with host cell trafficking, acquisition of lipids and cytoskeleton remodeling.** (a) Incs interfering with microfilaments and microtubules (IPAM, InaC) and Incs mediating Golgi redistribution around the inclusion (InaC). (b) Incs participating in ER-inclusion MCSs (IncD, IncV). (c) Incs subverting host cell vesicular transport (IncA, IncE, CpoS). PTM, post-translationally modified. RB, reticulate bodies. Reprinted from (Bugalhão & Mota, 2019).

1.6 Thesis Goals

The main goal of this PhD thesis was to increase the knowledge about how the human pathogen *C. trachomatis* manipulates host cells to survive and proliferate, by furthering the understanding on Incs. Considering the specific localization of these proteins, we anticipated that several Incs involved in the subversion of host vesicular trafficking or targeting specific host cell organelles remained to be identified. Therefore, our specific objectives were:

1) Discover novel Incs subverting eukaryotic vesicular trafficking and/or showing tropism for eukaryotic organelles;

2) Select one newly identified Inc and identify its host cell targets;

3) Provide insights on the mechanism of action of the newly identified Inc.

.

2

MATERIALS AND METHODS

2.1 Plasmids and oligonucleotides

Plasmids and oligonucleotides used in this work are listed in Annexes Table A.1 and A.2, respectively, as well as their relevant characteristics. In the case of *C. trachomatis* genes, oligonucleotides were designed using the corresponding DNA sequences from *C. trachomatis* L2/434. Plasmids were generated using restriction enzymes or by restriction-free cloning (Bond & Naus, 2012). For cloning using restriction enzymes, plasmids were constructed and purified using standard molecular biology procedures, using Phusion high-fidelity DNA polymerase (Thermo Fisher Scientific), restriction enzymes (Thermo Fisher Scientific), T4 DNA Ligase (Thermo Fisher Scientific), DreamTaq DNA polymerase (Thermo Fisher Scientific), NZYTaqII (NZYTech), DNA clean & concentrator™-5 kit, Zymoclean™ gel DNA recovery kit (Zymo Research), and GeneElute Plasmid Miniprep kit (Sigma-Aldrich) or NZYMidiprep kit (NZYTech) according to manufacturer's instructions. For restriction-free cloning, plasmids were generated using a PCR-based method (Bond & Naus, 2012) with Phusion high-fidelity DNA polymerase (Thermo Fisher Scientific), and DpnI (Thermo Fisher Scientific) was used to degrade parental plasmids. The accuracy of the nucleotide sequence of all the inserts in the constructed plasmids was confirmed by DNA sequencing.

2.2 *Escherichia coli* strains and growth conditions

Escherichia coli NEB 10β (New England Biolabs) was used for construction and purification of plasmids, and *E. coli* K12 ER2925 (New England Biolabs) was used to purify plasmids for transformation of *C. trachomatis*. *E. coli* strains were grown at 37 ^{o}C in liquid or solid lysogeny broth media (NZYTech) with the appropriate antibiotics and supplements. *E. coli* strains were transformed with plasmids by electroporation.

2.3 Yeast strains and vacuolar protein sorting assays

Yeast strains used in this work are listed in Annexes Table A.3. For vacuolar protein sorting assays (Vps), *Saccharomyces cerevisiae* NSY01 cells expressing the genes encoding green fluorescent protein (GFP) or GFP-Pep12$_{L\text{-}TM}$ fusion proteins were grown in plates with yeast nitrogen base uracil dropout (YNB-Ura) supplemented with 2% (w/v) fructose at 30 ºC for 3 days. Drops containing yeast cells at an amount equivalent to an optical density at 600 nm (OD_{600}) of 0.1 in 10 µl sterile dH_2O were plated on the same media supplemented with 2% (w/v) fructose (non-inducing media) or 2% (w/v) galactose (inducing media) and incubated at 30 ºC. After 2 days, normal (white colonies; Vps$^+$ phenotype) or mistrafficking (brown colonies; Vps$^-$ phenotype) was scored qualitatively by incubating yeast cells with agar containing a sucrose overlay solution [125 mM sucrose, 100 mM sodium acetate, pH 5.5, 0.5 mM *N*-ethylmaleimide (NEM), 10 µg/ml horseradish peroxidase, 8 U/ml glucose oxidase, and 2 mM *O*-dianisidine], indicating glucose production by formation of a brown precipitate (Franco *et al.*, 2012; Shohdy *et al.*, 2005).

2.4 Mammalian cell lines

HeLa 229, Vero and HEK 293T cells (from the European Collection of Cell Culture; ECACC) were maintained in Dulbecco's modified Eagle Medium (DMEM; Thermo Fisher Scientific) supplemented with 10% (v/v) heat-inactivated fetal bovine serum (FBS; Thermo Fisher Scientific) at 37 ºC in a 5% (v/v) CO_2 incubator. Cells were checked for *Mycoplasma* contamination by conventional PCR as described (Uphoff & Drexler, 2011).

2.5 Transient transfection of mammalian cells

For fluorescence microscopy analyses, 6x10^4 HeLa 229 cells were seeded onto 13 mm glass coverslips (VWR) in 24-well plates; for immunoblotting, 1x10^5 HeLa 229 cells were seeded in 24-well plates and for co-immunoprecipitation (co-IP) assays, 5x10^5 HEK 293T cells were seeded in 6-well plates previously coated with 0.001% (v/v) poly-L-Lysine (Sigma) in phosphate-buffered saline (PBS). At the following day, cells were transfected using the jetPEI™ reagent (Polyplus-Transfection) according to manufacturer's instructions. Briefly, cells seeded in 24-well plates were transfected with 250 ng of plasmid DNA and 1.5 µl of jetPEI™ reagent were added per well. The size of wells and the volumes used were scaled up when necessary. Plates were then centrifuged at 180 x *g* for 5 min at room temperature and then incubated at 37 °C in a 5% (v/v) CO_2 incubator. At the indicated times post-transfection, cells were collected for immunoblotting, co-IP assays or fixed for fluorescence

microscopy analysis. In the experiments where cells were transfected with plasmids and infected by *C. trachomatis*, the transfection was performed at time zero of infection.

2.6 Manipulation of *C. trachomatis*

2.6.1 Infection of HeLa 229 cells by *C. trachomatis*

C. trachomatis serovar L2 prototype strain 434/Bu (L2/434 from ATCC) was propagated in HeLa 229 cells using standard procedures (Scidmore, 2005). Throughout this work we used the nomenclature of the annotated *C. trachomatis* D/UW3 strain (Stephens *et al.* 1998). For infection assays, *C. trachomatis* L2/434 infectious particles were titrated as previously described (Scidmore, 2005). For fluorescence microscopy analysis, $6x10^4$ HeLa 229 cells were seeded onto 13 mm glass coverslips (VWR) in 24-well plates. For immunoblotting, $1x10^5$ HeLa cells were seeded in 24-well plates. Scaling-up was done for propagation of *C. trachomatis* strains in 6-well plates and in tissue culture flasks with a surface area of 25 cm^2 (T25 flask). After 24 h, cells were incubated for ~15 min with Hank's balanced salt solution (HBSS; Gibco) at 37 °C in a 5% (v/v) CO_2 incubator. HBSS was removed and cells were infected by *C. trachomatis* inocula prepared in HBSS or in sucrose-phosphate-glutamate buffer (SPG; 0.2 mM sucrose, 17 mM Na_2HPO4, 3 mM NaH_2PO_4, 5 mM L-glutamic acid) (200 µl per well for 24-well plates, 500 µl per well for 6-well plates or 2 ml for T25 flasks) for 30 min at 37 °C in a 5% (v/v) CO_2 incubator (plates) or for 1 h at room temperature with gentle rocking (T25 flasks). The inocula were then replaced by DMEM supplemented with 10% (v/v) FBS and 10 µg/ml gentamicin, and this time-point was considered the time zero of infection. At the indicated times post-infection, cells were fixed for fluorescence microscopy or harvested for immunoblotting.

2.6.2 Transformation of *C. trachomatis*

C. trachomatis transformants were generated essentially as described by Agaisse and Derré (Agaisse & Derré, 2013). Cell extracts containing *C. trachomatis* EBs in SPG at approximately $1x10^8$ IFUs/ml were mixed with 6 µg of plasmid DNA diluted in 200 µl $CaCl_2$ buffer (10 mM Tris pH 7.4, 50 mM $CaCl_2$) and incubated for 30 min at room temperature. In the meantime, $4x10^6$ HeLa 229 cells were washed in PBS by centrifugation at 237 x *g*. Pellets were then resuspended in $CaCl_2$ buffer and added to the mixture (*Chlamydia* and plasmid DNA). This final mixture (HeLa cells, *Chlamydia* and plasmid DNA) was incubated for 20 min at room temperature and mixed gently by pipetting every 5 min. Finally, 200 µl of the final mixture were added per well in a 6-well plate containing 3 ml per well of DMEM

supplemented with 10% (v/v) FBS and incubated for 44 h at 37 ºC in a 5% (v/v) CO_2 atmosphere. At 16 h post-transformation, the media was replaced by DMEM supplemented with 10% (v/v) FBS and 0.3 U/ml penicillin G. At 44 h post-transformation, cells were lysed with 500 µl per well of sterile dH_2O, 500 µl per well of 2x SPG were added to each well and the lysates from the 2 wells were pooled and centrifuged for 5 min at 237 x *g* at room temperature. The supernatant was added to HeLa cells seeded in a T25 flask previously incubated with HBSS. After 1 h of incubation at room temperature with gentle rocking, the inoculum was replaced by DMEM supplemented with 10% (v/v) FBS, 0.3 U/ml penicillin G and 1 µg/ml cycloheximide and the cells were incubated at 37 °C in a 5% (v/v) CO_2 atmosphere. After ~44 h, infected cells containing *C. trachomatis* transformants were lysed and used to re-infect HeLa cells previously seeded in T25 flasks and incubated for 37 ºC in a 5% (v/v) CO_2 atmosphere. After 2/3 days, wild type chlamydial inclusions, indicative of a successful transformation, were observed by phase-contrast microscopy. Infected cells containing *C. trachomatis* transformants were lysed and used to re-infect HeLa cells previously seeded in a T25 flask, as described above, except the concentration of penicillin G, which was increased for 1 U/ml. The transformants were passed several times to increase the number of bacteria and one passage was performed in the presence of 10 U/ml penicillin G before storing at -80 ºC.

2.6.3 Clone isolation of *C. trachomatis* strains by plaque purification

Clonal isolation of *C. trachomatis* strains was performed by plaque purification using Vero cells (Nguyen & Valdivia, 2013). $4x10^5$ Vero cells per well were seeded in 6-well plates and incubated at 37 ºC in a 5% (v/v) CO_2 atmosphere. At the following day, cells were incubated with HBSS while *C. trachomatis* strains previously stored at -80 ºC were thawed on ice and seven 10-fold dilutions were prepared in 1x SPG. Vero cells were then infected with 500 µl of each dilution and incubated for 30 min at 37 ºC in a 5% (v/v) CO_2 incubator. The inocula was replaced by DMEM (without phenol red) supplemented with 10% (v/v) FBS, 1 U/ml penicillin G and 1 µg/ml cycloheximide and infected cells were incubated at 37 °C in a 5% (v/v) CO_2 atmosphere. After 24 h, an overlay solution containing 0.54% (w/v) agarose diluted in DMEM (without phenol red) supplemented with 10% (v/v) FBS, 1 U/ml penicillin G and 1 µg/ml cycloheximide was prepared and kept at 55 ºC before adding to infected cells. The media were removed from the 6-well plate and 2 ml of the overlay solution were added to each well. Plates were incubated at room temperature for 15 min to allow the solidification of agarose, followed by the addition of 2 ml of DMEM (without phenol red) supplemented with 10% (v/v) FBS. Infected cells were incubated at 37 ºC in a 5% (v/v) CO_2 incubator.

After ~6 days, isolated plaques were picked with a 200 µl sterile barrier pipette tip and placed in a 1.5 ml tube containing 100 µl DMEM supplemented with 10% (v/v) FBS, 1 U/ml penicillin G and 1 µg/ml cycloheximide. The media from a 96-well plate containing Vero cells seeded the day before was removed, 100 µl of DMEM containing each plaque were added to each well and plates were incubated at 37 ºC in a 5% (v/v) CO_2 incubator. After 2 days, infected cells were lysed with 100 µl per well of sterile dH_2O, 100 µl per well of 2x SPG were added to each well and then each solution containing chlamydial infectious particles was added to HeLa 229 cells previously seeded in a 24-well plate. Each plaque-purified clone was propagated in HeLa 229 cells until a higher number of viable bacteria could be stored at -80ºC.

2.7 Co-immunoprecipitation assays

For co-IP assays, the GFP-Trap kit (Chromotek) was used essentially according to manufacturer's instructions. $5x10^5$ HEK 293T cells per well were seeded in 6-well plates, 2 wells per condition. At the following day, cells were co-transfected, in combinations of two, with plasmids encoding 14-3-3 isoforms fused to HA or FLAG-HA, and monomeric enhanced GFP (mEGFP) or IncL versions fused to the carboxy-terminal region of mEGFP. After 24 h, cells were scraped from wells and 2 wells per condition were pooled and centrifuged. Cell pellets were lysed in 200 µl of ice-cold co-IP lysis buffer [20 mM Tris-HCl pH 7.5, 137 mM NaCl, 2 mM ethylenediamine tetraacetic acid (EDTA), 1.0% NP40, protease inhibitors and phenylmethylsufonyl fluoride (PMSF)] for 30 min on ice and samples were mixed by pipetting every 10 min. The lysates were then centrifuged at 24100 x *g* at 4 ºC, 20 µl of each supernatant was stored (input of co-IP) and the remaining supernatant was diluted in 800 µl of ice-cold GFP-Trap buffer (10 mM Tris-HCl pH 7.5, 150 mM NaCl, 0.5 mM EDTA). Diluted lysates were incubated with previously washed GFP-Trap beads at 4 ºC with end-over-end mixing. After 4 h, beads were centrifuged at 2000 x *g* for 2 min at 4 ºC and the supernatants were stored (non-bound of co-IP). Beads were washed 6 times with GFP-Trap buffer by centrifugations with the same conditions and the supernatants from the last wash were stored (wash of co-IP). Finally, beads (bound of co-IP) and the previously harvested co-IP fractions (input, non-bound and wash fractions) were resuspended in 20 µl of 2x SDS-PAGE loading buffer [Tris-HCl 100 mM, pH 6.8, SDS 4.0% (w/v), glycerol 20% (v/v), β-mercaptoethanol 0.2 M, bromophenol blue 0.2% (w/v)], boiled for 10 min at 100 ºC and analyzed by immunoblotting.

2.8 Antibodies, fluorescent dyes and treatment with oleic acid

The following antibodies were used for immunoblotting: rabbit anti-GFP (Abcam; 1:1000), mouse anti-phosphoglycerate kinase 1 (PGK1) (Life Technologies; 1:1000), mouse anti-chlamydial heat-shock protein 60 (Hsp60) (A57-B9; Thermo Fisher Scientific; 1:1000), rat anti-hemagglutinin (HA) (3F10; Roche; 1:1000), mouse anti-α-tubulin (clone B-5-1-2; Sigma-Aldrich; 1:1000), rabbit anti-glycogen synthase kinase-3β (GSK3β) (Cell Signaling Technology; 1:5000) or rabbit anti-phospho-GSK3β (pGSK3β) (Cell Signaling Technology; 1:1000), followed by anti-rabbit, anti-mouse or anti-rat horseradish peroxidase (HRP)-conjugated secondary antibodies (GE Healthcare and Jackson ImmunoResearch; 1:10000).

For immunofluorescence microscopy, the following antibodies were used: rabbit anti-GFP (Abcam; 1:200), mouse anti-chlamydial Hsp60 (A57-B9; Thermo Fisher Scientific; 1:200), rat anti-HA (3F10; Roche; 1:200), goat anti-MOMP of *C. trachomatis* (Abcam; 1:200), rabbit anti-Cap1 [a gift from Agathe Subtil; (Gehre *et al.*, 2016); 1:200], mouse anti-c-Myc (clone 9E10, Calbiochem; 1:200), rabbit anti-pGSK3β (Cell Signaling Technology; 1:200), followed by appropriate fluorophore-conjugated anti-rabbit, anti-mouse, anti-rat or anti-goat antibodies (Jackson ImmunoResearch; 1:200).

To induce synthesis of lipid droplets (LDs), HeLa 229 cells were incubated with cell culture media containing 100 µM oleic acid (Sigma-Aldrich; stock solution at 100 mM in ethanol) for 6 hours and then fixed at the indicated time-points. For fluorescence microscopy analysis, LDs were stained with Oil Red O (Sigma-Aldrich; (3:2 v/v Oil Red stock solution diluted in water) or with BODIPY™ 493/503 (Invitrogen; 1:200 in PBS from a saturated stock solution).

To stain yeast mitochondria, yeast cells were incubated with 20 nM MitoRed (Sigma-Aldrich) diluted in YNB-Ura for 30 minutes at 30 °C (Sigma-Aldrich).

To stain yeast endocytic compartments, cells were incubated for 20 minutes with 0.5 µl of FM4-64 (stock solution at 3.2 µM) diluted in yeast extract peptone dextrose (YPD) media followed by a 20 minutes chase with unlabeled YNB media.

2.9 Fluorescence microscopy

Transfected and/or infected HeLa 229 cells were fixed in PBS containing 4% (w/v) paraformaldehyde (PFA) for 10 min at room temperature and permeabilized with PBS containing 0.1% (w/v) Saponin (PBSS; for transfected cells) or 0.1% (v/v) Triton X-100 (PBST; for infected cells). Immunostaining was performed with antibodies diluted in PBSS or

PBST containing 10% (v/v) horse serum. Cells were washed with PBS and dH_2O before assembling the coverslips on microscopy glass slides using Aqua-poly/Mount (Polysciences). Samples were analyzed by fluorescence microscopy and images were processed and assembled using Fiji software (Schindelin *et al.*, 2012).

For yeast microscopy, *S. cerevisiae* strains were grown in plates with YNB, with appropriate amino acids dropout, supplemented with 2% (w/v) fructose for 3 days at 30 °C, then streaked to YNB, with appropriate amino acids dropout, supplemented with 2% (w/v) galactose to induce the production of the proteins of interest and incubated for 48 h at 30 °C. Live yeast cells were visualized directly or after fluorescent staining by fluorescence microscopy.

To calculate the area of BODIPY positive LDs at *C. trachomatis* inclusions, images as those depicted in Figure 3.19 were randomly selected. Using FIJI software, the regions of interest were defined outlining individual inclusions plus 1 µm, in order to consider both LDs co-localizing with inclusions and LDs in close proximity with inclusions. Images were inverted, thresholds were applied by default settings and the area of LDs at the region of inclusions was calculated.

2.10 Immunoblotting

Transfected and/or infected HeLa cells were washed with PBS and detached from plates by incubation with TrypLE Express (Thermo Fisher Scientific) for 5 min at 37 °C in a 5% [v/v] CO_2 incubator. Cells were collected, centrifuged, and washed 2 times with ice-cold PBS. Pellets were resuspended in previously heated SDS-PAGE loading buffer, boiled for 10 min at 100 °C and incubated with benzonase (Novagen) to destroy DNA and reduce the viscosity of the samples before running on SDS-PAGE.

For detection of GFP fusion proteins in *S. cerevisiae*, yeast strains were grown for 3 days at 30 °C in YNB-Ura plates supplemented with 2% (w/v) fructose and then streaked into YNB-Ura supplemented with 2% (w/v) galactose for 2 days. An amount equivalent to OD_{600} 1.7 in 20 µl SDS-PAGE loading buffer was boiled for 10 minutes and run on SDS-PAGE.

The majority of proteins were separated by 12% (v/v) SDS-PAGE (15% for IncL-2HA versions and CT449-2HA) and transferred onto 0.2 µm nitrocellulose membranes (Bio-Rad) using Trans-Blot Turbo Transfer System (BioRad). Immunoblotting detection was done with SuperSignal West Pico Chemiluminescent Substrate (Thermo Fisher Scientific) or SuperSignal West Femto Maximum Sensitivity Substrate (Thermo Fisher Scientific) (as indicated in figure legends) and exposed to Amersham Hyperfilm ECL (GE Healthcare).

2.11 Statistical analyses

Statistical analyses were done using GraphPad Prism, version 7.00 for Windows, GraphPad Software, San Diego California, USA (www.graphpad.com). For comparisons, a Shapiro-Wilk normality test was performed. As normality could not be achieved in the Shapiro-Wilk normality test, Kruskal-Wallis test was used. The α-level was set to 0.05 and a difference with $P<0.05$ was considered to be statistically significant. For comparisons between values normalized against a control group, the Wilcoxon signed-rank test was used.

3

RESULTS

3.1 Screening of *C. trachomatis* Incs interfering with eukaryotic trafficking and/or showing tropism for eukaryotic organelles

C. trachomatis is predicted to encode more than 60 Incs, whose privileged localization suggests important roles in *Chlamydia*-host cell interactions. To increase the knowledge about the function of Incs, we started by performing a functional screen to find novel Incs subverting eukaryotic trafficking and fluorescence microscopy analysis to identify Incs showing tropism for eukaryotic organelles.

3.1.1 *C. trachomatis* Incs cause vacuolar protein sorting mistrafficking in yeast

To search for novel *C. trachomatis* Incs interfering with eukaryotic vesicular trafficking, we performed a functional screen using the yeast *S. cerevisiae* as a eukaryotic model. For this purpose, we focused on Incs which have been shown to localize at the inclusion membrane and with amino or carboxy-terminal regions longer than 40 amino acid residues predicted to be exposed to the host cell cytosol. We then generated *S. cerevisiae* NSY01 reporter strains (detailed in Annexes Table A.3) producing the predicted cytosolic domains of Incs fused to the green fluorescent protein (GFP) (Inc-GFP) (Figure 3.1a). It has been shown that for some Incs, the production of their cytosolic domains is sufficient to cause phenotypes in yeast, while other Inc fragments need to be fused to the localization signal (L) and transmembrane domains (TM) of the yeast SNARE Pep12p ($Pep12_{L\text{-}TM}$), which anchors the fragments to the cytosolic side of endosomes (Black & Pelham, 2000; Sisko *et al.*, 2006) to mimic their presence in a membrane and thus be able to exert their function.

Therefore, we also generated NSY01 reporter strains (detailed in Annexes Table A.3) producing the predicted cytosolic domains of Incs fused to GFP and to $Pep12_{L\text{-}TM}$ (Inc-GFP-$Pep12_{L\text{-}TM}$) (Figure 3.1a). In all strains, the genes encoding Inc-GFP and Inc-GFP-$Pep12_{L\text{-}TM}$ fusion proteins were expressed under the control of a galactose-inducible promoter. Immunoblotting revealed that most fusion proteins were produced and migrated on SDS-PAGE according to their predicted molecular mass (Annexes Figures A.1 and A.2 and summary of protein production in Tables 3.1 and 3.2).

The generated yeast strains were then used to screen for Incs causing vacuolar protein sorting (Vps) defects in yeast, based on the ability of the *S. cerevisiae* NSY01 reporter strain to produce a modified form of invertase (Carboxipeptidase Y-Invertase; CPY-Inv). CPY-Inv normally traffics to the yeast vacuole, but can be secreted to the outside of the cell due to Vps mistrafficking (Figure 3.1b) (Shohdy *et al.*, 2005). As illustrated in Figure 3.1b, normal (white colonies; Vps^+ phenotype) or mistrafficking (brown colonies; Vps^- phenotype) can be scored qualitatively (Shohdy *et al.*, 2005).

A representative result of the Vps assays performed is illustrated in Figure 3.2 (all data are shown in Annexes Figures A.3 and A.4 and are summarized in Tables 3.1 and 3.2). Yeast strains producing only GFP or GFP-$Pep12_{L\text{-}TM}$ were used as negative controls, and yeast strains producing proteins previously shown to induce a Vps^- phenotype, the dominant-negative form of the yeast ATPase Vps4 ($Vps4^{E233Q}$) (Shohdy *et al.*, 2005) and a fusion of the *Legionella pneumophila* effector VipA to GFP (VipA-GFP) (Franco *et al.*, 2012), were used as positive controls. Using this approach, we found 2 fusion proteins (out of 61) causing a Vps^- phenotype: $CT229_{91\text{-}215}$-GFP and $CT223_{192\text{-}268}$-GFP-$Pep12_{L\text{-}TM}$ (Figure 3.2). CT229 (CpoS) and CT223 (IPAM) have been previously shown to interfere with host cell trafficking during *C. trachomatis* infection (Alzhanov *et al.*, 2009; Dumoux *et al.*, 2015; Faris *et al.*, 2019; Rzomp *et al.*, 2006; Sixt *et al.*, 2017; Weber *et al.*, 2017). Therefore, although we only identified CT223 and CT229 as capable of causing sorting defects in yeast, these results validate the applicability of the yeast Vps assay to screen for *C. trachomatis* Incs interfering with eukaryotic trafficking.

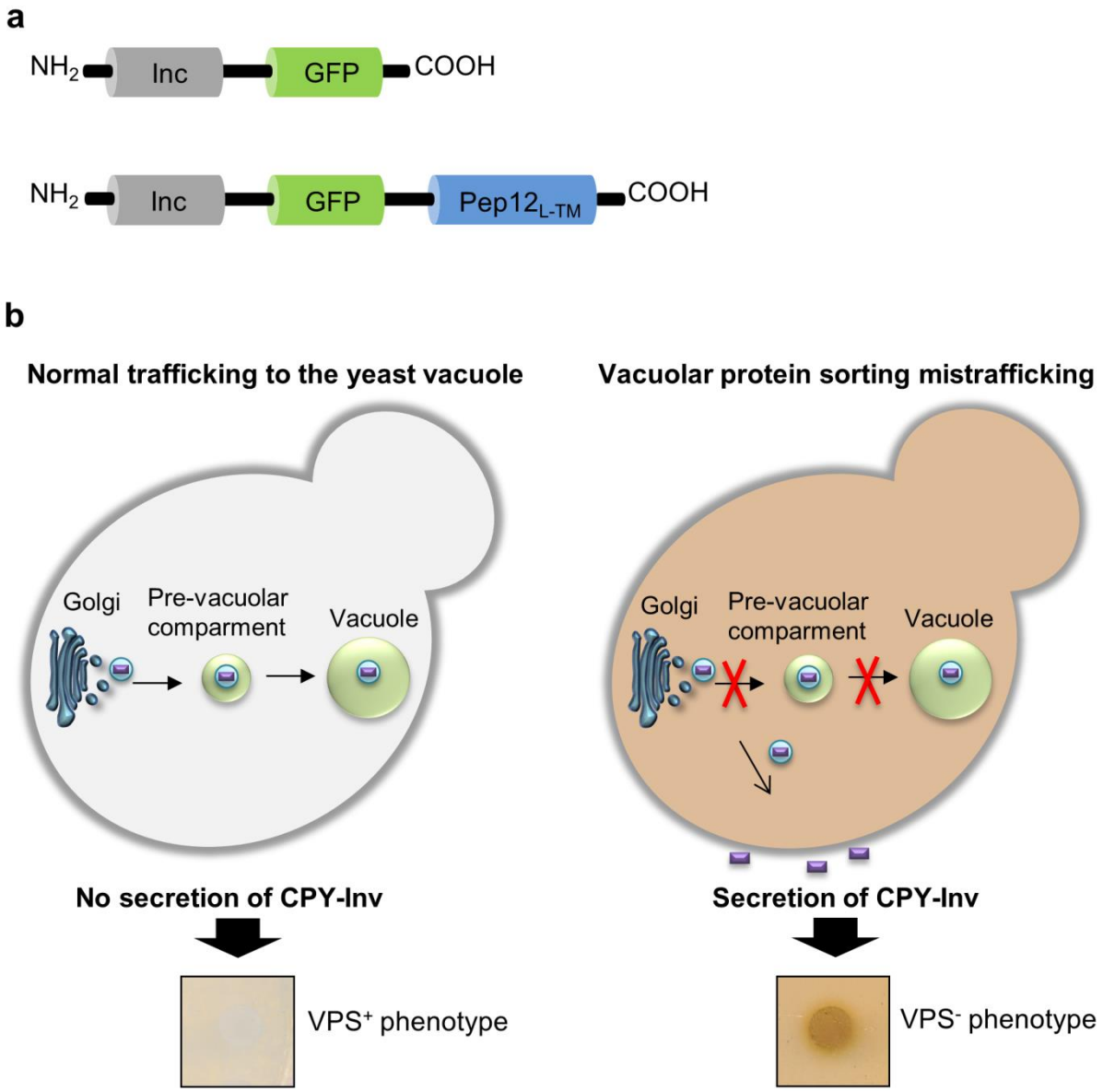

Figure 3.1 Schematic representation of vacuolar protein sorting assays. (a) The *S. cerevisiae* NSY01 reporter strain (Annexes Table A.3) was transformed with plasmids encoding the predicted cytosolic domains of Incs fused to GFP (Inc-GFP) or fused to GFP and to the localization signal (L) and transmembrane domains (TM) of the yeast SNARE Pep12p (Inc-GFP-Pep12$_{L\text{-}TM}$), under the control of a galactose-inducible promoter. The list of *S. cerevisiae* NSY01 reporter strains producing the Inc-GFP or Inc-GFP-Pep12$_{L\text{-}TM}$ proteins is detailed in Annexes Table A.3. (b) The generated yeast strains were used to screen for *C. trachomatis* Incs causing Vps defects, detected by an assay based on the ability of the NSY01 reporter strain to produce caboxypetidase Y-Invertase (CPY-Inv), which hydrolyses sucrose into glucose and fructose at the cell surface when trafficking to the vacuole is disrupted. Normal (Vps^{+} phenotype) or mistrafficking (Vps^{-} phenotype) can be scored qualitatively in solid media using a sucrose overlay solution, indicating glucose production by formation of a brown precipitate (Vps^{-} phenotype).

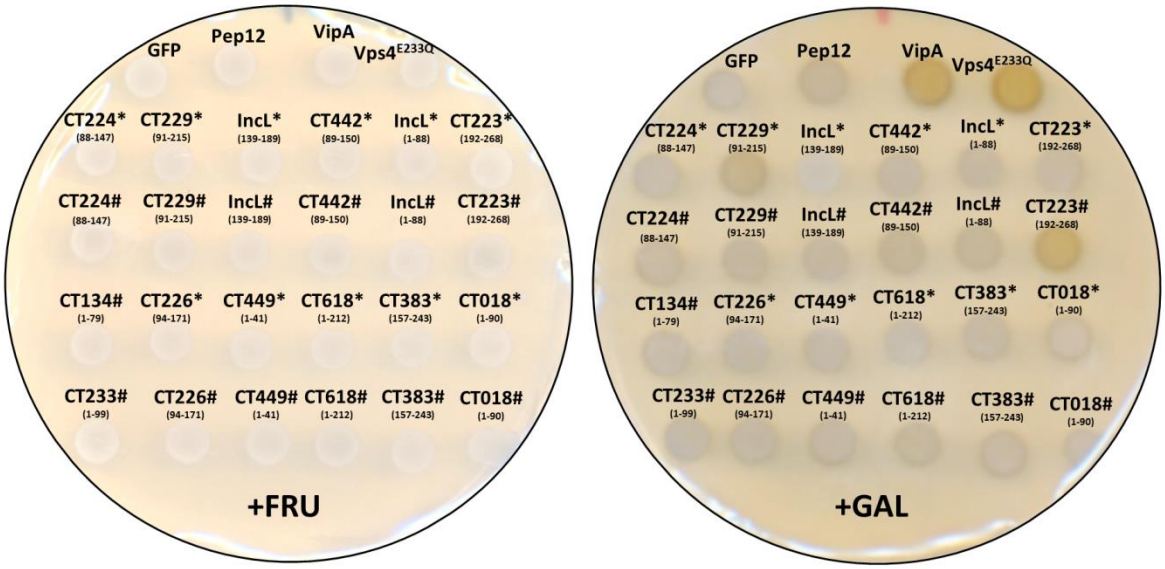

Figure 3.2 ***C. trachomatis*** **Incs cause vacuolar protein sorting mistrafficking in yeast.** Representative results from the Vps assay in yeast. *S. cerevisiae* strains encoding the indicated Inc fragments were grown in solid media under inducing (galactose; +GAL) or non-inducing (fructose; +FRU) conditions. After 48 h, the Vps phenotype was analyzed qualitatively in solid media. Two fusion proteins containing Inc fragments caused a Vps^- phenotype: $CT229_{91\text{-}215}$-GFP and $CT223_{192\text{-}268}$-GFP-$Pep12_{L\text{-}TM}$. GFP and GFP-$Pep12_{L\text{-}TM}$ were used as negative controls (Vps^+ phenotype) and a fusion to GFP of the *Legionella pneumophila* effector VipA (VipA-GFP) (Franco *et al.*, 2012) and the dominant-negative form of yeast ATPase Vps4 ($Vps4^{E233Q}$) (Shohdy *et al.*, 2005) were used as positive controls (Vps^- phenotype). * Represents Inc fragments fused to GFP and # represents Inc fragments fused to GFP-$Pep12_{L\text{-}TM}$. Vps results with all yeast strains analyzed are shown in Annexes Figures A.3 and A.4 and summarized in Tables 3.1 and 3.2.

3.1.2 *C. trachomatis* Incs co-localize with yeast organelles

To screen for *C. trachomatis* Incs targeting eukaryotic organelles, we analyzed the intracellular localization of Inc-GFP fusion proteins in yeast, on the assumption that their tropism for eukaryotic organelles could give insights about their functions. As depicted in Table 3.1, we were able to detect 19 Inc-GFP fusion proteins (out of 31) by fluorescence microscopy. Among these 19 Inc-GFP proteins, 12 were found spread in the yeast cytosol similarly to GFP alone and 7 appeared in a specific intracellular localization, suggesting tropism for endosomal compartments ($CT229_{91\text{-}215}$-GFP), mitochondria ($CT179_{53\text{-}170}$-GFP, $CT324_{119\text{-}303}$-GFP, $CT618_{1\text{-}212}$-GFP, $CT018_{1\text{-}90}$-GFP and $CT383_{157\text{-}243}$-GFP) or LDs (CT006, renamed IncL for Inc associating with LDs; $IncL_{1\text{-}88}$-GFP) (examples in Figure 3.3a and summary in Table 3.1). GFP-$Pep12_{L\text{-}TM}$ and Inc-GFP-$Pep12_{L\text{-}TM}$ fusion proteins localized predominantly at endosomal compartments, such as endosome-like puncta and vacuoles

(examples in Figure 3.3b and summary in Table 3.2), as previously described (Black & Pelham, 2000; Sisko *et al.*, 2006).

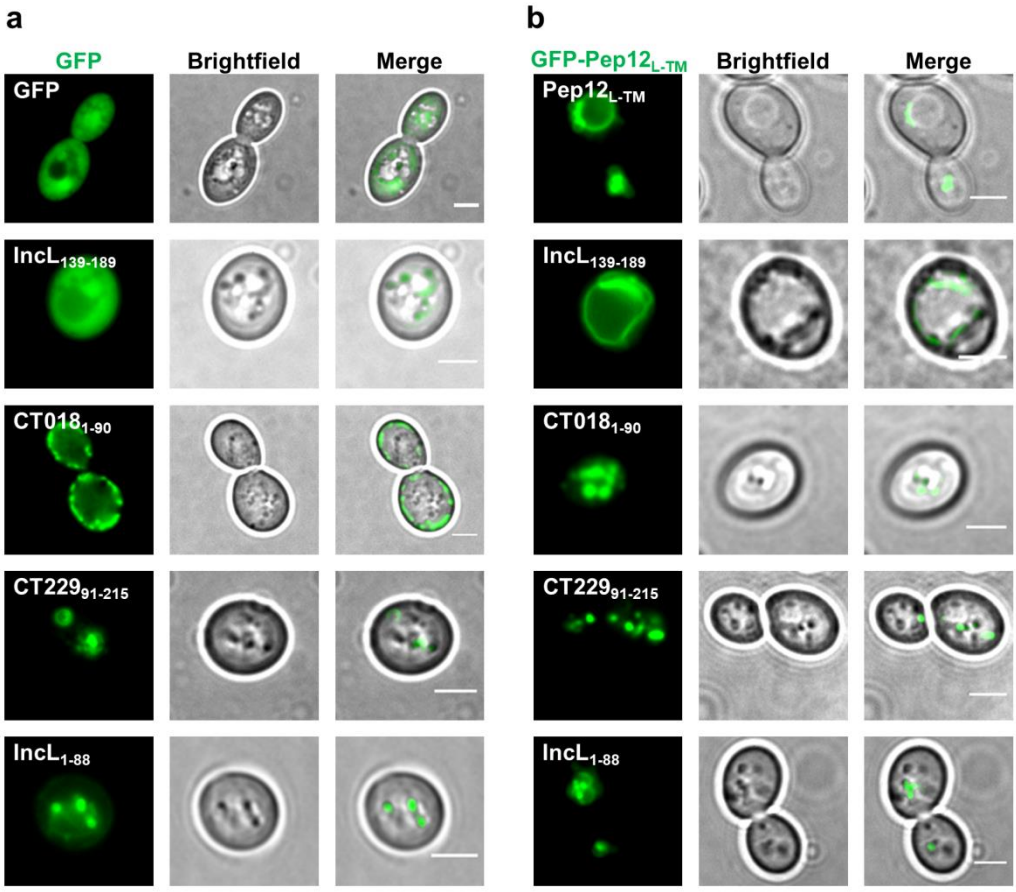

Figure 3.3 Intracellular localization of Inc-GFP and Inc-GFP-Pep12$_{L\text{-}TM}$ proteins in yeast. *S. cerevisiae* strains producing the indicated Inc-GFP proteins were grown in the presence of galactose. Live cells were visualized directly by fluorescence microscopy. Scale bars, 5 μm. (a) Examples for the intracellular localization of Inc-GFP proteins in yeast: cytosolic distribution (GFP and IncL$_{139\text{-}189}$-GFP), mitochondria-like puncta (CT018$_{1\text{-}90}$-GFP), endosomal compartments (CT229$_{1\text{-}215}$-GFP) and LDs (IncL$_{1\text{-}88}$-GFP). (b) Examples for the intracellular localization of Inc-GFP-Pep12$_{L\text{-}TM}$ proteins at endosomal compartments in yeast. The intracellular localization of all Inc-GFP and Inc-GFP-Pep12$_{L\text{-}TM}$ fusion proteins analyzed in this study is summarized in Tables 3.1 and 3.2.

Among the 5 Inc-GFP proteins that localized at mitochondria-like puncta, CT179$_{53\text{-}170}$-GFP and CT324$_{119\text{-}303}$-GFP migrated on SDS-PAGE according to their predicted molecular mass, while CT618$_{1\text{-}212}$-GFP, CT018$_{1\text{-}90}$-GFP and CT383$_{157\text{-}243}$-GFP migrated below their expected molecular mass (Annexes Figure A.1 and summary in Table 3.1). As the majority of mitochondrial matrix proteins contain an amino-terminal targeting signal that is cleaved upon import (Kunze & Berger, 2015), these differences might be due to differences in the length of the signal peptide that is cleaved.

To corroborate the observations on the localization of Incs in yeast, co-localization analyses by fluorescence microscopy between selected Inc-GFP proteins and organelle markers were performed. A yeast strain ectopically producing CT179$_{53\text{-}170}$-GFP was stained with MitoRed, a mitochondrial probe, which showed co-localization of CT179$_{53\text{-}170}$-GFP with mitochondria (Figure 3.4a). A yeast strain producing CT229$_{91\text{-}215}$-GFP, which induced a vacuolar protein traffic defect in yeast (Figure 3.2), was incubated with FM4-64 (a fluorescent endocytic probe). This showed that CT229$_{91\text{-}215}$-GFP co-localizes with endosomal compartments (Figure 3.4b).

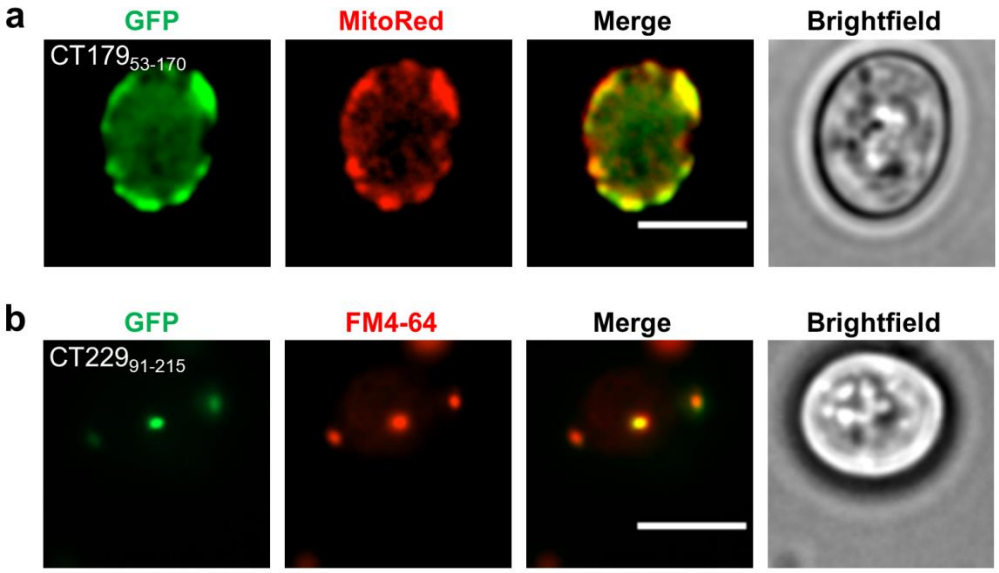

Figure 3.4 Co-localization analyses between Inc-GFP proteins and mitochondria or endosomal compartments. *S. cerevisiae* strains ectopically expressing the genes encoding the indicated Inc-GFP fusion proteins were grown in the presence of galactose. Live cells were visualized by fluorescence microscopy, directly or after the indicated staining. (a) Yeast strains producing CT179$_{53\text{-}170}$-GFP were stained with MitoRed, a mitochondrial probe, indicating that CT179$_{53\text{-}170}$-GFP co-localizes with mitochondria. (b) Yeast strains producing CT229$_{91\text{-}215}$ were incubated with FM4-64 and CT229$_{91\text{-}215}$ co-localized with FM4-64-stained endosomal compartments.

Finally, to test if IncL$_{1\text{-}88}$-GFP localized at LDs, we generated a yeast strain co-producing Erg6-mCherry (protein marker for LDs) (Khaddaj *et al.*, 2021) and IncL$_{1\text{-}88}$-GFP. This confirmed that IncL$_{1\text{-}88}$-GFP co-localizes with LDs (Figure 3.5). We also analyzed yeast strains co-producing Erg6-mCherry and GFP or IncL$_{139\text{-}189}$-GFP, which revealed that IncL$_{139\text{-}189}$-GFP has a cytosolic localization as GFP alone (Figure 3.5).

In summary, we found seven *C. trachomatis* Inc fragments associating with eukaryotic organelles. Five Incs associated with mitochondria but the relevance of this is unclear as a possible direct *C. trachomatis*-mitochondria interaction during infection has not been described. However, we found that IncL$_{1\text{-}88}$ localizes at LDs (Figure 3.5), which have been

shown to be targeted by several intracellular pathogens, including *C. trachomatis* [reviewed in (Roingeard & Melo, 2017)]. Therefore, we selected IncL for further characterization.

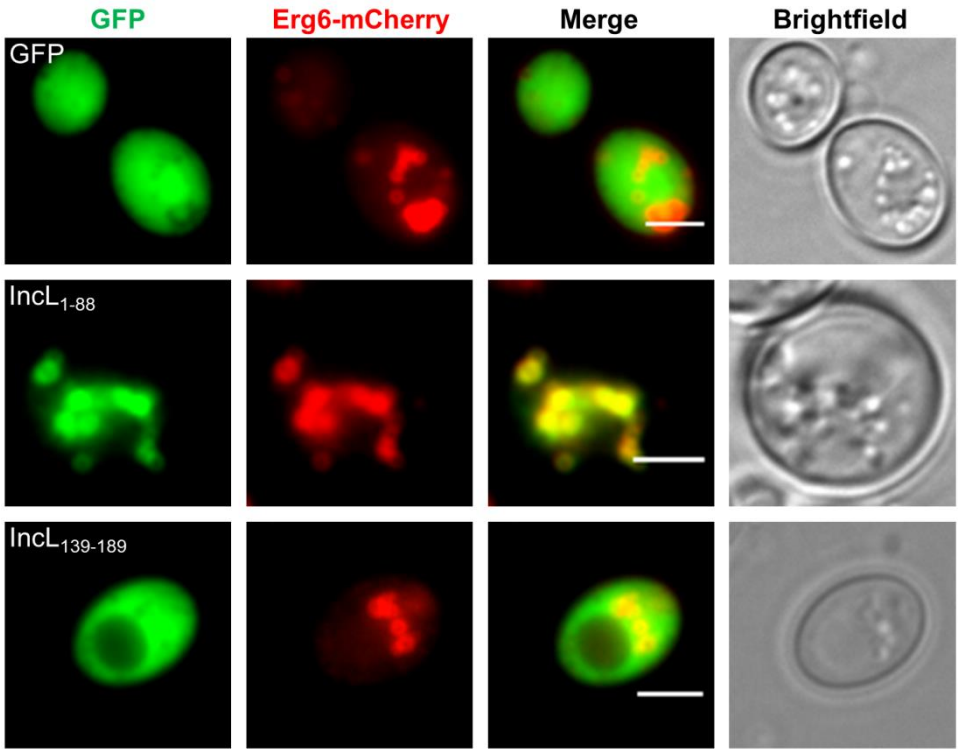

Figure 3.5 IncL$_{1-88}$-GFP localizes at LDs in yeast. *S. cerevisiae* strains ectopically co-expressing the genes encoding Erg6-mCherry (protein marker for lipid droplets) and GFP, IncL$_{1-88}$-GFP or IncL$_{139-189}$-GFP and were grown in the presence of galactose and live cells were visualized directly by fluorescence microscopy. Scale bar 5 μm. IncL$_{139-189}$-GFP was distributed in the yeast cytosol, similarly to GFP alone, while IncL$_{1-88}$-GFP co-localized with Erg6-mCherry, a protein marker for LDs.

Table 3.1 Inc-GFP fusion proteins - summary of production and localization in *S. cerevisiae*, and induction of a vacuolar protein sorting (Vps) defect.

Inc (aa-aa)	Produced	Subcellular localization	Vps defect
CT249 (1-50)	Yes	Cytosolic	No
CT134 (1-79)	No	Not detected	No
CT618 (1-212)	Below Mw	Mitochondria-like puncta	No
CT224 (88-147)	Yes	Cytosolic	No
CT228 (87-196)	No	Not detected	No
CT229 (91-215)	Yes	Endosomes	Yes
IncL (139-189)	Yes	Cytosolic	No
CT018 (1-90)	Below Mw	Mitochondria-like puncta	No
CT135 (269-360)	No	Not detected	No
CT225 (67-122)	Yes	Not detected	No
CT226 (94-171)	Yes	Not detected	No
CT227 (89-133)	Yes	Cytosolic	No
CT324 (1-74)	Yes	Not detected	No
CT383 (1-103)	No	Not detected	No
CT383 (157-243)	Below Mw	Mitochondria-like puncta	No
CT442 (89-150)	Yes	Cytosolic	No
CT449 (1-41)	Yes	Cytosolic	No
CT813 (95-264)	Yes	Not detected	No
CT837 (593-568)	Yes	Not detected	No
CT119 (57-246)	Yes	Cytosolic	No
CT115 (112-160)	Yes	Cytosolic	No
CT116 (88-132)	Yes	Cytosolic	No
CT118 (89-167)	Yes	Cytosolic	No
IncL (1-88)	Yes	Lipid droplets	No
CT135 (1-209)	No	Not detected	No
CT192 (82-231)	Yes	Cytosolic	No
CT223 (192-268)	Yes	Not detected	No
CT223 (92-268)	Yes	Not detected	No
CT324 (119-303)	Yes	Mitochondria-like puncta	No
CT556 (1-99)	Yes	Cytosolic	No
CT233 (1-99)	Not tested	Not tested	Not tested
CT179 (53-170)	Yes	Mitochondria-like puncta	No

Table 3.2 Inc-GFP-Pep12$_{L\text{-}TM}$ fusion proteins - summary of production and localization in *S. cerevisiae,* and induction of a vacuolar protein sorting (Vps) defect.

Inc (aa-aa)	Produced	Subcellular localization	Vps defect
CT249 (1-50)	Yes	Puncta	No
CT134 (1-79)	No	Puncta	No
CT618 (1-212)	Below Mw	Puncta	No
CT224 (88-147)	Yes	Vacuoles+puncta	No
CT228 (87-196)	Yes	Puncta	No
CT229 (91-215)	Yes	Puncta	No
IncL (139-189)	Yes	Vacuoles+puncta	No
CT018 (1-90)	Yes	Puncta	No
CT135 (269-360)	No	Not detected	No
CT225 (67-122)	Yes	Vacuoles+puncta	No
CT226 (94-171)	Yes	Vacuoles+puncta	No
CT227 (89-133)	Yes	Puncta	No
CT324 (1-74)	Yes	Vacuoles+puncta	No
CT383 (1-103)	Yes	Puncta	No
CT383 (157-243)	Yes	Puncta	No
CT442 (89-150)	Yes	Vacuoles+puncta	No
CT449 (1-41)	Yes	Vacuoles+puncta	No
CT813 (95-264)	Not tested	Not tested	No
CT837 (593-568)	Yes	Not detected	No
CT119 (57-246)	Yes	Not detected	No
CT115 (112-160)	Yes	Vacuoles	No
CT116 (88-132)	Yes	Vacuoles	No
CT118 (89-167)	Yes	Vacuoles	No
IncL (1-88)	Yes	Vacuoles+puncta	No
CT135 (1-209)	No	Not detected	Not tested
CT192 (82-231)	Yes	Vacuoles+puncta	No
CT223 (192-268)	Yes	Puncta	Yes
CT223 (92-268)	Yes	Puncta	Yes
CT324 (119-303)	Below Mw	Puncta	No
CT556 (1-99)	Yes	Puncta	No
CT179 (53-170)	Yes	Puncta	No

3.1.3 The first 88 amino acid residues of IncL fused to mEGFP co-localize with LDs in mammalian cells

The primary structure of CT006/IncL (189 amino acid residues; Figure 3.6) does not display significant similarities to known non-chlamydial proteins or domains. IncL has a predicted bilobed hydrophobic motif, characteristic of Incs, between a tyrosine residue at position 89 (Y_{89}) and a histidine residue at position 140 (H_{140}) (Dehoux *et al.*, 2011), which is composed of two transmembrane segments separated by a loop of 6 residues (Figures 3.6 and 3.7). IncL is predicted to have an additional hydrophobic and putative transmembrane domain between a glycine residue at position 47 (G_{47}) and a phenylalanine residue at position 69 (F_{69}) (Figures 3.6 and 3.7). To test whether IncL localizes at LDs in mammalian cells, HeLa 229 cells were transfected with plasmids encoding full length IncL ($IncL_{FL}$), its first 88 amino acid residues ($IncL_{1-88}$), or its last 51 amino acid residues ($IncL_{139-189}$) fused to the amino- or carboxy-terminus of monomeric enhanced green fluorescent protein (mEGFP) (Figure 3.6).

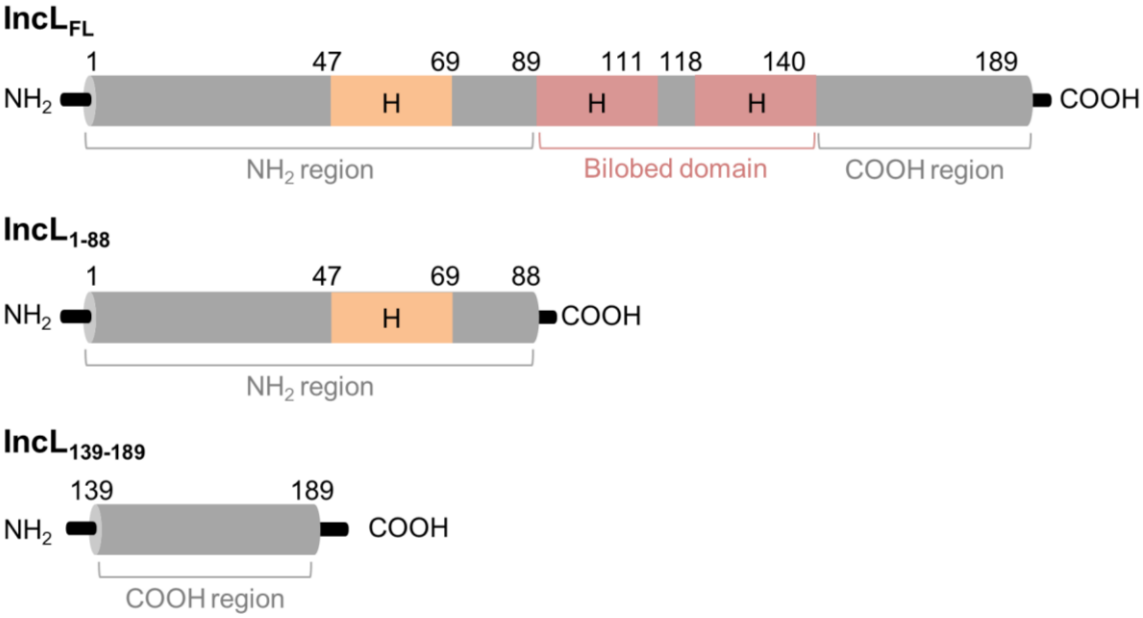

Figure 3.6 Schematic representation of *C. trachomatis* IncL. Full length IncL ($IncL_{FL}$) is composed of 189 amino acid residues. IncL has a predicted bilobed hydrophobic (H) motif between tyrosine residues at positions 89 (Y_{89}) and 140 (H_{140}), which is composed of two transmembrane segments separated by a loop of 6 residues (Dehoux *et al.*, 2011). In addition, IncL is predicted to have a hydrophobic and putative transmembrane domain between a glycine residue at position 47 (G_{47}) and a phenylalanine residue at position 69 (F_{69}). To analyse the intracellular localization of IncL in mammalian cells, we generated plasmids encoding $IncL_{FL}$, its first 88 amino acid residues ($IncL_{1-88}$) or its last 51 amino acid residues ($IncL_{139-189}$) fused to the amino or carboxy-terminus of mEGFP.

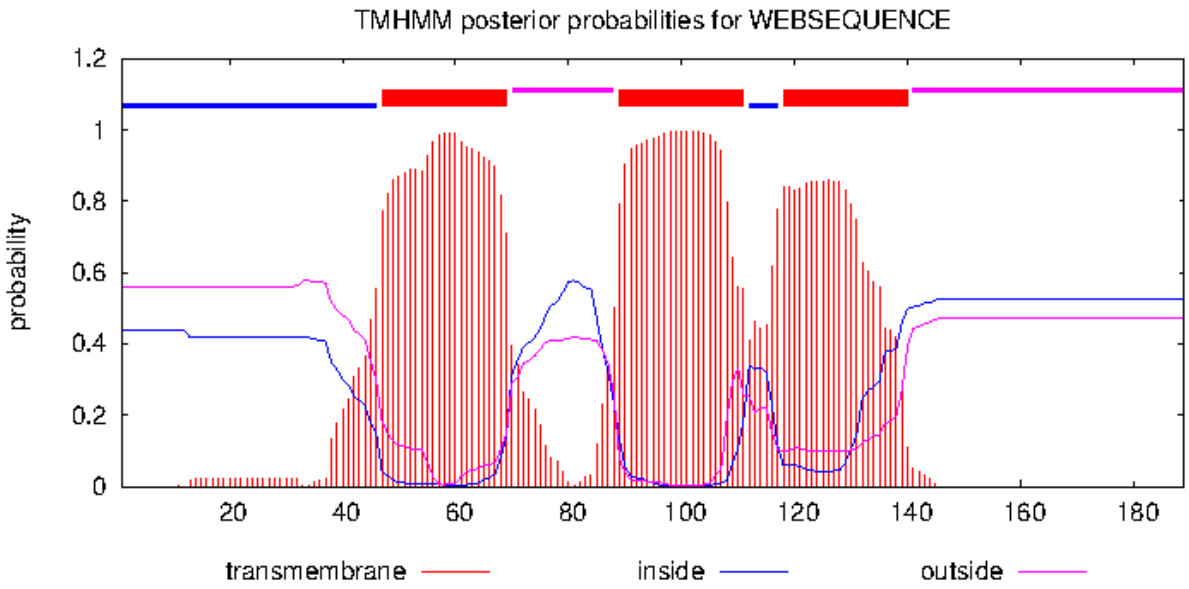

Figure 3.7 Prediction of transmembrane helices in IncL. According to TMHMM server, v 2.0 (Krogh *et al.*, 2001; Sonnhammer & Krogh, 1998), IncL is predicted to have 3 transmembrane domains between amino acid residues 47 and 69, 89 and 111, and 118 and 140. The positions of the last two hydrophobic motifs are approximately in agreement with the prediction of the bilobed hydrophobic motif described by Dehoux *et al*, 2011 (Dehoux *et al.*, 2011).

Fluorescence microscopy analysis revealed that the intracellular localization of IncL proteins fused to mEGFP is independent of the position of the mEGFP tag (Figure 3.8a). Immunoblotting of whole cell extracts from the transfected cells confirmed the production of fusion proteins with the predicted molecular mass, but revealed less degradation products for mEGFP-IncL versions comparing with IncL-mEGFP versions (Figure 3.8b). Therefore, subsequent analyses were performed with mEGFP-IncL versions. mEGFP-IncL$_{139\text{-}189}$ was not further analyzed, because it showed a cytosolic distribution as mEGFP alone (Figure 3.8a).

As HeLa 229 cells are poor in LDs, in our experiments LDs synthesis was induced by the addition of 100 μM of oleic acid (Cocchiaro *et al.*, 2008). Briefly, HeLa cells ectopically expressing the genes encoding mEGFP, mEGFP-IncL$_{FL}$ or mEGFP-IncL$_{1\text{-}88}$ were either incubated with the ethanol solvent alone (Figure 3.9a; left-hand side panel) or with 100 μM oleic acid (Figure 3.9a; right-hand side panel) for 6 h before fixation. The LDs were stained with the neutral lipid dye Oil Red O and the cells were analyzed by fluorescence microscopy. As expected, the incubation with oleic acid increased the number and size of LDs in HeLa cells, comparing with cells incubated only with the solvent (Figure 3.9a). The mEGFP-IncL$_{FL}$ protein did not co-localize with LDs, but instead it showed inconsistent localizations within cells, including a reticular distribution and an accumulation in puncta and patches in the cytosol and also near the plasma membrane (Figure 3.9a). Moreover, the localization of

mEGFP-IncL$_{FL}$ remained unaltered regardless of the incubation with oleic acid (Figure 3.9a). In contrast, the mEGFP-IncL$_{1-88}$ protein besides retaining some reticular distribution, partially appeared as circles surrounding Oil Red O-stained LDs (Figure 3.9a). Incubation with oleic acid led to an increase in number and size of LDs in all cells examined (Figure 3.9a), and, as shown in the zoomed images in Figure 3.9b, changed the localization of mEGFP-IncL$_{1-88}$ from small to large circles, all surrounding Oil Red O-stained LDs (Figure 3.9b).

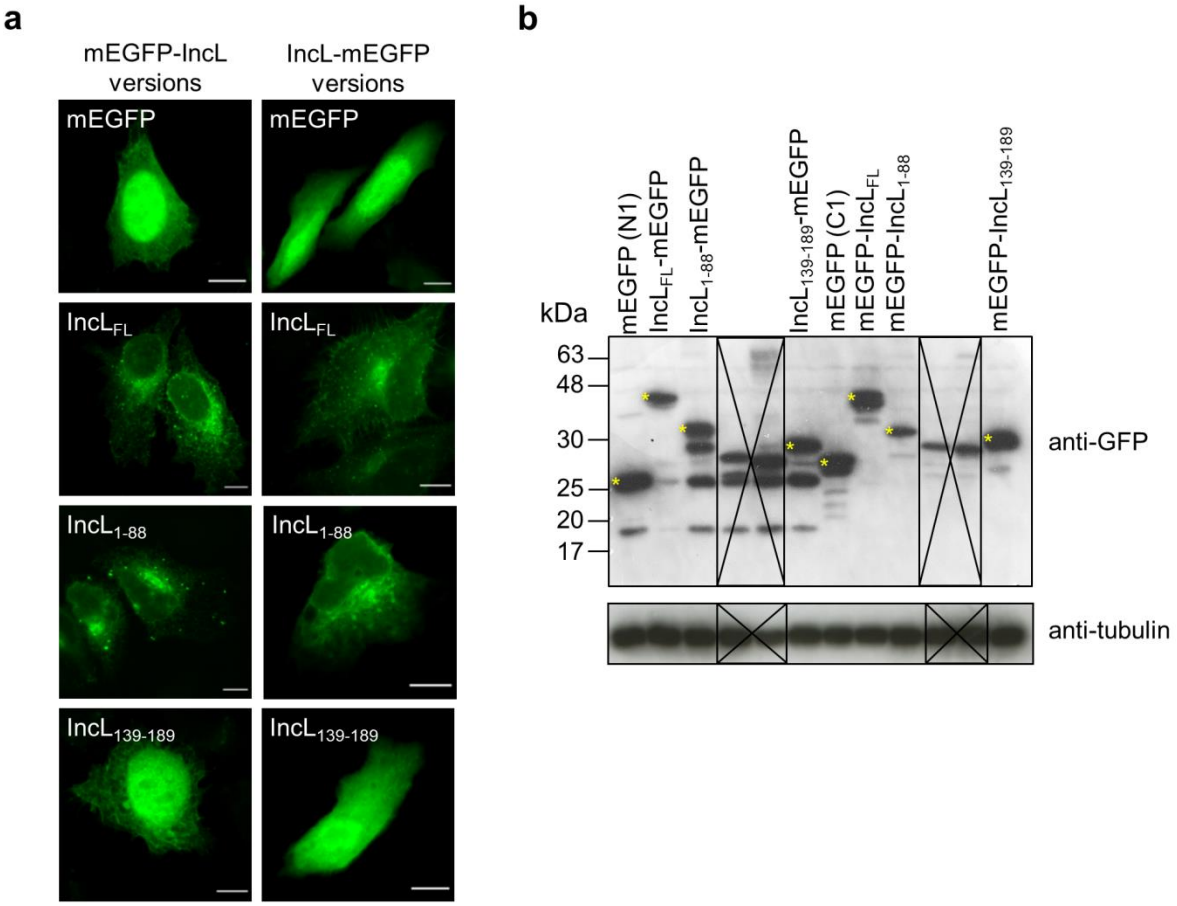

Figure 3.8 Analysis of the production and intracellular localization of IncL versions in mammalian cells. HeLa 229 cells were transfected for 24 h with plasmids encoding mEGFP or the indicated versions of IncL containing a mEGFP tag at their amino-termini (mEGFP-IncL proteins) or at their carboxy-termini (IncL-mEGFP proteins). (a) Transfected cells were fixed with 4% (w/v) PFA and imaged by fluorescence microscopy. Scale bars, 10 μm. (b) Whole cell extracts were analyzed by immunoblotting with antibodies against GFP and α-tubulin (HeLa 229 cells loading control) and appropriate HRP-conjugated secondary antibodies. Proteins were detected using SuperSignal West Pico detection kit (Thermo Fisher Scientific). The crosses in (b) correspond to proteins that were not analyzed in this study.

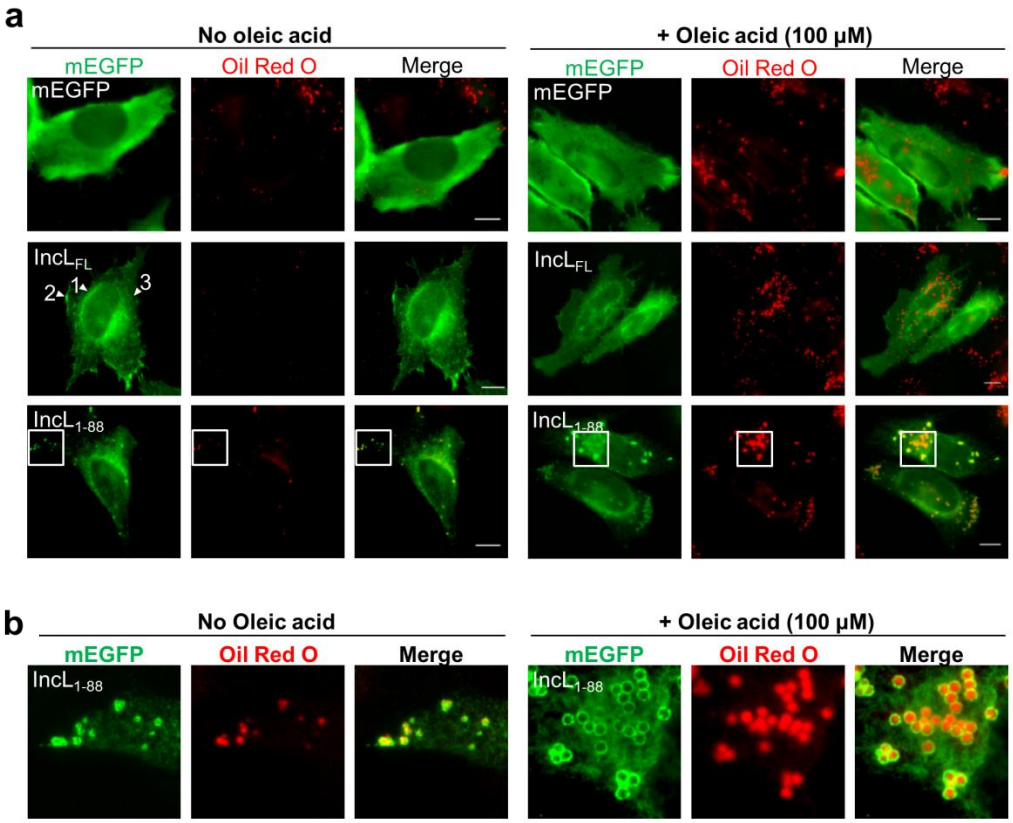

Figure 3.9 The first 88 amino acid residues of IncL fused to mEGFP co-localize with LDs in mammalian cells. HeLa 229 cells were transfected with plasmids encoding mEGFP or different regions of IncL containing a mEGFP tag at their amino-termini (mEGFP-IncL proteins). (a) At 18 h post-transfection, cells were either treated with ethanol (solvent control; left-hand side panel) or 100 µM oleic acid (right-hand side panel) for 6 h and then fixed with 4% (w/v) PFA. Fixed cells were labeled with anti-GFP and the appropriate fluorophore-conjugated secondary antibody, stained with Oil Red O (3:2 v/v Oil Red O stock solution diluted in water), and imaged by fluorescence microscopy. Scale bars, 10 µm. Arrowheads indicate the reticular distribution of mEGFP-IncL$_{FL}$ (1) and the accumulation in patches near the plasma membrane (2) or cytosol (3). (b) In the area delimited by white squares (Figure 3.9a) images were zoomed.

To clarify the reticular distribution of IncL, HeLa cells producing mEGFP-IncL$_{FL}$ or mEGFP-IncL$_{1-88}$ were immunolabeled with an antibody against protein disulfide isomerase (PDI), a protein marker for the endoplasmic reticulum (ER). This analysis revealed that both proteins partially co-localize with the ER (Figure 3.10).

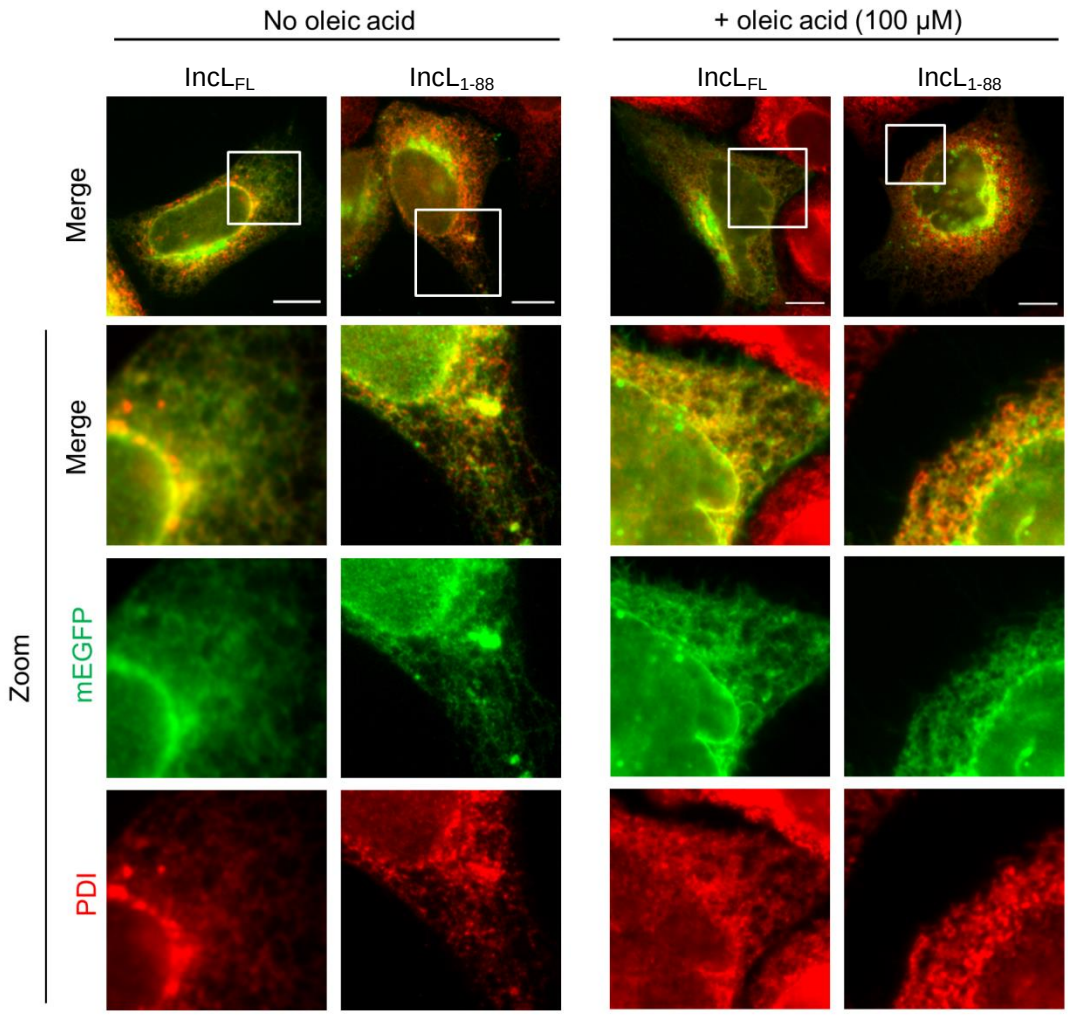

Figure 3.10 Full-length IncL and IncL$_{1-88}$ fused to mEGFP partially co-localize with the ER in mammalian cells. HeLa 229 cells were transfected with plasmids encoding mEGFP or the indicated versions of IncL containing a mEGFP tag at their amino-termini (mEGFP-IncL proteins). After 18 h, cells were treated ethanol (solvent control; left-hand side panel) or 100 µM oleic acid (right-hand side panel) for 6 h and fixed with 4% (w/v) PFA. Fixed cells were immunolabeled with an antibody against Protein disulfide isomerase (PDI), a protein marker for the ER, and an appropriate fluorophore-conjugated secondary antibody, and imaged by fluorescence microscopy. Scale bars, 10 µm.

3.1.4 Positively charged amino acids within IncL$_{1-88}$ are essential to target mEGFP-IncL$_{1-88}$ to LDs in mammalian cells

It was previously shown that association of caveolin with LDs is mediated by two motifs acting cooperatively (Ingelmo-torres *et al.*, 2010). A central hydrophobic domain anchors caveolin to the ER and then positively charged amino acid residues mediate its sorting to LDs (Ingelmo-torres *et al.*, 2010). Therefore, we searched for positively charged residues near the putative hydrophobic domain in IncL$_{1-88}$ (Figures 3.6 and 3.7) and five

candidates were identified: two lysine residues (K_{34}, K_{37}) upstream from the hydrophobic domain and arginine, histidine, and lysine (R_{72}, H_{80}, K_{81}) residues localized downstream from the hydrophobic domain (Figure 3.11a). To test for a role of these residues in targeting $IncL_{1-88}$ to LDs, we generated mammalian transfection plasmids encoding mEGFP-$IncL_{1-88}$ versions where the identified residues were replaced in different combinations by neutral glycine residues (K34G, K37G; H80G, K81G; R72G, H80G, K81G; K34G, K37G, H80G, K81G; or K34G, K37G, R72G, H80G, K81G). After transfection of HeLa cells with these plasmids we confirmed by immunoblotting that the mutant proteins were produced and migrated on SDS-PAGE according to their predicted molecular mass (Figure 3.11b).

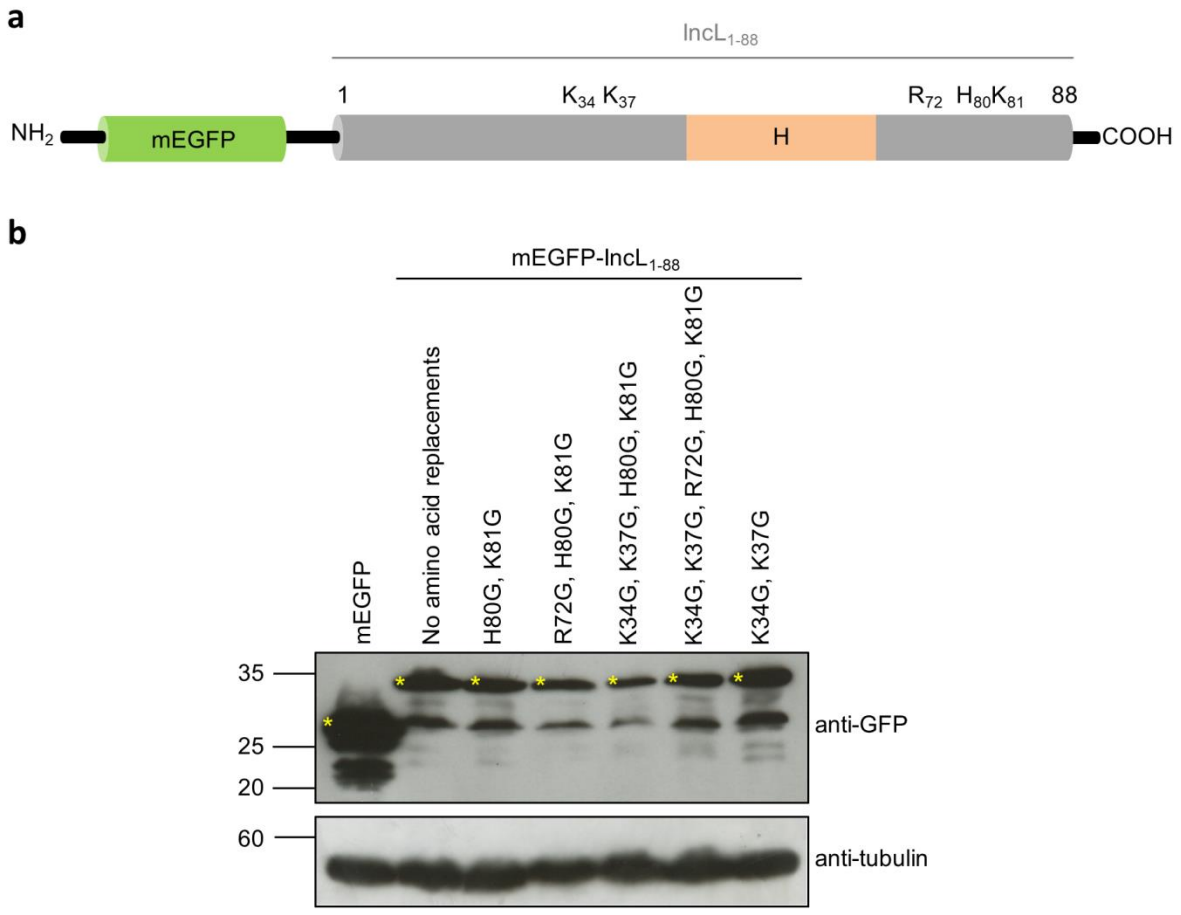

Figure 3.11 Analysis of the production of mEGFP-$IncL_{1-88}$ versions with positively charged amino acids replaced by glycines in mammalian cells. (a) Schematic representation of the position of five positively charged amino acids within $IncL_{1-88}$ (not drawn to scale); H, Hydrophobic domain. (b) HeLa 229 cells were transfected for 24 h with plasmids encoding mEGFP or the indicated versions of $IncL_{1-88}$ containing a mEGFP tag at their amino-termini. Whole cell extracts were analyzed by immunoblotting with antibodies against GFP and α-tubulin (HeLa 229 cells loading control) and appropriate HRP-conjugated secondary antibodies. Proteins were detected using SuperSignal West Pico detection kit (Thermo Fisher Scientific).

For fluorescence microscopy analysis, HeLa cells producing mEGFP, mEGFP-IncL$_{1-88}$ or mEGFP-IncL$_{1-88}$ variants with amino acid replacements were incubated with oleic acid to induce LD synthesis. The cells were then fixed, stained with Oil Red O and analyzed by fluorescence microscopy. The substitutions for glycines of $K_{34}K_{37}$, $H_{80}K_{81}$ or $K_{34}K_{37}H_{80}K_{81}$ resulted in mutant proteins localizing at LDs as mEGFP-IncL$_{1-88}$ (Figure 3.12). When the three positively charged amino acid residues ($R_{72}H_{80}K_{81}$) downstream from the hydrophobic domain were replaced by glycines, the protein became predominantly reticulated, but still retained some tropism for LDs. In contrast, when the five positively charged amino acid residues ($K_{34}K_{37}R_{72}H_{80}K_{81}$) were simultaneously replaced by glycines, the mutant protein showed almost solely a reticular distribution without defined circles surrounding LDs (Figure 3.12), suggesting that its sorting to LDs was substantially reduced. This analysis revealed that positively charged sequences close to the amino-terminal hydrophobic domain of IncL (Figure 3.11a) are important to target mEGFP-IncL$_{1-88}$ to LDs.

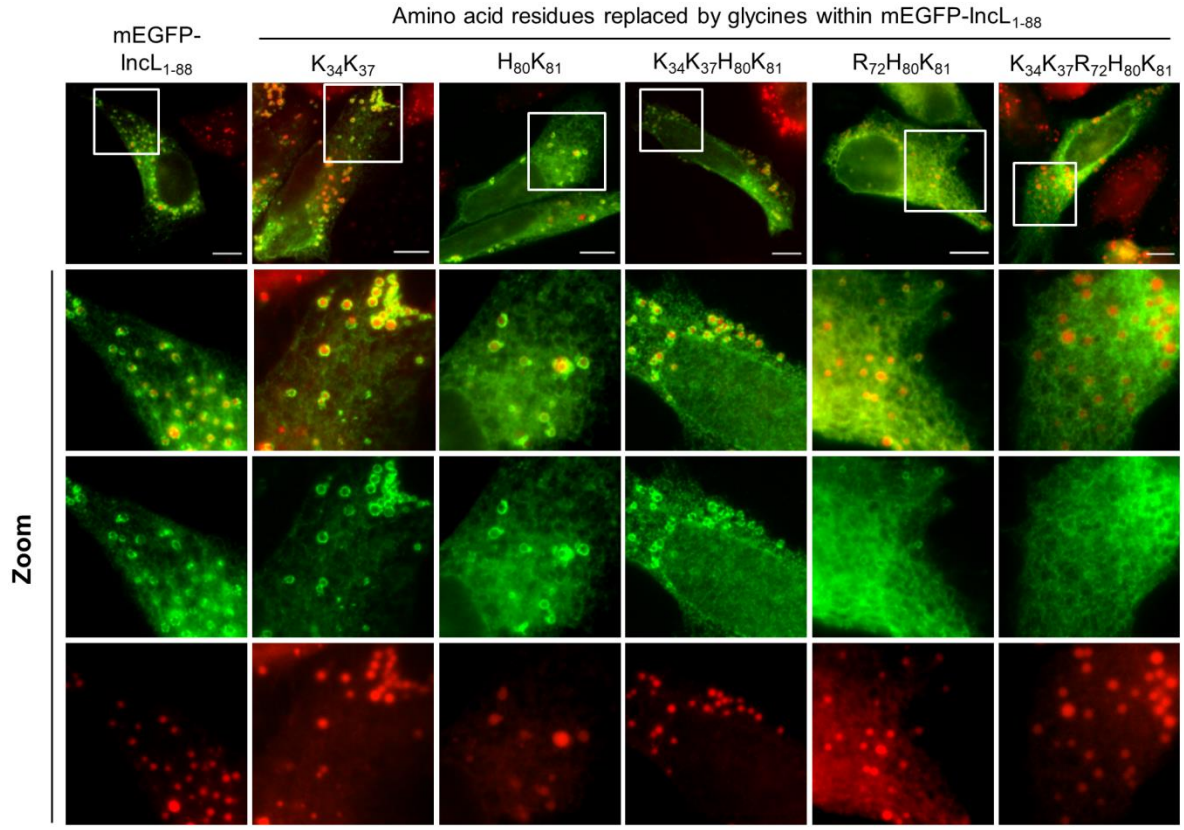

Figure 3.12 Positively charged amino acids within IncL$_{1-88}$ are important to target mEGFP-IncL$_{1-88}$ to LDs in mammalian cells. (a) Schematic representation of the position of positively charged amino acids within IncL$_{1-88}$ (not drawn to scale); H, Hydrophobic domain. (b) HeLa 229 cells were transfected with plasmids encoding mEGFP or different mEGFP-IncL$_{1-88}$ versions where the indicated amino acid residues were replaced by glycines (G). At 18 h post-transfection, cells were treated with 100 μM oleic acid for 6 h and then fixed with 4% (w/v) PFA. Fixed cells were labeled with anti-GFP and the appropriate fluorophore-conjugated secondary antibody, stained with Oil Red O (3:2 v/v Oil Red O stock solution diluted in water), and imaged by fluorescence microscopy. Scale bars, 10 μm. In the areas delimited by white squares images were zoomed.

3.2 IncL-2HA produced by *C. trachomatis* slightly increases the area of LDs at the region of inclusions

We found that the amino-terminal region of IncL localizes at LDs when transiently produced in mammalian cells, which suggests that IncL produced by *C. trachomatis* could have an important role in mediating the interaction between chlamydial inclusions and LDs. To give insights about the role of IncL during infection of tissue culture cells by *C. trachomatis*, we attempted to generate a chlamydial *incL* null mutant by group II intron-based insertional mutagenesis (Johnson & Fisher, 2013) or fluorescence-reported allelic exchange mutagenesis (FRAEM) (Mueller *et al.*, 2016), but after several attempts none of these approaches was successful. In addition, an anti-IncL antibody for fluorescence microscopy analyses is not currently available. To overcome these constraints and to be able to study IncL during *C. trachomatis* infection, we generated *C. trachomatis* L2/434 strains producing plasmid-encoded IncL with different epitope tags and analyzed the topology of IncL at the inclusion membrane and the effects caused by the overproduction of IncL during infection.

3.2.1 The putative cytosolic regions of IncL are exposed to the host cell cytosol

As the first 88 amino acids of IncL can mediate an association with LDs when this fragment is ectopically produced in eukaryotic cells, we sought to understand if this region of the protein is exposed to the host cytosol in infected cells. For this, we used *C. trachomatis* strains producing IncL or control proteins tagged with a 13-residue phosphorylatable peptide from glycogen synthase kinase (GSK)3β (Garcia *et al.*, 2006). This peptide is derived from GSK3β and when fused to bacterial proteins has been used to identify chlamydial and other bacterial effectors and to confirm the cytosolic exposure of Incs (Bauler & Hackstadt, 2014; Garcia *et al.*, 2006; Yanatori *et al.*, 2021). The GSK tag is phosphorylated by cytosolic eukaryotic protein kinases, allowing to use immunoblotting with phospho-specific GSK antibodies as indicative of protein localization outside of the chlamydial inclusion. Therefore, we transformed *C. trachomatis* serovar L2 strain 434/Bu (L2/434) with plasmids encoding different versions of IncL tagged with GSK under the control of the *incL* promoter. Specifically, to test if the carboxy-terminal region of IncL was exposed to the cell cytosol, GSK was fused to IncL after the last amino acid residue [IncL-GSK(189)]. As tagging GSK to the amino-terminus of IncL should interfere with the T3S signal, to test the localization of the amino-terminal region we generated *C. trachomatis* strains harboring fusion proteins with GSK integrated upstream from the putative hydrophobic domain between amino acid

residues 47 and 69 (Figures 3.6 and 3.7), specifically after the first 26 [IncL-GSK(26)] or 39 [IncL-GSK(39)] amino acid residues of IncL. *C. trachomatis* L2/434-derived strains producing the *C. trachomatis* ribosomal protein CT317/RplJ or the *C. trachomatis* T3S effector CteG (Pais *et al.*, 2019) with a carboxy-terminal GSK tag (RplJ-GSK or CteG-GSK) were generated and used as negative or positive control, respectively. The genes encoding RplJ-GSK or CteG-GSK were expressed under the control of the tetracycline inducible *tet* promoter.

HeLa cells were then infected with the different *C. trachomatis* L2/434-derived strains encoding GSK-tagged chlamydial proteins. After 24 h, infected cells were harvested and analyzed by immunoblotting using antibodies against total GSK (anti-GSK3β) or against phosphorylated GSK (anti-pGSK3β). Detection with the anti-GSK3*β* antibody revealed production of RplJ-GSK, CteG-GSK, IncL-GSK(189) and IncL-GSK(26) (Figures 3.13a). In contrast, IncL-GSK(39) could not be detected (Figure 3.13a) indicating that this tagged protein is likely unstable. Immunoblotting using anti-pGSK3β revealed the expected phosphorylation of CteG-GSK (Figure 3.13a), indicative of localization in the host cell cytosol, and lack of phosphorylation of RplJ-GSK (Figure 3.13a), confirming its retention within the inclusion, presumably inside bacteria. The results with these controls confirmed the validity of the assay. As IncL-GSK(189) and IncL-GSK(26) were both detected by the anti-pGSK3β antibody (Figure 3.13a), both the amino and the carboxy termini of IncL are exposed to the host cell cytosol, outside of the inclusion. By indirect immunofluorescence microscopy using anti-pGSK3β antibodies we further showed that both IncL-GSK(189) and IncL-GSK(26) concentrated at the inclusion membrane, while only background signal was detected for cells infected by L2/434 or by L2/434 producing RplJ-GSK (Figure 3.13b).

Altogether, these results indicate that the central bilobed hydrophobic domain of IncL mediates the insertion of IncL at the inclusion membrane, whereas its amino and carboxy-terminal regions are exposed to the host cell cytosol (Figure 3.13c). Therefore, the putative hydrophobic domain of IncL between amino acid residues 47 and 69 (Figures 3.6 and 3.7), should not cross the inclusion membrane (Figure 3.13c). Given its hydrophobicity, we speculate that this domain could insert in the leaflet of the inclusion membrane facing the host cell cytosol leaving one hydrophobic surface available to interact with LDs or with regions of the ER from where LDs originate.

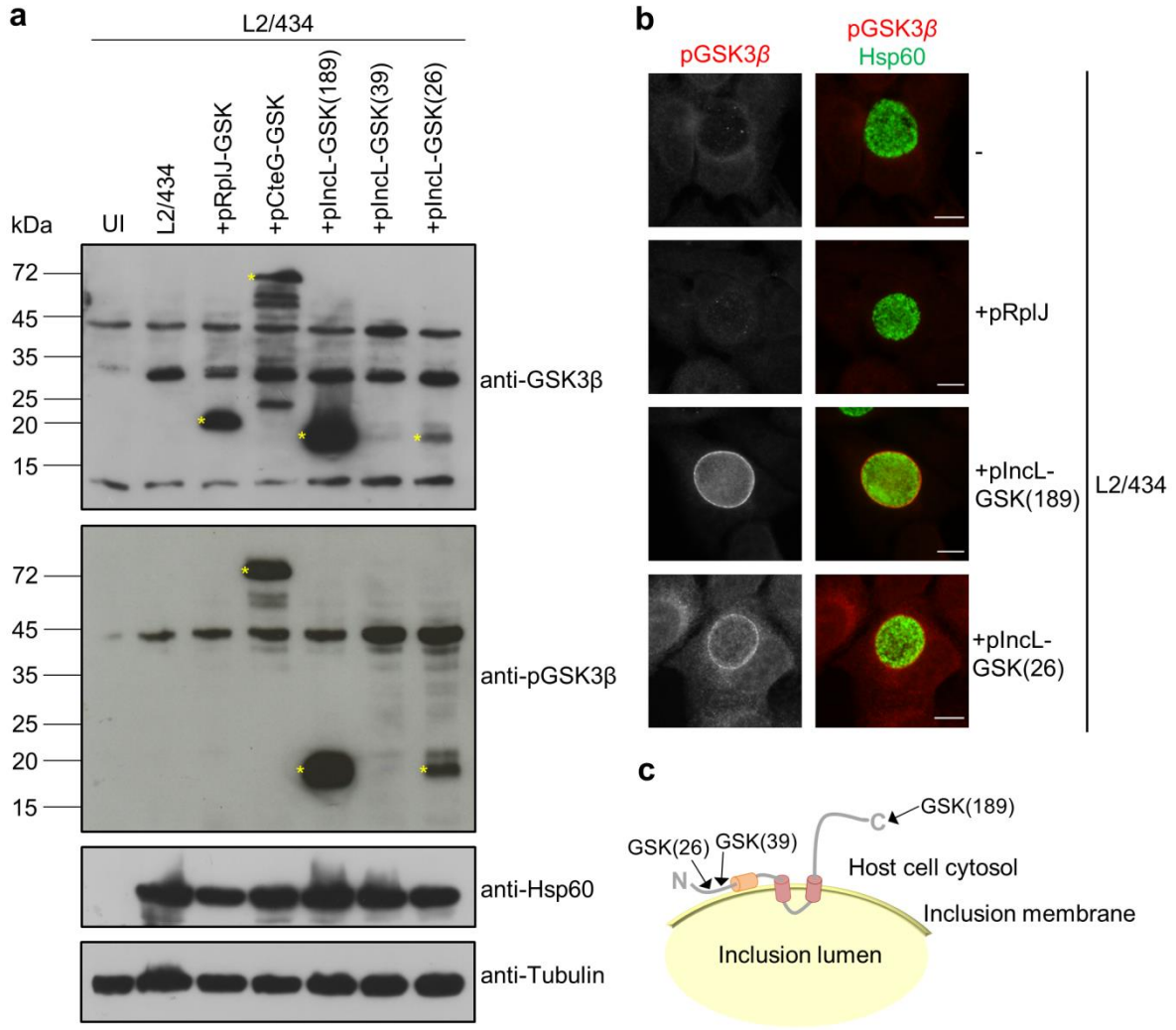

Figure 3.13 Analysis of the topology of IncL at the inclusion membrane. HeLa 229 cells were left uninfected (UI) or infected by *C. trachomatis* strains L2/434, L2/434+pRplJ-GSK, L2/434+pCteG-GSK, L2/434+pIncL-GSK(26), L2/434+pIncL-GSK(39) or L2/434+pIncL-GSK(189). (a) At 24 h post-infection, whole cell extracts were analyzed by immunoblotting using the antibodies anti-GSK3β, anti-pGSK3β, anti-*C. trachomatis* Hsp60 (bacterial loading control) and anti-α-tubulin (HeLa 229 cells loading control) and the appropriate HRP-conjugated secondary antibodies, followed by detection using SuperSignal West Femto (GSK and pGSK) or SuperSignal West Pico detection kit (Hsp60 and tubulin) (Thermo Fisher Scientific). (b) At 24 h post-infection, cells were fixed with 4% (w/v) PFA, immunolabeled with anti-pGSK3β (red) and anti-Hsp60 (green), and appropriate fluorophore-conjugated secondary antibodies. The labeled cells were then imaged by fluorescence microscopy. Scale bars, 10 μm. (c) Schematic representation of the deduced topology of IncL at the inclusion membrane. The arrows indicate the position where the GSK tag was fused. The analysis with the GSK tag showed that the putative hydrophobic domain of IncL between amino acid residues 47 and 69 (in orange) does not cross the inclusion membrane.

3.2.2 Characterization of IncL-2HA during *C. trachomatis* infection

To study IncL during *C. trachomatis* infection, we generated a *C. trachomatis* L2/434 strain harboring a plasmid encoding IncL with a double hemagglutinin (2HA) tag at its carboxy-terminus (pIncL-2HA) (L2/434+pIncL-2HA strain), under the control of the *incL* promoter. This strain produced IncL from the chromosome and IncL-2HA from an expression vector derived from the endogenous *C. trachomatis* virulence plasmid. Previous studies with other *C. trachomatis* T3S substrate genes (*ct142*, *ct143*, and *cteG*) expressed from the same backbone plasmid (pSVP247) (Da Cunha *et al.*, 2017; Pais *et al.*, 2019) reported a ~10-fold increase in total mRNA and protein levels relative to the endogenous genes and proteins. The levels of IncL-2HA in the L2/434+pIncL-2HA strain are thus expected to be much higher than of IncL in the L2/434 parental strain.

The *C. trachomatis* strain producing IncL-2HA was then characterized. Immunoblotting of extracts of infected HeLa cells revealed that IncL-2HA was detected from 16 to 44 hours post-infection and migrated on SDS-PAGE according to its predicted molecular mass (23 kDa) (Figure 3.14a). Indirect immunofluorescence microscopy of HeLa cells infected by L2/434+pIncL-2HA confirmed that IncL-2HA concentrates at the inclusion membrane and co-localizes with *C. trachomatis* Cap1 (known to localize at the inclusion membrane (Fling *et al.*, 2001) (Figure 3.14b). To investigate whether plasmid-encoded IncL-2HA could affect the intracellular growth of *C. trachomatis* in HeLa cells, the generation of infectious progeny and the area of the inclusions was compared between the parental and the L2/434+pIncL-2HA strains at 44 and 24 h post-infection, respectively. However, no significant differences were observed (Figure 3.14c and 3.14d), indicating that overproduction of IncL-2HA does not inhibit or promote *C. trachomatis* growth. Additional experiments where L2/434+pIncL-2HA was used to infect HeLa cells followed by analysis by indirect immunofluorescence microscopy, revealed that IncL-2HA was produced from 2 h post-infection and accumulated around the inclusion from at least 16 h post-infection (Figure 3.15). Furthermore, delivery of IncL-2HA into host cells could be detected from 2 h post-infection, while accumulation around the early inclusion was not always obvious (Figure 3.15). At 8 h post-infection IncL-2HA appeared in small tubules, which are a likely extension of the vacuolar membrane (Figure 3.15). Overall, this confirmed that IncL is a bona fide Inc, which is delivered into host cells at least from 2 h post-infection and accumulates at the inclusion membrane until late in the developmental cycle.

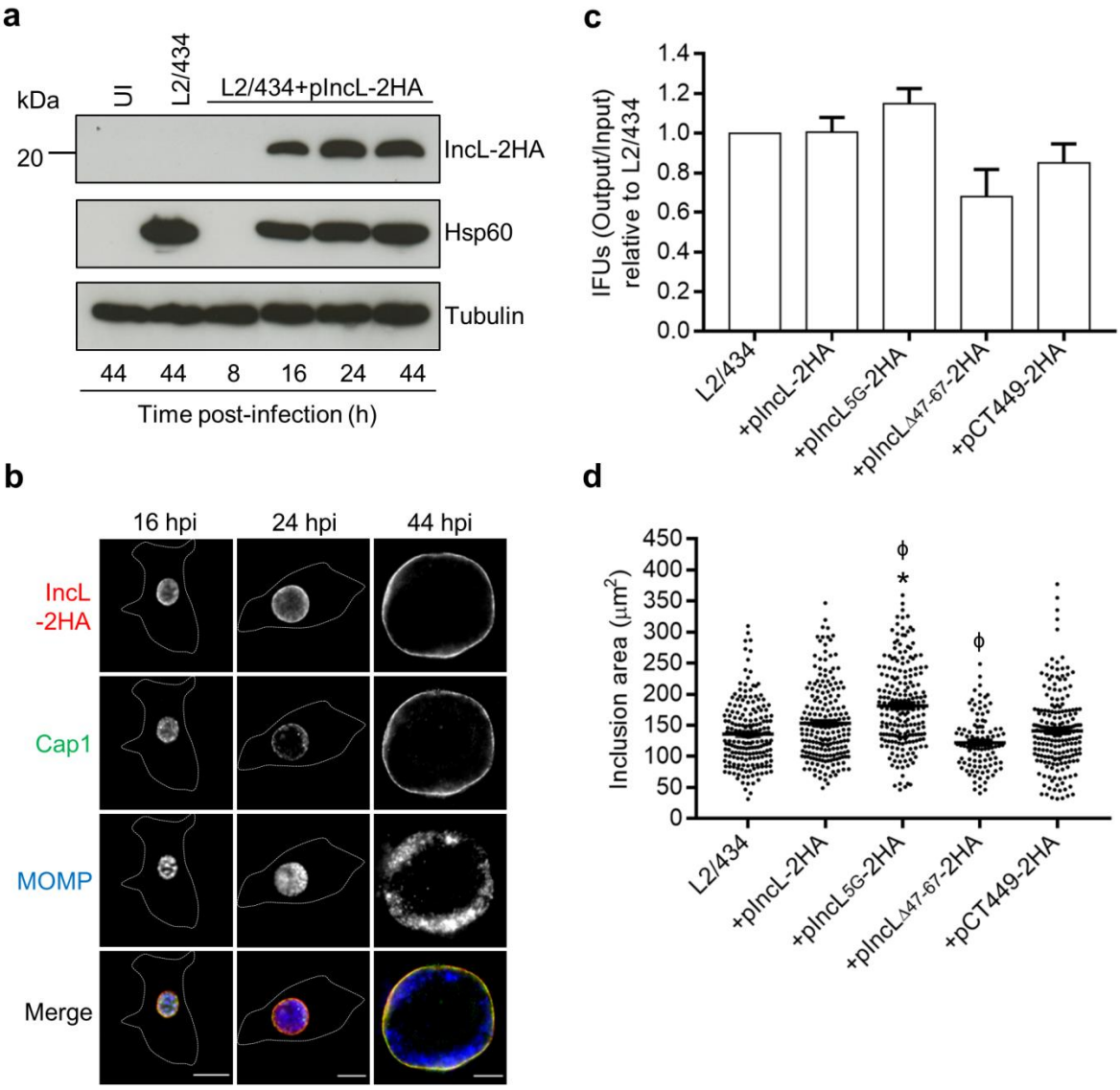

Figure 3.14 Characterization of *C. trachomatis* L2/434 strain harboring pIncL-2HA. HeLa 229 cells were left uninfected (UI) or infected by the *C. trachomatis* L2/434 parental strain or by *C. trachomatis* L2/434 strains harboring pIncL-2HA, pIncL$_{5G}$-2HA, pIncL$_{\Delta 47\text{-}67}$-2HA or pCT449-2HA. (a) At the indicated hours post-infection (hpi), whole cell extracts were analyzed by immunoblotting using antibodies against HA, Hsp60 (bacterial loading control) and α-tubulin (HeLa 229 cells loading control) and the appropriate HRP-conjugated secondary antibodies, followed by detection using SuperSignal West Pico detection kit (Thermo Fisher Scientific). (b) At the indicated hpi, infected cells were fixed with 4% (w/v) PFA, immunolabeled with antibodies against HA (red), *C. trachomatis* Cap1 (green), known to localize at the inclusion membrane (Fling *et al.*, 2001), and *C. trachomatis* MOMP (blue), and appropriate fluorophore-conjugated secondary antibodies. The labeled cells were then imaged by fluorescence microscopy. Scale bars, 10 μm. Dashed lines represent the limits of infected HeLa cells. (c) Output inclusions forming units (IFUs) per input IFUs was calculated for each *C. trachomatis* strain at 44 h post-infection and divided by the values obtained for the parental L2/434 strain. Data are represented as the mean and standard error of the mean of at least 3 independent experiments. Statistical analysis was performed using Wilcoxon signed-rank test. (d) At 24 hpi, the area of chlamydial inclusions was measured for more than 100 particles randomly selected from images from at least 3 independent experiments using Fiji software (Schindelin *et al.*, 2012). Statistical analysis was performed using Kruskal-Wallis and Dunn's multiple comparisons test. * Represents P<0.05 by comparison to the L2/434 strain; ϕ represents P<0.05 by comparison to the L2/434+pIncL-2HA strains.

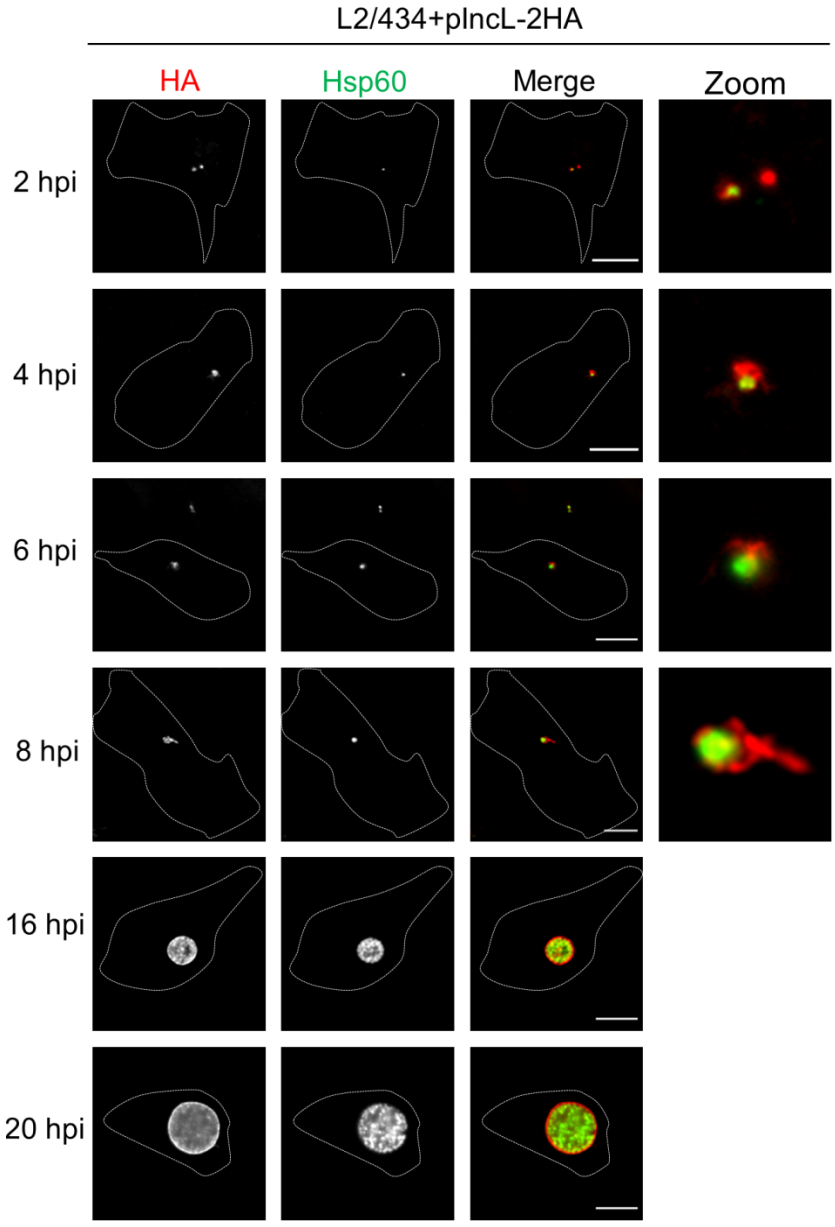

Figure 3.15 Plasmid-encoded IncL-2HA is produced at early times post-infection and accumulates at the periphery of the inclusion. HeLa 229 cells were infected by *C. trachomatis* L2/434 or *C. trachomatis* L2/434 harboring pIncL-2HA (L2/434+pIncL-2HA). At the indicated hours post-infection (hpi), cells were fixed with 4% (w/v) PFA, immunolabeled with antibodies against HA (red), *C. trachomatis* Hsp60 (green), and appropriate fluorophore-conjugated secondary antibodies, and imaged by fluorescence microscopy. Scale bars, 10 μm. Dashed lines represent the limits of infected HeLa cells and the chlamydial inclusions within were zoomed at 2, 4, 6 and 8 hpi.

3.2.3 The effect of IncL-2HA produced by *C. trachomatis* on host cell LDs

LDs are observed in close association with the inclusion membrane in HeLa cells infected by *C. trachomatis* L2/434 (Cocchiaro *et al.*, 2008). We questioned if increased production of plasmid-encoded IncL-2HA by *C. trachomatis* relative to the parental L2/434 strain could facilitate the association of LDs with the inclusion. To address this, we sought to use fluorescence microscopy images of cells infected by *C. trachomatis* for 10, 14, 18 and 22 h and quantify the area of LDs at the region of the inclusion. We reasoned that a possible effect of IncL-2HA overproduction in the association of LDs with the inclusion should not be seen by mutant IncL proteins with defects in the possible LD-targeting region and neither by a random Inc. Therefore, we generated three additional L2/434-derived strains: L2/434+pIncL$_{5G}$-2HA, harboring a plasmid-encoded IncL$_{5G}$-2HA mutant protein where the amino acid residues important for the localization of mEGFP-IncL$_{1-88}$ at LDs in transfected cells ($K_{34}K_{37}R_{72}H_{80}K_{81}$) were replaced by glycines (Figure 3.12); L2/434+pIncL$_{\Delta 47-67}$-2HA, harboring a plasmid-encoded IncL$_{\Delta 47-67}$-2HA mutant protein lacking amino acid residues 47 to 67, which comprise most of the putative hydrophobic motif possibly required for the association of IncL with LDs (Figure 3.11a and 3.12); and L2/434+pCT449-2HA, a strain harboring plasmid-encoded Inc CT449 with a carboxy-terminal 2HA tag. In these strains, the genes encoding the 2HA-tagged proteins are expressed from the corresponding *incL* or *ct449* promoters.

To test if Inc CT449 showed tropism for LDs in transfected HeLa cells, we generated mammalian transfection plasmids encoding CT449 or its predicted cytosolic regions (CT449$_{1-41}$ and CT449$_{88-110}$) with a mEGFP tag at their amino-termini. Immunoblotting analysis using extracts of HeLa cells ectopically expressing the genes encoding mEGFP-CT449$_{FL}$, mEGFP-CT449$_{1-41}$ or mEGFP-CT449$_{88-110}$ showed that all the proteins were produced with their predicted molecular mass (Figure 3.16a). Using fluorescence microscopy, we found that mEGFP-CT449$_{FL}$ was distributed in puncta, while their predicted cytosolic regions were spread in the cytosol (Figure 3.16b). To test if mEGFP-CT449$_{FL}$ puncta co-localized with LDs, HeLa cells transiently producing mEGFP-CT449$_{FL}$ were treated with oleic acid and stained with Oil Red O. As depicted in Figure 3.16c, mEGFP-CT449$_{FL}$ did not co-localize with LDs (Figure 3.16c), which is an indication that CT449 does not target LDs during *C. trachomatis* infection, being a suitable negative control for our experiments.

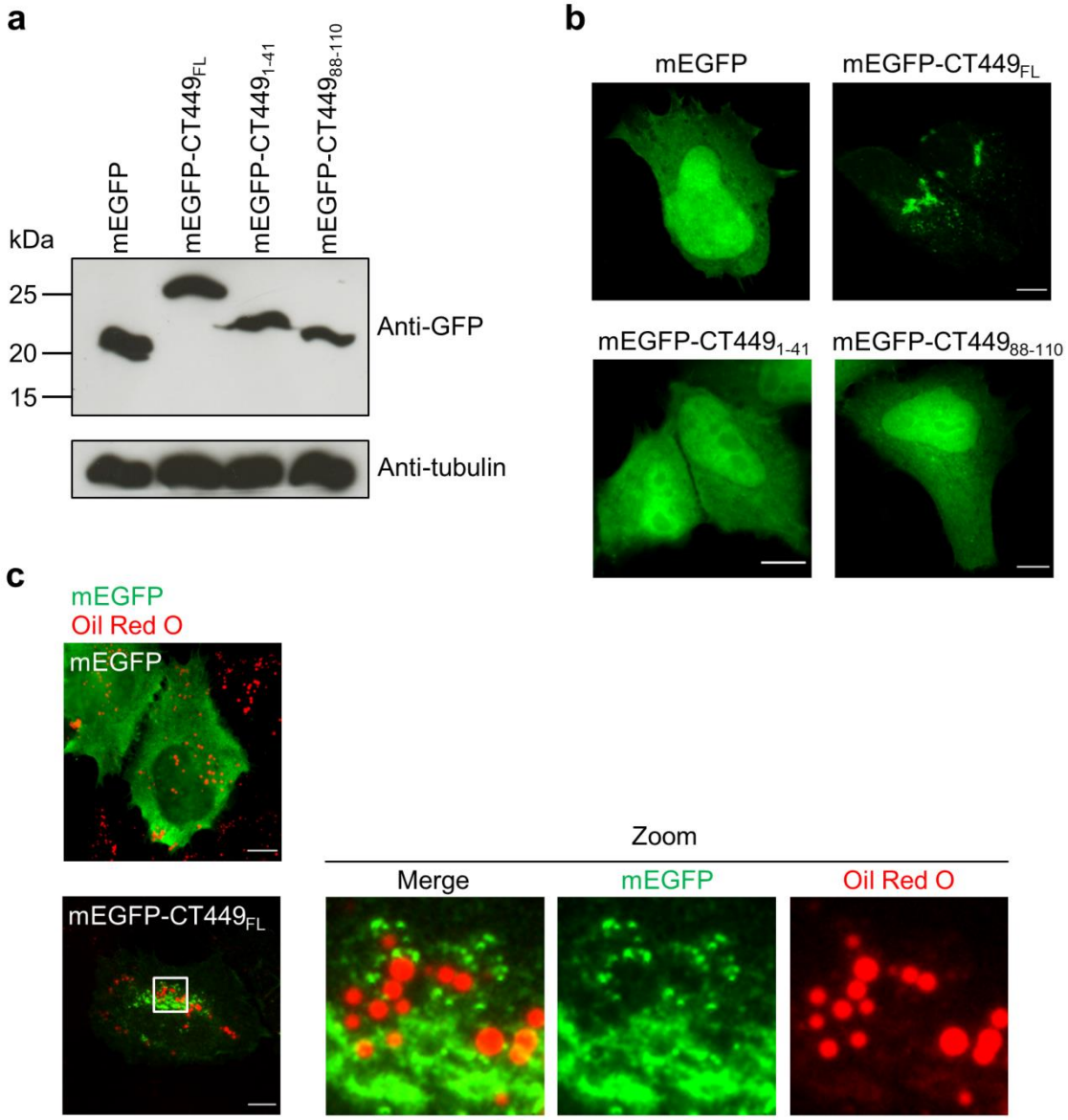

Figure 3.16 mEGFP-CT449 does not localize at lipid droplets in mammalian cells. HeLa 229 cells were transfected with plasmids encoding mEGFP or different versions of CT449 containing a mEGFP tag at their amino-termini (mEGFP-CT449$_{FL}$, mEGFP-CT449$_{1-41}$ or mEGFP-CT449$_{88-110}$). (a) At 24 h post-transfection, whole cell extracts were analyzed by immunoblotting with antibodies against GFP and α-tubulin (HeLa 229 cells loading control) and appropriate HRP-conjugated secondary antibodies. (b) At 24 h post-transfection, cells were fixed with 4% (w/v) PFA and analyzed by fluorescence microscopy. (c) At 18 h post-transfection, cells were treated with 100 µM oleic acid for 6 h and then fixed with 4% (w/v) PFA. Fixed cells were labeled with anti-GFP and the appropriate fluorophore-conjugated secondary antibody, stained with Oil Red O (3:2 v/v Oil Red O stock solution diluted in water), and imaged by fluorescence microscopy. Scale bars, 10 µm. The area delimited by a white square was zoomed.

We also confirmed that during infection of HeLa cells by *C. trachomatis*, plasmid-encoded IncL$_{5G}$-2HA, IncL$_{\Delta 47-67}$-2HA, and CT449-2HA are produced (Figure 3.17) and accumulate at the inclusion membrane (Figure 3.18). The production of IncL$_{5G}$-2HA, IncL$_{\Delta 47-67}$-2HA,

and CT449-2HA did not significantly affect the ability of *C. trachomatis* to generate infectious progeny (Figure 3.14c), but cells infected by the L2/434+pIncL$_{5G}$-2HA strain showed significantly larger inclusions than those infected by the L2/434 strain (Figure 3.14d). A comparison against the inclusions of cells infected by L2/434+pIncL-2HA also revealed that the production of IncL$_{5G}$-2HA resulted in larger inclusions, while the production of IncL$_{\Delta 47\text{-}67}$-2HA led to smaller inclusions (Figure 3.14d). As these strains were not significantly affected in their ability to generate infectious progeny, the differences in inclusion area might be related with alterations in inclusion morphology, composition and/or with the distribution of the chlamydiae within the inclusion, due to the accumulation of IncL mutant proteins at the inclusion membrane.

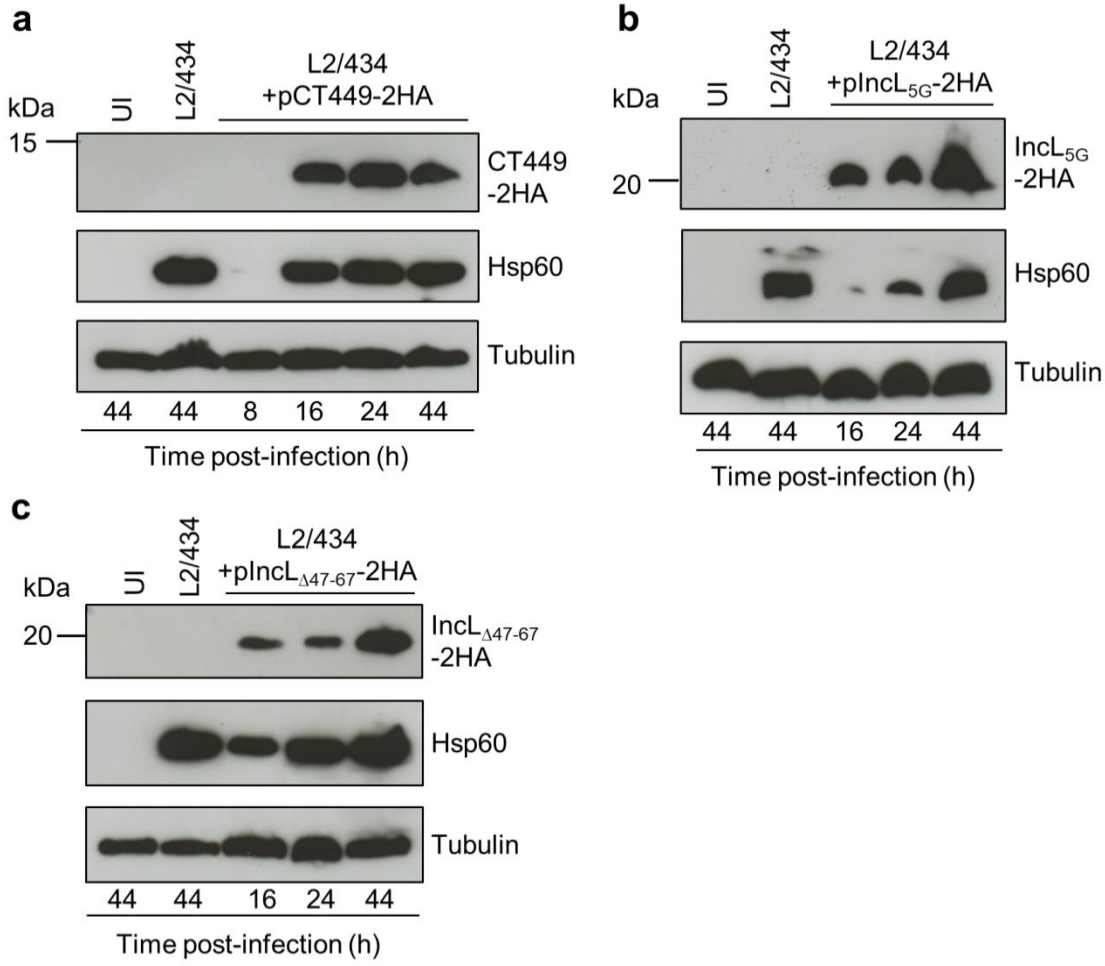

Figure 3.17 Analysis of the production of plasmid-encoded CT449-2HA, IncL$_{5G}$-2HA and IncL$_{\Delta 47\text{-}67}$-2HA by *C. trachomatis*. HeLa 229 cells were left uninfected (UI) or infected by *C. trachomatis* L2/434 or by L2/434 strains harboring (**a**) pCT449-2HA, (**b**) pIncL$_{5G}$-2HA, or (**c**) pIncL$_{\Delta 47\text{-}67}$-2HA. At the indicated times post-infection, whole cell extracts were analyzed by immunoblotting using antibodies against HA, Hsp60 (bacterial loading control) and α-tubulin (HeLa 229 cells loading control) and the appropriate HRP-conjugated secondary antibodies, followed by detection using SuperSignal West Pico detection kit (Thermo Fisher Scientific).

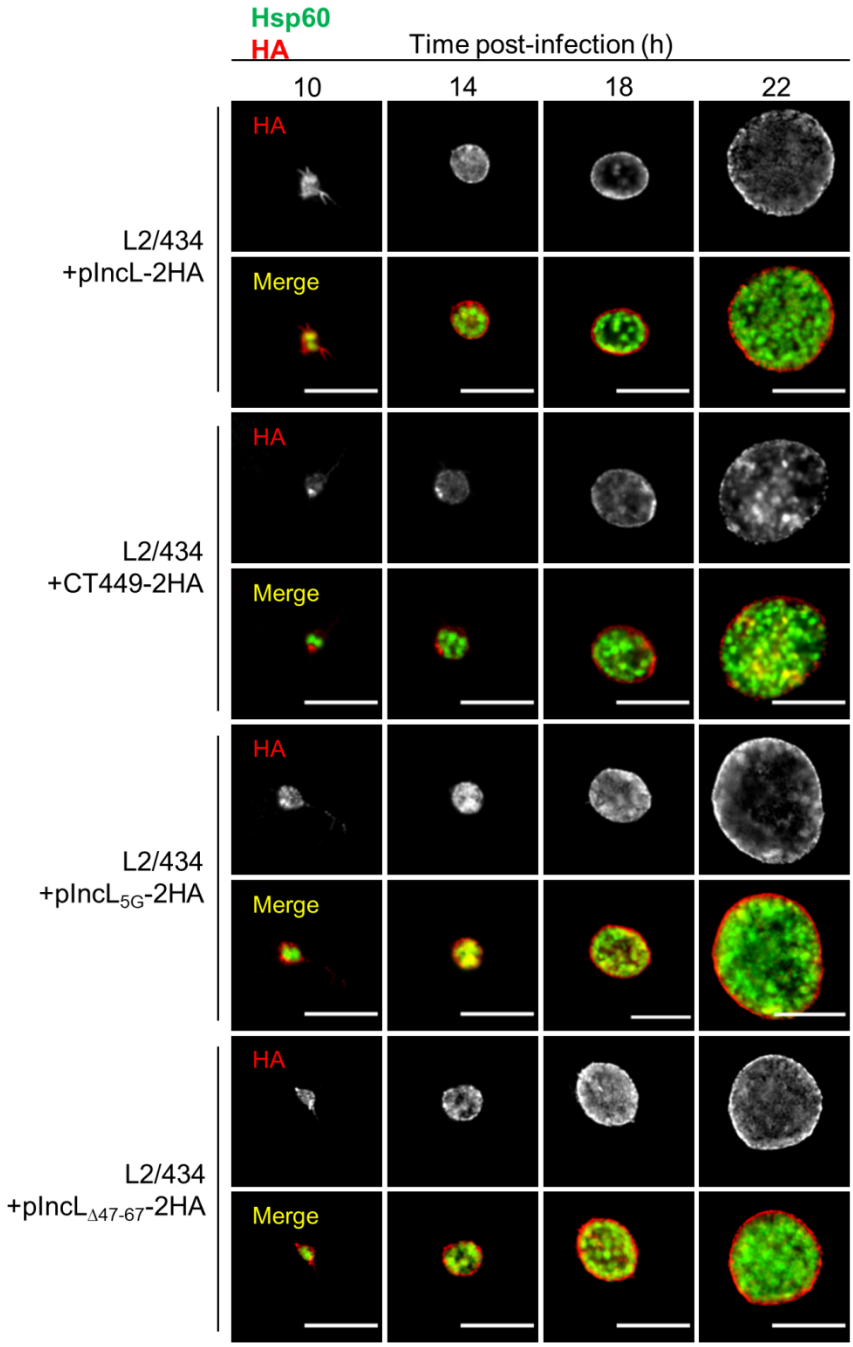

Figure 3.18 Analysis of the intracellular localization of plasmid-encoded IncL-2HA, CT449-2HA, IncL$_{5G}$-2HA and IncL$_{\Delta 47\text{-}67}$-2HA. HeLa 229 cells were left uninfected (UI) or infected by L2/434 strains harboring pIncL-2HA, pCT449-2HA, pIncL$_{5G}$-2HA or pIncL$_{\Delta 47\text{-}67}$-2HA. At the indicated times post-infection, infected cells were fixed with 4% (w/v) PFA, immunolabeled with antibodies against HA (red), Hsp60 (green) and appropriate fluorophore-conjugated secondary antibodies. The labeled cells were then imaged by fluorescence microscopy. Scale bars, 10 μm.

To test for a possible effect of the increased production of plasmid-encoded IncL-2HA on the distribution of LDs, HeLa cells were infected by *C. trachomatis* strains L2/434, L2/434+pIncL-2HA, L2/434+pIncL$_{5G}$-2HA, L2/434+pIncL$_{\Delta 47-67}$-2HA, or L2/434+pCT449-2HA. The cells were treated with oleic acid for 6 h, before fixation at 10, 14, 18 and 22 h post-infection. Fixed infected cells were labeled with anti-*C. trachomatis* Hsp60 and with the neutral lipid dye Bodipy 493/503 (which stains LDs) and analyzed by indirect immunofluorescence microscopy. At a first glance, the distribution of LDs was similar between cells infected by all *C. trachomatis* strains (Figure 3.19). To analyze this in further detail, the area of BODIPY-positive LDs within the region of chlamydial inclusions was measured from randomly selected images, as those depicted in Figure 3.19. For this analysis, both LDs localizing at the periphery of the inclusion or co-localizing with the inclusion were considered (see Materials and Methods).

Using the *C. trachomatis* strains indicated in Figure 3.20a, we did three separated experiments (Figures 3.20b, 3.20c and 3.20d), each one comprising three independent assays. Within each experiment, the three assays were performed with the same batches of culture media, HeLa cells and *C. trachomatis* stocks. In each of the three experiments, we observed a slight, but specific and significant, increase in the area of LDs within the inclusion region of cells infected by L2/434+pIncL-2HA comparing with cells infected by L2/434, or *vice-versa*, at 18 h (Figures 3.20b and 3.20d) or at 22 h (Figure 3.20c) post-infection. Apart from a difference between cells infected by the L2/434+pCT449-2HA and L2/434+pIncL-2HA strains at 22 h post-infection (Figure 3.20c), there were no significant differences in the area of LDs within the inclusion region when comparing cells infected by strains producing IncL$_{5G}$-2HA, IncL$_{\Delta 47-67}$-2HA, and CT449-2HA with cells infected by the L2/434 or L2/434+pIncL-2HA strains (Figures 3.20b, 3.20c and 3.20d).

In summary, a significant increase in the area of LDs at the region of inclusions was exclusively detected in cells infected by L2/434+pIncL-2HA. However, as we could not correlate this effect with the region and amino acid residues that promote the association of IncL with LDs in transfected cells, these results were inconclusive.

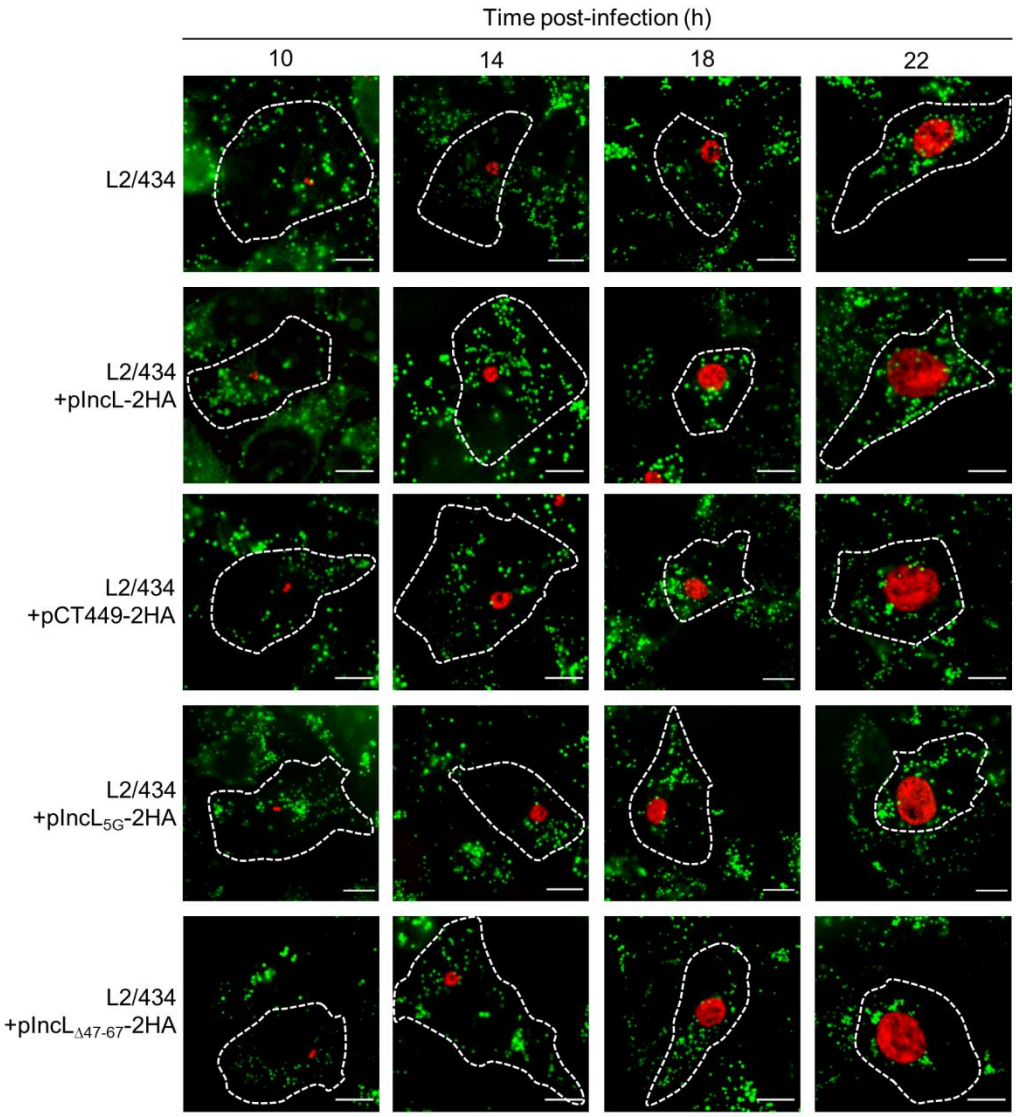

Figure 3.19 Analysis of the localization of LDs in cells infected by *C. trachomatis*. HeLa 229 cells were infected by *C. trachomatis* L2/434 parental strain or by *C. trachomatis* L2/434 strains harboring pIncL-2HA, pCT449-2HA, pIncL$_{5G}$-2HA or pIncL$_{\Delta 47-67}$-2HA. At the indicated times post-infection, infected cells previously treated with 100 µM oleic acid for 6 h were fixed with 4% (w/v) PFA, immunolabeled with an antibody against Hsp60 (red) and an appropriate fluorophore-conjugated secondary antibody, stained with the neutral lipid dye BODIPY (green) and imaged by fluorescence microscopy. Dashed lines represent the limits of infected HeLa 229 cells. Scale bars, 10 µm.

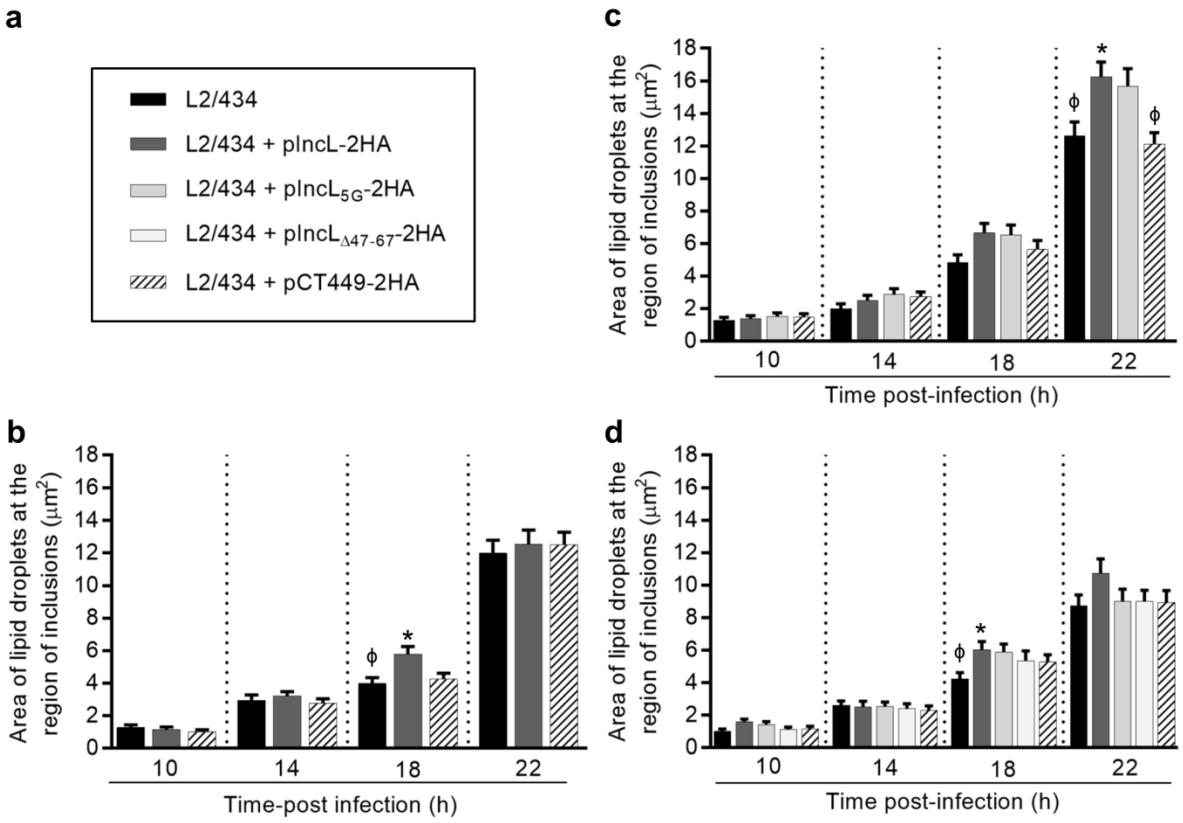

Figure 3.20 The effect of IncL-2HA produced by *C. trachomatis* on host cell lipid droplets. The area of BODIPY-positive LDs at the region of chlamydial inclusions was measured from randomly selected images, as those depicted in Figure 3.19, using Fiji software (Schindelin *et al.*, 2012). (a) Legend for *C. trachomatis* strains used. Graphs represented in (b), (c) and (d) correspond to the first, second and third set of experiments, each set composed of 3 independent assays. In each assay, 20 images were analyzed for cells infected by a given strain (60 images per experiment). Data are represented as the mean and standard error of the mean. Statistical analysis was performed using Kruskal-Wallis test with Dunn's multiple comparison test. * Represents $P<0.05$ by comparison to the L2/434 strain; ϕ represents $P<0.05$ by comparison to L2/434+pIncL-2HA.

3.3 Identification and validation of IncL host cell interacting proteins

The identification of eukaryotic proteins interacting with IncL could elucidate its function during *C. trachomatis* infection. Therefore, we wanted to explore possible interactions of IncL with host cell proteins, based on a previous large-scale proteomics screen (Mirrashidi *et al.*, 2015). Mirrashidi and colleagues screened for human proteins interacting with *Chlamydia* Incs, which revealed 14-3-3 proteins (14-3-3s) isoforms β, η and γ (phosphoserine/threonine binding proteins) and inactive protein tyrosine kinase (PTK7) (membrane receptor) as possible IncL interacting partners (Mirrashidi *et al.*, 2015), but this remained to be validated. Here, we analyzed the intracellular localization of 14-3-3s and PTK7 during *C. trachomatis* infection to test if these eukaryotic proteins were recruited to the inclusion membrane. To further validate their previously predicted interactions with IncL, we performed co-immunoprecipitation (co-IP) assays using mammalian cells transiently producing IncL and 14-3-3s or PTK7.

3.3.1 IncL interacts with 14-3-3β in mammalian cells

To investigate whether the previously predicted IncL eukaryotic interacting proteins were recruited to the inclusion membrane, HeLa cells were infected by the *C. trachomatis* strains L2/434 or L2/434+pIncL-2HA and transfected at time zero of infection with plasmids encoding 14-3-3β with a FLAG-HA tag at its amino-terminus (FLAG-HA-14-3-3β) or PTK7 with a myc tag at its carboxy-terminus (PTK7-myc). After 24 h, cells were fixed, immunolabeled for HA and for *C. trachomatis* MOMP, and analyzed by fluorescence microscopy.

As shown in Figure 3.21, FLAG-HA-14-3-3β presented a predominantly cytosolic distribution in non-infected cells, but accumulated at the periphery of the inclusion membrane in cells infected by *C. trachomatis* L2/434, as previously described for 14-3-3β (Scidmore & Hackstadt, 2001). A similar accumulation was observed in cells infected by *C. trachomatis* producing plasmid-encoded IncL-2HA (Figure 3.21a), indicating that overproduction of IncL does not seem to facilitate recruitment of FLAG-HA-14-3-3β to the inclusion periphery. PTK7-myc showed a reticular distribution in HeLa cells, which remained unaltered by *C. trachomatis* infection (Figure 3.21b).

To test for an interaction between IncL and 14-3-3β or PTK7, we performed co-IP assays using HEK 293T cells transfected with plasmids co-expressing, in combinations of two, the genes encoding mEGFP-IncL or mEGFP alone (as a control) and FLAG-HA-14-3-3β or PTK7-myc. Transfected cells were lysed and mEGFP fusion proteins were

immunoprecipitated using GFP-Trap beads (see Materials and Methods) and analyzed by immunoblotting. FLAG-HA-14-3-3β was pulled-down by mEGFP-IncL, but not by mEGFP alone (Figure 3.22a) and PTK7-myc was absent in all bound fractions (Figure 3.22b). Altogether, our results showed that IncL interacts with 14-3-3β after their transient production in HEK 293T cells, while the interaction between IncL and PTK7 was not validated in our experimental conditions.

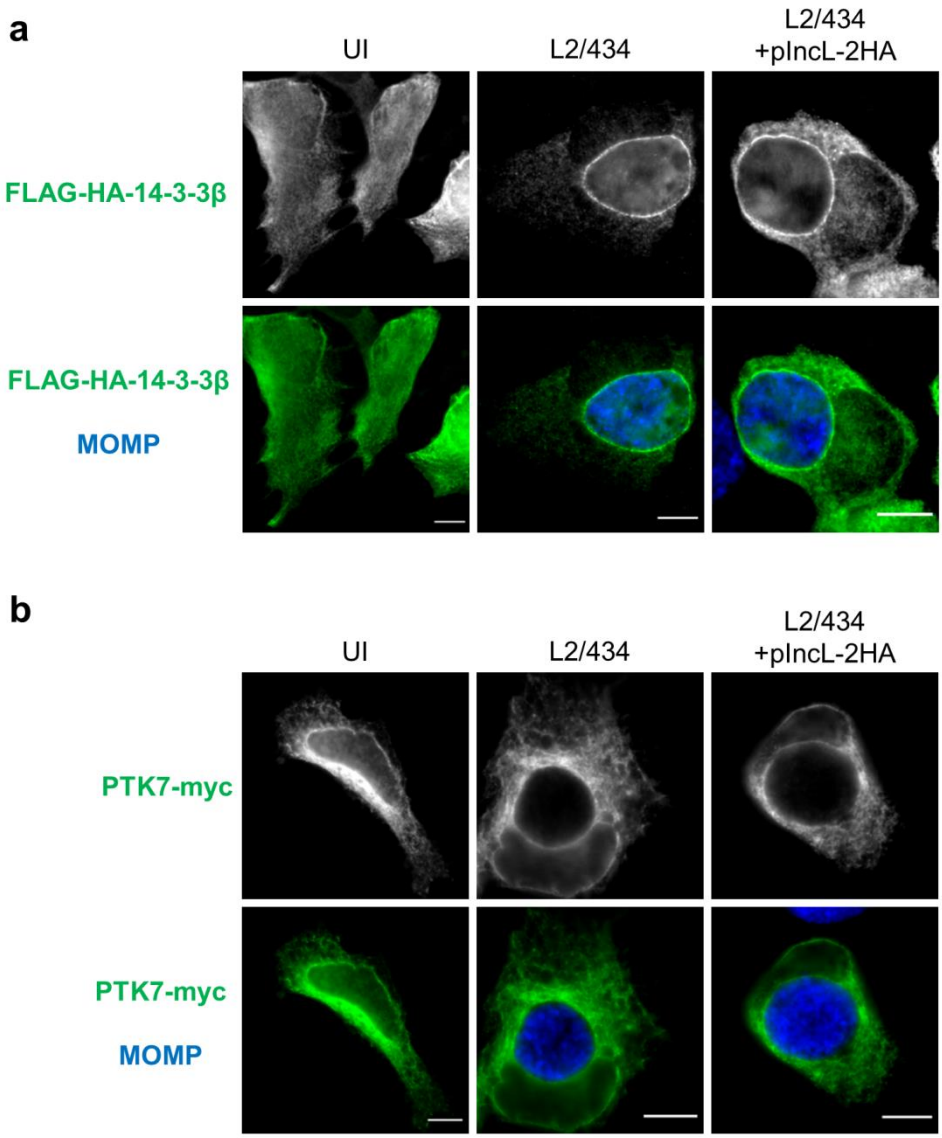

Figure 3.21 FLAG-HA-14-3-3β accumulates at the periphery of the inclusion membrane during *C. trachomatis* infection. HeLa 229 cells were infected by the *C. trachomatis* strains L2/434 or L2/434+pIncL-2HA. At time zero of infection, HeLa cells were transfected with plasmids encoding (a) FLAG-HA-14-3-3β or (b) PTK7-myc. After 24 h, cells were fixed with 4% (w/v) PFA, immunolabeled with antibodies against HA (green), myc (myc), *C. trachomatis* MOMP (blue), and appropriate fluorophore-conjugated secondary antibodies, and imaged by fluorescence microscopy. Scale bars, 10 μm.

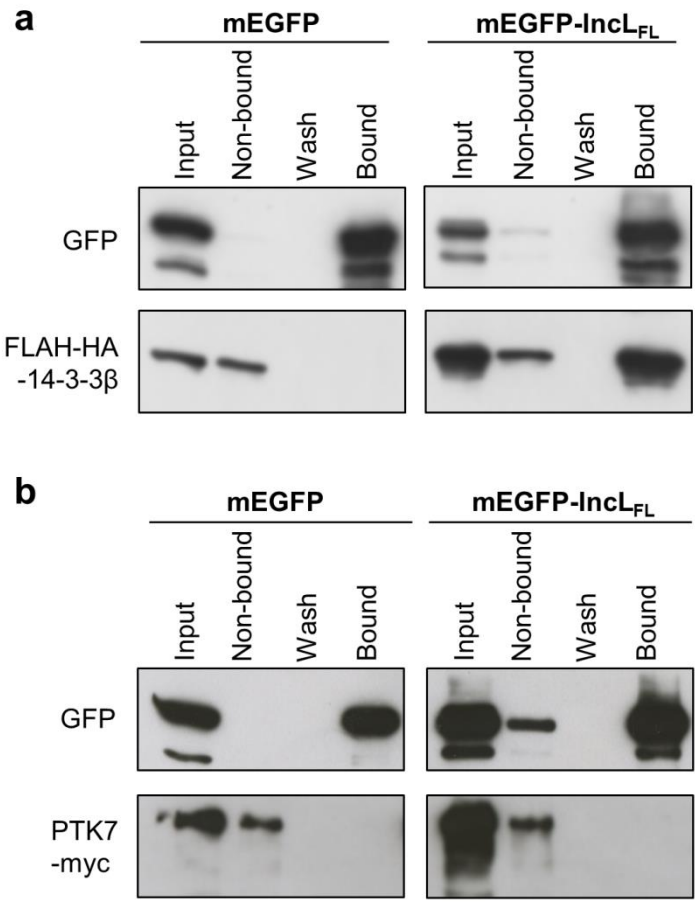

Figure 3.22 FLAG-HA-14-3-3β and mEGFP-IncL interact after their transient production in mammalian cells. HEK 293T cells were transfected with plasmids co-expressing, in combinations of two, the genes encoding mEGFP-IncL or mEGFP alone (as a control) and (a) FLAG-HA-14-3-3β or (b) PTK7-myc. Transfected cells were lysed and mEGFP fusion proteins were pulled-down using GFP-Trap beads (Chromotek) (see Materials and Methods). Proteins in the Input, non-bound, wash and bound fractions were analyzed by immunoblotting with antibodies against GFP, HA and myc and appropriate HRP-conjugated secondary antibodies. Proteins were detected using SuperSignal West Pico detection kit (Thermo Fisher Scientific).

3.3.2 The seven mammalian 14-3-3s are recruited to the periphery of *C. trachomatis* inclusions and IncL interacts with four isoforms

14-3-3s are present in all eukaryotic cells and mammalian cells produce seven isoforms of these proteins: Beta (β), Eta (η), Gamma (γ), Tau (τ), Zeta (ζ), Epsilon (ε) and Sigma (σ) (Aitken, 2002; Jones *et al.*, 1995). It had been previously shown by fluorescence microscopy that 14-3-3β and ε accumulate at the periphery of *C. trachomatis* inclusions (Kokes *et al.*, 2015). To test if all 14-3-3 isoforms were recruited to the inclusion membrane, HeLa cells were infected by *C. trachomatis* L2/434 and transfected with plasmids ectopically

expressing the genes encoding 14-3-3 isoforms with a HA or FLAG-HA tag at their amino-termini (FLAG-HA-14-3-3ε, FLAG-HA-14-3-3γ, HA-14-3-3η, HA-14-3-3ζ, FLAG-HA-14-3-3τ, FLAG-HA-14-3-3β, HA-14-3-3σ). Then cells were fixed, immunolabeled for HA and for *C. trachomatis* MOMP and analyzed by fluorescence microscopy. As depicted in Figure 3.23, we found that all the seven 14-3-3 isoforms accumulate at the periphery of the inclusion (Figure 3.23).

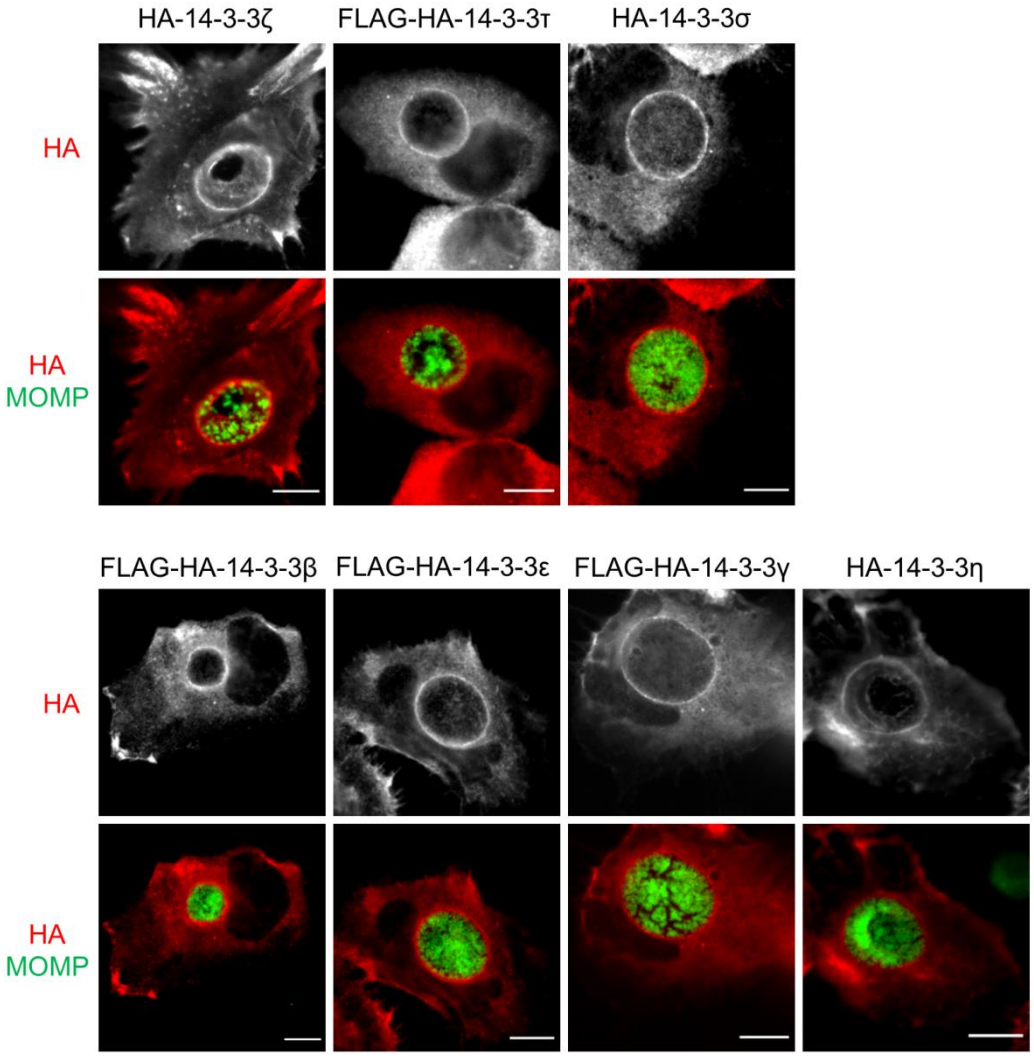

Figure 3.23 The seven mammalian isoforms of 14-3-3 proteins are recruited to the periphery of the inclusion membrane during *C. trachomatis* infection. HeLa 229 cells were infected by *C. trachomatis* L2/434 and transfected, at time zero of infection, with plasmids encoding the indicated 14-3-3 isoforms with a HA or FLAG-HA tag at their amino-termini. After 24 h, cells were fixed with 4% (w/v) PFA, immunolabeled with antibodies against HA (red), *C. trachomatis* MOMP (green), and appropriate fluorophore-conjugated secondary antibodies, and imaged by fluorescence microscopy. Scale bars, 10 μm. These experiments were performed with Carolina Brizida (master student in the host laboratory) under my direct supervison.

To test for an interaction between IncL and the seven 14-3-3 isoforms, we performed co-IP assays using HEK 293T cells ectopically co-expressing the genes encoding mEGFP or mEGFP-IncL and each one of the 14-3-3 isoforms fused to a HA or a FLAG-HA tag (Figure 3.24). With this approach, we validated the previously predicted interactions of IncL with the 14-3-3 isoforms β, η and γ and we also detected an interaction with the isoform σ. For FLAG-HA-14-3-3τ we obtained different outcomes in 3 independent experiments and therefore the results were inconclusive (Figure 3.24).

To understand if the ability of IncL to interact with only four 14-3-3 isoforms was related to major differences in their amino acid sequences, we first used the T-Coffee program to align the amino acid residues of the seven 14-3-3 isoforms. Then, the Jalview program was used to highlight differences in protein sequences by coloring amino acids according to their percentages of identity (Figure 3.25). As depicted in Figure 3.25, 14-3-3 isoforms are very similar, with few differences in their amino acid sequences and the carboxy-terminal regions showed the less degree of identity (Figure 3.25). Subsequently, BLAST was used to align 14-3-3 isoforms two by two to calculate the percentages of identity between them (Table 3.3). The percentages of identity varied between 60% and 88% and the ones showing the lowest values were 14-3-3ε and 14-3-3σ. Noteworthy, 14-3-3σ, which showed the less percentage of identity with the other isoforms, was able to interact with IncL, while 14-3-3 ζ, which is very similar to the IncL interacting isoform 14-3-3β, was not. Therefore, it was not possible to establish a relationship between the percentages of identity between 14-3-3 isoforms and their ability to interact with IncL.

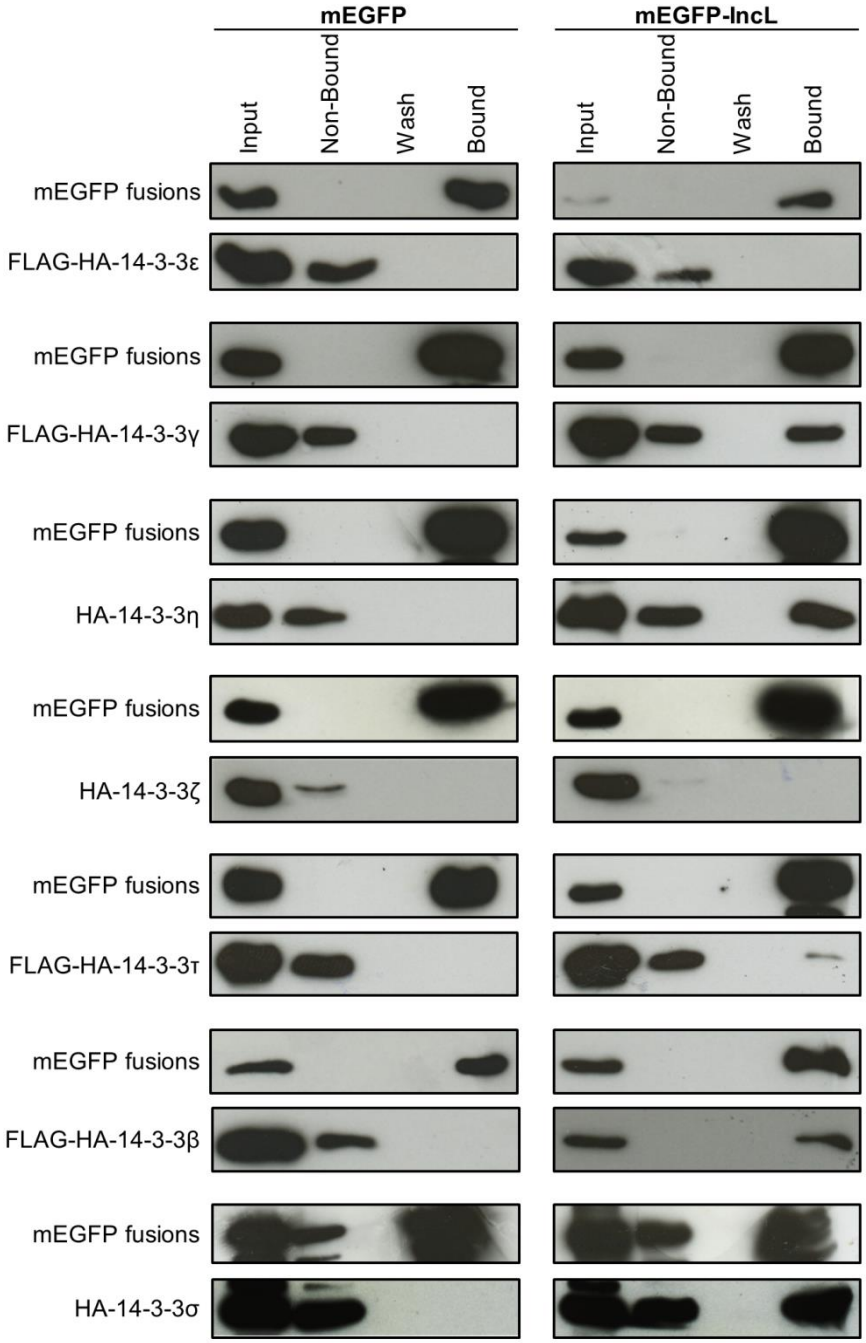

Figure 3.24 mEGFP-IncL interacts with FLAG-HA-14-3-3β, HA-14-3-3η, FLAG-HA-14-3-3γ and HA-14-3-3σ after transient production in HEK 293T cells. Co-IP assays were performed with GFP-Trap beads (Chromotek) (see Materials and Methods) using HEK 293T cells transfected for 24 h, in combinations of two, with plasmids encoding mEGFP (as a control) or mEGFP-IncL and the indicated 14-3-3 isoforms fused to a HA or FLAG-HA tag (FLAG-HA-14-3-3ε, FLAG-HA-14-3-3γ, HA-14-3-3η, HA-14-3-3ζ, FLAG-HA-14-3-3τ, FLAG-HA-14-3-3β e HA-14-3-3σ). Proteins in the Input, non-bound, wash and bound fractions were analyzed by immunoblotting with antibodies against GFP and HA and appropriate HRP-conjugated secondary antibodies. Proteins were detected using SuperSignal West Pico detection kit (Thermo Fisher Scientific). These experiments were performed with Carolina Brizida (master student in the host laboratory) under my direct supervison.

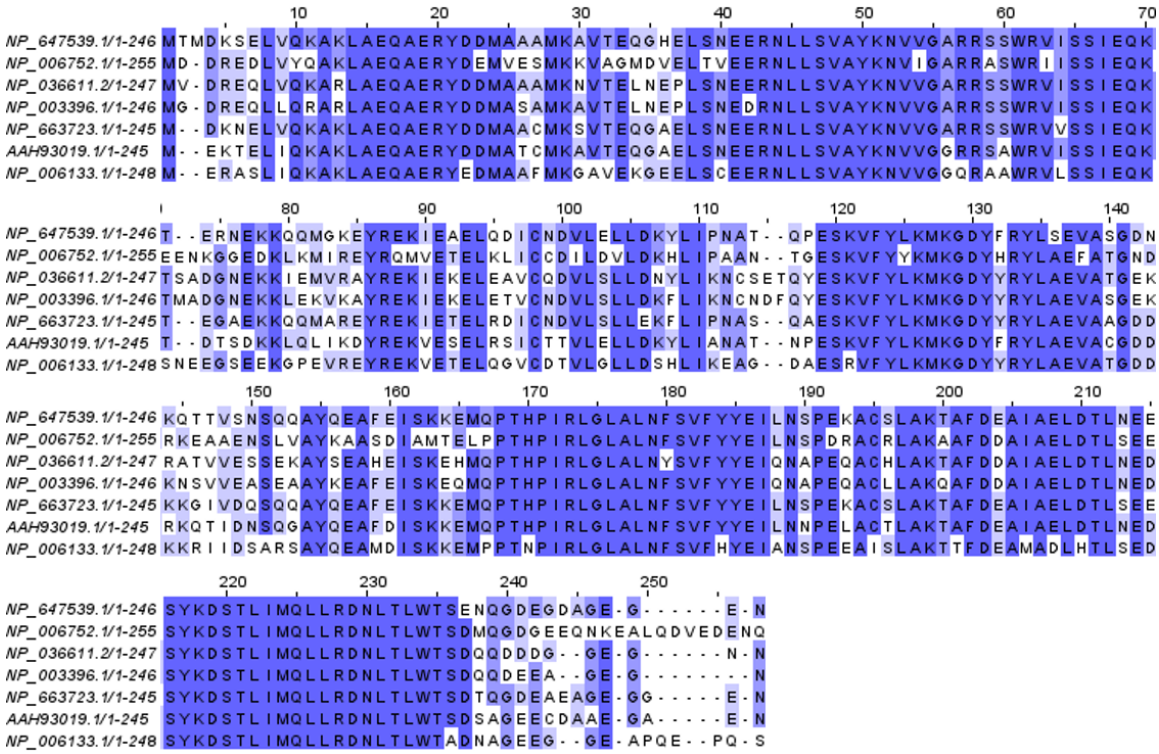

Figure 3.25 Alignment of the amino acid sequences of 14-3-3 isoforms. The amino acid sequences of 14-3-3 isoforms were aligned using the T-Coffee program and the percentage of identity was highlighted using the Jalview program. The intensity of the blue color is correlated with the percentage of identity between the seven 14-3-3 isoforms. The darkest blue highlights the presence of at least 6 isoforms sharing the same amino acid. The sequences of 14-3-3s are represented in the following order: 14-3-3β, 14-3-3ε, 14-3-3γ, 14-3-3η, 14-3-3ζ, 14-3-3τ, 14-3-3σ. These analyses were performed with Carolina Brizida (master student in the host laboratory) under my direct supervison.

Table 3.3 Percentage (%) of identity between 14-3-3 isoforms. Alignment using Blast program. These analyses were performed with Carolina Brizida (master student in the host laboratory) under my direct supervision.

14-3-3	Epsilon (ε)	Gama (γ)	Eta (η)	Zeta (ζ)	Tau (τ)	Beta (β)	Sigma (σ)
Epsilon (ε)	-	64	63	69	65	66	60
Gama (γ)	64	-	87	74	70	75	65
Eta (η)	63	87	-	74	71	76	64
Zeta (ζ)	69	74	74	-	80	88	71
Tau (τ)	65	70	71	80	-	82	71
Beta (β)	66	75	76	88	82	-	69
Sigma (σ)	60	65	64	71	71	69	-

3.3.3 IncL interacts via the carboxy-terminal region with 14-3-3β

14-3-3s frequently bind to their protein targets at phosphoserine/threonine binding motifs and the analysis of the primary sequence of IncL revealed the presence of two conserved 14-3-3 binding motifs [$R_{164}S_{165}S_{166}S_{167}A_{168}P_{169}$ and a serine as the penultimate amino acid residue (S_{188})] and an additional set of 3 consecutive serines ($S_{150}S_{151}S_{152}$) at the carboxy-terminal region (Figure 3.26a). As 14-3-3β interacts with another two Incs (IncG and InaC) (Kokes *et al.*, 2015; Scidmore & Hackstadt, 2001) and the interaction with IncG is mediated by a phosphoserine motif within IncG (Scidmore & Hackstadt, 2001), we decided to further explore the IncL-14-3-3β interaction. To define a region within IncL mediating the interaction with 14-3-3β, we performed co-IP assays, as described above, using HEK 293T cells ectopically co-expressing, in combinations of two, the genes encoding FLAG-HA-14-3-3β and mEGFP or mEGFP-IncL versions: mEGFP-$IncL_{FL}$, mEGFP-$IncL_{1-88}$ or mEGFP-$IncL_{139-189}$. FLAG-HA-14-3-3β was pulled-down by both mEGFP-$IncL_{FL}$ and mEGFP-$IncL_{139-189}$, but not by mEGFP or mEGFP-$IncL_{1-88}$, suggesting that IncL interacts with 14-3-3β through its last 51 amino acid residues (Figure 3.26b), which contain putative 14-3-3 binding motifs.

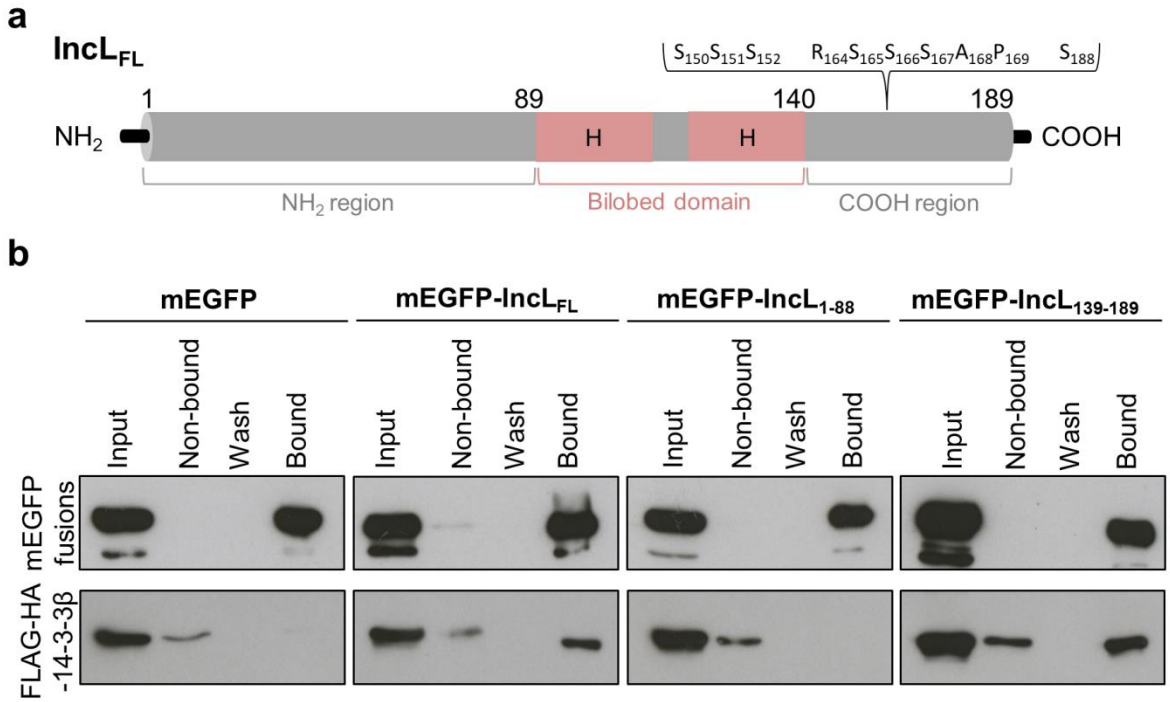

Figure 3.26 IncL interacts via the carboxy-terminal region with 14-3-3β. a) Schematic representation of the position of putative 14-3-3 binding motifs within IncL. IncL is predicted to have 2 conserved 14-3-3 binding motifs with the following amino acid sequences: $R_{164}S_{165}S_{166}S_{167}A_{168}P_{169}$ and S_{188}. In addition, IncL has 3 consecutive serines ($S_{150}S_{151}S_{152}$) at the carboxy-terminal region. (b) Co-IP assays were performed with GFP-Trap beads (Chromotek) using HEK 293T cells transfected for 24 h, in combinations of two, with plasmids encoding FLAG-HA-14-3-3β and mEGFP or the indicated mEGFP-IncL versions. Proteins in the Input, non-bound, wash and bound fractions were analyzed by immunoblotting with anti-GFP and anti-HA and appropriate HRP-conjugated secondary antibodies. Proteins were detected using SuperSignal West Pico detection kit (Thermo Fisher Scientific).

To test if one of the predicted 14-3-3 binding motifs was involved in IncL-14-3-3β interaction, we first generated 3 plasmids encoding mEGFP-IncL mutant proteins where each set of serines within each motif was individually replaced by alanines: mEGFP-IncL$_{S150-152->As}$ (replacement of $S_{150}S_{151}S_{152}$ to alanines), mEGFP-IncL$_{S165-167->As}$ (replacement of $S_{165}S_{166}S_{167}$ to alanines) and mEGFP-IncL$_{S188->A}$ (replacement of S_{188} to alanine). Then we performed co-IP assays using HEK 293T cells ectopically co-expressing, in combinations of two, the genes encoding FLAG-HA-14-3-3β and mEGFP or mEGFP-IncL mutant proteins. As shown in Figure 3.27, FLAG-14-3-3β was pulled-down by all mEGFP-IncL mutants, which means that none of the altered serines are essential for the interaction (Figure 3.27).

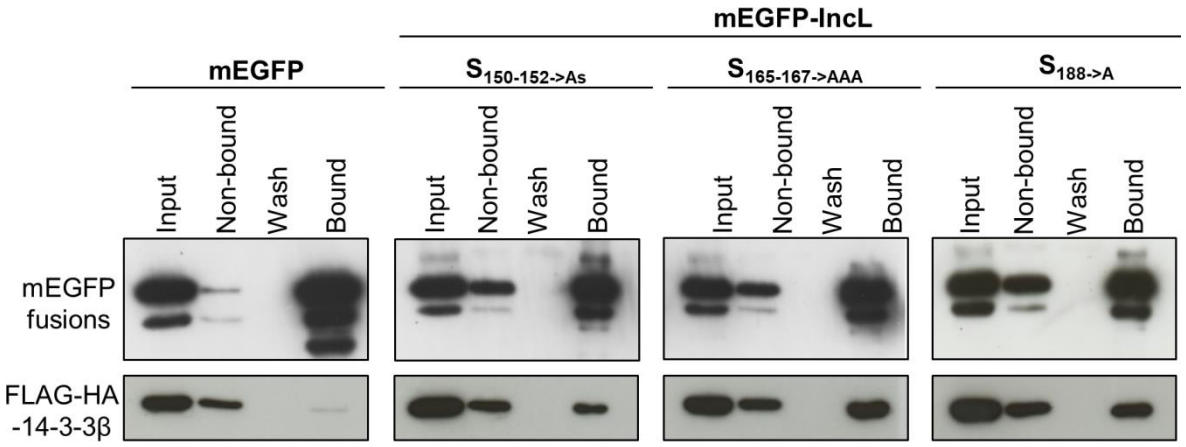

Figure 3.27 Analysis of the interaction between IncL mutant proteins and 14-3-3β. Co-IP assays were performed with GFP-Trap beads (Chromotek) using HEK 293T cells transfected for 24 h, in combinations of two, with plasmids encoding FLAG-HA-14-3-3β and mEGFP or mEGFP-IncL versions where the indicated serines were replaced by alanines. Proteins in the Input, non-bound, wash and bound fractions were analyzed by immunoblotting with anti-GFP and anti-HA and appropriate HRP-conjugated secondary antibodies. Proteins were detected using SuperSignal West Pico detection kit (Thermo Fisher Scientific).

Based on these results, we then hypothesized that, in mEGFP-IncL mutants, the presence of one or two putative 14-3-3 binding motifs could compensate the absence of only one motif. To test this, we performed co-IP assays using mEGFP-IncL mutants where each set of serines within each motif was replaced by alanines in double or triple combinations: mEGFP-IncL$_{S150-152,S165-169->As}$ (replacement of $S_{150}S_{151}S_{152}S_{165}S_{166}S_{167}$ to alanines), mEGFP-IncL$_{S150-152,S188->As}$ (replacement of $S_{150}S_{151}S_{152}S_{188}$ by alanines), mEGFP-IncL$_{S165-167,S188->As}$ (replacement of $S_{165}S_{166}S_{167}S_{188}$ by alanines) and mEGFP-IncL$_{S150-152,S165-169,S188->As}$ (replacement of $S_{150}S_{151}S_{152}S_{165}S_{166}S_{167}S_{188}$ by alanines). As all mEGFP-IncL mutants were able to interact with FLAG-HA-14-3-3β (Figure 3.28), the residues involved in the interaction of IncL with 14-3-3β remain to be identified.

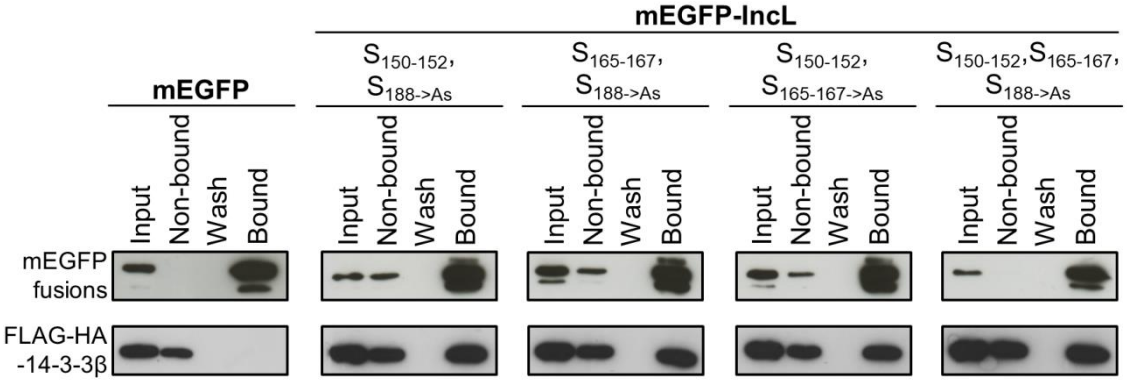

Figure 3.28 The substitution by alanines of all the serine residues within putative IncL 14-3-3 binding motifs does not affect IncL-14-3-3β interaction. Co-IP assays were performed with GFP-Trap beads (Chromotek) using HEK 293T cells transfected for 24 h, in combinations of two, with plasmids encoding FLAG-HA-14-3-3β and mEGFP or mEGFP-IncL versions where the indicated serines were replaced by alanines. Proteins in the Input, non-bound, wash and bound fractions were analyzed by immunoblotting with anti-GFP and anti-HA and appropriate HRP-conjugated secondary antibodies. Proteins were detected using SuperSignal West Pico detection kit (Thermo Fisher Scientific). These experiments were performed with Carolina Brizida (master student in the host laboratory) under my direct supervison.

4

DISCUSSION AND CONCLUSIONS

In this work, starting from a screen using *S. cerevisiae* as model organism, we identified a *C. trachomatis* Inc, CT006, which we named IncL, and revealed that it associates with the endoplasmic reticulum (ER) and lipid droplets (LDs) when its first 88 amino acid residues are ectopically produced in eukaryotic cells. Furthermore, we identified positively charged residues flanking a putative hydrophobic region that mediate the targeting of $IncL_{1-88}$ to mammalian LDs. Our results suggest that this putative hydrophobic region should be exposed to the outside of the inclusion, as well as the carboxy-terminal region, which supported the availability of these regions to interact with host cell factors. Using a *C. trachomatis* strain producing a plasmid-encoded IncL, we showed that IncL accumulates at the inclusion membrane throughout the chlamydial developmental cycle and its overproduction slightly, but significantly and reproducibly, increased the area of LDs within the region of chlamydial inclusions. Overall, this suggested that IncL might participate in mediating the association of LDs with the *C. trachomatis* inclusion. However, we could not correlate the increment in the area of LDs at the region of inclusions with the LDs targeting motifs within IncL. In addition, co-immunoprecipitation (co-IP) assays validated a previously predicted interaction of IncL with four isoforms of mammalian 14-3-3 proteins (14-3-3s) (Mirrashidi *et al.*, 2015). A detailed analysis on the interaction with the isoform β revealed that it is mediated by the carboxy-terminal region of IncL. This work demonstrated that a preliminary screen in yeast can be a valuable tool to expand the knowledge on *C. trachomatis* effectors as it was the starting point for the identification of IncL, which was further shown to target host cell LDs and eukaryotic 14-3-3s.

4.1 Using yeasts as a model to identify bacterial effector proteins subverting host cell pathways

As *S. cerevisiae* has been proved to be a useful system to study bacterial effectors, especially from bacteria that are difficult to genetically manipulate (Siggers & Cammie, 2008), this work started with a screen using *S. cerevisiae* as a model aiming to find novel functions for *C. trachomatis* Incs. We performed vacuolar protein sorting (Vps) assays in yeast, which have been previously used to identify bacterial effectors and protein regions interfering with eukaryotic vesicular trafficking, such as the *L. pneumophila* effector VipA (Bugalhão *et al.*, 2016; Franco *et al.*, 2012; Shohdy *et al.*, 2005) and the *C. trachomatis* effector CteG (Pais *et al.*, 2019). Here, we identified fragments of two *C. trachomatis* Incs causing mistrafficking in yeast, namely the CT229/CpoS fragment only when fused to GFP alone, and the CT223/IPAM fragment exclusively when fused to GFP-Pep12$_{L\text{-}TM}$. This further supported the importance of testing not only Inc fragments fused to GFP, but also fused to GFP-Pep12$_{L\text{-}TM}$, which anchors Inc fragments to the cytosolic side of endosomes, mimicking their presence in a membrane. By immunoblotting, a single band was detected for CT229/CpoS fragment fused to GFP and several degradation products when the fragment was fused to GFP-Pep12$_{L\text{-}TM}$, indicating that this latter fusion might be more susceptible to degradation, thus decreasing the concentration of the functional full-length fragment. With respect to CT223/IPAM, either the low levels detected for the GFP fusion were insufficient to cause mistrafficking or its Pep12$_{L\text{-}TM}$-mediated targeting to endosomal membranes was essential for its function. As these Incs are known to modulate host cell trafficking related processes, our results confirmed the applicability of the Vps assay to screen for *C. trachomatis* Incs causing Vps defects. The interference of CT229/CpoS with yeast vesicular trafficking might be related with its ability to interact with multiple Rab GTPases (Faris *et al.*, 2019; Rzomp *et al.*, 2006) and/or with its role in inhibiting host cell death during *C. trachomatis* infection (Sixt *et al.*, 2017; Weber *et al.*, 2017). CT223/IPAM is known to manipulate microtubules (Dumoux *et al.*, 2015) in *C. trachomatis*-infected cells and also blocks cytokinesis in transfected mammalian cells (Alzhanov *et al.*, 2009), which can be due to/or a consequence of a role in interfering with trafficking. Because we were looking for novel functions for Incs, we did not proceed with the analysis of CT229/CpoS or CT223/IPAM. Also, we do not exclude the possibility that other Incs are able to interfere with eukaryotic trafficking. For instance, the fragments of CT119/IncA and CT116/IncE were unable to cause Vps defects in yeast, but IncA inhibits endocytic membrane fusion during *C. trachomatis* infection (Delevoye *et al.*, 2008) and IncE is known to modulate the retromer-dependent

trafficking, which is associated with the recycling of cargo from endosomes to the plasma membrane or *trans*-Golgi network (TGN) (Mirrashidi *et al.*, 2015). Other Incs might interfere with endo-lysosomal trafficking only in the context of *C. trachomatis*-host cell interactions. Their function might be exerted only as full-length proteins, in complex with other *C. trachomatis* effectors and/or by interaction with mammalian targets that are not conserved in yeast. In future screens, Vps assays could be optimized, as several proteins were either not detected in yeast or presented low levels of production. To overcome this, fine-tuning of the Inc fragments used in these assays could be performed and other expression plasmids with stronger promoters could be tested. In addition, Inc fragments could be fused to GFP and/or GFP-Pep12$_{L\text{-}TM}$ at their amino-termini, as fusions at the carboxy-termini might, for some Inc fragments, prevent the interaction of these regions with host cell targets.

Vps assays were designed to search for bacterial proteins that might interfere, at some step, with the trafficking from the Golgi to the yeast vacuole via late endosomes (Shohdy *et al.*, 2005), possibly missing phenotypes caused by proteins that interfere with other trafficking pathways. Hypothesizing that other Incs might interfere with other trafficking pathways and/or target exclusively mammalian proteins, different types of screens could be performed. For instance, a human growth hormone (hGH) secretion assay was previously used to look for proteins that interfere with trafficking through the human secretory pathway (Selyunin *et al.*, 2011). Mammalian cells could be individually transfected with plasmids encoding Inc-GFP or GFP-Inc proteins and with prHom-Sec1 (Clontech), which encodes an hGH-hybrid protein that aggregates in the ER. Application of a drug directs hGH into the culture medium through the secretory pathway and ELISA could be used to monitor if expression of Incs affects secretion of hGH in the transfected and drug-induced cells (Selyunin *et al.*, 2011).

In the screen in yeast, we also analyzed the intracellular localization of Inc-GFP proteins as their tropism for eukaryotic organelles could give insights about their functions. We identified seven Incs whose putative cytosolic regions revealed relevant localizations. In addition to the localization of CpoS at endosomal compartments and IncL at LDs, fluorescence microscopy analysis led to the identification of five Inc-GFP fusion proteins localizing at mitochondria-like puncta (CT179$_{53\text{-}170}$-GFP, CT324$_{119\text{-}303}$-GFP, CT618$_{1\text{-}212}$-GFP, CT018$_{1\text{-}90}$-GFP and CT383$_{157\text{-}243}$-GFP). In particular, CT324 was previously predicted to interact with the core subunit of the mitochondrial membrane respiratory chain NADH dehydrogenase (Mirrashidi *et al.*, 2015), which might be related to the localization of CT324$_{119\text{-}303}$ at yeast mitochondria. Nevertheless, the tropism of these Incs for mitochondria remains to be tested in transfected mammalian cells and in the context of *C. trachomatis* infections. Although *C. trachomatis* is suggested to modulate mitochondrial dynamics (Al-

Zeer *et al.*, 2017; Chowdhury & Rudel, 2017; Kurihara *et al.*, 2019), there is no evidence for an active recruitment of these organelles to chlamydial inclusions, where Inc proteins localize, and therefore we did not select any of these proteins for further characterization. However, it is possible that some of these Incs mediate contacts between inclusions and mitochondria late in the developmental cycle when inclusions occupy almost the entire cytosol of the host cell.

At the early stages of this PhD work, more solid evidence was described in the literature for the interaction of *C. trachomatis* inclusions with host cell LDs (Cocchiaro *et al.*, 2008; Kumar *et al.*, 2006; Rank *et al.*, 2011; Saka *et al.*, 2015; Sisko *et al.*, 2006) and with the ER (Derré *et al.*, 2011; Stanhope *et al.*, 2017), from where LDs originate, which led to the selection of IncL for further characterization. LDs are translocated into the inclusion lumen by a mechanism that is not understood. Also, only a few *C. trachomatis* proteins had been implicated in this process and their functions still remain mostly unknown (Cocchiaro *et al.*, 2008; Kumar *et al.*, 2006; Rank *et al.*, 2011; Saka *et al.*, 2015; Sisko *et al.*, 2006). As we identified a novel *C. trachomatis* Inc associating with LDs, we considered that IncL deserved a detailed characterization, aiming to increase the knowledge on *C. trachomatis* effectors interacting with host cell LDs.

4.2 The dual intracellular localization of $IncL_{1-88}$ when ectopically produced in mammalian cells

We showed that the first 88 amino acid residues of IncL partially co-localized with LDs and with the ER when transiently produced in yeast and in HeLa cells. This suggests that $IncL_{1-88}$ have sorting motifs that directed it to LDs. Possibly, when $IncL_{1-88}$ is produced in eukaryotic cells, it is directed to the ER and then sorted to LDs. In addition to the bilobed hydrophobic motif, IncL has a predicted hydrophobic domain within the LD-targeting region, between glycine at position 47 (G_{47}) and phenyalanine at position 69 (F_{69}). We found that positively charged amino acids close to this hydrophobic domain are essential to target $IncL_{1-88}$ to LDs. LDs originate from the ER and, typically, eukaryotic class I proteins targeting LDs associate with membranes through hydrophobic hairpins and can localize both in the ER and LDs monolayer (Olzmann & Carvalho, 2019). In the case of caveolin (Cav), the central hydrophobic domain anchors Cav to the ER and then positively charged sequences mediate the sorting of Cav to LDs (Ingelmo-torres *et al.*, 2010), which is in agreement with our findings for $IncL_{1-88}$. In addition, $IncL_{1-88}$ does not seem to exclusively incorporate into oleic acid-induced LDs, as it also targets endogenous LDs in cells untreated with oleic acid. Full-length IncL showed a reticular distribution in HeLa cells, and accumulated in puncta

and patches in the cytosol and near the plasma membrane. The bilobed hydrophobic domain of IncL, which likely mediates the insertion of IncL at the inclusion membrane in infected cells, might lead to protein aggregation or to incorrect targeting to cellular membranes in transfected cells.

Our analysis of the topology of IncL indicates that both the amino and carboxy-terminal regions, flanking the bilobed hydrophobic domain, are exposed to the host cell cytosol. This agrees with the central bilobed hydrophobic motif mediating the insertion of IncL at the inclusion membrane, as predicted for an Inc. We speculate that in infected cells the same region and motifs that target $IncL_{1-88}$ to LDs might insert in the membrane leaflet of the inclusion membrane facing the host cell cytosol, similarly to monotopic membrane proteins, leaving one surface free to potentially interact with LDs or with regions of the ER originating LDs. While this needs to be tested, IncL has a proline residue near the center of the hydrophobic domain in its amino-terminal region, possibly aiding in hairpin formation, which is also present in the metyltransferase AAM-B (Zehmer *et al.*, 2008). The amino-terminal region of AAM-B associates with LDs with both ends facing the cytosol, indicating the formation of a hairpin loop in the phospholipid monolayer surrounding LDs (Zehmer *et al.*, 2008). In addition to AAM-B, the proline residue was also detected within the hydrophobic domain of other LDs proteins (ALDI, CYB5R3), but its substitution by leucine did not affect targeting (Zehmer *et al.*, 2008). The precise topology of IncL at the inclusion membrane remains to be elucidated. Nevertheless, the dual intracellular localization of the amino-terminal region in transfected cells and its exposure to the host cell cytosol during infection strongly indicates that this might be a functional region within IncL interacting with LDs and/or with regions of the ER originating LDs during *C. trachomatis* infection.

4.3 A possible role for IncL during *C. trachomatis* infection

The *C. trachomatis* inclusion establishes direct contact with the ER, where LDs are synthesized. This is mediated by at least one Inc protein, IncV, which interacts with the ER-resident proteins VAPA and VAPB, thus leading to the formation of ER-inclusion membrane contact sites (Stanhope *et al.*, 2017). Interestingly, the genes encoding IncL and IncV are organized next to each other on the same strand and separated by 127 nucleotides in the *C. trachomatis* genome. As the neighboring genes do not encode Incs, *incL* and *incV* correspond to a small island of *inc* genes, supporting that the functions of the encoded proteins could be related.

To understand the role of IncL during *C. trachomatis* infection, the generation of a *incL* null mutant will be important, but none of the most used strategies were successful, namely

group II intron-based insertional mutagenesis (Johnson & Fisher, 2013) and FRAEM (Mueller *et al.*, 2016), which might be related with technical specificities of our experimental conditions or an indication that *incL* is an essential gene. The latter is supported by the fact that a previous large mutagenesis screen did not isolate nonsense mutations for *incL* (Kokes *et al.*, 2015).

In the absence of an IncL-defective *C. trachomatis*, we tested if analyzing a strain with increased levels of IncL could provide us clues for its functions. Supporting a role for IncL in mediating *C. trachomatis*-LDs interactions, we showed that the production of plasmid-encoded IncL-2HA by *C. trachomatis* seems to increase slightly the area of LDs within the region of chlamydial inclusions. Our data indicated that this relative increment did not occur when cells were infected by *C. trachomatis* strains producing plasmid-encoded IncL-2HA proteins with mutations within the LDs-targeting region or CT449-2HA, supporting that it could be caused specifically by IncL. However, in general, we could not distinguish cells infected by the strain producing IncL-2HA from cells infected by strains producing IncL-2HA mutant proteins or CT449-2HA. As the effect caused by IncL-2HA was very minor, although consistent and somewhat specific, our experimental system might not have the sensitivity to clarify this. The generation of an *incL* mutant strain (conditional if the gene is essential) is required to test this and such strain is currently unavailable.

The chlamydial proteins Lda1, 2 and 3 are delivered by *C. trachomatis* into the host cell, where they associate with LDs (Kumar *et al.*, 2006). Lda3 also localizes at the inclusion membrane and lumen and it seems to play a major role in the recruitment of LDs by replacing adipocyte differentiation-related protein at the surface of LDs, probably facilitating the establishment of links between these organelles and the inclusion (Cocchiaro *et al.*, 2008). A model was previously proposed, in which unidentified Inc(s) could capture LDs at the inclusion membrane, which by invagination would deliver LDs into the lumen of the inclusion (Cocchiaro *et al.*, 2008). Although IncL was not previously detected in LDs isolated from *C. trachomatis*-infected cells, we propose that IncL could be involved in this process. In fact, different studies indicate that some Inc and non-Inc proteins interacting with LDs are being neglected. For instance, among several Incs tested, one study only detected IncA associated with LDs isolated from *C. trachomatis*-infected cells (Cocchiaro *et al.*, 2008), while another study only detected IncG, CT618 and Cap1 (Saka *et al.*, 2015).

LDs are composed by a hydrophobic core of neutral lipids surrounded by a phospholipid monolayer and associated proteins. They interact with other cellular organelles, regulate lipid and energy homeostasis (Olzmann & Carvalho, 2019) and are targeted by several intracellular pathogens (Roingeard & Melo, 2017; Vallochi *et al.*, 2018). For instance, LDs accumulate at the vicinity of *Mycobacterium tuberculosis*-containing

vacuoles followed by an accumulation of neutral lipids within the phagosome. Several protozoan parasites, including *Leishmania amazonensis* and *Toxoplasma gondii* induce the recruitment of LDs close to the parasite-containing vacuole, which favors parasite growth [reviewed in (Roingeard & Melo, 2017)]. With respect to *C. trachomatis*, LDs are known to accumulate at the periphery of the inclusion and to translocate into the inclusion lumen (Cocchiaro *et al.*, 2008; Kumar *et al.*, 2006). Moreover, the proteome of LDs was found to be altered during *C. trachomatis* infection (Saka *et al.*, 2015). It was also suggested that the absence of LDs impairs *C. trachomatis* growth (Kumar *et al.*, 2006), although this finding has been challenged in subsequent studies (Recuero-Checa *et al.*, 2016; Sharma *et al.*, 2018). Recently, it was demonstrated that the depletion of specific host SNAREs increased the content of LDs in *C. trachomatis*-infected cells and significantly decreased bacterial growth (Monteiro-Brás *et al.*, 2020). Whether the content of LDs influences or not *C. trachomatis* growth during infection of tissue cultured cells is still a matter of debate, but the relevance of LDs during chlamydial infections *in vivo* is further supported by their detection within inclusions from cells of mice infected by *Chlamydia muridarum* (Rank *et al.*, 2011), a chlamydial species that infects rodents. Future studies combining the ability to genetically manipulate *C. trachomatis* with knowledge on the different chlamydial proteins, such as IncL, that can target LDs should eventually clarify the significance of the *Chlamydia*-LDs interaction.

4.4 Searching for IncL host cell interacting proteins

Previous screens searching for host cell interacting partners for Incs predicted the interaction of IncL with host cell proteins. A large proteomics screen detected interactions between IncL and eukaryotic 14-3-3s and protein tyrosine kinase 7 (PTK7) (Mirrashidi *et al.*, 2015). More recently, a bacterial two-hybrid screen detected interactions between IncL and the SNAREs VAMP3 and VAMP4 (Bui *et al.*, 2021). However, all these predicted interactions remained to be validated.

At the beginning of this project, the only predicted IncL interacting partners had been published by Mirrashidi *et al.* In this study, full-length Incs and/or their predicted cytosolic domains fused to Strep tags were transiently produced in mammalian cells, affinity purified (AP), and the entire eluates were analyzed by mass spectrometry (MS). This led to the identification of hundreds of potential interacting partners for a total of 38 Incs. In particular, full length IncL was predicted to interact with the membrane receptor PTK7 and with the isoforms β, η and γ of 14-3-3s (Mirrashidi *et al.*, 2015). 14-3-3s regulate a wide variety of signaling pathways, including the cell cycle, intracellular trafficking and cytoskeleton

remodeling (Pennington *et al.*, 2018). They are present in all eukaryotic cells and, in particular, humans produce seven isoforms (β, γ, ε, η, σ, τ, and ζ), each one encoded by a different gene (Aitken, 2002; Jones *et al.*, 1995). Here, the interaction of IncL with these proteins was tested by co-IP assays using mammalian cells ectopically co-producing IncL and each one of the seven 14-3-3 isoforms or PTK7. IncL failed to interact with PTK7, which was not surprising as we did not observe a particular accumulation of this protein at the inclusion membrane. In contrast, we were able to confirm the previously predicted interactions of IncL with 14-3-3β, η and γ, and we also found an interaction with the isoform σ. In addition, we showed that all the seven isoforms are recruited to the inclusion membrane during infection, which had been previously shown by fluorescence microscopy solely for the isoforms β and ε (Kokes *et al.*, 2015). Considering our results and the possibility of false positives in AP-MS approaches, even with the employment of stringent algorithms (Mirrashidi *et al.*, 2015), we discarded PTK7 and explored the interaction between IncL and 14-3-3s.

In the context of *C. trachomatis* infections, 14-3-3β was the first eukaryotic protein found to be recruited to the inclusion membrane (Scidmore & Hackstadt, 2001). Site-directed mutagenesis of predicted 14-3-3 phosphorylation sites demonstrated that IncG binds to 14-3-3β via a conserved 14-3-3 binding motif ($RS_{164}RS_{166}F$) (Scidmore & Hackstadt, 2001). In addition, co-IP assays validated an interaction between InaC and 14-3-3β and ε, and these two isoforms were found to be recruited to the inclusion membrane in a InaC-dependent manner (Kokes *et al.*, 2015). Taking into account that would be ineffective to further analyze simultaneously the interaction of IncL with four 14-3-3 isoforms, and considering that two other Incs interact with the isoform β, we focused on identifying functional regions within IncL mediating the interaction with 14-3-3β.

The analysis of the primary sequence of IncL revealed the presence of two conserved 14-3-3 binding motifs [$R_{164}S_{165}S_{166}S_{167}A_{168}P_{169}$ and a serine as the penultimate amino acid residue (S_{188})] (Johnson *et al.*, 2010; Yaffe *et al.*, 1997) and an additional set of 3 consecutive serines ($S_{150}S_{151}S_{152}$) at the carboxy-terminal region. We successfully identified the carboxy-terminal region ($IncL_{139\text{-}189}$) as being essential and sufficient for IncL-14-3-3β interaction. However, IncL mutant proteins with all the serines within the putative 14-3-3 binding motifs replaced by alanines were still able to interact with IncL. Considering that the presence of these motifs is unlikely to occur by chance, especially the accuracy of the motif $R_{164}S_{165}S_{166}S_{167}A_{168}P_{169}$, we hypothesize that these motifs might be important for the interaction with other 14-3-3 isoforms and/or other unknown motifs are present within IncL. In our assays, these hypothetical unknown motifs could be sufficient to mediate the interaction of IncL mutant proteins with 14-3-3β. Supporting this hypothesis, 14-3-3s

preferentially bind to phosphoserine/threonine residues within conserved motifs (Yaffe *et al.*, 1997), but the interaction with these motifs in the absence of phosphorylation and with other types of sequences has already been described (Aitken, 2002). For instance, the interaction of the ADP-ribosyltransferase toxin, exoenzyme S (ExoS), secreted by the bacterium *Pseudomonas aeruginosa*, with 14-3-3s is independent of phosphorylation and depends on a DALDL sequence (Henriksson *et al.*, 2002). Other regulatory mechanisms involved in targets specificity include post-translation modifications of 14-3-3s, the state of phosphorylation of themselves or their targets and also the preference of 14-3-3s to form heterodimers with specific isoforms (Aitken, 2002; Aitken, 2011). In fact, 14-3-3 monomers are unstable and interact with their targets as hetero or homodimers, except the isoform σ, which is more structurally different and preferentially forms homodimers (Aitken, 2011).

The results obtained in our experimental system are insufficient to conclude if IncL binds 14-3-3s directly or via an intermediate eukaryotic protein. Moreover, we do not know if IncL is able to bind all the four isoforms β, η, γ and σ. The probability of IncL-14-3-3σ interaction is high, as 14-3-3σ tends to form homodimers, but the interaction with some other isoforms might be a consequence of heterodimerization between isoforms. In line with this, as all the isoforms are recruited to the inclusion membrane and so far only four isoforms were found to interact with Incs, this suggests that the remaining isoforms might be recruited to the inclusion membrane as a result of heterodimerization or other 14-3-3-binding Incs remain to be identified.

Before a further exploitation of other 14-3-3 binding motifs within IncL, it is essential to understand if these proteins interact directly with each other. This could be done by performing yeast or bacterial two-hybrid experiments or pull-down assays with purified IncL and 14-3-3s. Also, these interactions need to be validated in more physiological conditions, by performing co-IP assays using *C. trachomatis*-infected cells. Regarding the function of 14-3-3s in the context of *C. trachomatis* infections, it was suggested that the recruitment of 14-3-3β by Incs might sequester BCL2-associated agonist of cell death (BAD) protein at the inclusion membrane away from mitochondria, thus protecting host cell from apoptosis (Verbeke *et al.*, 2006). Besides this hypothesis, the role of 14-3-3s during *C. trachomatis* infection remains to be elucidated. It is reasonable to speculate for a relationship between the interaction of IncL with LDs and 14-3-3s, as some 14-3-3 isoforms were found associated with LDs isolated from mouse white adipocytes (Ding *et al.*, 2012) and also from uninfected and *C. trachomatis*-infected HeLa cells (Saka *et al.*, 2015). The recruitment of all the seven mammalian isoforms to the periphery of *C. trachomatis* inclusions and their interaction with at least three Incs indicate that the functions of 14-3-3s during infection deserve to be further investigated.

4.5 Model for the role of IncL during *C. trachomatis* infection

Based on our results, we hypothesize the mode of action of IncL during *C. trachomatis* infection (Figure 4.1). IncL is inserted into the inclusion membrane via a bilobed hydrophobic domain, while the amino and carboxy-terminal regions are exposed to the host cell cytosol and therefore available to interact with host cell partners. The carboxy-terminal region of IncL mediates a direct/indirect binding to four isoforms of 14-3-3s, however the meaning of these interactions is difficult to speculate taking into account the multitude of signaling pathways regulated by 14-3-3s. A putative hydrophobic domain (amino acids 47 to 69) within the amino-terminal region of IncL interacts with LDs and/or with regions of the ER originating LDs, which might facilitate the interaction of *C. trachomatis* inclusions with these organelles and their internalization into the lumen of the inclusion to be used as a source of proteins and lipids for bacterial growth. A relationship between the interaction of IncL with LDs and with 14-3-3s remains to be elucidated.

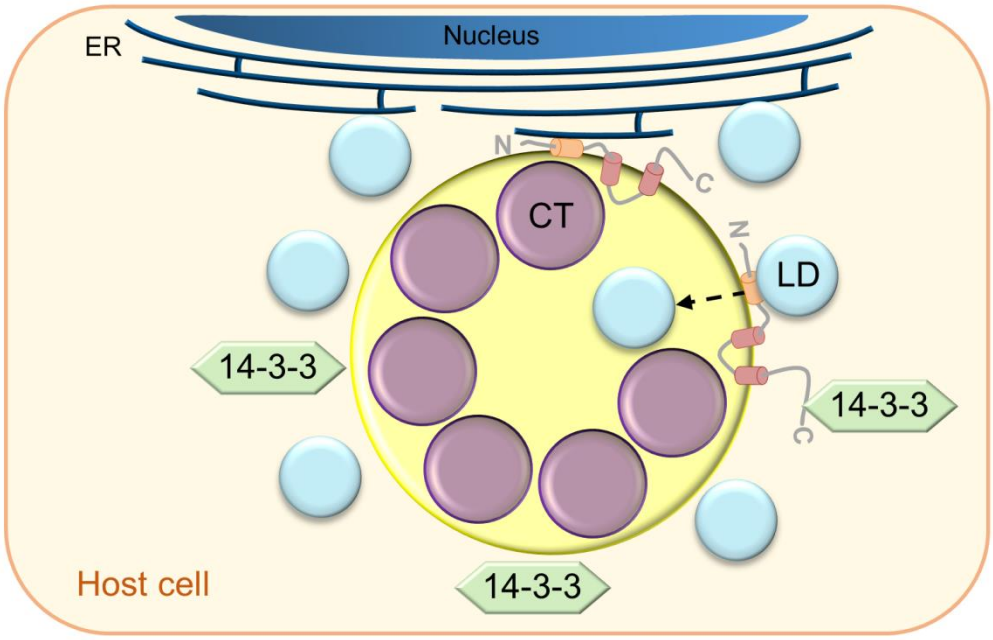

Figure 4.1 Model for the role of IncL during *C. trachomatis* infection. In *C. trachomatis* (CT)-infected cells, IncL is likely inserted into the inclusion membrane via a bilobed hydrophobic domain (amino acids 89 to 140; in red). The amino and carboxy-terminal regions of IncL are exposed to the host cell cytosol. The carboxy-terminal region interacts with eukaryotic 14-3-3s, while the amino-terminal region interacts with lipid droplets (LD) and/or with regions of the endoplasmic reticulum (ER) originating LDs, possibly via a putative hydrophobic domain (amino acids 47 to 69; in orange). IncL might facilitate the interaction of *C. trachomatis* inclusions with LDs and mediate their internalization into the lumen of the inclusion.

4.6 Concluding remarks and future directions

The results obtained throughout this PhD work contributed to expand the knowledge on the mechanisms evolved by the human pathogen *C. trachomatis* to subvert host mechanisms. In order to survive and proliferate within the inclusion, *C. trachomatis* must deliver effector proteins into host cells to selectively interact with organelles and pathways that favor bacterial growth and avoid pathways and immune responses leading to bacterial clearance. We successfully identified a *C. trachomatis* Inc, IncL, as a novel Inc targeting the host cell ER and LDs and also validated its interaction with mammalian 14-3-3s. IncL is a core Inc possibly involved in conserved interactions with host cells, as it is one of the 23 Incs conserved among at least five chlamydial species (*C. trachomatis*, *C. felis*, *C. pneumoniae*, *C. caviae*, and *C. muridarum*) (Lutter *et al.*, 2012). In infection experiments, the accumulation of LDs at the region of inclusions slightly and specifically increased in cells infected by a *C. trachomatis* strain overproducing IncL comparing with cells infected by the parental strain. However, this minor increment was not distinguishable from the ones caused by the overproduction of IncL with mutations within the LDs-targeting region. As all these chlamydial strains produce endogenous IncL, these results could only be clarified by generating a *C. trachomatis incL* null mutant. With such mutant strain, which we were unable to generate using FRAEM or the TargeTron method, it would be possible to make comparisons between the accumulation of LDs at the region of inclusions between cells infected by the parental strain producing endogenous IncL, the mutant strain lacking IncL and the mutant strains complemented with IncL or with IncL with mutations within the LDs-targeting region. The availability of this *C. trachomatis* strain lacking IncL, and possibly other double or triple mutant strains lacking simultaneously IncL and proteins with IncL-related functions, will make possible to clarify the role of IncL in mediating the recruitment of LDs and 14-3-3s to *C. trachomatis* inclusions. Also, it should reveal if IncL is important/essential for *C. trachomatis* growth and development. Hopefully, the recent developed strategies to use CRISPR interference for *C. trachomatis* essential genes (Ouellette, 2018; Ouellette *et al.*, 2021) might be appropriate to mutagenize *incL*. However, the reported reduction in transcript levels of 80-90% using CRISPRi (Ouellette *et al.*, 2021) might be insufficient to reveal a phenotype and constructing *incL* mutant strains might be challenging until CRISPRi is better established in the chlamydial field. With this in mind, efforts could be made in answering other questions that came out from this work. The relevance of IncL interaction with 14-3-3s is far from being understood, as well as the complex and diverse signaling pathways that might be regulated by these adaptor molecules in the context of infection. Taking into account that all the mammalian 14-3-3 isoforms are recruited to the

inclusion membrane and, in addition to IncG and InaC, IncL also interacts exclusively with some 14-3-3 isoforms, our work highlights the relevance of further exploring the meaning of these interactions to better understand the interplay between *C. trachomatis* and host cells. The subsequent work on this topic should focus on validating the interaction of IncL with 14-3-3s in the context of infection, as the diverse regulatory mechanisms involved in the ability of 14-3-3s to interact with their binding partners might differ between transfected and infected cells. Also, it is essential to determine if the interactions are direct or not, which can be answered in yeast or bacterial-two hybrid experiments between IncL and 14-3-3 isoforms. If the interaction is direct, the carboxy-terminal region of IncL should be examined in more detailed to search for 14-3-3 binding motifs, as novel binding domains might be discovered. This approach could start with the analysis of IncL versions with different portions of the carboxy-terminal region removed, to find a smaller region mediating the interaction. Subsequently, site-directed mutagenesis within this smaller region should reveal the 14-3-3 binding motif/s. In addition, IncL proteins with mutations within conserved 14-3-3 binding motifs, which were able to interact with 14-3-3β in our experiments, should be tested for their ability to interact with other isoforms, as the binding site may vary depending on the isoform and a single protein might interact with different isoforms via different motifs. If these approaches reveal that IncL does not bind directly to 14-3-3s, IncL binding partners can be searched by a MS analysis of mammalian proteins pulled down by transiently produced mEGFP-IncL. The identification of other IncL interacting proteins will help to understand the meaning of IncL interactions with 14-3-3s and LDs, and might also highlight novel IncL binding proteins, thus creating novel lines of research that could reveal other functions for IncL.

We identified an ER and LDs targeting region within the first 88 amino acid residues of IncL and also positively charged residues flanking a putative hydrophobic domain that are important for $IncL_{1-88}$ targeting to LDs in mammalian cells. To our knowledge, this is the first description of this type of motif mediating the targeting of chlamydial proteins to lipid droplets. However, it is still unclear how the putative hydrophobic domain, possibly mediating IncL-ER and IncL-LDs interactions, is exposed to host cell cytosol. To test if this domain is a hydrophobic hairpin inserted in a membrane leaflet as monotopic proteins, we could start by analyzing the topology of transiently produced $IncL_{1-88}$ in mammalian cells. Protease-protection assays could be performed using HeLa cells transfected with plasmids encoding $IncL_{1-88}$ with different tags at the amino and carboxy-terminal regions, such as mEGFP-$IncL_{1-88}$-2HA. In the case of smaller bands being detect by immunoblotting using anti-GFP and anti-HA, this would indicate that both regions were cleaved, meaning they

were exposed to the cytosol and therefore the hydrophobic motif would not cross the lipid membrane.

Despite the unanswered questions, this PhD work contributed to increase the knowledge on *C. trachomatis* effectors mediating interactions with host cells. We discovered a *C. trachomatis* Inc, named IncL for Inc associating with LDs, which also interacts with the adaptor molecules 14-3-3s. Our results highlight that a single *C. trachomatis* effector might interact with multiple host cell targets and possibly interfere with diverse cell functions, not discarding, however, the possibility of these interactions being related with the subversion of the same host pathway, as some 14-3-3 isoforms have been previously detected in the LDs proteome.

REFERENCES

AbdelRahman, Y. M., & Belland, R. J. (2005). The chlamydial developmental cycle. *FEMS Microbiol Rev*, *29*, 949–959.

Abraham, S., Juel, H. B., Bang, P., Cheeseman, H. M., Dohn, R. B., Cole, T., Kristiansen, M. P., Korsholm, K. S., Lewis, D., Olsen, A. W., McFarlane, L. R., Day, S., Knudsen, S., Moen, K., Ruhwald, M., Kromann, I., Andersen, P., Shattock, R. J., & Follmann, F. (2019). Safety and immunogenicity of the Chlamydia vaccine candidate CTH522 adjuvanted with CAF01 liposomes or aluminium hydroxide: a first-in-human, randomised, double-blind, placebo-controlled, phase 1 trial. *Lancet Infect Dis*, *19*, 1091–1100.

Aeberhard, L., Banhart, S., Fischer, M., Jehmlich, N., Rose, L., Koch, S., Laue, M., Renard, B. Y., Schmidt, F., & Heuer, D. (2015). The proteome of the isolated Chlamydia trachomatis containing vacuole reveals a complex trafficking platform enriched for retromer components. *PLoS Pathog*, *11*, e1004883.

Agaisse, H., & Derré, I. (2013). A C. trachomatis cloning vector and the generation of C. trachomatis strains expressing fluorescent proteins under the control of a C. trachomatis promoter. *PLoS One*, *8*, e57090.

Agaisse, H., & Derré, I. (2014). Expression of the effector protein IncD in Chlamydia trachomatis mediates recruitment of the lipid transfer protein CERT and the endoplasmic reticulum-resident protein VAPB to the inclusion membrane. *Infect Immun*, *82*, 2037–2047.

Aitken, A. (2002). Functional specificity in 14-3-3 isoform interactions through dimer formation and phosphorylation. Chromosome location of mammalian isoforms and variants. *Plant Mol Biol*, *50*, 993–1010.

Aitken, A. (2011). Post-translational modification of 14-3-3 isoforms and regulation of cellular function. *Semin Cell Dev Biol*, *22*, 673–680.

Al-Zeer, M. A., Xavier, A., Abu Lubad, M., Sigulla, J., Kessler, M., Hurwitz, R., & Meyer, T. F. (2017). Chlamydia trachomatis prevents apoptosis via activation of PDPK1-MYC and enhanced mitochondrial binding of hexokinase II. *EBioMedicine*, *23*, 100–110.

Almeida, F., Borges, V., Ferreira, R., Borrego, M. J., Gomes, J. P., & Jaime Mota, L. J. (2012). Polymorphisms in Inc proteins and differential expression of inc genes among Chlamydia trachomatis strains correlate with invasiveness and tropism of Lymphogranuloma venereum isolates. *J Bacteriol*, *194*, 6574–6585.

Almeida, F., Luís, M. P., Pereira, I. S., Pais, S. V., & Mota, L. J. (2018). The human centrosomal protein CCDC146 binds Chlamydia trachomatis inclusion membrane protein CT288 and is recruited to the periphery of the Chlamydia-containing vacuole. *Front Cell Infect Microbiol*, *8*, 254.

Alzhanov, D. T., Weeks, S. K., Burnett, J. R., & Rockey, D. D. (2009). Cytokinesis is blocked in mammalian cells transfected with Chlamydia trachomatis gene CT223. *BMC Microbiol*, *9*, 2.

Archuleta, T. L., & Spiller, B. W. (2014). A gatekeeper chaperone complex directs translocator secretion during type three secretion. *PLoS Pathog*, *10*, e1004498.

Bannantine, J. P., Griffiths, R. S., Viratyosin, W., Brown, W. J., & Rockey, D. D. (2000). A secondary structure motif predictive of protein localization to the chlamydial inclusion membrane. *Cell Microbiol*, *2*, 35–47.

Bastidas, R. J., Elwell, C. A., Engel, J. N., & Valdivia, R. H. (2013). Chlamydial intracellular survival strategies. *Cold Spring Harb Perspect Med*, *3*, a010256.

Bauler, L. D., & Hackstadt, T. (2014). Expression and targeting of secreted proteins from Chlamydia trachomatis. *J Bacteriol*, *196*, 1325–1334.

Becker, E., & Hegemann, J. H. (2014). All subtypes of the Pmp adhesin family are implicated in chlamydial virulence and show species-specific function. *Microbiology Open*, *3*, 544–556.

Belland, R. J., Scidmore, M. A., Crane, D. D., Hogan, D. M., Whitmire, W., McClarty, G., & Caldwell, H. D. (2001). Chlamydia trachomatis cytotoxicity associated with complete and partial cytotoxin genes. *Proc Natl Acad Sci U S A*, *98*, 13984–13989.

Belland, R. J., Zhong, G., Crane, D. D., Hogan, D., Sturdevant, D., Sharma, J., Beatty, W. L., & Caldwell, H. D. (2003). Genomic transcriptional profiling of the developmental cycle of Chlamydia trachomatis. *Proc Natl Acad Sci U S A*, *100*, 8478–8483.

Betts-Hampikian, H. J., & Fields, K. A. (2010). The chlamydial type III secretion mechanism: Revealing cracks in a tough nut. *Front Microbiol*, *1*, 114.

Binet, R., & Maurelli, A. T. (2009). Transformation and isolation of allelic exchange mutants of Chlamydia psittaci using recombinant DNA introduced by electroporation. *Proc Natl Acad Sci U S A*, *106*, 292–297.

Bishop, R. C., Boretto, M., Rutkowski, M. R., Vankelecom, H., & Derré, I. (2020). Murine endometrial organoids to model Chlamydia infection. *Front Cell Infect Microbiol*, *10*, 416.

Black, M. W., & Pelham, H. R. B. (2000). A selective transport route from Golgi to late endosomes that requires the yeast GGA proteins. *J Cell Biol*, *151*, 587–600.

Bodetti, T. J., Jacobson, E., Wan, C., Hafner, L., Pospischil, A., Rose, K., & Timms, P. (2002). Molecular evidence to support the expansion of the hostrange of Chlamydophila pneumoniae to include reptiles as well as humans, horses, koalas and amphibians. *Syst Appl Microbiol*, *25*, 146–152.

Bond, S. R., & Naus, C. C. (2012). RF-Cloning.org: an online tool for the design of restriction-free cloning projects. *Nucleic Acids Res*, *40*, W209–W213.

Borth, N., Massier, J., Franke, C., Sachse, K., Saluz, H. P., & Hänel, F. (2010). Chlamydial protease CT441 interacts with SRAP1 co-activator of estrogen receptor α and partially alleviates its co-activation activity. *J Steroid Biochem Mol Biol*, *119*, 89–95.

Brown, J. S. (2012). Community-acquired pneumonia. *Clin Med (Lond)*, *12*, 538–543.

Bugalhão, J. N., & Mota, L. J. (2019). The multiple functions of the numerous Chlamydia trachomatis secreted proteins: The tip of the iceberg. *Microb Cell*, *6*, 414–449.

Bugalhão, J. N., Mota, L. J., & Franco, I. S. (2016). Identification of regions within the Legionella pneumophila VipA effector protein involved in actin binding and polymerization and in interference with eukaryotic organelle trafficking. *Microbiology Open*, *5*, 118–133.

Bui, D. C., Jorgenson, L. M., Ouellette, S. P., & Rucks, E. A. (2021). Eukaryotic SNARE VAMP3 dynamically interacts with multiple chlamydial inclusion membrane proteins. *Infect Immun*, *89*, e00409-20.

Cai, Y., Fukushi, H., Koyasu, S., Kuroda, E., Yamaguchi, T., & Hirai, K. (2002). An etiological investigation of domestic cats with conjunctivitis and upper respiratory tract disease in Japan. *J Vet Med Sci*, *64*, 215–219.

Capmany, A., & Damiani, M. T. (2010). Chlamydia trachomatis intercepts Golgi-derived sphingolipids through a rab14-mediated transport required for bacterial development and replication. *PLoS One*, *5*, e14084.

Carlson, J. H., Hughes, S., Hogan, D., Cieplak, G., Sturdevant, D. E., McClarty, G., Caldwell, H. D., & Belland, R. J. (2004). Polymorphisms in the Chlamydia trachomatis cytotoxin locus associated with ocular and genital isolates. *Infect Immun*, *72*, 7063–7072.

Carlson, J. H., Whitmire, W. M., Crane, D. D., Wicke, L., Virtaneva, K., Sturdevant, D. E., Kupko, J. J., Porcella, S. F., Martinez-Orengo, N., Heinzen, R. A., Kari, L., & Caldwell, H. D. (2008). The Chlamydia trachomatis plasmid is a transcriptional regulator of chromosomal genes and a virulence factor. *Infect Immun*, *76*, 2273–2283.

Carpenter, V., Chen, Y.-S., Dolat, L., & Valdivia, R. H. (2017). The effector TepP mediates recruitment and activation of Phosphoinositide 3-kinase on early Chlamydia trachomatis vacuoles. *mSphere*, *2*, e00207-17.

Ceovic, R., & Gulin, S. J. (2015). Lymphogranuloma venereum: Diagnostic and treatment challenges. *Infect Drug Resist*, *8*, 39–47.

Chellas-Géry, B., Linton, C. N., & Fields, K. A. (2007). Human GCIP interacts with CT847, a novel Chlamydia trachomatis type III secretion substrate, and is degraded in a tissue-culture infection model. *Cell Microbiol*, *9*, 2417–2430.

Chen, A. L., Johnson, K. A., Lee, J. K., Sutterlin, C., & Tan, M. (2012). CPAF: A chlamydial protease in search of an authentic substrate. *PLoS Pathog*, *8*, e1002842.

Chen, C., Chen, D., Sharma, J., Cheng, W., Zhong, Y., Liu, K., Jensen, J., Shain, R., Arulanandam, B., & Zhong, G. (2006). The hypothetical protein CT813 is localized in the Chlamydia trachomatis inclusion membrane and is immunogenic in women urogenitally infected with C. trachomatis. *Infect Immun*, *74*, 4826–4840.

Chen, Y. S., Bastidas, R. J., Saka, H. A., Carpenter, V. K., Richards, K. L., Plano, G. V., & Valdivia, R. H. (2014). The Chlamydia trachomatis type III secretion chaperone Slc1 engages multiple early effectors, including TepP, a tyrosine-phosphorylated protein required for the recruitment of CrkI-II to nascent inclusions and innate immune signaling. *PLoS Pathog*, *10*, e1003954.

Chowdhury, S. R., & Rudel, T. (2017). Chlamydia and mitochondria - an unfragmented relationship. *Microb Cell*, *4*, 233–235.

Cingolani, G., McCauley, M., Lobley, A., Bryer, A. J., Wesolowski, J., Greco, D. L., Lokareddy, R. K., Ronzone, E., Perilla, J. R., & Paumet, F. (2019). Structural basis for the homotypic fusion of chlamydial inclusions by the SNARE-like protein IncA. *Nat Commun*, *10*, 2747.

Cocchiaro, J. L., Kumar, Y., Fischer, E. R., Hackstadt, T., & Valdivia, R. H. (2008). Cytoplasmic lipid droplets are translocated into the lumen of the Chlamydia trachomatis parasitophorous vacuole. *Proc Natl Acad Sci U S A*, *105*, 9379–9384.

Comanducci, M., Cevenini, R., Moroni, A., Giuliani, M.M., Ricci, S., Scarlato, V., and Ratti, G. (1993). Expression of a plasmid gene of Chlamydia trachomatis encoding a novel 28 kDa antigen. *J Gen Microbiol, 139,* 1083–1092

Cornelis, G. R. (2006). The type III secretion injectisome. *Nat Rev Microbiol*, *4*, 811–825.

Cossé, M. M., Barta, M. L., Fisher, D. J., Oesterlin, L. K., Niragire, B., Perrinet, S., Millot, G. A., Hefty, P. S., & Subtil, A. (2018). The loss of expression of a single type 3 effector (CT622) strongly reduces Chlamydia trachomatis infectivity and growth. *Front Cell Infect Microbiol*, *8*, 145.

Costa, T. R. D., Felisberto-Rodrigues, C., Meir, A., Prevost, M. S., Redzej, A., Trokter, M., & Waksman, G. (2015). Secretion systems in Gram-negative bacteria: Structural and mechanistic insights. *Nat Rev Microbiol*, *13*, 343–359.

Da Cunha, M., Milho, C., Almeida, F., Pais, S. V., Borges, V., Maurício, R., Borrego, M. J., Gomes, J. P., & Mota, L. J. (2014). Identification of type III secretion substrates of Chlamydia trachomatis using Yersinia enterocolitica as a heterologous system. *BMC Microbiol*, *14*, 40.

Da Cunha, M., Pais, S. V., Bugalhão, J. N., & Mota, L. J. (2017). The Chlamydia trachomatis type III secretion substrates CT142, CT143, and CT144 are secreted into the lumen of the inclusion. *PLoS One*, *12*, e0178856.

De Clercq, E., Kalmar, I., & Vanrompay, D. (2013). Animal models for studying female genital tract infection with Chlamydia trachomatis. *Infect Immun*, *81*, 3060–3067.

De Felipe, K. S., Glover, R. T., Charpentier, X., Anderson, O. R., Reyes, M., Pericone, C. D., & Shuman, H. A. (2008). Legionella eukaryotic-like type IV substrates interfere with organelle trafficking. *PLoS Pathog, 4*, e1000117.

De Puysseleyr, L., De Puysseleyr, K., Braeckman, L., Morré, S. A., Cox, E., & Vanrompay, D. (2017). Assessment of Chlamydia suis infection in pig farmers. *Transbound Emerg Dis*, *64*, 826–833.

Dehoux, P., Flores, R., Dauga, C., Zhong, G., & Subtil, A. (2011). Multi-genome identification and characterization of chlamydiae-specific type III secretion substrates: The Inc proteins. *BMC Genomics*, *12*, 109.

Delevoye, C., Nilges, M., Dautry-Varsat, A., & Subtil, A. (2004). Conservation of the biochemical properties of IncA from Chlamydia trachomatis and Chlamydia caviae: Oligomerization of IncA mediates interaction between facing membranes. *J Biol Chem*, *279*, 46896–46906.

Delevoye, C., Nilges, M., Dehoux, P., Paumet, F., Perrinet, S., Dautry-Varsat, A., & Subtil, A. (2008). SNARE protein mimicry by an intracellular bacterium. *PLoS Pathog*, *4*, e1000022.

Derré, I., Swiss, R., & Agaisse, H. (2011). The lipid transfer protein CERT interacts with the Chlamydia inclusion protein IncD and participates to ER-Chlamydia inclusion membrane contact sites. *PLoS Pathog*, *7*, e1002092.

Ding, Y., Wu, Y., Zeng, R., & Liao, K. (2012). Proteomic profiling of lipid droplet-associated proteins in primary adipocytes of normal and obese mouse. *Acta Biochim Biophys Sin (Shanghai)*, *44*, 394–406.

Dong, F., Pirbhai, M., Zhong, Y., & Zhong, G. (2004). Cleavage-dependent activation of a Chlamydia-secreted protease. *Mol Microbiol*, *52*, 1487–1494.

Dumoux, M., Menny, A., Delacour, D., & Hayward, R. D. (2015). A Chlamydia effector recruits CEP170 to reprogram host microtubule organization. *J Cell Sci*, *128*, 3420–3434.

Durand, N.J., Nicolas, J., and Favre, M. (1913). Lymphogranulomatose inguinale subaiguë d'origine génitale probable, peut-être vénérienne. *Bull la Société des Médecins des Hôpitaux Paris, 35,* 274–288.

Elwell, C. A., Ceesay, A., Jung, H. K., Kalman, D., & Engel, J. N. (2008). RNA interference screen identifies Abl kinase and PDGFR signaling in Chlamydia trachomatis entry. *PLoS Pathog*, *4*, e1000021.

Elwell, C. A., Czudnochowski, N., von Dollen, J., Johnson, J. R., Nakagawa, R., Mirrashidi, K., Krogan, N. J., Engel, J. N., & Rosenberg, O. S. (2017). Chlamydia interfere with an interaction between the mannose-6-phosphate receptor and sorting nexins to counteract host restriction. *eLife*, *6*, e22709.

Elwell, C., Mirrashidi, K., & Engel, J. (2016). Chlamydia cell biology and pathogenesis. *Nat Rev Microbiol*, *14*, 385–400.

Essig, A., & Longbottom, D. (2015). Chlamydia abortus: New aspects of infectious abortion in sheep and potential risk for pregnant women. *Curr Clin Microbiol Rep*, *2*, 22–34.

European Centre for Disease Prevention and Control. Lymphogranuloma venereum (2020).

Fabijan, J., Caraguel, C., Jelocnik, M., Polkinghorne, A., Boardman, W. S. J., Nishimoto, E., Johnsson, G., Molsher, R., Woolford, L., Timms, P., Simmons, G., Hemmatzadeh, F., Trott, D. J., & Speight, N. (2019). Chlamydia pecorum prevalence in South Australian koala (Phascolarctos cinereus) populations: Identification and modelling of a population free from infection. *Sci Rep*, *9*, 6261.

Falck, G., Heyman, L., Gnarpe, J., & Gnarpe, H. (1995). Chlamydia pneumoniae and chronic pharyngitis. *Scand J Infect Dis*, *27*, 179–182.

Faris, R., McCullough, A., Andersen, S. E., Moninger, T. O., & Weber, M. M. (2020). The Chlamydia trachomatis secreted effector TmeA hijacks the N-WASP-ARP2/3 actin remodeling axis to facilitate cellular invasion. *PLoS Pathog*, *16*, e1008878.

Faris, R., Merling, M., Andersen, S. E., Dooley, C. A., Hackstadt, T., & Weber, M. M. (2019). Chlamydia trachomatis CT229 subverts Rab GTPase-dependent CCV trafficking pathways to promote chlamydial infection. *Cell Rep*, *26*, 3380–3390.

Fehlner-Gardiner, C., Roshick, C., Carlson, J. H., Hughes, S., Belland, R. J., Caldwell, H. D., & McClarty, G. (2002). Molecular basis defining human Chlamydia trachomatis tissue tropism: A possible role for tryptophan synthase. *J Biol Chem*, *277*, 26893–26903.

Ferreira, R., Borges, V., Nunes, A., Borrego, M. J., & Gomes, J. P. (2013). Assessment of the load and transcriptional dynamics of Chlamydia trachomatis plasmid according to strains' tissue tropism. *Microbiol Res*, *168*, 333–339.

Fields, K. A., & Hackstadt, T. (2000). Evidence for the secretion of Chlamydia trachomatis CopN by a type III secretion mechanism. *Mol Microbiol*, *38*, 1048–1060.

Fischer, A., Harrison, K. S., Ramirez, Y., Auer, D., Chowdhury, S. R., Prusty, B. K., Sauer, F., Dimond, Z., Kisker, C., Hefty, P. S., & Rudel, T. (2017). Chlamydia trachomatis-containing vacuole serves as deubiquitination platform to stabilize Mcl-1 and to interfere with host defense. *eLife*, *6*, e21465.

Fling, S. P., Sutherland, R. A., Steele, L. N., Hess, B., D'Orazio, S. E. F., Maisonneuve, J. F., Lampe, M. F., Probst, P., & Starnbach, M. N. (2001). CD8+ T cells recognize an inclusion associated protein from the pathogen Chlamydia trachomatis. *Proc Natl Acad Sci U S A*, *98*, 1160–1165.

Franco, I. S., Shohdy, N., & Shuman, H. A. (2012). The Legionella pneumophila effector VipA is an actin nucleator that alters host cell organelle trafficking. *PLoS Pathog*, *8*, e1002546.

Galán, J. E., Lara-Tejero, M., Marlovits, T. C., & Wagner, S. (2014). Bacterial type III secretion systems: Specialized nanomachines for protein delivery into target cells. *Annu Rev Microbiol*, *68*, 415–438.

Garcia, J. T., Ferracci, F., Jackson, M. W., Joseph, S. S., Pattis, I., Plano, L. R. W., Fischer, W., & Plano, G. V. (2006). Measurement of effector protein injection by type III and type IV secretion systems by using a 13-residue phosphorylatable glycogen synthase kinase tag. *Infect Immun*, *74*, 5645–5657.

Gauliard, E., Ouellette, S. P., Rueden, K. J., & Ladant, D. (2015). Characterization of interactions between inclusion membrane proteins from Chlamydia trachomatis. *Front Cell Infect Microbiol*, *5*, 13.

Gehre, L., Gorgette, O., Perrinet, S., Prevost, M. C., Ducatez, M., Giebel, A. M., Nelson, D. E., Ball, S. G., & Subtil, A. (2016). Sequestration of host metabolism by an intracellular pathogen. *eLife*, *5*, e12552.

Ghosh, S., Ruelke, E. A., Ferrell, J. C., Bodero, M. D., Fields, K. A., & Travis J. J. (2020). Fluorescence-Reported Allelic Exchange Mutagenesis-mediated gene deletion indicates a requirement for Chlamydia trachomatis Tarp during in vivo infectivity and reveals a specific role for the C terminus during cellular invasion. *Infect Immun*, *88*, e00841-19.

Gitsels, A., Sanders, N., & Vanrompay, D. (2019). Chlamydial infection from outside to inside. *Front Microbiol, 10*, 2329.

Gomes, J. P., Nunes, A., Bruno, W. J., Borrego, M. J., Florindo, C., & Dean, D. (2006). Polymorphisms in the nine polymorphic membrane proteins of Chlamydia trachomatis across all serovars: Evidence for serovar Da recombination and correlation with tissue tropism. *J Bacteriol, 188*, 275–286.

Gong, S., Lei, L., Chang, X., Belland, R., & Zhong, G. (2011). Chlamydia trachomatis secretion of hypothetical protein CT622 into host cell cytoplasm via a secretion pathway that can be inhibited by the type III secretion system inhibitor compound 1. *Microbiology (Reading)*, *157*, 1134–1144.

Gong, S., Yang, Z., Lei, L., Shen, L., & Zhong, G. (2013). Characterization of Chlamydia trachomatis plasmid-encoded open reading frames. *J Bacteriol*, *195*, 3819–3826.

Hackstadt, T., Scidmore-Carlson, M. A., Shaw, E. I., & Fischer, E. R. (1999). The Chlamydia trachomatis IncA protein is required for homotypic vesicle fusion. *Cell Microbiol*, *1*, 119–130.

Halberstädter, L., & von Prowazek, S. (1907). Zur Aetiologie des Trachoms. *Dtsch Medizinische Wochenschrift, 33*, 1285-1287.

Hamaoui, D., Cossé, M. M., Mohan, J., Lystad, A. H., Wollert, T., & Subtil, A. (2020). The Chlamydia effector CT622/TaiP targets a nonautophagy related function of ATG16L1. *Proc Natl Acad Sci U S A*, *117*, 26784–26794.

Harkinezhad, T., Geens, T., & Vanrompay, D. (2009). Chlamydophila psittaci infections in birds: A review with emphasis on zoonotic consequences. *Vet Microbiol*, *135*, 68–77.

Harris, S. R., Clarke, I. N., Seth-Smith, H. M., Solomon, A. W., Cutcliffe, L. T., Marsh, P., Skilton, R. J., Holland, M. J., Mabey, D., Peeling, R. W., Lewis, D. A., Spratt, B. G., Unemo, M., Persson, K., Bjartling, C., Brunham, R., de Vries, H. J., Morré, S. A., Speksnijder, A., Bébéar, C. M., … Thomson, N. R. (2012). Whole-genome analysis of diverse Chlamydia trachomatis strains identifies phylogenetic relationships masked by current clinical typing. *Nat Genet,* 44, 413–419

Henriksson, M. L., Francis, M. S., Peden, A., Aili, M., Stefansson, K., Palmer, R., Aitken, A., & Hallberg, B. (2002). A nonphosphorylated 14-3-3 binding motif on exoenzyme S that is functional in vivo. *Eur J Biochem*, *269*, 4921–4929.

Heuer, D., Lipinski, A. R., Machuy, N., Karlas, A., Wehrens, A., Siedler, F., Brinkmann, V., & Meyer, T. F. (2009). Chlamydia causes fragmentation of the Golgi compartment to ensure reproduction. *Nature*, *457*, 731–735.

Ho, T. D., & Starnbach, M. N. (2005). The Salmonella enterica serovar typhimurium-encoded type III secretion systems can translocate Chlamydia trachomatis proteins into the cytosol of host cells. *Infect Immun*, *73*, 905–911.

Hobolt-Pedersen, A. S., Christiansen, G., Timmerman, E., Gevaert, K., & Birkelund, S. (2009). Identification of Chlamydia trachomatis CT621, a protein delivered through the type III secretion system to the host cell cytoplasm and nucleus. *FEMS Immunol Med Microbiol*, *57*, 46–58.

Hogan, R. J., Mathews, S. A., Mukhopadhyay, S., Summersgill, J. T., & Timms, P. (2004). Chlamydial persistence: beyond the biphasic paradigm. *Infect Immun*, *72*, 1843–1855.

Hou, S., Dong, X., Yang, Z., Li, Z., Liu, Q., & Zhong, G. (2015). Chlamydial plasmid-encoded virulence factor Pgp3 neutralizes the antichlamydial activity of human cathelicidin LL-37. *Infect Immun*, *83*, 4701–4709.

Hower, S., Wolf, K., & Fields, K. A. (2009). Evidence that CT694 is a novel Chlamydia trachomatis T3S substrate capable of functioning during invasion or early cycle development. *Mol Microbiol*, *72*, 1423–1437.

Huai, P., Li, F., Chu, T., Liu, D., Liu, J., & Zhang, F. (2020). Prevalence of genital Chlamydia trachomatis infection in the general population: A meta-analysis. *BMC Infectious Diseases*, *20*, 589.

Huang, J., Lesser, C. F., & Lory, S. (2008). The essential role of the CopN protein in Chlamydia pneumoniae intracellular growth. *Nature*, *456*, 112–115.

Huang, Z., Feng, Y., Chen, D., Wu, X., Huang, S., Wang, X., Xiao, X., Li, W., Huang, N., Gu, L., Zhong, G., & Chai, J. (2008). Structural basis for activation and inhibition of the secreted Chlamydia protease CPAF. *Cell Host Microbe*, *4*, 529–542.

Hui, X., Chen, Z., Lin, M., Zhang, J., Hu, Y., Zeng, Y., Cheng, X., Ou-Yang, L., Sun, M., White, A. P., & Wang, Y. (2020). T3SEpp: an integrated prediction pipeline for bacterial type III secreted effectors. *MSystems*, *5*, e00288-20.

Illingworth, M., Hooppaw, A. J., Ruan, L., Fisher, D. J., & Chen, L. (2017). Biochemical and genetic analysis of the Chlamydia GroEL chaperonins. *J Bacteriol*, *199*, e00844-16.

Ingelmo-torres, M., González-moreno, E., Kassan, A., Tebar, F., Herms, A., Grewal, T., Hancock, J. F., Enrich, C., Bosch, M., Gross, S. P., Parton, R. G., & Pol, A. (2010). Hydrophobic and basic domains target proteins to lipid droplets. *Traffic, 10*, 1785–1801.

Jewett, T. J., Dooley, C. A., Mead, D. J., & Hackstadt, T. (2008). Chlamydia trachomatis Tarp is phosphorylated by SRC family tyrosine kinases. *Biochem Biophys Res Commun*, *371*, 339–344.

Jewett, T. J., Fischer, E. R., Mead, D. J., & Hackstadt, T. (2006). Chlamydial TarP is a bacterial nucleator of actin. *Proc Natl Acad Sci U S A*, *103*, 15599–15604.

Jia, L., Sun, F., Wang, J., Gong, D., & Yang, L. (2019). Chlamydia trachomatis CT143 stimulates secretion of proinflammatory cytokines via activating the p38/MAPK signal pathway in THP-1 cells. *Mol Immunol*, *105*, 233–239.

Jia, T. J., Liu, D. W., Luo, J. H., & Zhong, G. M. (2007). Localization of the hypothetical protein CT249 in the Chlamydia trachomatis inclusion membrane. *Wei Sheng Wu Xue Bao*, *47*, 645–648.

Jiwani, S., Alvarado, S., Ohr, R. J., Romero, A., Nguyen, B., & Jewett, T. J. (2013). Chlamydia trachomatis Tarp harbors distinct G and F actin binding domains that bundle actin filaments. *J Bacteriol*, *195*, 708–716.

Johnson, C., Crowther, S., Stafford, M. J., Campbell, D. G., Toth, R., & MacKintosh, C. (2010). Bioinformatic and experimental survey of 14-3-3-binding sites. *Biochem J*, *427*, 69–78.

Johnson, C. M., & Fisher, D. J. (2013). Site-specific, insertional inactivation of incA in Chlamydia trachomatis using a group II intron. *PLoS One*, *8*, e83989.

Jones, D. H., Ley, S., & Aitken, A. (1995). Isoforms of 14-3-3 protein can form homo- and heterodimers in vivo and in vitro: implications for function as adapter proteins. *FEBS Letters*, *368*, 55–58.

Jorgensen, I., & Valdivia, R. H. (2008). Pmp-like proteins Pls1 and Pls2 are secreted into the lumen of the Chlamydia trachomatis inclusion. *Infect Immun*, *76*, 3940–3950.

Kari, L., Goheen, M. M., Randall, L. B., Taylor, L. D., Carlson, J. H., Whitmire, W. M., Virok, D., Rajaram, K., Endresz, V., McClarty, G., Nelson, D. E., & Caldwell, H. D. (2011). Generation of targeted Chlamydia trachomatis null mutants. *Proc Natl Acad Sci U S A*, *108*, 7189–7193.

Karnak, D., Bengsun, S., Beder, S., & Kayacan, O. (2001). Chlamydia pneumoniae infection and acute exacerbation of chronic obstructive pulmonary disease (COPD). *Respir Med*, *95*, 811–816.

Keb, G., Hayman, R., & Fields, K. A. (2018). Floxed-Cassette Allelic Exchange Mutagenesis enables markerless gene deletion in Chlamydia trachomatis and can reverse cassette-induced polar effects. *J Bacteriol, 200,* e00479-18.

Keb, G., Ferrell, J., Scanlon, K. R., Jewett, T. J., & Fields, K. A. (2021). Chlamydia trachomatis TmeA directly activates N-WASP to promote actin polymerization and functions synergistically with TarP during invasion. *mBio*, *12*, e02861-20.

Kessler, M., Hoffmann, K., Fritsche, K., Brinkmann, V., Mollenkopf, H. J., Thieck, O., Teixeira da Costa, A. R., Braicu, E. I., Sehouli, J., Mangler, M., Berger, H., & Meyer, T. F. (2019). Chronic Chlamydia infection in human organoids increases stemness and promotes age-dependent CpG methylation. *Nat Commun*, *10*, 1194.

Khaddaj, R., Mari, M., Cottier, S., Reggiori, F., & Schneite, R. (2021). The surface of lipid droplets constitutes a barrier for endoplasmic reticulum-resident integral membrane proteins. *J Cell Sci*, *135*, jcs256206.

Kohlmann, F., Shima, K., Hilgenfeld, R., Solbach, W., Rupp, J., & Hansen, G. (2015). Structural basis of the proteolytic and chaperone activity of Chlamydia trachomatis CT441. *J Bacteriol*, *197*, 211–218.

Kokes, M., Dunn, J. D., Granek, J. A., Nguyen, B. D., Barker, J. R., Valdivia, R. H., & Bastidas, R. J. (2015). Integrating chemical mutagenesis and whole genome sequencing as a platform for forward and reverse genetic analysis of Chlamydia. *Cell Host Microbe, 17*, 716–725.

Krogh, A., Larsson, B., Von Heijne, G., & Sonnhammer, E. L. L. (2001). Predicting transmembrane protein topology with a hidden Markov model: Application to complete genomes. *J Mol Biol*, *305*, 567–580.

Kumar, Y., Cocchiaro, J., & Valdivia, R. H. (2006). The obligate intracellular pathogen Chlamydia trachomatis targets host lipid droplets. *Curr Biol, 16,* 1646–1651.

Kumar, Y., & Valdivia, R. H. (2008). Actin and intermediate filaments stabilize the Chlamydia trachomatis vacuole by forming dynamic structural scaffolds. *Cell Host Microbe*, *4*, 159–169.

Kunze, M., & Berger, J. (2015). The similarity between N-terminal targeting signals for protein import into different organelles and its evolutionary relevance. *Front Physiol*, *6*, 259.

Kurarmoto, H., Hamano, M., & Imai, M. (2002). HEC-1 cells. *Hum Cell, 15*, 81–95.

Kurihara, Y., Itoh, R., Shimizu, A., Walenna, N. F., Chou, B., Ishii, K., Soejima, T., Fujikane, A., & Hiromatsu, K. (2019). Chlamydia trachomatis targets mitochondrial dynamics to promote intracellular survival and proliferation. *Cell Microbiol*, *21*, e12962.

Labrie, S. D., Dimond, Z. E., Harrison, K. S., Baid, S., Wickstrum, J., Suchland, R. J., & Hefty, P. S. (2019). Transposon mutagenesis in Chlamydia trachomatis identifies CT339 as a ComEC homolog important for DNA uptake and lateral gene transfer. *mBio*, *10*, e01343-19.

Lad, S. P., Li, J., da Silva, C. J., Pan, Q., Gadwal, S., Ulevitch, R. J., & Li, E. (2007). Cleavage of p65/RelA of the NF-κB pathway by Chlamydia. *Proc Natl Acad Sci U S A*, *104*, 2933–2938.

Lane, B. J., Mutchler, C., Al Khodor, S., Grieshaber, S. S., & Carabeo, R. A. (2008). Chlamydial entry involves TarP binding of guanine nucleotide exchange factors. *PLoS Pathog*, *4*, e1000014.

Le Negrate, G., Krieg, A., Faustin, B., Loeffler, M., Godzik, A., Krajewski, S., & Reed, J. C. (2008). Chla Dub1 of Chlamydia trachomatis suppresses NF-κB activation and inhibits IκBα ubiquitination and degradation. *Cell Microbiol*, *10*, 1879–1892.

Lei, L., Dong, X., Li, Z., & Zhong, G. (2013). Identification of a novel nuclear localization signal sequence in Chlamydia trachomatis-secreted hypothetical protein CT311. *PLoS One*, *8*, e64529.

Lei, L., Qi, M., Budrys, N., Schenken, R., & Zhong, G. (2011). Localization of Chlamydia trachomatis hypothetical protein CT311 in host cell cytoplasm. *Microb Pathog*, *51*, 101–109.

Lei, L., Yang, C., Patton, M. J., Smelkinson, M., Dorward, D., Ma, L., Karanovic, U., Firdous, S., McClarty, G., & Caldwell, H. D. (2021). A chlamydial plasmid-dependent secretion system for the delivery of virulence factors to the host cytosol. *mBio*, *12*, e01179-21.

Li, Z., Chen, C., Chen, D., Wu, Y., Zhong, Y., & Zhong, G. (2008a). Characterization of fifty putative inclusion membrane proteins encoded in the Chlamydia trachomatis genome. *Infect Immun*, *76*, 2746–2757.

Li, Z., Chen, D., Zhong, Y., Wang, S., & Zhong, G. (2008b). The chlamydial plasmid-encoded protein Pgp3 is secreted into the cytosol of Chlamydia-infected cells. *Infect Immun*, *76*, 3415–3428.

Lindner, K. (1910) Zur atiologie der gonokokken-freien urethritis. *Wien Klin Wochenschr, 8*, 283–284.

Lindner, K. (1911). Gonoblennorrhöe, Einschlußblennorrhöe und Trachom. *A. von Graefe's Arch. Ophthalmol, 78*, 345–38

Liechti, G., Kuru, E., Packiam, M., Hsu, Y. P., Tekkam, S., Hall, E., Rittichier, J. T., VanNieuwenhze, M., Brun, Y. V., & Maurelli, A. T. (2016). Pathogenic Chlamydia lack a classical sacculus but synthesize a narrow, mid-cell peptidoglycan ring, regulated by MreB, for cell division. *PLoS Pathog*, *12*, e1005590.

Liechti, G. W., Kuru, E., Hall, E., Kalinda, A., Brun, Y. V, Vannieuwenhze, M., & Maurelli, A. T. (2014). A new metabolic cell-wall labelling method reveals peptidoglycan in Chlamydia trachomatis. *Nature*, *506*, 507–510.

Lipinski, A. R., Heymann, J., Meissner, C., Karlas, A., Brinkmann, V., Meyer, T. F., & Heuer, D. (2009). Rab6 and Rab11 regulate Chlamydia trachomatis development and golgin-84-dependent Golgi fragmentation. *PLoS Pathog*, *5*, e1000615.

Lovett, M., Kuo, C. C., Holmes, K., and Falkow, S. (1980). Plasmids of the genus Chlamydia. *Curr Chemother Infect Dis, 2,* 1250–1252.

Liu, Y., Chen, C., Gong, S., Hou, S., Qi, M., Liu, Q., Baseman, J., & Zhong, G. (2014a). Transformation of Chlamydia muridarum reveals a role for Pgp5 in suppression of plasmid-dependent gene expression. *J Bacteriol*, *196*, 989–998.

Liu, Y., Huang, Y., Yang, Z., Sun, Y., Gong, S., Hou, S., Chen, C., Li, Z., Liu, Q., Wu, Y., Baseman, J., & Zhong, G. (2014b). Plasmid-encoded Pgp3 is a major virulence factor for Chlamydia muridarum to induce hydrosalpinx in mice. *Infect Immun*, *82*, 5327–5335.

Lowden, N. M., Yeruva, L., Johnson, C. M., Bowlin, A. K., & Fisher, D. J. (2015). Use of aminoglycoside 3′ adenyltransferase as a selection marker for Chlamydia trachomatis intron-mutagenesis and in vivo intron stability. *BMC Res Notes*, *8*, 570.

Lutter, E. I., Barger, A. C., Nair, V., & Hackstadt, T. (2013). Chlamydia trachomatis inclusion membrane protein CT228 recruits elements of the myosin phosphatase pathway to regulate release mechanisms. *Cell Rep*, *3*, 1921–1931.

Lutter, E. I., Bonner, C., Holland, M. J., Suchland, R. J., Stamm, W. E., Jewett, T. J., McClarty, G., & Hackstadt, T. (2010). Phylogenetic analysis of Chlamydia trachomatis tarp and correlation with clinical phenotype. *Infect Immun*, *78*, 3678–3688.

Lutter, E. I., Martens, C., & Hackstadt, T. (2012). Evolution and conservation of predicted inclusion membrane proteins in chlamydiae. *Comp Funct Genomics*, *2012*, 362104.

Lutz-Wohlgroth, L., Becker, A., Brugnera, E., Huat, Z. L., Zimmermann, D., Grimm, F., Haessig, M., Greub, G., Kaps, S., Spiess, B., Pospischil, A., & Vaughan, L. (2006). Chlamydiales in guinea-pigs and their zoonotic potential. *J Vet Med A Physiol Pathol Clin Med*, *53*, 185–193.

Matsumoto, A., Izutsu, H., Miyashita, N., & Ohuchi, M. (1998). Plaque formation by and plaque cloning of Chlamydia trachomatis biovar trachoma. *J Clin Microbiol*, *36*, 3013–3019.

McKuen, M. J., Mueller, K. E., Bae, Y. S., & Fields, K. A. (2017). Fluorescence-reported allelic exchange mutagenesis reveals a role for Chlamydia trachomatis TmeA in invasion that is independent of host AHNAK. *Infect Immun*, *85*, e00640-17.

Mehlitz, A., Banhart, S., Hess, S., Selbach, M., & Meyer, T. F. (2008). Complex kinase requirements for Chlamydia trachomatis Tarp phosphorylation. *FEMS Microbiol Lett*, *289*, 233–240.

Mehlitz, A., Banhart, S., Mäurer, A. P., Kaushansky, A., Gordus, A. G., Zielecki, J., MacBeath, G., & Meyer, T. F. (2010). Tarp regulates early Chlamydia-induced host cell survival through interactions with the human adaptor protein SHC1. *J Cell Biol*, *190*, 143–157.

Meyer, T. (2016). Diagnostic procedures to detect Chlamydia trachomatis infections. *Microorganisms*, *4*, 25.

Mirrashidi, K. M., Elwell, C. A., Verschueren, E., Johnson, J. R., Frando, A., Von Dollen, J., Rosenberg, O., Gulbahce, N., Jang, G., Johnson, T., Jager, S., Gopalakrishnan, A. M., Sherry, J., Dan Dunn, J., Olive, A., Penn, B., Shales, M., Cox, J. S., Starnbach, M. N., … Engel, J. (2015). Global mapping of the Inc-human interactome reveals that retromer restricts Chlamydia infection. *Cell Host Microbe*, *18*, 109–121.

Misaghi, S., Balsara, Z. R., Catic, A., Spooner, E., Ploegh, H. L., & Starnbach, M. N. (2006). Chlamydia trachomatis-derived deubiquitinating enzymes in mammalian cells during infection. *Mol Microbiol*, *61*, 142–150.

Mital, J., Lutter, E. I., Barger, A. C., Dooley, C. A., & Hackstadt, T. (2015). Chlamydia trachomatis inclusion membrane protein CT850 interacts with the dynein light chain DYNLT1 (Tctex1). *Biochem Biophys Res Commun*, *462*, 165–170.

Mital, J., Miller, N. J., Fischer, E. R., & Hackstadt, T. (2010). Specific chlamydial inclusion membrane proteins associate with active Src family kinases in microdomains that interact with the host microtubule network. *Cell Microbiol*, *12*, 1235–1249.

Miyagawa, Y., Mitamura, T., Yaoi, H., Ishii, N., and Okanishi, J. (1935). Studies on the virus of lymphogranuloma inguinale Nicolas, Favre and Durand. *Jpn J Exp Med, 13,* 733–738.

Mohamad, K. Y., & Rodolakis, A. (2010). Recent advances in the understanding of Chlamydophila pecorum infections, sixteen years after it was named as the fourth species of the Chlamydiaceae family. *Vet Res*, *41*, 27.

Monteiro-Brás, T., Wesolowski, J., & Paumet, F. (2020). Depletion of SNAP-23 and Syntaxin 4 alters lipid droplet homeostasis during Chlamydia infection. *Microb Cell*, *7*, 46–58.

Moulder, J.W. (1966). The Relation of the Psittacosis Group (Chlamydiae) to Bacteria and Viruses. *Annu Rev Microbiol, 20,* 107–130.

Mueller, K. E., & Fields, K. A. (2015). Application of β-Lactamase reporter fusions as an indicator of effector protein secretion during infections with the obligate intracellular pathogen Chlamydia trachomatis. *Plos One, 10*, e0135295.

Mueller, K. E., Wolf, K., & Fields, K. A. (2016). Gene deletion by Fluorescence-Reported Allelic Exchange Mutagenesis in Chlamydia trachomatis. *mBio*, *7*, e01817-15.

Muschiol, S., Boncompain, G., Vromman, F., Dehoux, P., Normark, S., Henriques-Normark, B., & Subtil, A. (2011). Identification of a family of effectors secreted by the type III secretion system that are conserved in pathogenic chlamydiae. *Infect Immun*, *79*, 571–580.

Nguyen, B. D., & Valdivia, R. H. (2013). Forward genetic approaches in Chlamydia trachomatis. *J Vis Exp*, e50636.

Nguyen, P. H., Lutter, E. I., & Hackstadt, T. (2018). Chlamydia trachomatis inclusion membrane protein MrcA interacts with the inositol 1,4,5-trisphosphate receptor type 3 (ITPR3) to regulate extrusion formation. *PLoS Pathog*, *14*, e1006911.

Nunes, A., & Gomes, J. P. (2014). Evolution, phylogeny, and molecular epidemiology of Chlamydia. *Infect Genet Evol*, *23*, 49–64.

O'Connel, C. M., & Ferone, M. E. (2016). Chlamydia trachomatis genital infections. *W V Med J*, *3*, 390–403.

O'Connell, C. M., AbdelRahman, Y. M., Green, E., Darville, H. K., Saira, K., Smith, B., Darville, T., Scurlock, A. M., Meyer, C. R., & Belland, R. J. (2011). Toll-like receptor 2 activation by Chlamydia trachomatis is plasmid dependent, and plasmid-responsive chromosomal loci are coordinately regulated in response to glucose limitation by C. trachomatis but not by C. muridarum. *Infect Immun*, *79*, 1044–1056.

O'Connell, C. M., & Nicks, K. M. (2006). A plasmic-cured Chlamydia muridarum strain displays altered plaque morphology and reduced infectivity in cell culture. *Microbiology (Reading)*, *152*, 1601–1607.

Olzmann, J. A., & Carvalho, P. (2019). Dynamics and functions of lipid droplets. *Nat Rev Mol Cell Biol*, *20*, 137–155.

Omsland, A., Sixt, B. S., Horn, M., & Hackstadt, T. (2014). Chlamydial metabolism revisited: Interspecies metabolic variability and developmental stage-specific physiologic activities. *FEMS Microbiol Rev*, *38*, 779–801.

Ouellette, S. P. (2018). Feasibility of a conditional knockout system for Chlamydia based on CRISPR interference. *Front Cell Infect Microbiol, 8*, 59.

Ouellette, S. P., Blay, E. A., Hatch, N. D., & Fisher-Marvin, L. A. (2021). CRISPR interference to inducibly repress gene expression in Chlamydia trachomatis. *Infect Immun*, *89*, e00108-21.

Paba, P., Bonifacio, D., Di Bonito, L., Ombres, D., Favalli, C., Syrjänen, K., & Ciotti, M. (2008). Co-expression of HSV2 and Chlamydia trachomatis in HPV-positive cervical cancer and cervical intraepithelial neoplasia lesions is associated with aberrations in key intracellular pathways. *Intervirology*, *51*, 230–234.

Pais, S. V., Key, C. E., Borges, V., Pereira, I. S., Gomes, J. P., Fisher, D. J., & Mota, L. J. (2019). CteG is a Chlamydia trachomatis effector protein that associates with the Golgi complex of infected host cells. *Sci Rep*, *9*, 6133.

Pais, S. V., Milho, C., Almeida, F., & Mota, L. J. (2013). Identification of novel Type III secretion chaperone-substrate complexes of Chlamydia trachomatis. *PLoS One*, *8*, e56292.

Panzetta, M. E., Luján, A. L., Bastidas, R. J., Damiani, M. T., Valdivia, R. H., & Saka, H. A. (2019). Ptr/CTL0175 is required for the efficient recovery of Chlamydia trachomatis from stress induced by gamma-interferon. *Front Microbiol*, *10*, 756.

Paschen, S. A., Christian, J. G., Vier, J., Schmidt, F., Walch, A., Ojcius, D. M., & Häcker, G. (2008). Cytopathicity of Chlamydia is largely reproduced by expression of a single chlamydial protease. *J Cell Biol*, *182*, 117–127.

Patton, M. J., Chen, C., Yang, C., Mccorrister, S., Grant, C., Westmacott, G., Yuan, X., Ochoa, E., Fariss, R., Whitmire, W. M., Carlson, J. H., & Caldwell, H. D. (2018). Plasmid negative regulation of CPAF expression is Pgp4 independent and restricted to invasive Chlamydia trachomatis biovars. *mBio*, *9*, e02164-17.

Paul, B., Kim, H. S., Kerr, M. C., Huston, W. M., Teasdale, R. D., & Collins, B. M. (2017). Structural basis for the hijacking of endosomal sorting nexin proteins by Chlamydia trachomatis. *eLife*, *6*, e22311.

Paumet, F., Wesolowski, J., Garcia-Diaz, A., Delevoye, C., Aulner, N., Shuman, H. A., Subtil, A., & Rothman, J. E. (2009). Intracellular bacteria encode inhibitory SNARE-like proteins. *PLoS One*, *4*, e7375.

Pennington, K., Chan, T., Torres, M., & Andersen, J. (2018). The dynamic and stress-adaptive signaling hub of 14-3-3: emerging mechanisms of regulation and context-dependent protein–protein interactions. *Oncogene*, *37*, 5587–5604.

Pennini, M. E., Perrinet, S., Dautry-Varsat, A., & Subtil, A. (2010). Histone methylation by NUE, a novel nuclear effector of the intracellular pathogen Chlamydia trachomatis. *PLoS Pathog*, *6*, e1000995.

Phillips, D. M., Swenson, C. E., & Schachter, J. (1984). Ultrastructure of Chlamydia trachomatis infection of the mouse oviduct. *J Ultrasruct Res*, *88*, 244–256.

Phillips, S., Quigley, B. L., & Timms, P. (2019). Seventy years of Chlamydia vaccine research - Limitations of the past and directions for the future. *Front Microbiol*, *10*, 70.

Pickett, M. A., Everson, J. S., Pead, P. J., & Clarke, I. N. (2005). The plasmids of Chlamydia trachomatis and Chlamydophila pneumoniae (N16): Accurate determination of copy number and the paradoxical effect of plasmid-curing agents. *Microbiology*, *151*, 893–903.

Pinho-Bandeira, T., Cabral Veríssimo, V., & Sá Machado, R. (2020). The epidemiology of chlamydia, gonorrhoea and syphilis in Portugal: where do we go from now? *European Journal of Public Health*, *30*, ckaa165.538.

Podleschny, M., Grund, A., Berger, H., Rollwitz, E., & Borchers, A. (2015). A PTK7/Ror2 co-receptor complex affects xenopus neural crest migration. *PLoS One*, *10*, e0145169.

Pospischil, A., Thoma, R., Hilbe, M., Grest, P., & Gebbers, F. O. (2002). Abortion in woman caused by caprine Chlamydophila abortus (Chlamydia psittaci serovar 1). *Swiss Med Wkly*, *132*, 64–66.

Pruneda, J. N., Bastidas, R. J., Bertsoulaki, E., Swatek, K. N., Santhanam, B., Clague, M. J., Valdivia, R. H., Urbé, S., & Komander, D. (2018). A Chlamydia effector combining deubiquitination and acetylation activities induces Golgi fragmentation. *Nat Microbiol*, *3*, 1377–1384.

Qi, M., Lei, L., Gong, S., Liu, Q., DeLisa, M. P., & Zhong, G. (2011). Chlamydia trachomatis secretion of an immunodominant hypothetical protein (CT795) into host cell cytoplasm. *J Bacteriol*, *193*, 2498–2509.

Rajeeve, K., Das, S., Prusty, B. K., & Rudel, T. (2018). Chlamydia trachomatis paralyses neutrophils to evade the host innate immune response. *Nature Microbiology*, *3*, 824–835.

Rank, R. G., Whittimore, J., Bowlin, A. K., & Wyrick, P. B. (2011). In vivo ultrastructural analysis of the intimate relationship between polymorphonuclear leukocytes and the chlamydial developmental cycle. *Infect Immun*, *79*, 3291–3301.

Recuero-Checa, M. A., Sharma, M., Lau, C., Watkins, P. A., Gaydos, C. A., & Dean, D. (2016). Chlamydia trachomatis growth and development requires the activity of host Long-chain Acyl-CoA Synthetases (ACSLs). *Sci Rep*, *6*, 23148.

Rockey, D. D., Scidmore, M. A., Bannantine, J. P., & Brown, W. J. (2002). Proteins in the chlamydial inclusion membrane. *Microbes Infect*, *4*, 333–340.

Roingeard, P., & Melo, R. C. N. (2017). Lipid droplet hijacking by intracellular pathogens. *Cell Microbiol*, *19*, e12688.

Ronzone, E., & Paumet, F. (2013). Two coiled-coil domains of Chlamydia trachomatis IncA affect membrane fusion events during infection. *PLoS One*, *8*, e69769.

Ronzone, E., Wesolowski, J., Bauler, L. D., Bhardwaj, A., Hackstadt, T., & Paumet, F. (2014). An α-helical core encodes the dual functions of the chlamydial protein IncA. *J Biol Chem*, *289*, 33469–33480.

Rowley, J., Hoorn, S. Vander, Korenromp, E., Low, N., Unemo, M., Abu-Raddad, L. J., Chico, R. M., Smolak, A., Newman, L., Gottlieb, S., Thwin, S. S., Broutet, N., & Taylor, M. M. (2019). Chlamydia, gonorrhoea, trichomoniasis and syphilis: Global prevalence and incidence estimates, 2016. *Bull World Health Organ*, *97*, 548–562.

Rzomp, K. A., Moorhead, A. R., & Scidmore, M. A. (2006). The GTPase Rab4 interacts with Chlamydia trachomatis inclusion membrane protein CT229. *Infect Immun*, *74*, 5362–5373.

Saka, H. A., Thompson, J. W., Chen, Y. S., Dubois, L. G., Haas, J. T., Moseley, A., & Valdivia, R. H. (2015). Chlamydia trachomatis infection leads to defined alterations to the lipid droplet proteome in epithelial cells. *PLoS One*, *10*, e0124630.

Samudrala, R., Heffron, F., & McDermott, J. E. (2009). Accurate prediction of secreted substrates and identification of a conserved putative secretion signal for type III secretion systems. *PLoS Pathog*, *5*, e1000375.

Seth-Smith, H. M. B., Harris, S. R., Skilton, R. J., Radebe, F. M., Golparian, D., Shipitsyna, E., Duy P. T., Scott P., Cutcliffe L. T., O'Neill C., Parmar S., Pitt R., Baker S., Ison C. A., Marsh P., Jalal H., Lewis D. A., Unemo M., Clarke I. N., Parkhill J., Thomson N. R. (2013). Whole-genome sequences of Chlamydia trachomatis directly from clinical samples without culture. *Genome Res, 23,* 855–866.

Schindelin, J., Arganda-Carreras, I., Frise, E., Kaynig, V., Longair, M., Pietzsch, T., Preibisch, S., Rueden, C., Saalfeld, S., Schmid, B., Tinevez, J. Y., White, D. J., Hartenstein, V., Eliceiri, K., Tomancak, P., & Cardona, A. (2012). Fiji: An open-source platform for biological-image analysis. *Nature Methods*, *9*, 676–682.

Scidmore-Carlson, M. A., Shaw, E. I., Dooley, C. A., Fischer, E. R., & Hackstadt, T. (1999). Identification and characterization of a Chlamydia trachomatis early operon encoding four novel inclusion membrane proteins. *Mol Microbiol*, *33*, 753–765.

Scidmore, M. A. (2005). Cultivation and laboratory maintenance of Chlamydia trachomatis. *Curr Protoc Microbiol,* Chapter 11, Unit 11A.1.

Scidmore, M. A., & Hackstadt, T. (2001). Mammalian 14-3-3β associates with the Chlamydia trachomatis inclusion membrane via its interaction with IncG. *Mol Microbiol*, *39*, 1638–1650.

Selyunin, A. S., Sutton, S. E., Weigele, B. A., Reddick, L. E., Orchard, R. C., Bresson, S. M., Tomchick, D. R., & Alto, N. M. (2011). The assembly of a GTPase-kinase signalling complex by a bacterial catalytic scaffold. *Nature*, *469*, 107–113.

Sharma, J., Zhong, Y., Dong, F., Piper, J. M., Wang, G., & Zhong, G. (2006). Profiling of human antibody responses to Chlamydia trachomatis urogenital tract infection using microplates arrayed with 156 chlamydial fusion proteins. *Infect Immun*, *74*, 1490–1499.

Sharma, M., Machuy, N., Böhme, L., Karunakaran, K., Mäurer, A. P., Meyer, T. F., & Rudel, T. (2011). HIF-1α is involved in mediating apoptosis resistance to Chlamydia trachomatis-infected cells. *Cell Microbiol*, *13*, 1573–1585.

Sharma, M., Recuero-Checa, M. A., Fan, F. Y., & Dean, D. (2018). Chlamydia trachomatis regulates growth and development in response to host cell fatty acid availability in the absence of lipid droplets. *Cell Microbiol*, *20*, e12801.

Shaw, E. I., Dooley, C. A., Fischer, E. R., Scidmore, M. A., Fields, K. A., & Hackstadt, T. (2000). Three temporal classes of gene expression during the Chlamydia trachomatis developmental cycle. *Mol Microbiol*, *37*, 913–925.

Shaw, J. H., Key, C. E., Snider, T. A., Sah, P., Shaw, E. I., Fisher, D. J., & Lutter, E. I. (2018). Genetic Inactivation of Chlamydia trachomatis inclusion membrane protein CT228 alters MYPT1 recruitment, extrusion production, and longevity of infection. *Front Cell Infect Microbiol*, *8*, 415.

Scherer, W. F., Syverton J. T., Gey G. O. (1953). Studies on the propagation in vitro of poliomyelitis viruses. IV. Viral multiplication in a stable strain of human malignant epithelial cells (strain HeLa) derived from an epidermoid carcinoma of the cervix. *J Exp Med*, *97*, 695–710.

Shohdy, N., Efe, J. A., Emr, S. D., & Shuman, H. A. (2005). Pathogen effector protein screening in yeast identifies Legionella factors that interfere with membrane trafficking. *Proc Natl Acad Sci U S A*, *102*, 4866–4871.

Sigar, I. M., Schripsema, J. H., Wang, Y., Clarke, I. N., Cutcliffe, L. T., Seth-Smith, H. M. B., Thomson, N. R., Bjartling, C., Unemo, M., Persson, K., & Ramsey, K. H. (2014). Plasmid deficiency in urogenital isolates of Chlamydia trachomatis reduces infectivity and virulence in a mouse model. *Pathog Dis*, *70*, 61–69.

Siggers, K. A., & Cammie, F. L. (2008). The yeast Saccharomyces cerevisiae: A versatile model system for the identification and characterization of bacterial virulence proteins. *Cell Host Microbe*, *4*, 8–15.

Sisko, J. L., Spaeth, K., Kumar, Y., & Valdivia, R. H. (2006). Multifunctional analysis of Chlamydia-specific genes in a yeast expression system. *Mol Microbiol*, *60*, 51–66.

Sixt, B. S., Bastidas, R. J., Finethy, R., Baxter, R. M., Carpenter, V. K., Kroemer, G., Coers, J., & Valdivia, R. H. (2017). The Chlamydia trachomatis inclusion membrane protein CpoS counteracts STING-mediated cellular surveillance and suicide programs. *Cell Host Microbe*, *21*, 113–121.

Snavely, E. A., Kokes, M., Dunn, J. D., Saka, H. A., Nguyen, B. D., Bastidas, R. J., Mccafferty, D. G., & Valdivia, R. H. (2014). Reassessing the role of the secreted protease CPAF in Chlamydia trachomatis infection through genetic approaches. *Pathog Dis*, *71*, 336–351.

Song, L., Carlson, J. H., Whitmire, W. M., Kari, L., Virtaneva, K., Sturdevant, D. E., Watkins, H., Zhou, B., Sturdevant, G. L., Porcella, S. F., McClarty, G., & Caldwell, H. D. (2013). Chlamydia trachomatis plasmid-encoded Pgp4 is a transcriptional regulator of virulence-associated genes. *Infect Immun, 81*, 636–644.

Sonnhammer, E. L. L., & Krogh, A. (1998). A hidden Markov model for predicting transmembrane helices in protein sequence. *Proc Int Conf Intell Syst Mol Biol, 6*, 175–182.

Stanhope, R., Flora, E., Bayne, C., & Derré, I. (2017). IncV, a FFAT motif-containing Chlamydia protein, tethers the endoplasmic reticulum to the pathogen-containing vacuole. *Proc Natl Acad Sci U S A, 114*, 12039–12044.

Starnbach, M. N., Loomis, W. P., Ovendale, P., Regan, D., Hess, B., Alderson, M. R., & Fling, S. P. (2003). An inclusion membrane protein from Chlamydia trachomatis enters the MHC class I pathway and stimulates a CD8+ T Cell response. *J Immunol*, *171*, 4742–4749.

Stephens, R., Kalman, S., Lammel, C., Fan, J., Marathe, R., & Aravind, L. (1998). Genome sequence of an obligate intracellular pathogen of humans: Chlamydia trachomatis. *Science, 282*, 754–759.

Stephens, R. S., Myers, G., Eppinger, M., and Bavoil, P. M. (2009). Divergence without difference: phylogenetics and taxonomy of Chlamydia resolved. *FEMS Immunol Med Microbiol, 55,* 115–119

Sturdevant, G. L., Carlson, J. H., Whitmire, W. M., Zhou, B., Song, L., & Caldwell, H. D. (2014). Infectivity of urogenital Chlamydia trachomatis plasmid-deficient, CT135-null, and double-deficient strains in female mice. *Pathog Dis*, *71*, 90–92.

Sturdevant, G. L., Kari, L., Gardner, D. J., Olivares-Zavaleta, N., Randall, L. B., Whitmire, W. M., Carlson, J. H., Goheen, M. M., Selleck, E. M., Martens, C., & Caldwell, H. D. (2010). Frameshift mutations in a single novel virulence factor alter the in vivo pathogenicity of Chlamydia trachomatis for the female murine genital tract. *Infect Immun*, *78*, 3660–3668.

Subtil, A., Delevoye, C., Balañá, M. E., Tastevin, L., Perrinet, S., & Dautry-Varsat, A. (2005). A directed screen for chlamydial proteins secreted by a type III mechanism identifies a translocated protein and numerous other new candidates. *Mol Microbiol*, *56*, 1636–1647.

Suchland, R. J., Rockey, D. D., Bannantine, J. P., & Stamm, W. E. (2000). Isolates of Chlamydia trachomatis that occupy nonfusogenic inclusions lack IncA, a protein localized to the inclusion membrane. *Infect Immun*, *68*, 360–367.

Sun, Q., Yong, X., Sun, X., Yang, F., Dai, Z., Gong, Y., Zhou, L., Zhang, X., Niu, D., Dai, L., Liu, J. J., & Jia, D. (2017). Structural and functional insights into sorting nexin 5/6 interaction with bacterial effector IncE. *Signal Transduct Target Ther*, *2*, 17030.

Tam, J. E., Davis, C. H., & Wyrick, P. B. (1994). Expression of recombinant DNA introduced into Chlamydia trachomatis by electroporation. *Can J Microbiol*, *40*, 583–591.

Tang, L., Chen, J., Zhou, Z., Yu, P., Yang, Z., & Zhong, G. (2015). Chlamydia-secreted protease CPAF degrades host antimicrobial peptides. *Microbes Infect*, *17*, 402–408.

Taylor-Brown, A., Vaughan, L., Greub, G., Timms, P., & Polkinghorne, A. (2015). Twenty years of research into Chlamydia-like organisms: A revolution in our understanding of the biology and pathogenicity of members of the phylum Chlamydiae. *Pathogens and Disease*, *73*, 1–15.

Taylor, H. R., Burton, M. J., Haddad, D., West, S., & Wright, H. (2014). Trachoma. *The Lancet*, *384*, 2142–2152.

Thalmann, J., Janik, K., May, M., Sommer, K., Ebeling, J., Hofmann, F., Genth, H., & Klos, A. (2010). Actin re-organization induced by Chlamydia trachomatis serovar D - evidence for a critical role of the effector protein CT166 targeting Rac. *PLoS One*, *5*, e9887.

Trachoma Fact Sheets, World Health Organization (WHO) (2021).

Unterweger, C., Schwarz, L., Jelocnik, M., Borel, N., Brunthaler, R., Inic-Kanada, A., & Marti, H. (2020). Isolation of tetracycline-resistant chlamydia suis from a pig herd affected by reproductive disorders and conjunctivitis. *Antibiotics (Basel)*, *9*, 187.

Uphoff, C. C., & Drexler, H. G. (2011). Detecting Mycoplasma contamination in cell cultures by polymerase chain reaction. *Methods Mol Biol*, *731*, 93–103.

Vallochi, A. L., Teixeira, L., Oliveira, K. da S., Maya-Monteiro, C. M., & Bozza, P. T. (2018). Lipid droplet, a key player in host-parasite interactions. *Front Immunol*, *9*, 1022.

Verbeke, P., Welter-Stahl, L., Ying, S., Hansen, J., Häcker, G., Darville, T., & Ojcius, D. M. (2006). Recruitment of BAD by the Chlamydia trachomatis vacuole correlates with host-cell survival. *PLoS Pathog*, *2*, 408–417.

Vromman, F., Perrinet, S., Gehre, L., & Subtil, A. (2016). The DUF582 Proteins of Chlamydia trachomatis bind to components of the ESCRT machinery, which is dispensable for bacterial growth in vitro. *Front Cell Infect Microbiol*, *6*, 123.

Wang, J., Zhang, Y., Lu, C., Lei, L., Yu, P., & Zhong, G. (2010). A genome-wide profiling of the humoral immune response to Chlamydia trachomatis infection reveals vaccine candidate antigens expressed in humans. *J Immunol, 185*, 1670–1680.

Wang, X., Hybiske, K., & Stephens, R. S. (2018). Direct visualization of the expression and localization of chlamydial effector proteins within infected host cells. *Pathog Dis*, *76*, fty011.

Wang, Y., Kahane, S., Cutcliffe, L. T., Skilton, R. J., Lambden, P. R., & Clarke, I. N. (2011). Development of a transformation system for Chlamydia trachomatis: Restoration of glycogen biosynthesis by acquisition of a plasmid shuttle vector. *PLoS Pathog*, *7*, e1002258.

Weber, M. M., Bauler, L. D., Lam, J., & Hackstadt, T. (2015). Expression and localization of predicted inclusion membrane proteins in Chlamydia trachomatis. *Infect Immun*, *83*, 4710–4718.

Weber, M. M., Lam, J. L., Dooley, C. A., Noriea, N. F., Hansen, B. T., Hoyt, F. H., Carmody, A. B., Sturdevant, G. L., & Hackstadt, T. (2017). Absence of specific Chlamydia trachomatis inclusion membrane proteins triggers premature inclusion membrane lysis and host cell death. *Cell Rep*, *19*, 1406–1417.

Weber, M. M., Noriea, N. F., Bauler, L. D., Lam, J. L., Sager, J., Wesolowski, J., Paumet, F., & Hackstadt, T. (2016). A functional core of IncA is required for Chlamydia trachomatis inclusion fusion. *J Bacteriol*, *198*, 1347–1355.

Wesolowski, J., Weber, M. M., Nawrotek, A., Dooley, C. A., Calderon, M., St. Croix, C. M., Hackstadt, T., Cherfils, J., & Paumet, F. (2017). Chlamydia hijacks ARF GTPases to coordinate microtubule posttranslational modifications and Golgi complex positioning. *mBio, 8*, e02280-16.

Wickstrum, J., Sammons, L. R., Restivo, K. N., & Hefty, P. S. (2013). Conditional gene expression in Chlamydia trachomatis using the tet system. *PLoS One*, *8*, e76743.

Wons, J., Meiller, R., Bergua, A., Bogdan, C., & Geißdörfer, W. (2017). Follicular conjunctivitis due to Chlamydia felis-Case report, review of the literature and improved molecular diagnostics. *Front Med*, *4*, 105.

Yaffe, M. B., Rittinger, K., Volinia, S., Caron, P. R., Aitken, A., Leffers, H., Gamblin, S. J., Smerdon, S. J., Cantley, L. C., & Street, W. (1997). The structural basis for 14-3-3: phosphopeptide binding specificity. *Cell*, *91*, 961–971.

Yanatori, I., Miura, K., Chen, Y. S., Valdivia, R. H., & Kishi, F. (2021). Application of a Chlamydia trachomatis expression system to identify Chlamydia pneumoniae proteins translocated into host cells. *J Bacteriol, 203*, e00511-20.

Yang, C., Starr, T., Song, L., Carlson, J. H., Sturdevant, G. L., Beare, P. A., Whitmire, W. M., & Caldwell, H. D. (2015). Chlamydial lytic exit from host cells is plasmid regulated. *mBio*, *6*, e01648-15.

Zehmer, J. K., Bartz, R., Liu, P., & Anderson, R. G. W. (2008). Identification of a novel N-terminal hydrophobic sequence that targets proteins to lipid droplets. *J Cell Sci*, *121*, 1852–1860.

Zhong, G. (2011). Chlamydia trachomatis secretion of proteases for manipulating host signaling pathways. *Front Microbiol*, *2*, 14.

Zhong, G. (2017). Chlamydial Plasmid-Dependent Pathogenicity. *Trends Microbiol*, *25*, 141–152.

Zou, Y., Lei, W., Su, S., Bu, J., Zhu, S., Huang, Q., & Li, Z. (2019). Chlamydia trachomatis plasmid-encoded protein Pgp3 inhibits apoptosis via the PI3K-AKT-mediated MDM2-p53 axis. *Mol Cell Biochem*, *452*, 167–176.

Zuck, M., & Hybiske, K. (2019). The Chlamydia trachomatis extrusion exit mechanism is regulated by host abscission proteins. *Microorganisms*, *7*, 149.

ANNEXES

Table A.1 Plasmids used in this work

Plasmid	Description	Source/Reference
	Plasmids for production of proteins in *Saccharomyces cerevisiae*	
pGreg505	Erg6-mCherry; (Amp^R)	Kindly provided by Roger Schneiter (Khaddaj *et al.*, 2021)
pKS84	GFP; pKS84 derivatives were used for ectopic production of GFP fusion proteins in *Saccharomyces cerevisiae* from a galactose-inducible promoter (Amp^R).	(De Felipe *et al.*, 2008)
pIF206	VipA-GFP	(Franco *et al.*, 2012)
pJB27	$CT249_{1-50}$-GFP; $ct249_{1-50}$ was amplified from *C. trachomatis* L2/434 chromosomal DNA by PCR with oligos 1977 and 1978, digested with BamHI-HindIII and inserted in the same sites of pKS84.	This work
pJB28	$CT134_{1-79}$-GFP; $ct134_{1-79}$ was amplified from *C. trachomatis* L2/434 chromosomal DNA by PCR with oligos 1979 and 1980, digested with BamHI-HindIII and inserted in the same sites of pKS84.	This work
pJB29	$CT618_{1-212}$-GFP; $ct618_{1-212}$ was amplified from *C. trachomatis* L2/434 chromosomal DNA by PCR with oligos 1981 and 1982, digested with BamHI-HindIII and inserted in the same sites of pKS84.	This work
pJB30	$CT224_{88-147}$-GFP; $ct224_{88-147}$ was amplified from *C. trachomatis* L2/434 chromosomal DNA by PCR with oligos 1983 and 1984 and inserted by restriction-free cloning in pKS84.	This work

pJB31	CT228$_{87-196}$-GFP; *ct228*$_{87-196}$ region was amplified from *C. trachomatis* L2/434 chromosomal DNA by PCR with oligos 1985 and 1986 and inserted by restriction-free cloning in pKS84.	This work
pJB32	CT229$_{91-215}$-GFP; *ct229*$_{91-215}$ was amplified from *C. trachomatis* L2/434 chromosomal DNA by PCR with oligos 1987 and 1988 and inserted by restriction-free cloning in pKS84.	This work
pJB33	CT135$_{269-360}$-GFP; c*t135*$_{269-360}$ was amplified from *C. trachomatis* L2/434 chromosomal DNA by PCR with oligos 2002 and 2003, digested with BamHI-HindIII and inserted in the same sites of pKS84.	This work
pJB34	CT383$_{157-243}$-GFP; *ct383*$_{157-243}$ was amplified from *C. trachomatis* L2/434 chromosomal DNA by PCR with oligos 2014 and 2015, digested with BamHI-HindIII and inserted in the same sites of pKS84.	This work
pJB35	IncL$_{139-189}$-GFP; *incL*$_{139-189}$ was amplified from *C. trachomatis* L2/434 chromosomal DNA by PCR with oligos 1998 and 1999, digested with BamHI-HindIII and inserted in the same sites of pKS84.	This work
pJB36	CT226$_{94-171}$-GFP; *ct226*$_{94-171}$ was amplified from *C. trachomatis* L2/434 chromosomal DNA by PCR with oligos 2006 and 2007, digested with BamHI-HindIII and inserted in the same sites of pKS84.	This work
pJB37	CT324$_{1-74}$-GFP; *ct324*$_{1-74}$ was amplified from *C. trachomatis* L2/434 chromosomal DNA by PCR with oligos 2010 and 2011, digested with BamHI-HindIII and inserted in the same sites of pKS84.	This work
pJB38	CT449$_{1-41}$-GFP; *ct449*$_{1-41}$ was amplified from *C. trachomatis* L2/434 chromosomal DNA by PCR with oligos 2018 and 2019, digested with BamHI-HindIII and inserted in the same sites of pKS84.	This work
pJB39	CT115$_{112-160}$-GFP; *ct115*$_{112-160}$ was amplified from *C. trachomatis* L2/434 chromosomal DNA by PCR with oligos 2026 and 2027, digested with BamHI-HindIII and inserted in the same sites of pKS84.	This work
pJB40	CT383$_{1-103}$-GFP; *ct383*$_{1-103}$ was amplified from *C. trachomatis* L2/434 chromosomal DNA by PCR with oligos 2012 and 2013, digested with BamHI-HindIII and inserted in the same sites of pKS84.	This work

pJB41	CT813$_{95-264}$-GFP; *ct813*$_{95-264}$ was amplified from *C. trachomatis* L2/434 chromosomal DNA by PCR with oligos 2020 and 2021, digested with BamHI-HindIII and inserted in the same sites of pKS84.	This work
pJB42	CT837$_{593-658}$-GFP; *ct837*$_{593-658}$ was amplified from *C. trachomatis* L2/434 chromosomal DNA by PCR with oligos 2022 and 2023, digested with BamHI-HindIII and inserted in the same sites of pKS84.	This work
pJB43	CT119$_{57-246}$-GFP; *ct119*$_{57-246}$ was amplified from *C. trachomatis* L2/434 chromosomal DNA by PCR with oligos 2024 and 2025, digested with BamHI-HindIII and inserted in the same sites of pKS84.	This work
pJB44	CT116$_{88-132}$-GFP; *ct116*$_{88-132}$ was amplified from *C. trachomatis* L2/434 chromosomal DNA by PCR with oligos 2028 and 2029, digested with BamHI-HindIII and inserted in the same sites of pKS84.	This work
pJB45	CT118$_{89-167}$-GFP; *ct118*$_{89-167}$ was amplified from *C. trachomatis* L2/434 chromosomal DNA by PCR with oligos 2030 and 2031, digested with BamHI-HindIII and inserted in the same sites of pKS84.	This work
pJB46	IncL$_{1-88}$-GFP; *incL*$_{1-88}$ was amplified from *C. trachomatis* L2/434 chromosomal DNA by PCR with oligos 2048 and 2049 and inserted by restriction-free cloning in pKS84.	This work
pJB47	CT135$_{1-209}$-GFP; *ct135*$_{1-209}$ was amplified from *C. trachomatis* L2/434 chromosomal DNA by PCR with oligos 2050 and 2051 and inserted by restriction-free cloning in pKS84.	This work
pJB48	CT223$_{92-268}$-GFP; *ct223*$_{92-268}$ was amplified from *C. trachomatis* L2/434 chromosomal DNA by PCR with oligos 2055 and 2056 and inserted by restriction-free cloning in pKS84.	This work
pJB49	CT192$_{82-231}$-GFP; *ct192*$_{82-231}$ was amplified from *C. trachomatis* L2/434 chromosomal DNA by PCR with oligos 2052 and 2053 and inserted by restriction-free cloning in pKS84.	This work
pJB50	CT223$_{192-268}$-GFP; *ct223*$_{192-268}$ was amplified from *C. trachomatis* L2/434 chromosomal DNA by PCR with oligos 2054 and 2055 and inserted by restriction-free cloning in pKS84.	This work

pJB51	CT324$_{119-303}$-GFP; *ct324$_{119-303}$* was amplified from *C. trachomatis* L2/434 chromosomal DNA by PCR with oligos 2057 and 2058 and inserted by restriction-free cloning in pKS84.	This work
pJB52	CT556$_{1-99}$-GFP; *ct556$_{1-99}$* was amplified from *C. trachomatis* L2/434 chromosomal DNA by PCR with oligos 2059 and 2060 and inserted by restriction-free cloning in pKS84.	This work
pJB54	CT179$_{53-170}$-GFP; *ct179$_{53-170}$* was amplified from *C. trachomatis* L2/434 chromosomal DNA by PCR with oligos 2069 and 2070 and inserted by restriction-free cloning in pKS84.	This work
pLJM1076	CT018$_{1-90}$-GFP; *ct018$_{1-90}$* was amplified from *C. trachomatis* L2/434 chromosomal DNA by PCR with oligos 2000 and 2001, digested with BamHI-HindIII and inserted in the same sites of pKS84.	This work
pLJM1077	CT225$_{67-122}$-GFP; *ct225$_{67-122}$* was amplified from *C. trachomatis* L2/434 chromosomal DNA by PCR with oligos 2004 and 2005, digested with BamHI-HindIII and inserted in the same sites of pKS84.	This work
pLJM1078	CT227$_{89-133}$-GFP; *ct227$_{89-133}$* was amplified from *C. trachomatis* L2/434 chromosomal DNA by PCR with oligos 2008 and 2009, digested with BamHI-HindIII and inserted in the same sites of pKS84.	This work
pLJM1079	CT442$_{89-150}$-GFP; *ct442$_{89-150}$* was amplified from *C. trachomatis* L2/434 chromosomal DNA by PCR with oligos 2016 and 2017, digested with BamHI-HindIII and inserted in the same sites of pKS84.	This work
pSDY-1	GFP-Pep12$_{L-TM}$; plasmid used to amplify Pep12$_{L-TM}$.	Kindly provided by Raphael Valdivia (Sisko *et al.*, 2006)
pJB55	GFP-Pep12$_{L-TM}$; *pep12$_{L-TM}$* was amplified from pSDY-1 with oligos 2046 and 2047 and inserted by restriction-free cloning in pKS84.	This work
pJB57	CT249$_{1-50}$-GFP-Pep12$_{L-TM}$; *pep12$_{L-TM}$* was amplified from pSDY-1 by PCR with oligos 2046 and 2047 and inserted by restriction-free cloning in pJB27.	This work
pJB58	CT134$_{1-79}$-GFP-Pep12$_{L-TM}$; *pep12$_{L-TM}$* was amplified from pSDY-1 by PCR with oligos 2046 and 2047 and inserted by restriction-free cloning in pJB28.	This work

pJB59	$CT618_{1-212}$-GFP-$Pep12_{L-TM}$; $pep12_{L-TM}$ was amplified from pSDY-1 by PCR with oligos 2046 and 2047 and inserted by restriction-free cloning in pJB29.	This work
pJB60	$CT224_{88-147}$-GFP-$Pep12_{L-TM}$; $pep12_{L-TM}$ was amplified from pSDY-1 by PCR with oligos 2046 and 2047 and inserted by restriction-free cloning in pJB30.	This work
pJB61	$CT228_{87-196}$-GFP-$Pep12_{L-TM}$; $pep12_{L-TM}$ was amplified from pSDY-1 by PCR with oligos 2046 and 2047 and inserted by restriction-free cloning in pJB31.	This work
pJB62	$CT229_{91-215}$-GFP-$Pep12_{L-TM}$; $pep12_{L-TM}$ was amplified from pSDY-1 by PCR with oligos 2046 and 2047 and inserted by restriction-free cloning in pJB32.	This work
pJB63	$IncL_{139-189}$-GFP-$Pep12_{L-TM}$; $pep12_{L-TM}$ was amplified from pSDY-1 by PCR with oligos 2046 and 2047 and inserted by restriction-free cloning in pJB35.	This work
pJB64	$CT018_{1-90}$-GFP-$Pep12_{L-TM}$; $pep12_{L-TM}$ was amplified from pSDY-1 by PCR with oligos 2046 and 2047 and inserted by restriction-free cloning in pLJM1076.	This work
pJB65	$CT135_{269-360}$-GFP-$Pep12_{L-TM}$; $pep12_{L-TM}$ was amplified from pSDY-1 by PCR with oligos 2046 and 2047 and inserted by restriction-free cloning in pJB33.	This work
pJB66	$CT225_{67-122}$-GFP-$Pep12_{L-TM}$; $pep12_{L-TM}$ was amplified from pSDY-1 by PCR with oligos 2046 and 2047 and inserted by restriction-free cloning in pLJM1077.	This work
pJB67	$CT324_{1-74}$-GFP-$Pep12_{L-TM}$; $pep12_{L-TM}$ was amplified from pSDY-1 by PCR with oligos 2046 and 2047 and inserted by restriction-free cloning in pJB37.	This work
pJB68	$CT227_{89-133}$-GFP-$Pep12_{L-TM}$; $pep12_{L-TM}$ was amplified from pSDY-1 by PCR with oligos 2046 and 2047 and inserted by restriction-free cloning in pLJM1078.	This work
pJB69	$CT383_{1-103}$-GFP-$Pep12_{L-TM}$; $pep12_{L-TM}$ was amplified from pSDY-1 by PCR with oligos 2046 and 2047 and inserted by restriction-free cloning in pJB40.	This work

pJB70	$CT383_{157-243}$-GFP-$Pep12_{L-TM}$; $pep12_{L-TM}$ was amplified from pSDY-1 by PCR with oligos 2046 and 2047 and inserted by restriction-free cloning in pJB34.	This work
pJB71	$CT442_{89-150}$-GFP-$Pep12_{L-TM}$; $ct442_{89-150}$ was amplified from pLJM1079 by PCR with oligos 2162 and 2163 and inserted by restriction-free cloning in pJB55.	This work
pJB72	$CT449_{1-41}$-GFP-$Pep12_{L-TM}$; $pep12_{L-TM}$ was amplified from pSDY-1 by PCR with oligos 2046 and 2047 and inserted by restriction-free cloning in pJB38.	This work
pJB74	$CT837_{593-658}$-GFP-$Pep12_{L-TM}$; $pep12_{L-TM}$ was amplified from pSDY-1 by PCR with oligos 2046 and 2047 and inserted by restriction-free cloning in pJB42.	This work
pJB75	$CT115_{112-160}$-GFP-$Pep12_{L-TM}$; $pep12_{L-TM}$ was amplified from pSDY-1 by PCR with oligos 2046 and 2047 and inserted by restriction-free cloning in pJB39.	This work
pJB76	$CT116_{88-132}$-GFP-$Pep12_{L-TM}$; $pep12_{L-TM}$ was amplified from pSDY-1 by PCR with oligos 2046 and 2047 and inserted by restriction-free cloning in pJB44.	This work
pJB77	$CT223_{192-268}$-GFP-$Pep12_{L-TM}$; $pep12_{L-TM}$ was amplified from pSDY-1 by PCR with oligos 2046 and 2047 and inserted by restriction-free cloning in pJB50.	This work
pJB78	$CT223_{92-268}$-GFP-$Pep12_{L-TM}$; $pep12_{L-TM}$ was amplified from pSDY-1 by PCR with oligos 2046 and 2047 and inserted by restriction-free cloning in pJB48.	This work
pJB79	$CT118_{89-167}$-GFP-$Pep12_{L-TM}$; $pep12_{L-TM}$ was amplified from pSDY-1 by PCR with oligos 2046 and 2047 and inserted by restriction-free cloning in pJB45.	This work
pJB80	$CT226_{94-171}$-GFP-$Pep12_{L-TM}$; $pep12_{L-TM}$ was amplified from pSDY-1 by PCR with oligos 2046 and 2047 and inserted by restriction-free cloning in pJB36.	This work
pJB81	$IncL_{1-88}$-GFP-$Pep12_{L-TM}$; $incL_{1-88}$ was amplified from pJB46 by PCR with oligos 2048 and 2049 and inserted by restriction-free cloning in pJB55.	This work

pJB82	CT192$_{82-231}$-GFP-Pep12$_{L-TM}$; *ct192$_{82-231}$* was amplified from pJB49 by PCR with oligos 2052 and 2053 and inserted by restriction-free cloning in pJB55.	This work
pJB83	CT324$_{119-303}$-GFP-Pep12$_{L-TM}$; *ct324$_{119-303}$* was amplified from pJB51 by PCR with oligos 2058 and 2059 and inserted by restriction-free cloning in pJB55.	This work
pJB84	CT135$_{1-209}$-GFP-Pep12$_{L-TM}$; *ct135$_{1-209}$* was amplified from pJB47 by PCR with oligos 2050 and 2051 and inserted by restriction-free cloning in pJB55.	This work
pJB85	CT556$_{1-99}$-GFP-Pep12$_{L-TM}$; *ct556$_{1-99}$* was amplified from pJB52 by PCR with oligos 2059 and 2060 and inserted by restriction-free cloning in pJB55.	This work
pJB86	CT233$_{1-99}$-GFP-Pep12$_{L-TM}$; *ct233$_{1-99}$* was amplified from *C. trachomatis* L2/434 chromosomal DNA by PCR with oligos 2065 and 2066 and inserted by restriction-free cloning in pJB55.	This work
pJB87	CT179$_{53-170}$-GFP-Pep12$_{L-TM}$; *ct179$_{53-170}$* was amplified from pJB54 by PCR with oligos 2069 and 2070 and inserted by restriction-free cloning in pJB55.	This work
pJB88	CT119$_{57-246}$-GFP-Pep12$_{L-TM;}$ *ct119$_{57-246}$* was amplified from pJB43 by PCR with oligos 2164 and 2165 and inserted by restriction-free cloning in pJB55.	This work
	Plasmids for production of proteins in mammalian cells	
pALT1	mEGFP; pALT1 derivatives were used for ectopic production of IncL-mEGFP fusion proteins in mammalian cells (Km^R).	(Pais *et al.*, 2019)
pALT2	mEGFP; pALT2 derivatives were used for ectopic production of mEGFP-IncL fusion proteins in mammalian cells (Km^R).	(Pais *et al.*, 2019)
pJB104	mEGFP-IncL$_{FL}$; *incL$_{FL}$* was amplified from *C. trachomatis* L2/434 chromosomal DNA by PCR with oligos 2237 and 2238, digested with XhoI-BamHI and inserted in the same sites of pALT2.	This work

pJB105	mEGFP-IncL$_{1-88}$; *incL$_{1-88}$* was amplified from *C. trachomatis* L2/434 chromosomal DNA by PCR with oligos 2237 and 2241, digested with XhoI-BamHI and inserted in the same sites of pALT2.	This work
pJB106	IncL$_{FL}$-mEGFP; *incL$_{FL}$* was amplified from *C. trachomatis* L2/434 chromosomal DNA by PCR with oligos 2239 and 2263, digested with XhoI-BamHI and inserted in the same sites of pALT1.	This work
pJB107	IncL$_{1-88}$-mEGFP; *incL$_{1-88}$* was amplified from *C. trachomatis* L2/434 chromosomal DNA by PCR with oligos 2239 and 2242, digested with XhoI-BamHI and inserted in the same sites of pALT1.	This work
pJB110	IncL$_{139-189}$-mEGFP; *incL$_{139-189}$* was amplified from *C. trachomatis* L2/434 chromosomal DNA by PCR with oligos 2271 and 2263, digested with XhoI-BamHI and inserted in the same sites of pALT1.	This work
pJB113	mEGFP-IncL$_{139-189}$; *incL$_{139-189}$* was amplified from *C. trachomatis* L2/434 chromosomal DNA by PCR with oligos 2272 and 2238, digested with XhoI-BamHI and inserted in the same sites of pALT2.	This work
pJB116	mEGFP-IncL with residues $S_{165}S_{166}S_{167}$ substituted by $A_{165}A_{166}A_{167}$; *incL$_{S165-167->As}$* was generated by two distinct PCR reactions from pJB104 with oligos 2237 and 2399, and oligos 2398 and 628. The two resulting PCR products were used as templates to perform an overlapping PCR with oligos 2237 and 628. The final PCR product was digested with XhoI-BamHI and inserted in the same sites of pALT2.	This work
pJB117	mEGFP-IncL with residues $S_{150}S_{151}S_{152}$ substituted by $A_{150}A_{151}A_{152}$; *incL$_{S150-152->As}$* was generated by two distinct PCR reactions from pJB104 with oligos 2237 and 2442, and oligos 2441 and 628. The two resulting PCR products were used as templates to perform an overlapping PCR with oligos 2237 and 628. The final PCR product was digested with XhoI-BamHI and inserted in the same sites of pALT2.	This work

pJB118	mEGFP-IncL with residues S_{188} substituted by A_{188}; *incL*$_{S188->A}$ was generated by two distinct PCR reactions from pJB104 with oligos 2237 and 2444, and oligos 2443 and 628. The two resulting PCR products were used as templates to perform an overlapping PCR with oligos 2237 and 628. The final PCR product was digested with XhoI-BamHI and inserted in the same sites of pALT2.	This work
pJB140	mEGFP-IncL$_{1-88}$ with residues $H_{80}K_{81}$ substituted by $G_{80}G_{81}$; *incL*$_{1-88}$ with nucleotide substitutions was generated by two distinct PCR reactions from pJB105 with oligos 2639 and 628, and oligos 2237 and 2640. The two resulting PCR products were used as templates to perform an overlapping PCR with oligos 2237 and 628. The final PCR product was digested with XhoI-BamHI and inserted in the same sites of pALT2.	This work
pJB141	mEGFP-IncL$_{1-88}$ with residues $R_{72}H_{80}K_{81}$ substituted by $G_{72}G_{80}G_{81}$; *incL*$_{1-88}$ with nucleotide substitutions was generated by two distinct PCR reactions from pJB140 with oligos 2637 and 628, and oligos 2237 and 2638. The two resulting PCR products were used as templates to perform an overlapping PCR with oligos 2237 and 628. The final PCR product was digested with XhoI-BamHI and inserted in the same sites of pALT2.	This work
pJB142	mEGFP-IncL$_{1-88}$ with residues $K_{34}K_{37}H_{80}K_{81}$ substituted by $G_{34}G_{37}G_{80}G_{81}$; *incL*$_{1-88}$ with nucleotide substitutions was generated by two distinct PCR reactions from pJB140 with oligos 2635 and 628, and oligos 2237 and 2636. The two resulting PCR products were used as templates to perform an overlapping PCR with oligos 2237 and 628. The final PCR product was digested with XhoI-BamHI and inserted in the same sites of pALT2.	This work

pJB143	mEGFP-IncL_{1-88} with residues $K_{34}K_{37}R_{72}H_{80}K_{81}$ substituted by $G_{34}G_{37}G_{72}G_{80}G_{81}$; *incL*$_{1-88}$ with nucleotide substitutions was generated by two distinct PCR reactions from pJB141 with oligos 2635 and 628, and oligos 2237 and 2636. The two resulting PCR products were used as templates to perform an overlapping PCR with oligos 2237 and 628. The final PCR product was digested with XhoI-BamHI and inserted in the same sites of pALT2.	This work
pJB144	mEGFP-IncL_{1-88} with residues $K_{34}K_{37}$ substituted by $G_{34}G_{37}$; *incL*$_{1-88}$ with nucleotide substitutions was generated by two distinct PCR reactions from pJB105 with oligos 2635 and 628, and oligos 2237 and 2636. The two resulting PCR products were used as templates to perform an overlapping PCR with oligos 2237 and 628. The final PCR product was digested with XhoI-BamHI and inserted in the same sites of pALT2.	This work
pCS2-hPTK7-MT	Protein Tyrosine kinase 7 (PTK7)-myc	Kindly provided by Annette Borchers (Podleschny *et al.*, 2015)
pcDNA3-FLAG-HA-14-3-3β	FLAG-HA-14-3-3β	Addgene #8999
pcDNA3.1-HA-14-3-3ε	HA-14-3-3ε	Addgene #48797
pcDNA3-FLAG-HA-14-3-3γ	FLAG-HA-14-3-3γ	Addgene #9000
HA-14-3-3η	HA-14-3-3η	Addgene #116887
pGEX-4T2-GST-14-3-3τ	GST- 14-3-3τ	Addgene #13281
HA-14-3-3ζ	HA-14-3-3ζ	Addgene #116888

pcDNA3-HA-14-3-3σ	HA-14-3-3σ	Addgene #11946
pCB1	FLAG-HA-14-3-3τ; 14-3-3τ was amplified from pGEX-4T2-GST-14-3-3τ by PCR with oligos 2540 and 2541, digested with EcoRI-XhoI and inserted in the same sites of pcDNA3-FLAG-HA-14-3-3γ.	This work
pCB4	FLAG-HA-14-3-3ε; 14-3-3ε was amplified from pcDNA3.1-HA-14-3-3ε by PCR with oligos 2633 and 2634, digested with EcoRI-XhoI and inserted in the same sites of pcDNA3-FLAG-HA-14-3-3γ.	This work
pCB7	mEGFP-IncL with residues $S_{150}S_{151}S_{152}S_{188}$ substituted by $A_{150}A_{151}A_{152}A_{188}$; *incL* with nucleotide substitutions was generated by two distinct PCR reactions from pJB117 with oligos 2237 and 2444, and oligos 2443 and 628. The two resulting PCR products were used as templates to perform an overlapping PCR with oligos 2237 and 628. The final PCR product was digested with XhoI-BamHI and inserted in the same sites of pALT2.	This work
pCB8	mEGFP-IncL with residues $S_{150}S_{151}S_{152}S_{165}S_{166}S_{167}$ substituted by $A_{150}A_{151}A_{152}A_{165}A_{166}A_{167}$; *incL* with nucleotide substitutions was generated by two distinct PCR reactions from pJB116 with oligos 2237 and 2442, and oligos 2441 and 628. The two resulting PCR products were used as templates to perform an overlapping PCR with oligos 2237 and 628. The final PCR product was digested with XhoI-BamHI and inserted in the same sites of pALT2.	This work
pCB9	mEGFP-IncL with residues $S_{165}S_{166}S_{167}S_{188}$ substituted by $A_{165}A_{166}A_{167}A_{188}$; *incL* with nucleotide substitutions was generated by two distinct PCR reactions from pJB116 with oligos 2237 and 2444, and oligos 2443 and 628. The two resulting PCR products were used as templates to perform an overlapping PCR with oligos 2237 and 628. The final PCR product was digested with XhoI-BamHI and inserted in the same sites of pALT2.	This work

pCB10	mEGFP-IncL with residues $S_{150}S_{151}S_{152}S_{165}S_{166}S_{167}S_{188}$ substituted by $A_{150}A_{151}A_{152}A_{165}A_{166}A_{167}A_{188}$; *incL* with nucleotide substitutions was generated by two distinct PCR reactions from pCB7 with oligos 2237 and 2399, and oligos 2398 and 628. The two resulting PCR products were used as templates to perform an overlapping PCR with oligos 2237 and 628. The final PCR product was digested with XhoI-BamHI and inserted in the same sites of pALT2.	This work
	Plasmids for production of proteins in *C. trachomatis*	
p2TK2--SW2	*C. trachomatis* vector for expression of proteins (Amp^R).	(Agaisse & Derré, 2013)
pSVP247 Derivatives	pSVP247 derivatives were used for production of proteins with a carboxy-terminal double HA (2HA) tag in *C. trachomatis*. Contain the terminator of the *incDEFG* operon (T*incD*) of *C. trachomatis* L2/434 (Amp^R).	(Da Cunha *et al.*, 2014)
pAV4/pIncL-2HA	IncL-2HA; *incL* and its predicted endogenous promoter were amplified from *C. trachomatis* L2/434 chromosomal DNA by PCR with oligos 2250 and 2251, digested with KpnI-NotI and inserted in the same sites of pSVP247.	This work
pJB134/pCT449-2HA	CT449-2HA; *ct449* and its predicted endogenous promoter were amplified from *C. trachomatis* L2/434 chromosomal DNA by PCR with oligos 2616 and 2617, digested with KpnI-NotI and inserted in the same sites of pSVP247.	This work
pJB151/pIncL$_{5G}$-2HA	IncL$_{5G}$-2HA: IncL-2HA with residues $K_{34}K_{37}R_{72}H_{80}K_{81}$ substituted by $G_{34}G_{37}G_{72}G_{80}G_{81}$; *incL* with nucleotide substitutions was generated by several PCR reactions. Firstly, PCR product (PP) 1 was generated from pAV4 with oligos 2250 and 2663; PP2 was generated from pJB143 with oligos 2662 and 2665 and PP3 was generated from pAV4 with oligos 2664 and 2251. PP1 and PP2 and were then used as templates to perform an overlapping PCR with oligos 2250 and 2665, generating PP4. Finally, PP2 and PP4 were used as templates to perform an overlapping PCR with oligos 2250 and 2251 and this final PCR product was digested with NotI-KpnI and inserted in the same sites of pSVP247	This work

pSVP277	pSVP277 is a derivative of p2TK2--SW2(Agaisse & Derré, 2013) for production of proteins with a carboxy-terminal GSK peptide and contains the terminator of the *incDEFG* operon (T*incD*) of *C. trachomatis* L2/434.	This work
pSVP284	RplJ-GSK. The gene encoding RplJ-GSK is expressed under the control of the promoter of *ct694.*	This work
pSVP302/pTet-CteG-2HA	CteG-2HA. The gene encoding CteG-2HA is expressed under the control of the tetracycline-inducible promoter (P*tet*).	(Pais *et al.*, 2019)
pIP12	pIP12 is a derivative of pSVP277 without the first 3 nucleotides (ATG) of the DNA sequence encoding the GSK peptide and contains the terminator of the *incDEFG* operon (T*incD).* The DNA sequence from the gene encoding the GSK peptide (without the first ATG) to the end of the T*incD* was amplified by PCR from pSVP277 with oligos 2132 and 1483, digested with NotI-SalI and inserted in the same sites of p2TK2--SW2.	This work
pIP13/pTet-CteG-GSK	CteG-GSK; The DNA sequence encoding CteG under the control of the tetracycline-inducible promoter (P*tet*) was amplified by PCR from pSVP302 with oligos 1803 and 1552, digested with NotI-KpnI and inserted in the same sites of pIP12.	This work
pIP14/pRplJ-GSK	RplJ-GSK; The DNA sequence encoding RplJ under the control of the tetracycline-inducible promoter (P*tet*) was generated by two PCR reactions. A DNA fragment containing P*tet* was amplified by PCR from pSVP302 with oligos 1803 and 1808, and a DNA fragment encoding RplJ was amplified from pSVP284 with oligos 1809 and 1756. The two resulting PCR products were used as templates to perform an overlapping PCR with oligos 1803 and 1756. The final PCR product was digested with NotI-KpnI and inserted in the same sites of pIP12.	This work
pJB166/pIncL-GSK	IncL-GSK; *incL* and its predicted endogenous promoter were amplified by PCR from pAV4 with oligos 2250 and 2251, digested with KpnI-NotI and inserted in the same sites of pIP12.	This work

pJB167	A DNA sequence containing the terminator of the *incDEFG* operon (T*incD)* was amplified by PCR from pIP12 with oligos 2778 and 1483, digested with NotI-SalI and inserted in the same sites of p2TK2--SW2.	This work
pJB168/pIncL-GSK(26)	IncL-GSK(26): GSK peptide fused to IncL between amino acid residues 26 and 27. A DNA fragment encoding IncL-GSK(26) under the control of the *incL* promoter was generated by sequential PCRs. A partial DNA fragment was amplified by PCR from pAV4 using oligos 2250 and 2781, and another DNA fragment was amplified with oligos 2780 and 2779. These PCR products were used as templates to perform an overlapping PCR with oligos 2250 and 2779. This final PCR product was digested with NotI-KpnI and inserted in the same sites of pJB167.	This work
pJB169/pIncL-GSK(39)	IncL-GSK(39): GSK peptide fused to IncL between amino acid residues 39 and 40. A DNA fragment encoding IncL-GSK(39) under the control of the *incL* promoter was generated by sequential PCRs. A DNA fragment was amplified by PCR from pAV4 using oligos 2250 and 2783, and another DNA fragment was amplified with oligos 2782 and 2779. These PCR products were used as templates to perform an overlapping PCR with oligos 2250 and 2779. This final PCR product was digested with NotI-KpnI and inserted in the same sites of pJB167.	This work
pJB170/pIncL$_{\Delta 47-67}$-2HA	IncL$_{\Delta 47-67}$-2HA: IncL-2HA lacking 21 amino acids from a putative hydrophobic domain (from amino acid residues A_{47} to V_{67}); *incL*$_{\Delta 47-67}$ was generated by two PCR reactions from pAV4 with oligos 2250 and 2788, and oligos 2787 and 2251, followed by a PCR reaction where the two resulting PCR products were used as templates to perform an overlapping PCR with oligos 2250 and 2251. The final PCR product was digested with NotI-KpnI and inserted in the same sites of pSVP247.	This work

Table A.2 Oligonucleotides used in this work.

Number	Description	Sequence (5′ - 3′)	Restriction Site
628	Reverse oligo to construct pJB140, pJB141, pJB142, pJB143 and pJB144	TTATGTTTCAGGTTCAGGG	-
1483	Reverse oligo to construct pSVP277 and pIP12	GATCGTCGACGTCTTAGGAGC TTTTTGCAATGC	SalI
1552	Reverse oligo to construct pIP13	GATCGCGGCCGCGGATAGAG GAGCTTTGCACACC	NotI
1756	Reverse oligo to construct pIP14	GATCGCGGCCGCGCTCTTGAG TTTTTTCTGCTTTCTGG	NotI
1803	Forward oligo to construct pIP13 and pIP14	GATCGGTACCTTAAGACCCAC TTTCACATTTAA	KpnI
1808	Reverse overlap oligo to construct pIP14	GCAACTTTTTCTCTTCTTTCATT TCACTTTTCTCTATCACTGATA GGGAGTGG	-
1809	Forward overlap oligo to construct pIP14	CCACTCCCTATCAGTGATAGA GAAAAGTGAAATGAAAGAAG AGAAAAAGTTGC	-
1977	Forward oligo to construct pJB27	AAAAGGATCCATGGGTATCA AACCTCATG	BamHI
1978	Reverse oligo to construct pJB27	GGGGAAGCTTGCGAGCAACTT TTGCTGC	HindIII
1979	Forward oligo to construct pJB28	AAAAGGATCCATGGCTTGTTG CGCATGTG	BamHI
1980	Reverse oligo to construct pJB28	GGGGAAGCTTTTCAGCACGGC TTTCTGTG	HindIII
1981	Forward oligo to construct pJB29	AAAAGGATCCATGGCAGCAA CGGTACCC	BamHI
1982	Reverse oligo to construct pJB29	GGGGAAGCTTACTTGCACGAG CTCTTTTAAG	HindIII
1983	Forward oligo to construct pJB30 by restriction-free cloning	GTCAAGGAGAAAAAACCCCG GATCCATGTCTGGCTATGGTG GAGA	-
1984	Reverse oligo to construct pJB30 by restriction-free cloning	CAGTGAAAAGTTCTTCTCCTTT ACTCATAAGCTTATCATTGGG AAAAATTGAGTGTAGA	-
1985	Forward oligo to construct pJB31 by restriction-free cloning	GTCAAGGAGAAAAAACCCCG GATCCATGCGTCTTATGTATC GATCCTC	-
1986	Reverse oligo to construct pJB31 by restriction-free cloning	CAGTGAAAAGTTCTTCTCCTTT ACTCATAAGCTTAGAAGCTTG GTTAGCGTCTATA	-

1987	Forward oligo to construct pJB32 by restriction-free cloning	GTCAAGGAGAAAAAACCCCG GATCCATGAGAGCACGAAGT CGTC	-
1988	Reverse oligo to construct pJB32 by restriction-free cloning	CAGTGAAAAGTTCTTCTCCTTT ACTCATAAGCTTTTTTTTACGA CGGGATGCCT	-
1998	Forward oligo to construct pJB35	GATCGGATCCATGACCCACCT TTTCCC	BamHI
1999	Reverse oligo to construct pJB35	GATCAAGCTTAGCGGAAAAG CGTTGG	HindIII
2000	Forward oligo to construct pLJM1076	GATCGGATCCATGCAGCATGC CCATAATG	BamHI
2001	Reverse oligo to construct pLJM1076	GATCAAGCTTTTTTGTGTGCAC TTGTGGC	HindIII
2002	Forward oligo to construct pJB33	GATCGGATCCATGATCTGCCA GCGCAAC	BamHI
2003	Reverse oligo to construct pJB33	GATCAAGCTTCTCTATACGCG CATCTAAAGG	HindIII
2004	Forward oligo to construct pLJM1077	GATCGGATCCATGTCTGTGAT ACGCAATTC	BamHI
2005	Reverse oligo to construct pLJM1077	GATCAAGCTTATCCCACCCAT GAAATTTAGC	HindIII
2006	Forward oligo to construct pJB36	GATCGGATCCATGTATGGGTT TTCTTTAAAACCG	BamHI
2007	Reverse oligo to construct pJB36	GATCAAGCTTTCTCAGACTTT CTTCCAATAC	HindIII
2008	Forward oligo to construct pLJM1078	GATCGGATCCATGTGTAGTCG GGGATTGC	BamHI
2009	Reverse oligo to construct pLJM1078	GATCAAGCTTTGAGACACTTA TAGTCACATCTGC	HindIII
2010	Forward oligo to construct pJB37	GATCGGATCCATGGTCAAAGC CGCTCATC	BamHI
2011	Reverse oligo to construct pJB37	GATCAAGCTTCTTCCAGTTTCT TTGTAAAAAGTCTCCG	HindIII
2012	Forward oligo to construct pJB40	GATCGGATCCATGTTCGGATC TATCCCTTG	BamHI
2013	Reverse oligo to construct pJB40	GATCAAGCTTGCAATGAACAC GAGCGC	HindIII
2014	Forward oligo to construct pJB34	GATCGGATCCATGCGGATCTC TCAAAAAGATACTC	BamHI
2015	Reverse oligo to construct pJB34	GATCAAGCTTGTGGCCGCGCT GGTTTTTC	HindIII

2016	Forward oligo to construct pLJM1079	GATCGGATCCATGGAAGGATACTGTTCTCCG	BamHI
2017	Reverse oligo to construct pLJM1079	GATCAAGCTTTTGGGTCTGATCCACCAG	HindIII
2018	Forward oligo to construct pJB38	GATCGGATCCATGAAATTACCAGAAGTGAG	BamHI
2019	Reverse oligo to construct pJB38	GATCAAGCTTTTGCACCCAATTCATTGAC	HindIII
2020	Forward oligo to construct pJB41	GATCGGATCCATGCAAGTTGAGAAATCTCAATG	BamHI
2021	Reverse oligo to construct pJB41	GATCAAGCTTTATCGAACCACGTCTTCC	HindIII
2022	Forward oligo to construct pJB42	GATCGGATCCATGTGGGATGAAGACAGTTTG	BamHI
2023	Reverse oligo to construct pJB42	GATCAAGCTTAATACCTGAGAATTGCCACC	HindIII
2024	Forward oligo to construct pJB43	GATCGGATCCATGCTACAGAAAACCGCTAATC	BamHI
2025	Reverse oligo to construct pJB43	GATCAAGCTTGGAGCTTTTTGTAGAGGG	HindIII
2026	Forward oligo to construct pJB39	GATCGGATCCATGAGAGAGCGGTTGCATC	BamHI
2027	Reverse oligo to construct pJB39	GATCAAGCTTGCTCGCCCCTTTTTTACTC	HindIII
2028	Forward oligo to construct pJB44	GATCGGATCCATGGATGTTCTAGAGAATCATGG	BamHI
2029	Reverse oligo to construct pJB44	GATCAAGCTTTTGAGTTACTAAAATCACTTGGTCTG	HindIII
2030	Forward oligo to construct pJB45	GATCGGATCCATGTCAGCAGTTGTTCAG	BamHI
2031	Reverse oligo to construct pJB45	GATCAAGCTTGAAGGAGCGTGATCGAGAAC	HindIII
2046	Forward oligo to construct pJB55, by restriction-free cloning	ACTATACAAAGTCGACCGATGCCCTATGTCGGAAGACGAATTTTTTGG	-
2047	Reverse oligo to construct pJB55, by restriction-free cloning	GCTGACTGGGTTGAAGGCTCTCATTACAATTTCATAATGAGAAAAATAAAAAG	-
2048	Forward oligo to construct pJB46 and pJB81 by restriction-free cloning	GTCAAGGAGAAAAAACCCCGGATCCATGCCCTCCACTGTTGCAC	-

2049	Reverse oligo to construct pJB46 and pJB81 by restriction-free cloning	CAGTGAAAAGTTCTTCTCCTTTACTCATAAGCTTTCCGGAGCAACCCTGAAAG	-
2050	Forward oligo to construct pJB47 and pJB84 by restriction-free cloning	GTCAAGGAGAAAAAACCCCGGATCCATGGTAAGCTTCGATTTAAATGATC	-
2051	Reverse oligo to construct pJB47 and pJB84 by restriction-free cloning	CAGTGAAAAGTTCTTCTCCTTTACTCATAAGCTTTGTGATCATTTTGTTTCTTAATTTTC	-
2052	Forward oligo to construct pJB49 and pJB82 by restriction-free cloning	GTCAAGGAGAAAAAACCCCGGATCCATGTGTCACATCCGAAGCAG	-
2053	Reverse oligo to construct pJB49 and pJB82 by restriction-free cloning	CAGTGAAAAGTTCTTCTCCTTTACTCATAAGCTTACAATCATTGGAAACTAAATCATTAATC	-
2054	Forward oligo to construct pJB50 by restriction-free cloning	GTCAAGGAGAAAAAACCCCGGATCCATGGAGCACTACTCTCGTATTTG	-
2055	Reverse oligo to construct pJB48 and pJB50 by restriction-free cloning	CAGTGAAAAGTTCTTCTCCTTTACTCATAAGCTTCACCCGAGAGCCGTAATTG	-
2056	Forward oligo to construct pJB48 by restriction-free cloning	GTCAAGGAGAAAAAACCCCGGATCCATGTGTAGTTGTTGCTTGAGATC	-
2057	Forward oligo to construct pJB51 and pJB83 by restriction-free cloning	GTCAAGGAGAAAAAACCCCGGATCCATGCTAGATAAAGAAAACAAATACC	-
2058	Reverse oligo to construct pJB51 and pJB83 by restriction-free cloning	CAGTGAAAAGTTCTTCTCCTTTACTCATAAGCTTTTGTTCAATAACTCGTGTTGGAC	-
2059	Forward oligo to construct pJB52 and pJB85 by restriction-free cloning	GTCAAGGAGAAAAAACCCCGGATCCATGCCATTCGCAAAAGAAGC	-
2060	Reverse oligo to construct pJB52 and pJB85 by restriction-free cloning	CAGTGAAAAGTTCTTCTCCTTTACTCATAAGCTTATATTGTAGCCAGTCCCACTG	-
2065	Forward oligo to construct pJB86 by restriction-free cloning	GTCAAGGAGAAAAAACCCCGGATCCATGACGTACTCTATGTCCGATATAG	-
2066	Reverse oligo to construct pJB86 by restriction-free cloning	CAGTGAAAAGTTCTTCTCCTTTACTCATAAGCTTCTGCGGGCCGAGTCCTAAAG	-

2069	Forward oligo to construct pJB54 and pJB87 by restriction-free cloning	GTCAAGGAGAAAAAACCCCG GATCCATGAAAGAACAAAAG CTTGCAGC	-
2070	Reverse oligo to construct pJB54 and PJB87 by restriction-free cloning	CAGTGAAAAGTTCTTCTCCTTT ACTCATAAGCTTACCTTTGGG AGAAGTATTTGCT	-
2132	Forward oligo to construct pIP12	GATCGCGGCCGCAGTGGTCGC CCTCGCACTACTAGTTTCG	NotI
2162	Forward oligo to construct pJB71 by restriction-free cloning	GTCAAGGAGAAAAAACCCCG GATCCATGGAAGGATACTGTT CTCCG	-
2163	Reverse oligo to construct pJB71 by restriction-free cloning	CAGTGAAAAGTTCTTCTCCTTT ACTCATAAGCTTTTGGGTCTG ATCCACCAGAC	-
2164	Forward oligo to construct pJB88 by restriction-free cloning	GTCAAGGAGAAAAAACCCCG GATCCATGCTACAGAAAACC GCTAATCTAC	-
2165	Reverse oligo to construct pJB88 by restriction-free cloning	CAGTGAAAAGTTCTTCTCCTTT ACTCATAAGCTTGGAGCTTTTT GTAGAGGGTGATG	-
2237	Forward oligo to construct pJB104 and pJB105	GATCCTCGAGAACCCTCCACT GTTGCACC	XhoI
2238	Reverse oligo to construct pJB104 and pJB113	GATCGGATCCTTAAGCGGAAA AGCGTTGG	BamHI
2239	Forward oligo to construct pJB106 and pJB107	GATCCTCGAGATGCCCTCCAC TGTTGC	XhoI
2241	Reverse oligo to construct pJB105	GATCGGATCCTTATCCGGAGC AACCCTG	BamHI
2242	Reverse oligo to construct pJB107	GATCGGATCCTCCGGAGCAAC CCTGAAAG	BamHI
2250	Forward oligo to construct pAV4	GATCGGTACCACAATCAGCTT ATCTCCCTAG	KpnI
2251	Reverse oligo to construct pAV4	GATCGCGGCCGCGAGCGGAA AAGCGTTGGG	NotI
2263	Reverse oligo to construct pJB106 and pJB110	GATCGGATCCAAAGCGGAAA AGCGTTGGG	BamHI
2264	Reverse oligo to construct pJB107	GATCGGATCCAATCCGGAGC AACCCTGAAAG	BamHI
2271	Forward oligo to construct pJB110	GATCCTCGAGATGACCCACCT TTTCCCAGC	XhoI
2272	Forward oligo to construct pJB113	GATCCTCGAGAAACCCACCTT TTCCCAGC	XhoI
2398	Forward overlap oligo to construct pJB116 and pCB10	CCAAGCTCCCCCGTGCTGCCG CTGCTCCCGATCTG	-

2399	Reverse overlap oligo to construct pJB116 and pCB10	CAGATCGGGAGCAGCGGCAG CACGGGGGAGCTTGG	-
2441	Forward overlap oligo to construct pJB117 and pCB8	GAACATAAACCAGCTGCTGCC CTTAAAATCG	-
2442	Reverse overlap oligo to construct pJB117 and pCB8	CGATTTTAAGGGCAGCAGCTG GTTTATGTTC	-
2443	Forward overlap oligo to construct pJB118, pCB7 and pCB9	CCTTCCCAACGCTTTGCCGCTT AA	-
2444	Reverse overlap oligo to construct pJB118, pCB7 and pCB9	TTAAGCGGCAAAGCGTTGGG AAGG	-
2540	Forward oligo to construct pCB1	GACTGAATTCATGGAGAAGA CTGAGCTGATCC	EcoRI
2541	Reverse oligo to construct pCB1	GACTCTCGAGTTAGTTTTCAG CCCCTTCTGCCGCATCAC	XhoI
2616	Forward oligo to construct pJB134	GATCGGTACCATAGATAATGA TTATTATCAAG	KpnI
2617	Reverse oligo to construct pJB134	GATCGCGGCCGCGCTGAATAG GCGCTTCAG	NotI
2633	Forward oligo to construct pCB4	GATCGAATTCGATGATCGAGA GGATCTGG	EcoRI
2634	Reverse oligo to construct pCB4	GATCCTCGAGTTACTGATTTTC GTCTTCCACGTCC	XhoI
2635	Forward overlap oligo to construct pJB142, pJB143 and pJB144	CCTCTAGCTCAAGGATACCCT GGAGCAGCATTATCCATAG	-
2636	Reverse overlap oligo to construct pJB142, pJB143 and pJB144	CTATGGATAATGCTGCTCCAG GGTATCCTTGAGCTAGAGG	-
2637	Forward overlap oligo to construct pJB141	GTATTTCCTATCGGAGGTCTG ATCTCCTGC	-
2638	Reverse overlap oligo to construct pJB141	GCAGGAGATCAGACCTCCGA TAGGAAATAC	-
2639	Forward overlap oligo to construct pJB140	GATCTCCTGCCTATTCGGTGG AAGCTTTCAGGGTTGC	-
2640	Reverse overlap oligo to construct pJB140	GCAACCCTGAAAGCTTCCACC GAATAGGCAGGAGATC	-
2662	Forward overlap oligo to construct pJB151	CATAACACCTAGTTGGAAAA ATGCCCTCCACTGTTGCACC	-
2663	Reverse overlap oligo to construct pJB151	GGTGCAACAGTGGAGGGCAT TTTTCCAACTAGGTGTTATG	-

2664	Forward overlap oligo to construct pJB151	GCTTTCAGGGTTGCTCCGGAT ATGTTCTAGCAACCTTTC	-
2665	Reverse overlap oligo to construct pJB151	GAAAGGTTGCTAGAACATATC CGGAGCAACCCTGAAAGC	-
2778	Forward oligo to construct pJB167	GATCGCGGCCGCGGATGACAT GTGATTCGCG	NotI
2779	Reverse oligo to construct pJB168 and pJB169	GATCGCGGCCGCGTTAAGCGG AAAAGCGTTGGGAAGG	NotI
2780	Forward overlap oligo to construct pJB168	GAAAGAGTTGCCGCTGCCAGT GGTCGCCCTCGCACTACTAGT TTCGCTGAAAGTTACATGAGC CCTCTAGC	-
2781	Reverse overlap oligo to construct pJB168	GCTAGAGGGCTCATGTAACTT TCAGCGAAACTAGTAGTGCGA GGGCGACCACTGGCAGCGGC AACTCTTTC	-
2782	Forward overlap oligo to construct pJB169	CCCTAAAGCAGCAAGTGGTC GCCCTCGCACTACTAGTTTCG CTGAAAGTTTATCCATAGCCT CTTTAG	-
2783	Reverse overlap oligo to construct pJB169	CTAAAGAGGCTATGGATAAA CTTTCAGCGAAACTAGTAGTG CGAGGGCGACCACTTGCTGCT TTAGGG	-
2787	Forward overlap oligo to construct pJB170	CCATAGCCTCTTTAGCAGTAT TTCCTATCAGAGG	-
2788	Reverse overlap oligo to construct pJB170	CCTCTGATAGGAAATACTGCT AAAGAGGCTATGG	-

Table A.3 *S. cerevisiae* strains used in this work.

Strains	Relevant Genotype	Source/Reference
NSY01	BHY10 diploid a/α, CPY-Inv, *inv-*, *ura-*	(Shohdy *et al.*, 2005)
SCIF00	NSY01 P*gal-gfp* (pKS84)	(Franco *et al.*, 2012)
SCIF01	NSY01 P*gal-vipA-gfp* (pIF206)	(Franco *et al.*, 2012)
SCNS00	NSY01 P*gal-vps4*^{E233Q}	(Shohdy *et al.*, 2005)
SCJNB01	NSY01 P*gal-ct249*$_{1-50}$*-gfp* (pJB27)	This work
SCJNB02	NSY01 P*gal-ct134*$_{1-79}$*-gfp* (pJB28)	This work
SCJNB03	NSY01 P*gal-ct618*$_{1-212}$*-gfp* (pJB29)	This work
SCJNB04	NSY01 P*gal-ct224*$_{88-147}$*-gfp* (pJB30)	This work
SCJNB05	NSY01 P*gal-ct228*$_{87-196}$*-gfp* (pJB31)	This work
SCJNB06	NSY01 P*gal- ct229*$_{91-215}$*-gfp* (pJB32)	This work
SCJNB07	NSY01 P*gal-incL*$_{139-189}$*-gfp* (pJB35)	This work
SCJNB08	NSY01 P*gal-ct018*$_{1-90}$*-gfp* (pLJM1076)	This work
SCJNB09	NSY01 P*gal-ct135*$_{269-360}$*-gfp* (pJB33)	This work
SCJNB10	NSY01 P*gal-ct225*$_{67-122}$*-gfp* (pLJM1077)	This work
SCJNB11	NSY01 P*gal-ct226*$_{94-171}$*-gfp* (pJB36)	This work
SCJNB12	NSY01 P*gal-ct227*$_{89-133}$*-gfp* (pLJM1078)	This work
SCJNB13	NSY01 P*gal-ct324*$_{1-74}$*-gfp* (pJB37)	This work
SCJNB14	NSY01 P*gal-ct383*$_{1-103}$*-gfp* (pJB40)	This work
SCJNB15	NSY01 P*gal-ct383*$_{157-243}$*-gfp* (pJB34)	This work
SCJNB16	NSY01 P*gal-ct442*$_{89-150}$*-gfp* (pLJM1079)	This work
SCJNB17	NSY01 P*gal-ct449*$_{1-41}$*-gfp* (pJB38)	This work
SCJNB18	NSY01 P*gal-ct813*$_{95-264}$*-gfp* (pJB41)	This work
SCJNB19	NSY01 P*gal-ct837*$_{593-658}$*-gfp* (pJB42)	This work
SCJNB20	NSY01 P*gal-ct119*$_{57-246}$*-gfp* (pJB43)	This work
SCJNB21	NSY01 *Pgal-ct115*$_{112-160}$*-gfp* (pJB39)	This work
SCJNB22	NSY01 P*gal-ct116*$_{88-132}$*-gfp* (pJB44)	This work
SCJNB23	NSY01 P*gal-ct118*$_{89-167}$*-gfp* (pJB45)	This work
SCJNB25	NSY01 P*gal-incL*$_{1-88}$*-gfp* (pJB46)	This work
SCJNB26	NSY01 P*gal-ct135*$_{1-209}$*-gfp* (pJB47)	This work
SCJNB27	NSY01 P*gal-ct192*$_{82-231}$*-gfp* (pJB49)	This work
SCJNB28	NSY01 P*gal-ct223*$_{192-268}$*-gfp* (pJB50)	This work
SCJNB29	NSY01 P*gal-ct223*$_{92-268}$*-gfp* (pJB48)	This work
SCJNB30	NSY01 P*gal-ct324*$_{119-303}$*-gfp* (pJB51)	This work
SCJNB31	NSY01 P*gal-ct556*$_{1-99}$*-gfp* (pJB52)	This work
SCJNB36	NSY01 P*gal-ct179*$_{53-170}$*-gfp* (pJB54)	This work
SCJNB37	NSY01 P*gal-gfp-pep12*$_{L-TM}$ (pJB55)	This work

SCJNB38	NSY01 P*gal-ct249*$_{1\text{-}50}$*-gfp-pep12*$_{L\text{-}TM}$ (pJB57)	This work
SCJNB39	NSY01 P*gal-ct134*$_{1\text{-}79}$*-gfp-pep12*$_{L\text{-}TM}$ (pJB58)	This work
SCJNB40	NSY01 P*gal-ct618*$_{1\text{-}212}$*-gfp-pep12*$_{L\text{-}TM}$ (pJB59)	This work
SCJNB41	NSY01 P*gal-ct224*$_{88\text{-}147}$*-gfp-pep12*$_{L\text{-}TM}$ (pJB60)	This work
SCJNB42	NSY01 P*gal-ct228*$_{87\text{-}196}$*-gfp-pep12*$_{L\text{-}TM}$ (pJB61)	This work
SCJNB43	NSY01 P*gal- ct229*$_{91\text{-}215}$*-gfp-pep12*$_{L\text{-}TM}$ (pJB62)	This work
SCJNB44	NSY01 P*gal-incL*$_{139\text{-}189}$*-gfp-pep12*$_{L\text{-}TM}$ (pJB63)	This work
SCJNB45	NSY01 P*gal-ct018*$_{1\text{-}90}$*-gfp-pep12*$_{L\text{-}TM}$ (pJB64)	This work
SCJNB46	NSY01 P*gal-ct135*$_{269\text{-}360}$*-gfp-pep12*$_{L\text{-}TM}$ (pJB65)	This work
SCJNB47	NSY01 P*gal-ct225*$_{67\text{-}122}$*-gfp-pep12*$_{L\text{-}TM}$ (pJB66)	This work
SCJNB48	NSY01 P*gal-ct226*$_{94\text{-}171}$*-gfp-pep12*$_{L\text{-}TM}$ (pJB80)	This work
SCJNB49	NSY01 P*gal-ct227*$_{89\text{-}133}$*-gfp-pep12*$_{L\text{-}TM}$ (pJB68)	This work
SCJNB50	NSY01 P*gal-ct324*$_{1\text{-}74}$*-gfp-pep12*$_{L\text{-}TM}$ (pJB67)	This work
SCJNB51	NSY01 P*gal-ct383*$_{1\text{-}103}$*-gfp-pep12*$_{L\text{-}TM}$ (pJB69)	This work
SCJNB52	NSY01 P*gal-ct383*$_{157\text{-}243}$*-gfp-pep12*$_{L\text{-}TM}$ (pJB70)	This work
SCJNB53	NSY01 P*gal-ct442*$_{89\text{-}150}$*-gfp-pep12*$_{L\text{-}TM}$ (pJB71)	This work
SCJNB54	NSY01 P*gal-ct449*$_{1\text{-}41}$*-gfp-pep12*$_{L\text{-}TM}$ (pJB72)	This work
SCJNB56	NSY01 P*gal-ct837*$_{593\text{-}658}$*-gfp-pep12*$_{L\text{-}TM}$ (pJB74)	This work
SCJNB57	NSY01 P*gal-ct119*$_{57\text{-}246}$*-gfp-pep12*$_{L\text{-}TM}$ (pJB88)	This work
SCJNB58	NSY01 *Pgal-ct115*$_{112\text{-}160}$*-gfp-pep12*$_{L\text{-}TM}$ (pJB75)	This work
SCJNB59	NSY01 P*gal-ct116*$_{88\text{-}132}$*-gfp-pep12*$_{L\text{-}TM}$ (pJB76)	This work
SCJNB60	NSY01 P*gal-ct118*$_{89\text{-}167}$*-gfp-pep12*$_{L\text{-}TM}$ (pJB79)	This work
SCJNB61	NSY01 P*gal-incL*$_{1\text{-}88}$*-gfp-pep12*$_{L\text{-}TM}$ (pJB81)	This work
SCJNB62	NSY01 P*gal-ct135*$_{1\text{-}209}$*-gfp-pep12*$_{L\text{-}TM}$(pJB84)	This work
SCJNB63	NSY01 P*gal-ct192*$_{82\text{-}231}$*-gfp-pep12*$_{L\text{-}TM}$ (pJB82)	This work
SCJNB64	NSY01 P*gal-ct223*$_{192\text{-}268}$*-gfp-pep12*$_{L\text{-}TM}$ (pJB77)	This work
SCJNB65	NSY01 P*gal-ct223*$_{92\text{-}268}$*-gfp-pep12*$_{L\text{-}TM}$ (pJB78)	This work
SCJNB66	NSY01 P*gal-ct324*$_{119\text{-}303}$*-gfp-pep12*$_{L\text{-}TM}$ (pJB83)	This work
SCJNB67	NSY01 P*gal-ct556*$_{1\text{-}99}$*-gfp-pep12*$_{L\text{-}TM}$ (pJB85)	This work
SCJNB70	NSY01 P*gal-ct233*$_{1\text{-}99}$*-gfp-pep12*$_{L\text{-}TM}$ (pJB86)	This work
SCJNB72	NSY01 P*gal-ct179*$_{53\text{-}170}$*-gfp-pep12*$_{L\text{-}TM}$ (pJB87)	This work
YPH499	*MATa ura3-52 lys2-801_amber ade2-101_ochre trp1-Δ63 his3-Δ200 leu2-Δ1*	Kindly provided by Victor J. Cid
SCJNB79	YPH499 P*gal-gfp* (pKS84) + (pGreg505 Erg6-mCherry)	This work
SCJNB80	YPH499 P*gal-incL*$_{1\text{-}88}$*-gfp* (pJB46) + (pGreg505 Erg6-mCherry)	This work
SCJNB82	YPH499 P*gal-gfp* (pJB81) + (pGreg505 Erg6-mCherry)	This work

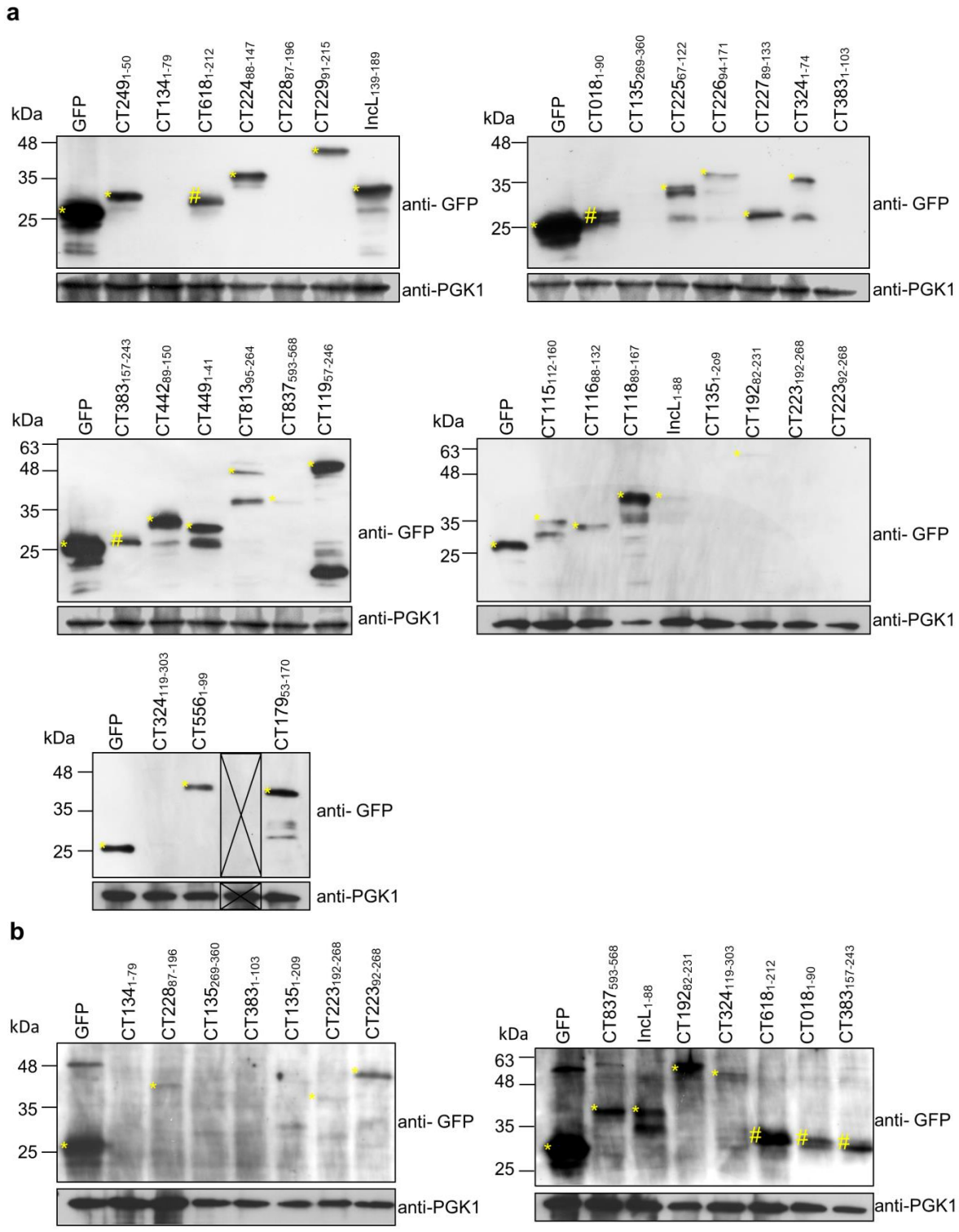

Figure A.1 Analysis of the production of Inc-GFP fusion proteins in yeast by immunoblotting. Whole cell extracts from *S. cerevisiae* NSY01 producing the indicated Inc fragments fused to GFP were analyzed by immunoblotting using antibodies against GFP and PGK1 (yeast loading control) and appropriate HRP-conjugated secondary antibodies. (a) Proteins were detected using SuperSignal West Pico detection kit (Thermo Fisher Scientific). (b) Proteins were detected using SuperSignal West Femto detection kit (Thermo Fisher

Scientific). * Represents proteins that migrated according to the predicted molecular mass; # represents proteins that migrated below the predicted molecular mass; the cross in (**a**) corresponds to a fusion protein that was not analyzed in this study.

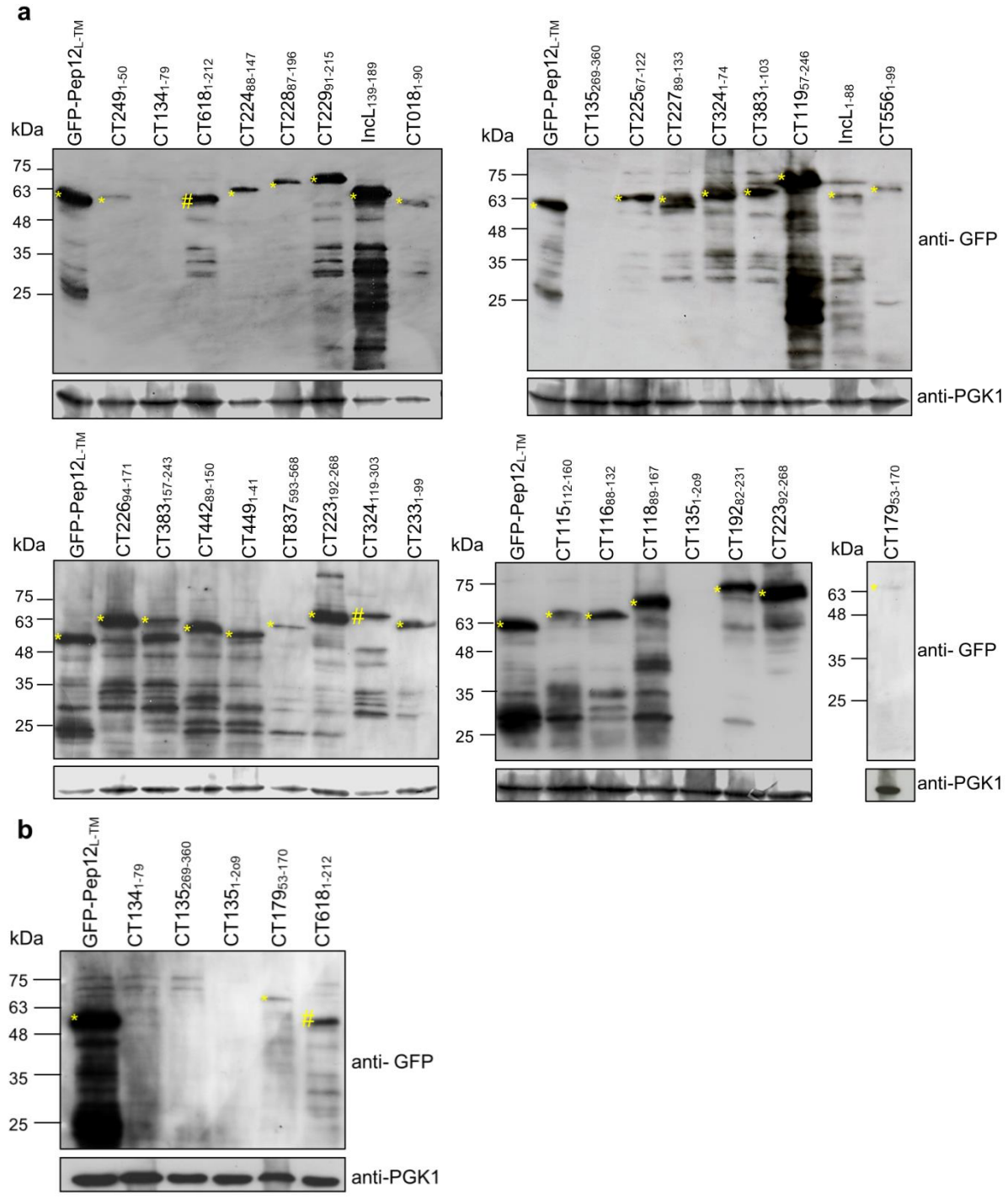

Figure A.2 Analysis of the production of Inc-GFP-Pep12L-TM fusion proteins in yeast by immunoblotting. Whole cell extracts from *S. cerevisiae* NSY01 producing the indicated Inc fragments fused to GFP-Pep12L-TM were analyzed by immunoblotting using antibodies against GFP and PGK1 (yeast loading control) and appropriate HRP-conjugated secondary antibodies. (**a**) Proteins were detected using SuperSignal West Pico detection kit (Thermo Fisher Scientific). (**b**) Proteins were detected using SuperSignal West Femto detection kit (Thermo Fisher Scientific). * represents proteins that migrated according to the predicted molecular mass; # represents proteins that migrated below the predicted molecular mass.

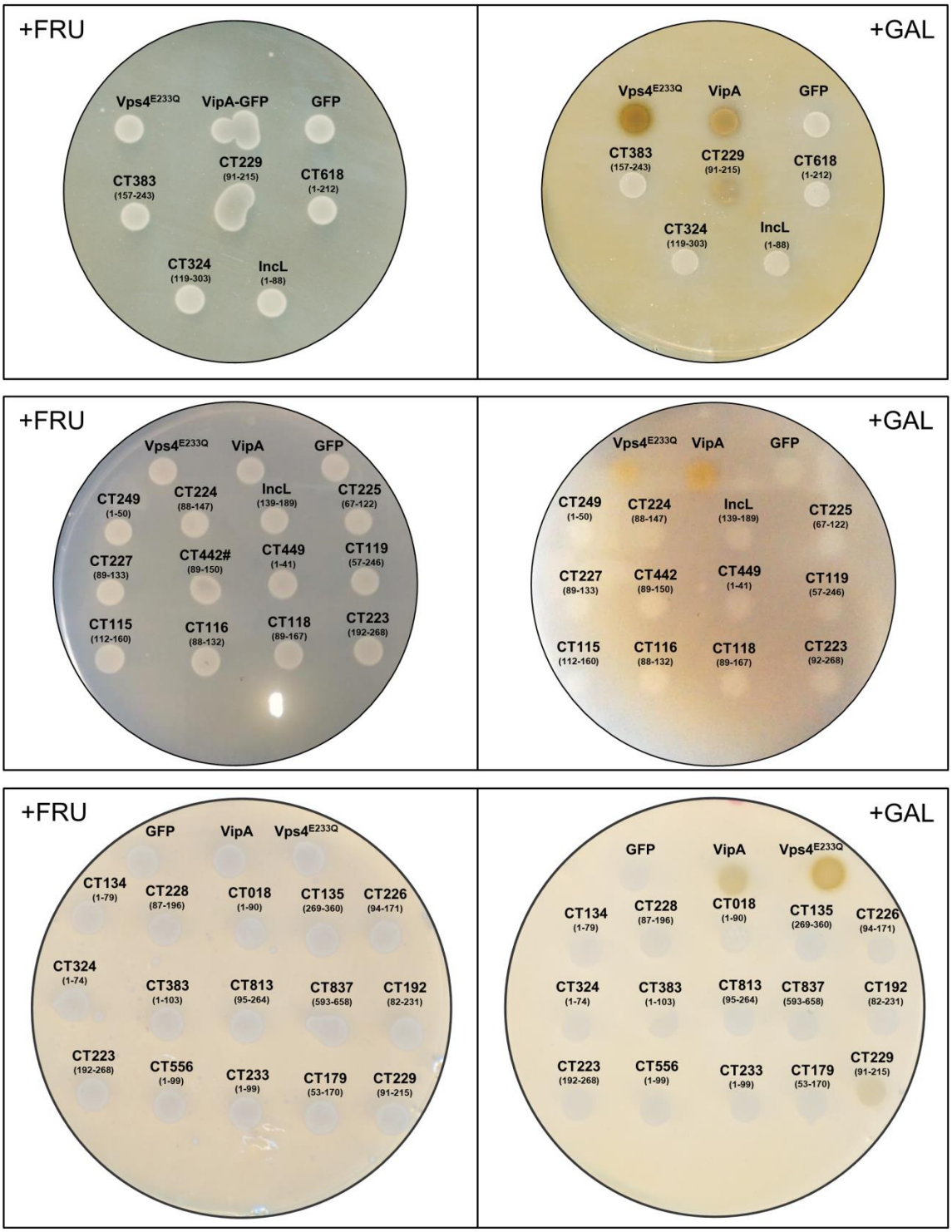

Figure A.3 - The effect of Inc-GFP proteins on vacuolar protein sorting in yeast. *S. cerevisiae* NSY01 strains producing the indicated Inc fragments fused to GFP (Inc-GFP) were grown in solid media under inducing (galactose; +GAL) or non-inducing (fructose; +FRU) conditions. After 48 h, the Vps phenotype was analyzed qualitatively in solid media. Inc-GFP protein interfering with trafficking: CT229$_{91\text{-}215}$-GFP; Negative control: GFP; Positive controls: the *Legionella pneumophila* effector VipA and the dominant-negative form of the yeast ATPase Vps4 (Vps4^{E233Q}). Vps results with all yeast strains producing Inc-GFP proteins are summarized in Table 3.1.

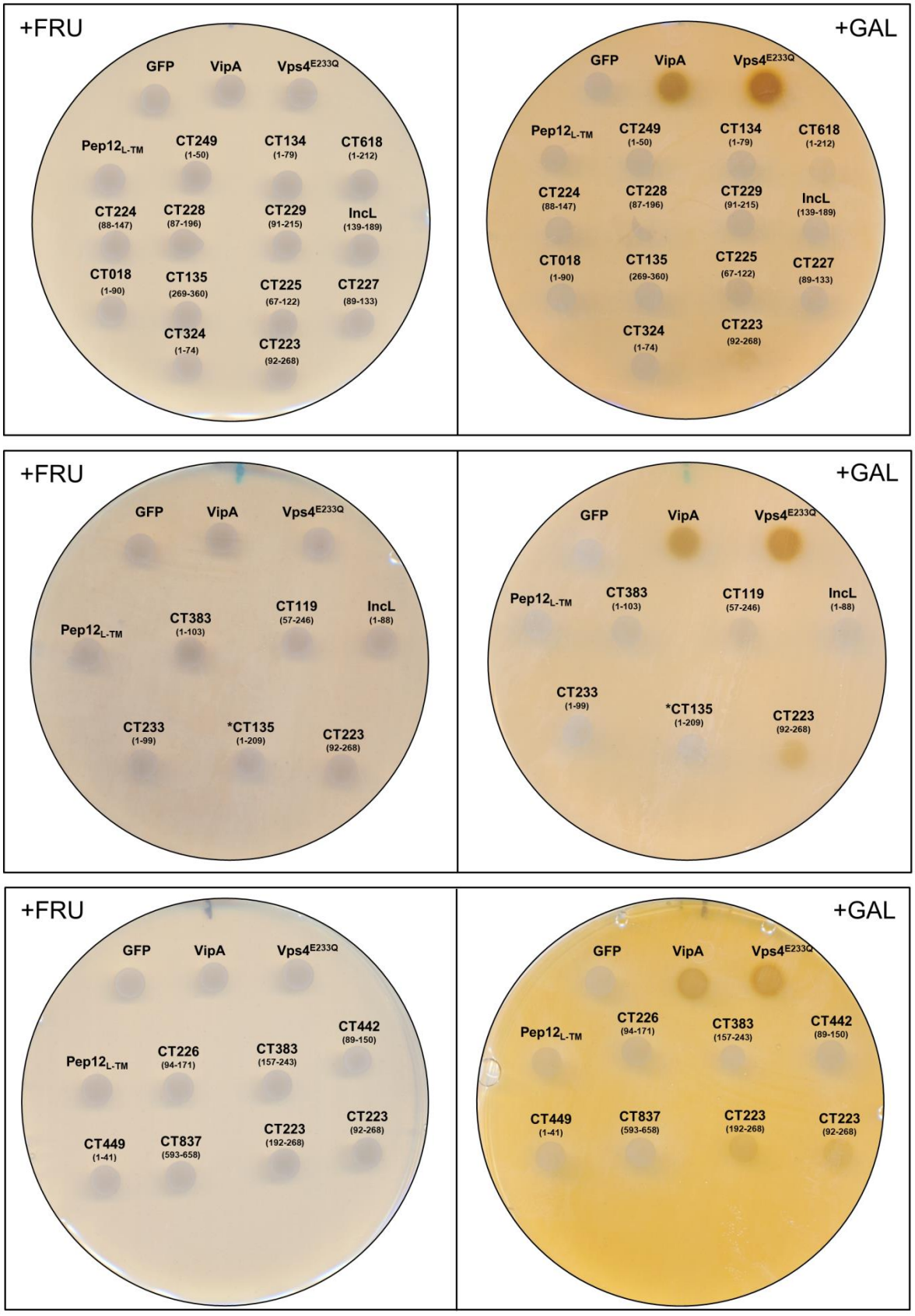

Figure A.4 The effect of Inc-GFP-Pep12L-TM proteins on vacuolar protein sorting in yeast. *S. cerevisiae* strains producing the indicated Inc fragments fused to GFP-Pep12L-TM (Inc-GFP-Pep12L-TM) were grown in solid media

under inducing (galactose; +GAL) or non-inducing (fructose; +FRU) conditions. After 48 h, the Vps phenotype was analyzed qualitatively in solid media. Inc-GFP-Pep12$_{L\text{-}TM}$ protein interfering with trafficking: CT223$_{192\text{-}268}$-GFP-Pep12$_{L\text{-}TM}$; Negative controls: GFP and GFP-Pep12$_{L\text{-}TM}$; Positive controls: the *Legionella pneumophila* effector VipA and the dominant-negative form of the yeast ATPase Vps4 (Vps4^{E233Q}). *CT135$_{1\text{-}209}$ is fused only to GFP (*CT135$_{1\text{-}209}$-GFP). Vps results with all yeast strains producing Inc-GFP-Pep12$_{L\text{-}TM}$ proteins are summarized in Table 3.2.

2021

JOANA MARGARIDA NUNES BUGALHÃO

IDENTIFICATION AND CHARACTERIZATION OF INCL: A *CHLAMYDIA TRACHOMATIS* PROTEIN ASSOCIATING WITH HOST CELL LIPID DROPLETS AND 14-3-3 PROTEINS